Small Molecule and Macromolecular Donors of Reactive Sulfur Species: Insights Into Reactivity and Therapeutic Potential

Kearsley Matthew Dillon

Dissertation submitted to the faculty of the Virginia Polytechnic Institute and State University in partial fulfillment of the requirements for the degree of

Doctor of Philosophy

In

Chemistry

John B. Matson, Chair

Webster L. Santos

Richard D. Gandour

Michael D. Schulz

July 7th, 2021

Blacksburg, VA

Keywords: Gasotransmitter, Drug Delivery, Prodrug, Persulfide, Hydrogen Sulfide

Small Molecule and Macromolecular Donors of Reactive Sulfur Species: Insights Into Reactivity and Therapeutic Potential

Kearsley Matthew Dillon

ABSTRACT

Hydrogen sulfide (H_2S) has been recognized as a biological signaling molecule for over twenty years now. Since these important findings emerged, many collaborative projects among chemists, biologists, and clinicians have demonstrated the physiological roles and potential therapeutic benefits of exogenous H_2S delivery. As our understanding of the active roles H_2S plays in biological systems has increased, so has the desire to investigate other related sulfur species (i.e. persulfides, R–SSH) for their physiological interactions with H_2S and potential therapeutic efficacy. This recent interest in persulfides has stimulated a flurry of research in the field and created a new set of scientific problems to solve and opportunities to improve our understanding of persulfides in a biological context. With this surge of interest in persulfides, chemists set out to synthesize and characterize a variety of stimuli-responsive compounds that release persulfides under specific, biologically relevant conditions.

In order to better understand persulfide reactivity and biological activity, and provide several prodrug platforms that respond to a variety of stimuli, this dissertation describes four persulfide-releasing prodrug systems, a pyrene-based fluorescent probe that measures H_2S release in the presence of thiols, and efforts toward a peptide-based system for the release of H_2S from a peptide thioacid (C(O)SH). The first four systems described utilize the well-known 1,6-benzyl elimination reaction (sometimes called self-immolation) to trigger release of a persulfide from a small molecule, polymeric, or peptide-based prodrug platform.

Importantly, the first self-immolative small molecule persulfide prodrug (termed BDP-NAC) was designed to respond to reactive oxygen species (ROS). Specifically, BDP-NAC utilized a *para*-positioned boronic acid pinacol ester functionality to selectively react with H_2O_2, yielding *N*-acetylcysteine persulfide (NAC-SSH) and *p*-hydroxybenzyl alcohol as a byproduct. BDP-NAC showed trigger specificity towards H_2O_2, as determined by the use of a structurally analogous fluorescent probe (termed BDP-fluor). The prodrug also exhibited antioxidant properties *in vitro,* and served as the first example in the literature of a self-immolative persulfide donor.

The second group of donors, self-immolative small molecule and peptide-based persulfide prodrugs (termed SOPD-Pep and SOPD-NAC), were designed to be responsive to superoxide ($O_2^{\bullet -}$), the primary precursor to all other ROS. In this work, the advantages of attaching small molecule persulfide donors to peptides were explored. *In vitro* experiments showed that SOPD-Pep mitigated toxicity induced by phorbol 12-myristate 13-acetate (PMA) more effectively than its small molecule counterpart SOPD-NAC and several common H_2S donors. It is proposed that peptide scaffolds offer increased cellular uptake due to their nanoscale size, allowing for better antioxidant activity, as confirmed by fluorescence microscopy.

The third section of this dissertation compares an esterase-responsive small molecule to an analogous polymeric persulfide releasing prodrug (termed EDP-NAC and polyEDP-NAC) and their abilities to decrease oxidative stress in response to immediate (H_2O_2) and sustained (5-fluorouracil, 5-FU) forms of ROS. Persulfide release half-lives were characterized using ^{1}H NMR spectroscopy and showed over one order of magnitude difference between EDP-NAC and polyEDP-NAC. In vitro evaluation of the donors showed polyEDP-NAC was better suited to combat sustained production of ROS induced by 5-FU, whereas EDP-NAC was better suited to combat immediately available ROS from H_2O_2. These discrepancies in antioxidant activity

between the two donors were deemed to be a result of their different persulfide release half-lives, indicating that scientists must take these factors into consideration when designing R–SSH prodrugs for specific disease indications.

The fourth donor, NDP-NAC, responded to the bacteria-specific enzyme nitroreductase to release its persulfide payload. NDP-NAC elicited gastroprotective effects in mice that were not observed in animals treated with control compounds incapable of persulfide release or in animals treated with Na_2S. NDP-NAC induced these effects by the upregulation of beneficial small and medium chain fatty acids and through increasing growth of *Turicibacter sanguinis*, a beneficial gut bacterium. It also decreased the populations of *Synergistales* bacteria, opportunistic pathogens implicated in gastrointestinal infections.

Lastly, two appendices are provided in this dissertation that briefly describe the synthesis of a pyrene-based H_2S sensor and efforts toward a readily accessible peptide-based thioacids as H_2S donors.

Small Molecule and Macromolecular Donors of Reactive Sulfur Species: Insights Into Reactivity and Therapeutic Potential

Kearsley Matthew Dillon

GENERAL AUDIENCE ABSTRACT

Hydrogen sulfide (H_2S), produced naturally in hydrothermal vents and as a byproduct of industrial processes, has historically been known for its potent smell and toxicity. However, the recent discovery of H_2S as a naturally-produced signaling molecule (termed gasotransmitter) in mammals has changed the way scientists view this malodorous gas. Our understanding of the biological roles and production of H_2S is still growing, and recent research has suggested various links between changes in H_2S concentrations in the body and a variety of disease states, including Alzheimer's, cardiovascular disease, and inflammation. Because of this link between various diseases and alterations in natural H_2S production, collaborative efforts among chemists, biologists, and pharmacologists have demonstrated the usefulness of therapeutics that contain H_2S-donating moieties, in an effort to alleviate these disease conditions.

Persulfides (R-SSH), biological signaling molecules related to H_2S, have emerged as critical species in sulfur signaling because of the similar observed antioxidative effects compared to H_2S. This dissertation focuses on the synthesis and characterization of several compounds that release persulfides in response to specific stimuli (called persulfide donors). The first donor system described here releases persulfides in response to hydrogen peroxide (H_2O_2), a major cellular oxidant, and reduces oxidative stress in response to H_2O_2. The second donor system responds to superoxide ($O_2^{\bullet -}$), a precursor oxidant to H_2O_2 in cells, to release persulfides. Specifically, two

variants of these donors, a small molecule and a peptide-based donor, exhibited antioxidant activity in response to $O_2^{\bullet -}$, but to varying degrees based on differences in cellular uptake of small molecules and self-assembled peptide nanostructures. The third donor system compares persulfide release from a small molecule and polymeric scaffold, both of which release persulfides in response to esterase enzymes. A large persulfide release half-life range was observed between the two donor systems, and antioxidant activity in response to H_2O_2 also varied based on the source and timescale of oxidant (H_2O_2 versus 5-fluorouracil). The fourth section of this dissertation focuses on a persulfide donor that responds to the bacterial enzyme nitroreductase. This donor increased levels of beneficial bacteria and short and medium chain fatty acids in murine models, while simultaneously decreasing levels of a niche subset of harmful bacteria. Taken together, these persulfide donor systems exhibit the strong reducing ability of persulfides in a biological context, showcasing the potential for therapeutic efficacy and avenues for more advanced donors to be synthesized in the future.

Dedication

This dissertation is dedicated to my mother, Pamela Gordon, for her unwavering support, love, and influence.

Acknowledgements

First, I would like to thank Dr. John Matson for allowing me the freedom to pursue my own interests in lab, providing the resources for me to be able to quickly synthesize compounds, and bringing me in on collaborative activities with experts in other fields. Secondly, I would like to thank my committee members Dr. Richard Gandour, Dr. Webster Santos, and Dr. Michael Schulz for their advice, guidance, and constructive criticism. I would also like to thank Dr. Johan Foster for his helpful role as a member of my Ph.D. Committee in my first two years at Virginia Tech. Additional thanks goes to Dr. Andrew Lowell for serving as a stand-in committee member during my defense.

Next, I would like to thank my mother, Pamela Gordon, for her unwavering support and encouragement during my Ph.D. work. She always encouraged me to do the very best I could with the resources at hand, and greatly helped me financially during this time. Thank you for helping me navigate the graduate school experience with loving, thoughtful advice on personal and professional interactions with others.

I would like to thank my family for their continued support scattered across the country. To my step-dad, Glenn Gordon, thank you for always providing positive reinforcement and having a great attitude. To my brother Josh and his lovely wife Erin Stanley, thank you both for being supportive and encouraging me to finish strong. To my dad, David Dillon, thanks for always offering to help and being available. I love all of you and sincerely appreciate the support system I have in the form of my family.

To my lab folks, I thank you all for having such a positive impact on my life. Thank you for listening to me ramble about outlandish chemistry ideas, and for providing constructive

criticism in my own personal research. I hope we stay in touch in the future. I first want to thank Dr. Chad Powell and Dr. Kyle Arrington for instilling the classic Matson lab "work hard, play hard" mentality in me. We always found ways to have fun on the job, but at the end of the day, we were productive. Without you two, I would not be the same chemist (or person) I am today, and I will never forget some of the funny moments we had together in and outside of lab. To Dr. Ryan Carrazzone, thank you for being available to talk about anything, any time, and for becoming one of my best friends. Thank you for the fun and interesting chemistry whiteboard sessions we'd have drawing up potential ideas. Also, thank you for all the fun times we had in downtown Blacksburg. I'm excited to see where your career goes. To Samantha Scannelli and Dr. Christy Orsino, thank you for providing your home and backyard for cookouts and parties. You both are kind, genuine people and I'm thankful for the times we shared together. To Sarah Swilley, thank you for participating in our lab banter and helping make Hahn Hall South 2008 a fun environment to work in. You truly are a good friend and I wish you and your husband Mike all the best. To Erin Crater, thank you for the times we spent together toward the end of my tenure at Virginia Tech. Your talent and work ethic are impeccable, and your drive and motivation are inspiring. I'll never forget how supportive you were during the week of my defense, and for that I'll be eternally grateful. To Dr. Yin Wang, thank you for allowing me to collaborate with you on your peptide-based projects and for offering advice on nanoscience-related subjects. I look forward to hearing of your successful academic career back in China, and I promise one day I'll visit! To Dr. Josh Wolfgang, thank you for our weightlifting sessions at the Blacksburg Weight Club (and on campus) and for the fun times we had at bars/cookouts. To Dr. Mark Paradzinksy, thank you for our friendship and our time spent together during our first year of graduate school. Several fond memories of us

working through MSD homework in the Johnston Student Center while eating Subway come to mind.

To my undergraduate researcher, Ethan Winckler, I want to thank you sincerely. You picked up on many lab techniques very quickly, and developed some of the best "chemistry hands" I've ever seen from an undergrad. It is very rare that in one year an undergraduate researcher can develop such skills and become a reliable synthetic chemist, so for that, I applaud you. I also thank you for our conversations, lunches, and the fun times that we spent together at bars downtown. You have a bright future ahead of you, Ethan, and I am excited to see where you go.

To Logan Smith, my best friend of 15+ years, thank you for always putting on a smile and brightening the mood. You quickly integrated into my graduate school friend group and I'm pretty sure they ended up preferring you over me most times. ☺ You were always there for me, through the Preliminary Exam in second year, through tough times of paper edits and writing, through the pandemic of 2020 and all the isolation that went with that, and during the weeks before and after my defense. I will be forever grateful for our friendship and your unwavering support.

Lastly, I would like to thank all the support staff in the Department of Chemistry at Virginia Tech. To Ken Knott, Geno Iannaccone, and Mehdi Ashraf-Khorassani, thank you for your work in keeping NMR and HPLC/LCMS/MS running smoothly throughout my time at Virginia Tech. You all have proven to be an invaluable resource to both the department and its graduate students, and I sincerely appreciate the work you did to help me throughout my 5 year tenure at VT.

Table of Contents

Attribution

Many colleagues and coworkers helped in writing, editing, research, and data analysis in this dissertation. A concise description of their contributions and personal backgrounds are included in this section.

Chapter 1: Kearsley M. Dillon (graduate student, Department of Chemistry, Virginia Tech) performed writing and editing of this chapter. John B. Matson (Ph.D., Department of Chemistry, Virginia Tech) is the advisor and committee chair who provided guidance, writing, and editing of this chapter.

Chapter 2: Chad Powell (Ph.D., Department of Chemistry, Virginia Tech) performed most synthesis, characterization, writing, cell culture, and developed the initial concept of the self-immolative persulfide-releasing prodrug. Kearsley M. Dillon (graduate student, Department of Chemistry, Virginia Tech) performed synthesis and characterization for this chapter. Yin Wang (post-doctoral researcher, Department of Chemistry, Virginia Tech) both performed and instructed how to properly do cell viability experiments. Ryan J. Carrazzone (graduate student, Department of Chemistry, Virginia Tech) aided in experiment design and ^{1}H NMR experiments. John B. Matson (Ph.D., Department of Chemistry, Virginia Tech) is the advisor and committee chair who provided guidance, writing, and editing of this chapter.

Chapter 3: Kearsley M. Dillon (graduate student, Department of Chemistry, Virginia Tech) performed partial synthesis, characterization, and writing for this chapter. Yin Wang (post-doctoral researcher, Department of Chemistry, Virginia Tech) performed peptide synthesis, characterization, and writing for this chapter. Zhao Li (graduate student, Department of Chemistry, Virginia Tech) aided in peptide synthesis and experimental design for this chapter. Ethan Winckler

(undergraduate researcher, Department of Biochemistry, Virginia Tech) performed partial synthesis for this chapter. John B. Matson (Ph.D., Department of Chemistry, Virginia Tech) is the advisor and committee chair who provide guidance, writing, and editing of this chapter.

Chapter 4: Kearsley M. Dillon (graduate student, Department of Chemistry, Virginia Tech) performed synthesis, partial characterization, and writing for this chapter. Ryan J. Carrazzone (graduate student, Department of Chemistry, Virginia Tech) performed characterization and writing for this chapter. Yin Wang (post-doctoral researcher, Department of Chemistry, Virginia Tech) aided in data analysis and experimental design in this chapter. Chad Powell (Ph.D., Department of Chemistry, Virginia Tech) aided in experimental design and guidance for synthesis in this chapter. John B. Matson (Ph.D., Department of Chemistry, Virginia Tech) is the advisor and committee chair who provided guidance, writing, and editing of this chapter.

Chapter 5: Kearsley M. Dillon (graduate student, Department of Chemistry, Virginia Tech) performed synthesis, characterization, eukaryote cell culture and writing for this chapter. Holly A. Morrison (graduate student, Department of Biomedical Sciences and Pathobiology, Virginia-Maryland College of Veterinary Medicine, Virginia Tech) performed most biological (mouse and bacterial) experiments and aided in writing this chapter. Chadwick R. Powell (Ph.D., Department of Chemistry, Virginia Tech) provided synthetic and conceptual guidance for this chapter. Ryan J. Carrazzone (graduate student, Department of Chemistry, Virginia Tech) performed ^{1}H NMR kinetics for this chapter. Veronica M. Ringel-Scaia (Ph.D., Department of Biomedical Sciences and Pathobiology, Virginia-Maryland College of Veterinary Medicine, Virginia Tech) performed biological (mouse and bacterial) experiments for this chapter. Ethan W. Winckler (undergraduate researcher, Department of Biochemistry, Virginia Tech) performed partial synthesis and aided in LCMS experiments. R. McAlister Council-Troche (Analytical Chemist, Department of

Biomedical Sciences and Pathobiology, Virginia-Maryland College of Veterinary Medicine, Virginia Tech) performed UPLC/MS analysis on mouse blood/plasma samples. Irving C. Allen (Ph.D., Department of Biomedical Sciences and Pathobiology, Virginia-Maryland College of Veterinary Medicine, Virginia Tech) aided in biological experiment design and writing in this chapter. John B. Matson (Ph.D., Department of Chemistry, Virginia Tech) is the advisor and committee chair who provided guidance, writing, and editing of this chapter.

Appendices A and B: Kearsley M. Dillon (graduate student, Department of Chemistry, Virginia Tech) performed synthesis, characterization, and writing for this chapter. John B. Matson (Ph.D., Department of Chemistry, Virginia Tech) is the advisor and committee chair who provided guidance, writing, and editing of this chapter.

Chapter 1: A Review of Chemical Tools for Studying Small Molecule Persulfides: Detection and Delivery

Adapted with permission from: Dillon, K. M., et al., "A Review of Chemical Tools for Studying Small Molecule Persulfides: Detection and Delivery" ACS Chemical Biology, *accepted*

1.1. Authors

Kearsley M. Dillon and John B. Matson*

Department of Chemistry and Virginia Tech Center for Drug Discovery, Virginia Tech, Blacksburg, Virginia 24061, United States

1.2. Abstract

Hydrogen sulfide (H_2S) has gained significant attention as a potent bioregulator in the redox metabolome, but it is just one of many reactive sulfur species (RSS). Recently, small molecule persulfides (RSSH) have emerged as an RSS of particular interest due to their enhanced antioxidant abilities compared to H_2S and their ability to directly convert protein thiols into protein persulfides, suggesting that persulfides may have distinct physiological functions from H_2S. However, persulfides exhibit instability and cross-reactivity that hampers the elucidation of their precise biological roles. As such, chemists have designed chemical tools and techniques to facilitate the study of persulfides under various conditions. These molecules and methods include persulfide trapping reagents and sensors, as well as compounds that degrade in response to various triggers to release persulfides, termed persulfide donors. There now exist a variety of persulfide donor classes, some of which possess tissue-targeting capabilities designed to mimic localized endogenous production of RSS. This review briefly covers the physicochemical properties of persulfides, the endogenous production of small molecule persulfides, and their reactions with

protein thiols and other reactive species. These introductory sections are followed by a discussion of chemical tools used in persulfide chemical biology, with critical analysis of recent advancements in the field and commentary on potential directions for future research.

1.3. Introduction

Reactive sulfur species (RSS) are widely implicated in a variety of physiological and pathophysiological processes and have attracted significant attention over the past decade.[1] RSS include hydrogen sulfide (H_2S),[2] persulfides (RSSH),[3] polysulfides (RSS_nSR),[4] sulfur dioxide (SO_2),[5] carbonyl sulfide (COS),[6] and carbon disulfide (CS_2),[7] among others. Early efforts focused heavily on hydrogen sulfide (H_2S),[8-9] which is considered a gasotransmitter alongside carbon monoxide (CO)[10] and nitric oxide (NO).[11] H_2S mediates a number of biological processes,[12-14] and exogenous delivery of this gas through a variety of means (e.g., inhalation, sulfide salts, prodrugs) has helped reveal how endogenous H_2S functions while also demonstrating some therapeutic promise.[15-16] Recently, persulfides have begun to pique the interest of chemists, chemical biologists, pharmacologists, and others interested in RSS, in large part because of their presumptive roles as H_2S signaling products along with studies suggesting that native persulfides possess antioxidative physiological functions.[17] In fact, mounting evidence indicates that persulfides possess physiological roles similar to and related to H_2S, indicating that some of the effects originally attributed to H_2S may actually be derived from persulfides.

H_2S and persulfides both have major roles as redox modulators (mostly reducing) that help maintain redox homeostasis. Both species also play active roles in the regulation of enzyme activity and chelation of metals.[18] Additionally, persulfides are proposed as players in biosynthesis of various biological sulfur-containing cofactors including biotin, lipoic acid, and iron-sulfur clusters.[19-20] Beyond its relationship to H_2S, one could ask what makes persulfides, among all RSS,

compelling enough to warrant such significant research efforts? For instance, all RSS are redox modulators (mostly reducing), and there exist many other endogenously produced bioreductants (vitamins C and E, for example). Is the persulfide functional group just one of many forms of RSS and bioreductants in what has recently been termed the reactive species interactome?[21] In other words, do persulfides serve a unique biological purpose? These are important questions that researchers have pondered over the past several years, leading to the development of chemical tools to study persulfides, which are now actively being applied to shed some light onto the role of persulfides in the greater biological signaling and redox webs.

Currently, the most compelling evidence supporting a specific role for endogenously produced small molecule persulfides is their ability to react with cysteine (Cys) residues in proteins in a process called persulfidation, by which a protein thiol is converted into a protein persulfide (RSH + "S^0"→ RSSH). Protein persulfidation appears to be a prominent means of biological regulation and oxidative protection of enzymes and therefore may play a critical role in maintaining redox homeostasis.[22] A critical difference between H_2S and small molecule persulfides arises here: While H_2S (sulfur oxidation state = +2) can provide the sulfur source for protein persulfidation, the protein thiol must first be oxidized (e.g., to a sulfenic acid, RS(O)H); in contrast, small molecule persulfides (oxidation state of internal sulfur = 0) can persulfidate proteins without this oxidation step.[23] Therefore, persulfide donors should be considered alongside H_2S donors in the development of chemical tools to study RSS chemical biology, as well as in the design of therapeutic agents aiming to reestablish cellular redox balance by taking advantage of natural RSS signaling pathways. Similarly, detection of persulfides, separately from H_2S, is also critical in probing the roles of endogenous small molecule and protein persulfides.

In this review, we discuss the state of the art in trapping, sensing, and delivery of small molecule persulfides. We begin with a short overview of the physicochemical properties of persulfides, as well as the physiological roles of persulfides as we currently understand them. We then highlight recent progress in the development of persulfide detection and donor compounds. We aim throughout to provide the reader with an understanding of the capabilities and limitations of these chemical tools with a view toward what the future of this field may hold.

1.4. Physicochemical properties of persulfides

Persulfides have significantly different physicochemical properties compared to structurally analogous thiols (RSH) and H_2S. For example, the pK_a of the Cys thiol (CysSH) is around 8.3, and the pK_a of H_2S is 7.0, whereas the pK_a of cysteine persulfide (Cys–SSH) is 4.3 (predicted).[23-25] This difference in acidity leads to thiols being predominantly protonated at physiological pH, H_2S existing as 30% H_2S and 70% HS^-, and persulfides existing nearly exclusively in their anionic form (RSS^-). For sake of simplicity, in this review the term thiol refers to RSH/RS^-, H_2S refers to H_2S/HS^-, and persulfide refers to RSSH/RSS^-, with specific protonation state noted only when needed. Because persulfides exist primarily in their anionic state at physiological pH, their nucleophilicity is greatly enhanced relative to thiols and H_2S. Additionally, persulfides are proposed to have increased nucleophilicity compared with thiols with similar basicity due to the alpha effect, which suggests that the presence of lone pairs on the adjacent internal sulfur increases reactivity.[26] Because of this enhanced nucleophilicity, persulfides readily react with biologically relevant electrophiles. For example, 8-nitroguanosine 3',5'-cyclic monophosphate (8-nitro-cGMP) is an endogenously produced electrophile with well-known activity as a second messenger in redox signaling.[27] Persulfides possess the ability to convert 8-nitro-cGMP into 8-mercapto-cGMP under

conditions where H_2S cannot, changing the function of this second messenger in redox signaling pathways.[28]

Although anionic persulfides (as RSS^-) are good nucleophiles at physiological pH, neutral persulfides (RSSH) exhibit electrophilicity similar to disulfides (RSSR'). Both species are considered soft electrophiles and react with soft nucleophiles.[29] A significant difference between persulfides and disulfides is that persulfides are readily deprotonated under physiological conditions, offering a rapid means of changing the reactivity of persulfides from electrophilic to nucleophilic, leading to dual reactivity that is not observed in disulfides. Disulfides have long been known to react with thiols in disulfide exchange reactions, and persulfides exhibit analogous reactivity with thiols and also other persulfides in biological systems, affording complex mixtures of polysulfides, hydrogen polysulfides ($R\text{-}SS_nSH$), thiols, and potentially H_2S. Biologically, this process of sulfur shuttling is often called transpersulfidation.[26] This speciation (cross-reactivity) of persulfides with themselves and thiols is a result of the pH-controlled, dual reactivity of persulfides, changing from nucleophilic to electrophilic as pH decreases.[29]

The S–H bond strength of persulfides versus thiols also varies drastically (~70 versus ~92 kcal/mol for persulfides and thiols, respectively).[30] This difference in bond strength is related to the increased stability of the perthiyl radical ($RSS^{\bullet}$) compared to the thiyl radical ($RS^{\bullet}$), caused by the neighboring sulfur atom stabilizing $RSS^{\bullet}$ through resonance effects.[31] Enhanced stability protects the perthiyl radical from reaction with both O_2 and NO, potentially allowing this radical species to exhibit some biological reactivity on its own, but this utility has not, to our knowledge, been confirmed experimentally.[32-33] Additionally, perthiyl radical stability leads to persulfides being more potent H-atom donors than thiols, and similarly allows anionic perthiols (as RSS^-) to be superior one electron reductants when compared to corresponding anionic thiols (as RS^-)

(reduction potentials at pH = 7 are 0.68 V (calculated) and 0.92 V, for RSS$^{\bullet}$/RSSH and RS$^{\bullet}$/RSH respectively).[34] Enzymatically, glutathione persulfide (GSSH) and coenzyme A-SSH can be readily oxidized into sulfites (SO_3^{2-}) via mitochondrial enzymes called persulfide dioxygenases (ETHE1).[35] The potent reducing properties of persulfides were verified experimentally using assays that monitored the reduction of ferric (Fe^{3+}) heme proteins to ferrous (Fe^{2+}) hemes under conditions where thiols remain unreactive.[33] Importantly, the superior reducing qualities of persulfides relative to thiols suggest that persulfides can act as potent antioxidants, able to trap and quench oxidizing radical species.

1.5. Endogenous production and reactions of persulfides

Small molecule persulfides are biologically synthesized mainly via enzymatic catalysis and thiol/disulfide exchange reactions. The most common forms of naturally-occurring small molecule persulfides are cysteine persulfide (Cys–SSH) and GSSH, with liver and heart concentrations ranging from 50–100 and 1–5 μM in mice, respectively.[3] Cys–SSH is endogenously formed via cystathionine-β-synthase (CBS) or cystathionine-γ-lyase (CSE) catalysis from cystine through β-elimination (Figure 1A).[22] However, neither CBS or CSE can convert Cys into Cys-SSH.[3] Interestingly, kinetic analyses of these enzymes suggest that as the concentrations of cystine increases in cells (oxidizing conditions), more Cys–SSH is produced, providing a natural biological means of maintaining redox homeostasis under oxidative stress.[22, 36] Cysteinyl tRNA synthetases (CARs) also produce Cys-SSH through more complicated mechanisms involving Cys transfer to the 2'ribosyl -OH group at the 3' terminus of tRNA.[37]

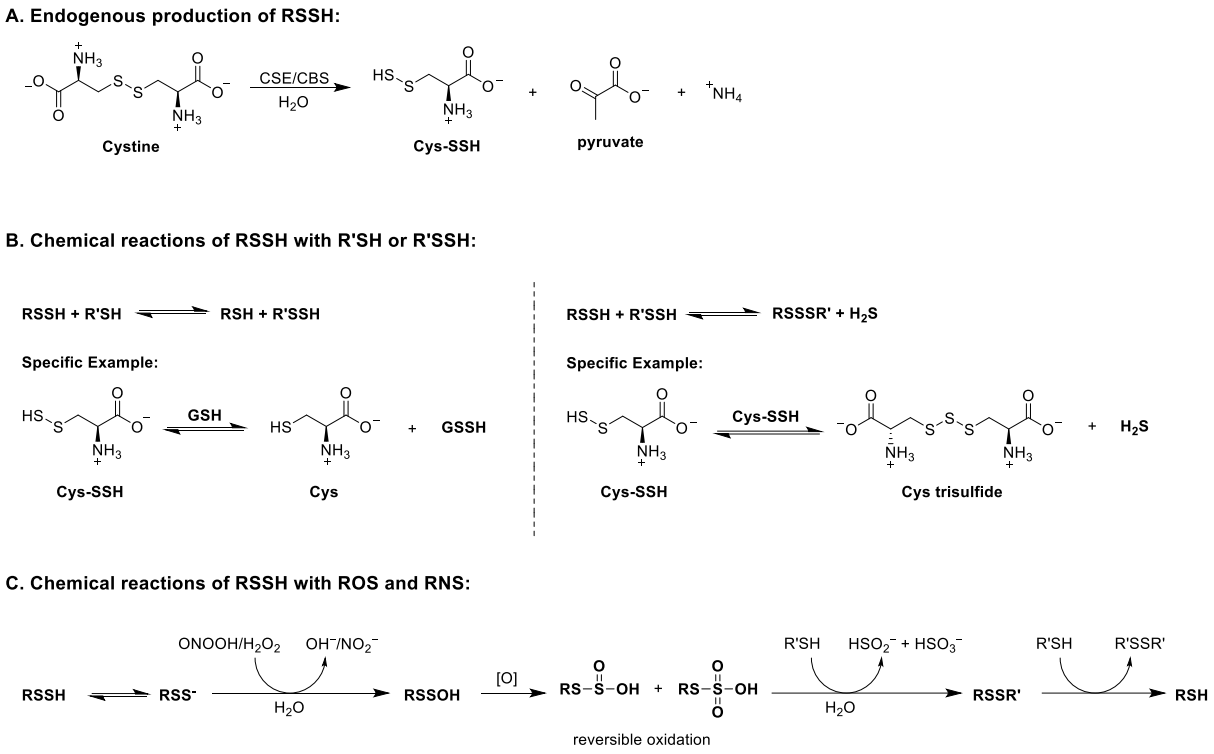

Figure 1. Summary of major endogenous production pathways and some pertinent chemical reactions of persulfides.

The differences in physicochemical properties of persulfides relative to H_2S enable unique biological reactivity. For example, persulfides can directly persulfidate enzymes, where H_2S cannot (it requires initial oxidation of the protein thiol, as noted above). The chemical process of persulfidation relies on the reaction of a protein-bound thiol with the terminal persulfide sulfur, resulting in a persulfidated Cys residue with the release of a thiol. Prominent examples of protein persulfidation and resulting biological effects include H-Ras activation in heart tissue, which modulates cellular redox signaling,[38] and increased parkin protein activity, which decreases Parkinson's symptoms.[39]

In addition to reaction with Cys residues in proteins, small molecule persulfides can react with thiols to form another persulfide and thiol, or a disulfide and H_2S. Small molecule persulfides can also react with themselves to form complex mixtures of various polysulfides, thiols, and H_2S (Figure 1B). For example, Cys–SSH can disproportionate to form cysteine trisulfide (Cys–SSS–Cys) and H_2S. This disproportionation process can continue, yielding higher order cysteine persulfides (Cys–SS_nSH), polysulfides (Cys–SS_nS–Cys), and more H_2S, although low in vitro concentrations of these species may limit the biological relevance of these higher-order reactions. However, some researchers have proposed that exogenously delivered Cys polysulfides may be useful because of their high sulfane sulfur load and innocuous metabolites.[40] Additionally, GSSH can be formed via the reaction of Cys–SSH and glutathione (GSH), which can also disproportionate following a pathway analogous to disproportionation and further reactions of Cys–SSH.

Finally, persulfides also exhibit reactivity with reactive oxygen and nitrogen species (ROS and RNS, respectively).[41] In various model reactions, persulfides react with two electron oxidants like hydrogen peroxide (H_2O_2) and peroxynitrite (ONOOH/$ONOO^-$) (Figure 1C). In one particular study, Li reported GSSH reacted with H_2O_2 at 50 times the rate of H_2S at pH = 7.4.[42] In another study, albumin persulfide reacted with peroxynitrite 10x faster than the corresponding thiol.[23] Additionally, other experiments have shown GSH to be unreactive to oxidation by H_2O_2 under conditions where GSSH exhibited strong reactivity.[3] The likely product of the reaction of H_2O_2 and persulfides is a perthiosulfenic acid (RSSOH), and density functional theory (DFT) calculations have corroborated this proposed reactivity.[3] Further oxidation of perthiosulfenic acids in the presence of excess oxidant also occurs, forming perthiosulfinic and perthiosulfonic acids ($RSSO_2H$ and $RSSO_3H$, respectively).[43] These oxidized persulfide derivatives have been detected

in a number of proteins including papain and albumin.[23, 44] Protein sulfinic and sulfonic acids (RSO_2H and RSO_3H) *cannot* be reduced by biological reductants, but protein perthiosulfinic and perthiosulfonic acids (($RSSO_2H$ and $RSSO_3H$)) *can* be reduced to regenerate the original protein thiol, showcasing the ability of persulfidation to protect enzymes from irreversible oxidation.

Persulfides have rich reactivity far beyond what we have described here. Considering that these compounds can be both nucleophilic and electrophilic and can react in both one- and two-electron redox processes, it is not surprising that persulfide reactions continue to be an area of intense investigation. While further discussion on this topic is beyond the scope of this review, for a comprehensive analysis on persulfide chemical biology, we direct the reader to an excellent recent review on this topic.[45]

1.6. Chemical tools for detection and trapping of persulfides

Due to their speciation and cross-reactivity, small molecule persulfides are difficult to detect directly by high resolution mass spectrometry (HRMS). Accordingly, researchers in the field of persulfide donor chemistry have leveraged the nucleophilicity of persulfides to aid in their quantification/identification via the addition of electrophilic trapping reagents to their kinetic assays. Several trapping reagents have been utilized for these purposes, including dinitrofluorobenzene (DNFB),[46] *N*-ethylmaleimide (NEM),[47] iodoacetamide (IAM) derivatives,[48] *S*-methyl methanethiosulfonate (MMTS),[49] and monobromobimane (mBBr).[50] DNFB reacts with persulfides in a nucleophilic aromatic substitution reaction, displacing the fluorine on the aromatic ring, while NEM relies on a thiol(persulfide)-Michael addition across the electron-deficient olefin, yielding a disulfide linkage. IAM, MMTS, and mBBr all rely on nucleophilic substitution reactions between persulfides and these electrophiles, also resulting in the formation of disulfide linkages (Figure 2A). For protein persulfide quantification, similar techniques have been used; we direct

the reader to recent reports showing a unique tag-switch assay using two reagents to selectively block thiols and then label persulfides in two reaction steps.[51]

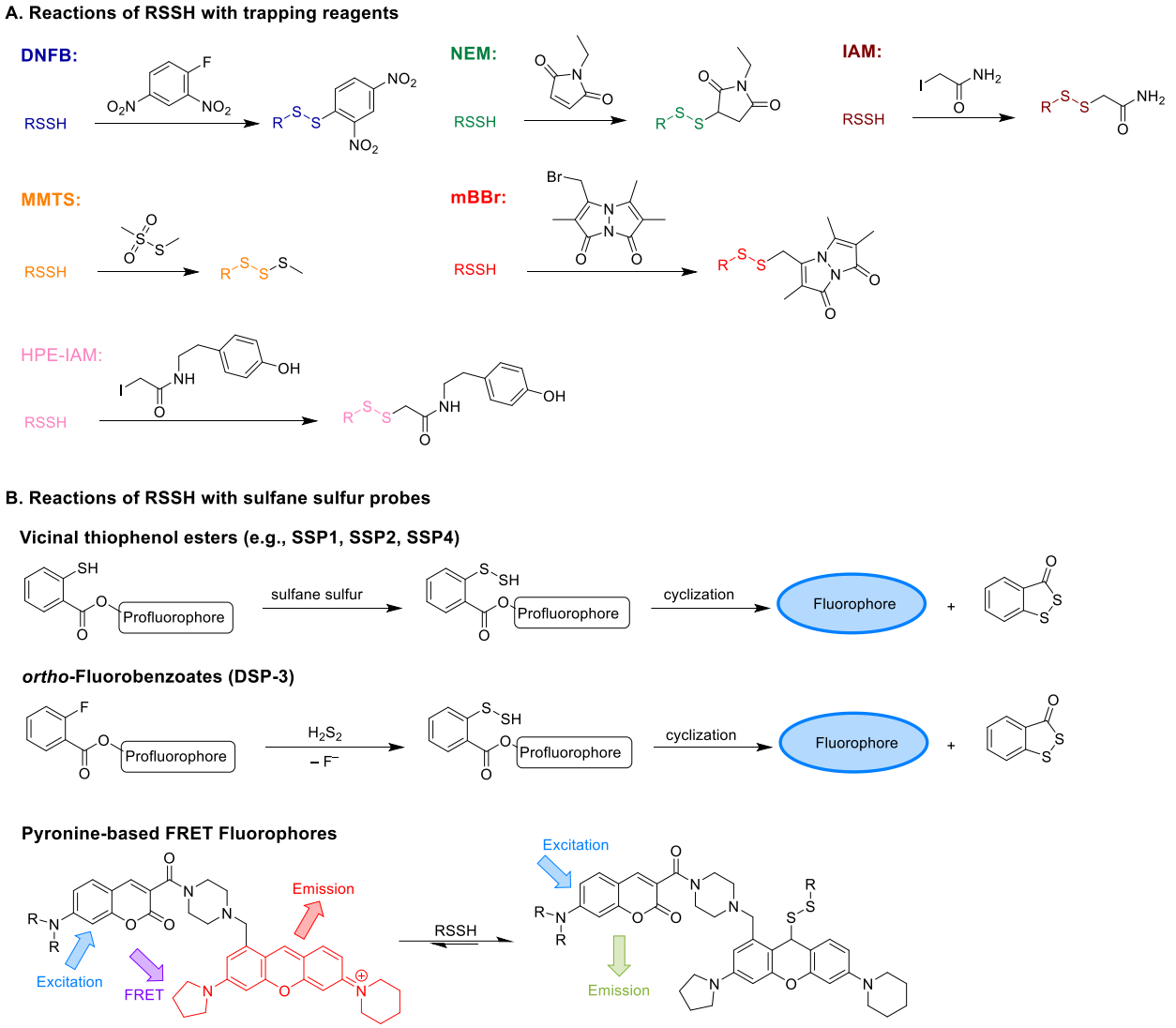

Figure 2. A) Summary of chemical reactions of persulfides with several common trapping reagents. B) Reactions of persulfides with selected chemical probes of sulfane sulfur

Unfortunately, there appears to be no consistent "best choice" reagent for persulfide trapping, as different electrophilic trapping reagents appear to work best for specific persulfides, even

structurally similar ones.[47, 52] Yields of trapped persulfide vary widely with different trapping reagents, often with no apparent rationale. Some possible reasons for the inconsistency in certain trapping reagents towards persulfide donors include the reaction conditions used to trap persulfides (i.e., pH, nature and amount of organic solvent, temperature, experiment timescale), and the pK_a and/or nucleophilicity of the released persulfide (e.g., alkyl-SSH vs. Cys-SSH vs. aromatic-SSH). We caution readers that because of the tendency for persulfides to disproportionate, any reported yield is likely lower than the true amount of persulfide produced because a significant amount may be lost to these side reactions. Thus, persulfide trapping reagents are more useful for verifying that a persulfide has indeed formed rather than quantifying the amount produced.

Persulfide trapping requires subsequent analysis by mass spectrometry, liquid chromatography, or other analytical techniques. In contrast, turn-on fluorescent probes can provide real-time analysis of persulfide formation. Development of fluorescent persulfide probes has been challenging because thiols, H_2S, and sulfane sulfur (including RSSH, RSS_nR, S_8, and H_2S_n) are related analytes with similar reactivity profiles. To this extent, a few probes have been developed. The most well-known turn-on fluorescent probes capable of detecting persulfides are SSP1/SSP2 (Figure 2B).[53] These fluorescent probes are actually not selective for persulfides but rather quantify total sulfane sulfur, where persulfides are a major contributor. SSP1/SSP2 are each connected to a fluorophore via an ester linkage, with an *ortho*-positioned thiophenol. This thiophenol reacts with sulfane sulfur and then undergoes a ring-closing step to release a fluorophore and a benzodithialone byproduct. Despite the publication of a handful of sulfane sulfur-selective profluorophores,[54-57] no persulfide-specific turn-on probes are currently available. The synthesis of reliable, persulfide-specific fluorescent probes would prove immensely useful in the field of RSS biology, potentially providing real-time bioimaging of persulfide generation or release *in vivo*.

Despite the lack of traditional fluorophores with specific persulfide-sensing capabilities, there exist a few examples of ratiometric probes that utilize Förster resonance energy transfer (FRET) and preferentially react with sulfane sulfur species such as persulfides over other related functional groups and compounds (i.e., RSH and H_2S). Ojida designed several FRET-based dual-emission fluorescent probes that leverage the enhanced reactivity of persulfides (relative to thiols).[58] These probes initially emit in the red region, but in response to reaction with persulfides, the emission is blue-shifted, providing easily distinguishable fluorescence differences in reacted/unreacted fluorophore. In particular, one pyronine derivative showed good selectivity for Na_2S_2 over thiols (Figure 2B). In related work, Urano also developed persulfide-sensing probes based on FRET.[59] These silicon-based rhodamine probes exhibited varying degrees of selectivity for persulfides over thiols, with one derivative showing 10,000-fold increased selectivity for Na_2S_2 over GSH. Both of these FRET-based systems achieved some level of selectivity for specific persulfides over thiols, and we expect further iteration to yield increases in sensitivity and selectivity for persulfides over other RSS.

1.7. Synthetic persulfide donors

As interest in the biological interactions of persulfides has increased, the need for clearly defined chemical tools for studying those interactions has also expanded. These chemical tools mostly include persulfide donors (sometimes called persulfide prodrugs, persulfide precursors, or "caged" persulfides) and degrade in response to a specific stimulus to release a persulfide payload. To properly evaluate the biological significance of persulfides, a variety of persulfide donors are required. Although this review is not a comprehensive look at all currently available persulfide donors, here we aim to critically analyze recent developments in persulfide donor chemistry,

focusing on specific examples and discussing important considerations in prodrug design and choosing appropriate donors for biological applications.

1.7.1. Hydrolysis/nucleophile-triggered persulfide donors

One subset of persulfide donors utilizes hydrolysis or nucleophiles to generate a small molecule persulfide. These donors possess varied release rates and rely on nucleophilic addition by water, thiols, or amines to elicit persulfide release. Notably, some of the first hydrolysis/nucleophile-triggered persulfide donor systems were initially reported as H_2S donor systems and likely release both H_2S and persulfides,[60-61] but we do not describe those in detail here. Chemical structures and relevant information describing several persulfide donors triggered by hydrolysis or nucleophiles appear in Table 1.

Table 1. Hydrolysis/nucleophile-triggered persulfide donors

Persulfide Donor	General Structure	Released Persulfide	Trapping Reagent	Ref
Penicillamine acyl persulfide	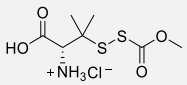	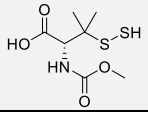	NEM	62
O-Silyl mercaptans	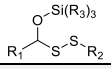		IAM	64
Diacyl disulfides	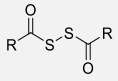	H_2S_2, sulfane sulfur	mBBr, NEM	65
Isothioureas	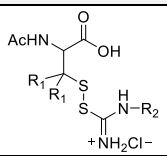	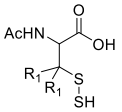	NEM	47
Perthiocarbamates	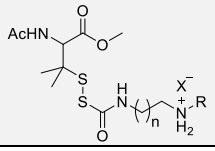	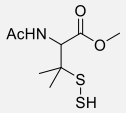	HPE-IAM	52

One of the first persulfide donors, reported by Galardon et al., was penicillamine acyl persulfide, which generates a persulfide analogue of the nitrosothiol SNAP.[62] Due to acidic reaction conditions required for synthesis, the product of this reaction is an ammonium salt, allowing for a long shelf-life at room temperature. The mechanism of persulfide release from this donor system relies on a pH-driven S→N methoxycarbonyl transfer reaction, similar to native chemical ligation strategies commonly employed in peptide synthesis.[63] The authors found that this SNAP analogue was relatively stable in millimolar concentrations at pH 2.7, but upon increasing pH to 7.4, unmasking of the persulfide readily occurred. This "unmasking rate" continued to accelerate with increasing pH, as expected. The free persulfide was trapped using NEM, and this donor converted 8-nitro-GMP to 8-mercapto-cGMP.

Xian et al. recently reported a more general hydrolysis-triggered persulfide donor system in the form of *O*-silyl geminal mercaptans and disulfides.[64] The chemical basis of this system leverages the enhanced stability of oxygen-centered protecting groups over thiol protecting groups in biological systems. Because deprotection of an oxygen-centered protecting group is required to release persulfides from these donors, the authors described this release mechanism as O→S relay deprotection. In this work *O*-silyl geminal mercaptans (which can release H_2S) were converted into asymmetric disulfides (which release persulfides). The asymmetric disulfides released their persulfide payloads more quickly at more acidic pH values with trapping using IAM. In addition, bulkier silyl protecting groups (i.e., triethylsilyl, TES) showed enhanced pH stability over smaller protecting groups (i.e., trimethylsilyl, TMS), with TES-protected donors exhibiting slower release rates than TMS-protected ones. Finally, by swapping out *O*-silyl protecting groups with acetyl esters, persulfide donors with the possibility of degradation and persulfide release in the presence of biologically ubiquitous esterases were generated. The ability to modify the triggers to change

the stimuli-responsiveness of these compounds is unique among most persulfide donors. Using creative chemistry, it may be possible to further derivatize these compounds, affording a set of persulfide donors with a variety of triggers and similar release rates. Related symmetric diacyl disulfides were also studied by Xian as donors of hydrogen persulfide (H_2S_2), the simplest persulfide.[65] H_2S_2 release was observed in pH 7.4 PBS buffer, and trapping with mBBr and phenyl 2-fluoro-5-nitrobenzoate confirmed H_2S_2 release.

Reactions of H_2S_2 released from symmetric acyl persulfides with various fluorescence probes highlighted some of the difficulties in following H_2S_2, persulfides, and RSS in general.[65] Decomposition of diacyl disulfides in pH 7.4 PBS buffer showed minor fluorescence turn-on in the presence of WSP-5[66] (an H_2S-sensitive probe), as expected. However. DSP-3[67] (an H_2S_2-sensitive probe) also did not generate much response, while SSP4[68] (a sulfane-sulfur sensitive probe) showed a large fluorescence turn-on response. These results indicated that released H_2S_2 reacted more quickly with itself to generate various forms of sulfane sulfur than with DSP-3. Additional side reactions also occurred; for example, hydrolysis and subsequent disproportionation of the resulting acyl persulfide generated H_2S and a thioacid, and the large fluorescent turn-on of SSP4 indicated that a significant amount of S_8 was produced, which agrees with the theoretical end products of disproportionation of acyl persulfides. Despite these complications due to reactivity of H_2S_2, acyl persulfides were demonstrated to raise H_2S_2 levels inside PC3 prostate cancer cells, as confirmed using DPS-3.

Toscano et al. reported a unique persulfide donor platform based on *S*-substituted isothioureas.[47] The authors confirmed persulfide release via UPLC-MS using NEM as a trapping reagent, but not all persulfides were efficiently trapped. Structure-activity relationships were then determined using this same *S*-isothiourea-based system by the addition of electron-withdrawing or donating

substituents on the aromatic ring attached to the thiourea (R_2 in the *S*-isothioureas in Table 1). These modified *S*-isothioureas showed tunable persulfide release kinetics, with half-lives ranging from 5.0 to 17.3 min based on aromatic thiourea electronics. Importantly, these donors were stable on the benchtop in the solid state for several months. The modular synthesis of these donors, coupled with their water solubility, place them in a uniquely advantageous position. Furthermore, the known biological activity of thiourea-containing compounds as anticancer/antimicrobial agents[69] may serve as a starting point for *S*-substituted isothiourea-based drugs.

Finally, Toscano et al. also reported an extremely tunable persulfide donor platform utilizing alkylamine-substituted perthiocarbamates.[52] This donor system was designed to exploit the reactivity of a protonated amine that could cyclize and release persulfides in response to changes in pH. Persulfides were efficiently trapped using 4-(hydroxyphenyl)ethyl iodoacetamide (HPE-IAM). The cyclization mechanism of persulfide release was then evaluated using a control compound that that lacked a terminal amine/ammonium group. This control showed no persulfide release under similar conditions, confirming that the presence of the terminal amine is necessary for persulfide release. Structural modifications, including changing the length of the terminal amine linker and the degree of methylation on the terminal amine, drastically changed the persulfide release kinetics, with half-lives ranging from 1.4 to 484 min, the largest reported range of any donor system thus far. Finally, H9c2 cells were pre-treated with alkylamine-substituted perthiocarbamates for 2 h before addition of H_2O_2, revealing a dose-dependent attenuation of H_2O_2-induced toxicity.

An impressive array of hydrolysis/nucleophile-triggered persulfide donors with a variety of release rates have been reported. Many have good water solubility, enabling simple in vivo administration with minimal organic solvent. However, although water solubility is advantageous from a drug

administration point of view, the presence of charged components in some of these donors may limit absorption through the gastrointestinal (GI) tract in animal studies using oral administration. While ideal for study and potential treatment of GI diseases, lack of systemic absorption would limit tissue concentrations of the donor in other areas of the body, preventing tissue-specific targeting outside of the GI tract. However, hydrolysis/nucleophile-triggered persulfide donors are ideal for cell and animal studies where systemic delivery of reduced sulfur is needed.

1.7.2. Enzyme triggered persulfide donors

Enzymes are of utmost importance to all living organisms for the catalysis of biochemical reactions. The utilization of enzymes as donor triggers can offer a broad range of targeting capabilities, based on the chemical properties of the trigger installed on the donor and the localization of the enzyme within an organism. Additionally, overexpression of enzymes is commonplace in many diseases,[70] offering yet another layer of targeting capabilities with thoughtful donor design. A handful of persulfide donors that respond to enzymes have been recently reported, with their structures and relevant information tabulated in Table 2.

Table 2. Enzyme-triggered persulfide donors

Persulfide Donor	General Structure	Released Persulfide	Trapping Reagent	Ref
TML-based H_2S_2 donors	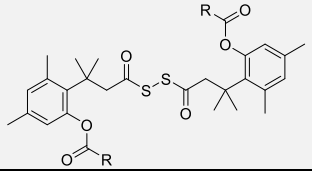	H_2S_2	mBBr	71
TML-based GSSH donor	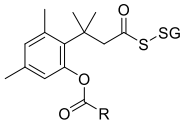	GSSH	DNFB	73
Esterase-responsive benzyl disulfide	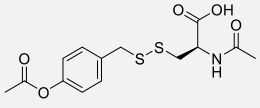	NAC-SSH	DNFB	74

(EDP-NAC)				
NR-responsive benzyl disulfide (NDP-NAC)	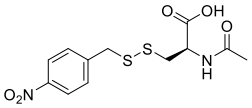	NAC-SSH	DNFB	76

One of the first enzyme-responsive persulfide donors was reported by Wang et al in 2018.[71] These persulfide precursors utilized the popular "trimethyl lock" lactonization system (TML)[72] to efficiently release H_2S_2 in response to esterases. Specifically, the action of an esterase enzyme first cleaves an ester, revealing a phenol that then cyclizes with the aid of three specifically placed methyl substituents, uncaging one half of the donor and converting the initial disulfide structure into an acyl persulfide (RC(O)SSH). This process repeats on the other half of the molecule to release H_2S_2. The H_2S_2-triggered fluorescent turn-on probe DSP-3 confirmed H_2S_2 release from a representative donor (R = CH_3) in the presence of porcine liver esterase (PLE) in PBS (pH = 7.4). Little fluorescence was observed in control experiments without PLE, indicating stability of the donors towards hydrolysis. The authors also used mBBr to trap H_2S_2 as its stable, dimeric adduct (bimane-SS-bimane). H_2S_2 release rates could be tuned by changing the steric bulk of the ester substituent (R group), with half-lives ranging from 24 to 172 min in response to 10 U/mL PLE. Installation of a phosphoester functionality enabled H_2S_2 release in response to alkaline phosphatase (ALP), with a half-life of 28 min in response to 2 U/mL ALP.

Structurally similar to the previously discussed H_2S_2 donor system, Wang recently reported an esterase-triggered GSSH (glutathione persulfide) donor.[73] The compound possessed a TML-based caging group on one side of an asymmetric disulfide, with GSH making up the other half. The authors evaluated GSSH production by trapping GSSH using DNFB and monitoring lactone

byproduct formation by HPLC. Although only a 10% yield of trapped GSSH was obtained, near quantitative conversion of lactone byproduct after 50 min was observed in response to PLE (2 U/mL). A large amount of glutathione trisulfide (GSSSG) was also produced, which the authors attributed to disproportionation and general instability of GSSH, explaining the low trapping yield. Finally, this TML-based GSSH donor compound reduced oxidative stress in an H_2O_2-induced oxidative cell model, functioning as a more potent antioxidant than either H_2S or GSH at equivalent concentrations (150 μM) and maintaining the highest viability after cells were pretreated with donor compound and then exposed to H_2O_2 (450 μM).

These TML-based H_2S_2 and GSSH donors enabled a study of enzyme persulfidation, comparing H_2S_2 and GSSH to H_2S.[71] In the first study, a TML-based H_2S_2 donor (R=Me) persulfidated GAPDH (glyceraldehyde 3-phosphate dehydrogenase) using a tag-switch assay,[51] decreasing GAPDH activity to 18% of maximal activity. This particular assay entailed the blocking of all protein thiols and persulfides followed by subsequent treatment of the resulting thioethers/disulfides with specific nucleophiles attached to a reporter molecule. Treatment of GAPDH with an equivalent amount of H_2S (200 μM) resulted in no enzyme persulfidation, confirming that H_2S cannot directly persulfidate GAPDH. In another GAPDH persulfidation assay, the TML-based GSSH donor (100 μM) decreased catalytic activity to 37% of maximal activity upon treatment.[73] Although no direct comparison was made between the TML-based H_2S_2 and GSSH donors at the same concentrations, these papers demonstrate how persulfides, including H_2S_2 and GSSH, have enhanced abilities to persulfidation enzymes compared with H_2S.

Our group reported the synthesis and evaluation of a benzyl disulfide-based esterase-responsive persulfide donor.[74] This donor, termed EDP-NAC (Ester disulfide prodrug *N*-acetylcysteine), relied on the cleavage of an acetyl ester by PLE, uncaging a free phenol that then underwent 1,6-

elimation (also called self-immolation), a common transformation widely used in the field of stimuli-responsive drug delivery. Persulfide release was evaluated using DNFB as a trapping reagent, as confirmed by LCMS analysis with an authentic sample of the disulfide product. In this work, EDC-NAC was attached to a polymeric scaffold to serve as a comparison between polymeric and monomeric esterase-responsive persulfide donors. This donor and its polymeric analog are discussed in more detail in Section 5.4.

Because several links between host/microbe health and RSS have been established,[75] we suspected a persulfide donor that responded to specific bacterial stimuli might prove useful in the elucidation of the roles persulfides may play at the host-bacterial pathogen interface. Using a similar framework to EDP-NAC, we very recently reported the first tissue-specific persulfide donor termed NDP-NAC (Nitroreductase disulfide prodrug- *N*-acetylcysteine).[76] NDP-NAC released NAC persulfide (NAC-SSH) and *p*-aminobenzyl alcohol as a byproduct in response to bacterial nitroreductase (NR). The mechanism of persulfide release requires initial reduction of a *para*-position nitro group to an amine,[77] followed by 1,6-elimination.[78] Utilizing DNFB as a trapping reagent, HPLC confirmed NAC-SSH release via comparison to an authentic standard. ^{1}H NMR spectroscopy was used to evaluate reaction kinetics, yielding a decomposition half-life of 1.5 h under mildly basic conditions similar to those found in the small intestine, monitoring the conversion of the starting donor aromatic peaks to the *p*-aminobenzyl alcohol byproduct.

NDP-NAC enabled a study of the effect of persulfide delivery on general bacterial populations in the mouse microbiome after oral administration of NDP-NAC or one of several control compounds.[76] Using biased sampling and MALDI-TOF analysis, the number of unique non-*Bacillus* species present was quantified, showing 8 unique species present in the donor treatment group, and negligible changes in control groups, including both Na_2S (as an H_2S donor) and

structurally analogous control compounds that lacked the ability to release persulfides. Utilizing the same mouse samples, short and medium chain fatty acid (SCFA and MCFA) analysis was performed, showing that NDP-NAC-treated animals exhibited much higher levels of heptanoic acid, which plays gastroprotective roles in Crohn's disease and ulcerative colitis.[79] Furthermore, shotgun metagenomics analysis revealed substantial changes in genes responsible for translation, lipid metabolism, and endocrine and metabolic diseases, consistent with changes in markers for various niche bacteria. Thus, persulfide release from NDP-NAC elicited noticeable changes the mouse microbiome, generally increasing populations of beneficial bacteria and reducing the population of some pathogenic bacteria, suggesting that controlled delivery of persulfides to the gut may be useful for modulating the microbiome to treat various diseases.

Importantly, persulfide donors with enzyme triggers that are compartmentalized in specific tissues are more desirable than ubiquitous enzyme triggers to treat acute diseases, like localized inflammation (oxidative stress), to minimize off-target effects. Nitroreductase, as discussed above, is only one of many possible compartmentalized enzymes that may be useful in the development of targeted, enzyme-responsive persulfide donors. We note that esterase-responsive donors accomplish systemic persulfide release due to the pervasive nature of these enzymes. From a therapeutic perspective, this could be advantageous for systemic disease indications, but these donors are unlikely to exhibit specific targeting capabilities. We foresee researchers leveraging the reactivity of many other compartmentalized enzymes in the future, adding more specialized chemical tools to help elucidate biological roles of persulfides in specific tissues.

1.7.3. Redox and light-activated persulfide donors

Reactive sulfur species are heavily implicated in the maintenance of redox homeostasis.[17] Because of their enhanced nucleophilicity and activity as strong bioreductants, persulfides tend to act as

potent scavengers of reactive oxygen species (ROS). These factors make it advantageous to design persulfide precursors that respond to ROS, releasing persulfides to ultimately reduce local oxidative stress.

Utilizing light as a trigger to release persulfides holds therapeutic promise due to the bioorthogonality of visible light as a productive stimulus. Light possesses unique advantages over other choices of stimuli due to the ability to spatiotemporally control its application in desired tissues without major perturbation of most biochemical processes. However, utilizing light as a trigger is limited to the penetration depth and safe limit of light with a given wavelength and intensity. Several redox- and light-activated persulfide donors and relevant information are tabulated below in Table 3.

Table 3. Redox and light-activated persulfide donors

Persulfide Donor	General Structure	Released Persulfide	Trapping Reagent	Ref
H_2O_2-responsive benzyl disulfide (BDP-NAC)	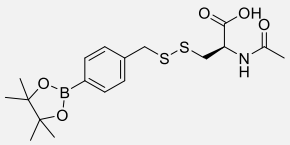	NAC-SSH	n/a	80
Allyl disulfide boronate esters	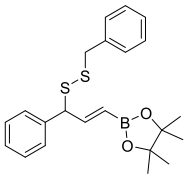	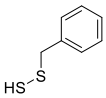	DNFB, mBBr	82
TML-based boronate esters	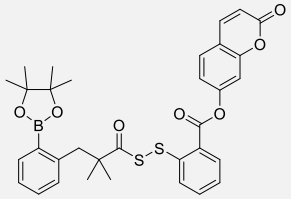 Self-reporter 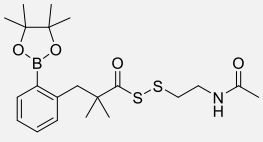 Donor used in biological studies	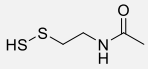	DNFB	83

Superoxide-responsive benzyl disulfide (SOPD-NAC)	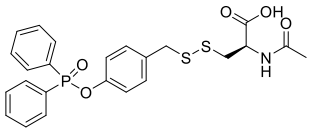	NAC-SSH	n/a	84
o-Nitrobenzyl disulfides	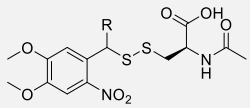	NAC-SSH	DNFB, mBBr	87

A benzyl disulfide-based persulfide donor termed BDP-NAC (Bpin-disulfide prodrug-*N*-acetyl cysteine) was reported by our group in 2018.[80] This persulfide donor released NAC-SSH after deprotection of a boronic acid pinacol ester (Bpin) functionality by H_2O_2 through a mechanism similar NDP-NAC, discussed above, and to COS-releasing compounds reported by Pluth.[81] We confirmed NAC-SSH release from BDP-NAC using LCMS, following the disappearance of the NDP-NAC peak the appearance of free NAC-SSH after 1 h, as confirmed by HRMS. ^{1}H NMR spectroscopy was also used to monitor conversion of NDP-NAC from starting material to byproduct in response to H_2O_2. Finally, trigger specificity of BDP-NAC was evaluated using a profluorophore (termed BDP-fluor) based on the WSP-2 H_2S probe,[66] which showed a 100x fluorescence turn-on in response to H_2O_2 but only minor response to other common oxidants and biological reductants.

In a cell model of oxidative stress, treatment of H9c2 cardiomyocytes with BDP-NAC (100-200 μM) and H_2O_2 (100 μM) revealed a dose-depending increase in cell viability.[80] Control experiments using structurally similar compounds lacking either the Bpin trigger or the disulfide linkage showed little efficacy in mitigating cytotoxicity, indicating that NAC-SSH release from the donor was imparting the majority of observed antioxidative activity. Additional control experiments showed that Na_2S, an instantaneous H_2S donor, and GYY4137, a slow-releasing H_2S

donor did not retain the high cell viabilities after H_2O_2 exposure observed after treatment with BDP-NAC. This work highlighted how persulfides may be more effective than H_2S donors at regulating the cellular redox environment.

Chakrapani reported an H_2O_2-responsive persulfide donor that cleverly utilized a 1,4-O→S-relay decomposition mechanism to release persulfides and cinnamaldehyde.[82] Triggered by using H_2O_2 to remove a BPin group, DNFB and mBBr were utilized to trap persulfides, as confirmed by HPLC analysis. Cinnamaldehyde release was then confirmed with HPLC analysis, observing minimal scavenging of aldehyde by persulfides in the presence of an electrophilic trapping reagent. The authors observed dose-dependent cytoprotection by this dual persulfide/cinnamaldehyde donor compound (0–100 μM) in DLD-1 adenocarcinoma cells after exposure to an oxidative treatment of menadione (50 μM) and JCHD (50 μM), a derivative of juglone. Importantly, a control compound lacking a disulfide and therefore unable to release a persulfide provided no protection from oxidative stress, indicating that the persulfide released by this donor compound was the major contributor to the observed cytoprotective effects.

Another H_2O_2-responsive persulfide donor was recently reported by Lukesh et al., drawing inspiration from Wang to synthesize TML-containing analogues with H_2O_2-sensitive Bpin triggers.[83] The authors designed and synthesized a self-reporting, ROS-responsive persulfide donor, equipped both a disulfide functionality and 7-hydroxycoumarin. This compound relies on the oxidation of a boronate ester, which triggers lactonization to release a free persulfide. The free persulfide then cyclizes to release 7-hydroxycoumarin, providing a self-reporting persulfide donor. Fluorescence experiments conducted with this donor/reporter hybrid revealed a large fluorescence increase in response to H_2O_2, while negligible fluorescence turn-on was observed from a control compound lacking a Bpin group. The authors also identified the cyclic disulfide byproduct of these

experiments, confirming persulfide release and subsequent cyclization is favored over direct oxidation of the released persulfides by H_2O_2. This clever molecular design avoids electrophilic byproducts and generates a fluorescent response, but the cyclization event to generate the fluorophore consumes the persulfide, producing a cyclic acyl disulfide in the process.

To study the biological effects of these TML-based boronate esters, an *N*-acetylcysteamine disulfide analog was prepared, with persulfide trapping confirmed using DNFB.[83] Pretreatment of HeLa cells with this *N*-acetylcysteamine donor before H_2O_2 exposure yielded complete cytoprotection, retaining near 100% cell viability. Importantly, controls lacking various integral components (Bpin trigger, disulfide functionality, *gem*-dimethyl groups) lacked the ability to rescue cells from oxidative damage, suggesting persulfide release from this donor platform was the cause of the observed cytoprotection.

Moving away from boronate esters, which react with H_2O_2, we developed small molecule and peptide-based persulfide donors that responded to superoxide ($O_2^{\bullet-}$).[84] Biologically, $O_2^{\bullet-}$ acts as a more damaging form of ROS (compared to H_2O_2) and is converted into H_2O_2 by the action of superoxide dismutases (SOD) in mitochondria.[85] Thus, we envisioned a persulfide donor that is capable of quenching $O_2^{\bullet-}$ would be beneficial for reducing oxidative damage under conditions where $O_2^{\bullet-}$ levels are high. The small molecule donor, termed SOPD-NAC (Superoxide-triggered persulfide donor *N*-acetylcysteine), relied on a diphenylphosphinate group that selectively reacts with $O_2^{\bullet-}$,[86] allowing for the uncaging of a free phenol that then underwent 1,6-elimination. The donors responded to $O_2^{\bullet-}$, as confirmed by fluorescence assays using WSP-2 with added Cys to convert released persulfides into H_2S. They did not respond significantly to H_2O_2, highlighting the selectivity of this approach for $O_2^{\bullet-}$. An analog of SOPD-NAC that included a self-assembling

peptide, termed SOPD-Pep, was also prepared. More information regarding the comparison studies between these two superoxide-responsive donors can be found in Section 5.4.

Taken together, this collection of ROS-responsive persulfide donors highlights how ROS, including H_2O_2 and $O_2^{\bullet-}$, can be used to trigger release of reducing persulfides. Because of the enhanced stability and trigger specificity imparted by Bpin moiety, donors that possess this functional group exhibit targeting capabilities with the ability to quench local oxidative stress in tissues where H_2O_2 concentrations are high. Additionally, the diphenylphosphinate group acted as a trigger to release persulfides in response to $O_2^{\bullet-}$. This donor platform provided a means of quenching a precursor oxidant to H_2O_2, possibly acting as a means of preventing H_2O_2 production.

Singh et al. developed the first light-responsive persulfide donors, developing one- and two-photon-activated donors based on an *ortho*-nitrobenzyl (ONB) phototrigger.[87] Both persulfide donors (R = H, Me)) were stable in ACN/PBS (3:7, pH = 7.4) containing 10% FBS and cellular thiols (NAC/GSH, 1 mM), with less than 20% decomposition after 10 d under these conditions. HPLC and ^{1}H NMR spectroscopy suggested persulfide generation in response to UV light ($\lambda \geq$ 365 nm) by demonstrating high conversion to the photobyproduct. Persulfide trapping in this system was accomplished using mBBr, with the ONB persulfide donor eliciting a large fluorescence increase, indicating the formation of bimane-SS-NAC. Notably, a control compound that lacked a nitro group and a control experiment lacking UV light showing little fluorescence increase, indicating that both a nitro group and UV light were required for persulfide release. DNFB was also used to quantitatively monitor persulfide release in an HPLC study using alternating light and dark conditions, clearly indicating the unique ability of this system to be turned on and off. The authors then utilized the profluorophore DCFDA (DCFDA = 2',7'-

dichlorodihydrofluorescein diacetate) to visualize intracellular ROS generation, observing a fluorescence turn-off upon administration of their persulfide donor in HeLa cells.

Because of the bioorthogonality of the photostimulus used to elicit persulfide release, light-triggered persulfide donors are uniquely poised to make significant contributions in the elucidation of their biological roles. By tuning the photochemical properties of light-triggered persulfide donors, one could imagine donors that respond to less energetic light, providing a safer means of spatiotemporally controlled persulfide release.

1.7.4. Macromolecular/supramolecular persulfide donors

Macromolecular and supramolecular persulfide delivery systems offer a means of modulating physical, chemical, and pharmacokinetic properties of donors bound to a macromolecular scaffold without directly changing the chemical reactivity of the persulfide payload.[88] For example, polymeric or self-assembling peptide-based scaffolds can enhance the water solubility of hydrophobic donors, extend release rates, and allow for further targeting capabilities based on the functionalities installed on the macromolecular scaffold.[89-90] Additionally, macromolecular scaffolds decrease the rate at which a therapeutic is released in biological systems, sometimes dramatically, enabling access to controlled release profiles.[91]

Table 4. Macromolecular/supramolecular persulfide donors

Persulfide Donor	General Structure	Released Persulfide	Trapping Reagent	Ref
Esterase-responsive benzyl disulfides (EDP-NAC and poly[EDP-NAC])	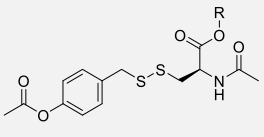 R = H, poly(HEMA-*co*-OEGMA)	NAC-SSH	DNFB	74

Superoxide-responsive benzyl disulfides (SOPD-NAC and SOPD-Pep)	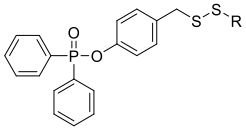 R = NAC, Bz-Cys-Phe-Phe-Glu	NAC-SSH, Bz-Cys(SSH)-Phe-Phe-Glu	n/a	84

We recently reported on a macromolecular persulfide donor in the form of esterase-responsive benzyl disulfides.[74] Due to the limited half-life of most small molecule persulfide donors (generally minutes to hours), we set out to extend persulfide release kinetics via the attachment of a 1,6-elimination-based benzyl disulfide donor to a polymeric scaffold. EDP-NAC (discussed in section 5.2) was coupled to a poly(HEMA-*co*-OEGMA) copolymer that was synthesized via reversible addition-fragmentation chain transfer (RAFT) polymerization[92] to yield a polymeric analog, termed poly(EDP-NAC). ^{1}H NMR spectroscopy was applied to measure the decomposition kinetics of the small molecule and polymeric persulfide donors in response to porcine liver esterase (PLE) (1 U/mL), observing decomposition half-lives of 1.6 and 36 h, respectively. Both EDP-NAC and poly(EDP-NAC) showed no cytotoxicity in H9c2 cardiomyocytes up to concentrations of 400 μM.

This range of release rates allowed us to compare the effects of slow and fast persulfide release in several cell assays. In an H_2O_2-induced cytotoxicity assay, EDP-NAC rescued cells from an immediate form of ROS (H_2O_2), where the polymer showed limited ability to ameliorate oxidative damage under these conditions. However, when H9c2 cells were treated with 5-fluorouricil, a sustained producer of ROS,[93] poly(EDP-NAC) showed a much greater capacity to rescue cells from oxidative damage than EDP-NAC, indicating that the persulfide release half-life must be on the same order of magnitude with the intracellular ROS production rate to achieve maximal protection.

We also reported on a peptide-based supramolecular persulfide delivery system in the form of superoxide ($O_2^{\bullet-}$)-responsive benzyl disulfide donors.[84] This study, similar to the previously mentioned polymeric persulfide donors, compared a small molecule persulfide donor, SOPD-NAC, to peptide-based nanoassemblies (See section 5.3 for discussion on the small molecule donor). The structure of the peptide-based donor, termed SOPD-Pep (Superoxide-triggered persulfide donor peptide), was similar, substituting NAC for the peptide sequence Bz-Cys-Phe-Phe-Glu. Conventional transmission electron microscopy revealed that SOPD-Pep self-assembled into twisted nanoribbons in aqueous solution. We demonstrated the trigger specificity of the diphenylphosphinate group in both persulfide donors to potential oxidants and reductants using WSP-2, finding the largest fluorescence turn-on in the treatment group that included $O_2^{\bullet-}$ and Cys. In these experiments, Cys was used to liberate H_2S from the released persulfides because WSP-2 is an H_2S-sensitive fluorescent probe. There were no significant differences in these fluorescence assays between the small molecule or the peptide, indicating both were capable of persulfide release in response to $O_2^{\bullet-}$.

Fluorescence microscopy was then utilized to investigate whether H_2S could be liberated in cells in the presence of $O_2^{\bullet-}$. In this study, L-buthionine-(*S*,*R*)-sulfoximine (BSO) was used to induce oxidative stress via depletion of intracellular GSH to generate $O_2^{\bullet-}$ in vitro[94-95], and WSP-5 was chosen as an H_2S-selective probe to monitor H_2S accumulation in the cells upon administration of the persulfide donors. BSO and WSP-5 alone showed no fluorescence increase, but pretreatment with SOPD-Pep for 6 h, followed by addition of BSO and WSP-5, drastically increased fluorescence intensity after 30 min. Interestingly, the small molecule analog SODP-NAC showed limited fluorescence increase, which we attributed to the increased ability for peptide assemblies to enter and remain in cells due to their nanoscale size.[96]

The area of macromolecular/supramolecular persulfide donors is perhaps the least explored at this point. In polymer-based systems, monomer choice, degree of polymerization, blockiness, and polymer topology are a few examples of variables researchers could leverage to synthesize a variety of polymeric persulfide donors ranging from solution-based assemblies to functional materials. Targeting groups, fluorophores, and other drugs could be included in the polymers or polymer assemblies. Additionally, numerous changes could be made to the resulting peptide-based donors by varying the appended amino acid sequence, possibly achieving robust biological targeting and/or desirable material properties (e.g., localized release from hydrogels). The area of macromolecular/supramolecular persulfide donor chemistry is in its infancy, but it may yield widely tunable, water-soluble, and bench-stable persulfide donor platforms with greater targeting capabilities and longer release periods than can be achieved with small molecule donors.

1.8. Conclusions

An impressive amount of progress has been made in the field of persulfide donor chemistry in the few years since substantial interest in persulfide biology emerged. Continued innovation and collaboration among researchers from different fields is required to drive the field forward at this fast pace. Many challenges remain in persulfide chemical biology, such as determining biological targets of small molecules persulfides, accurately measuring persulfide concentrations in different tissues, and establishing the specific roles of persulfides among all other RSS. It is also unclear whether persulfides simply act as sacrificial reductants to quench oxidants, or if specific biological targets that uniquely respond to persulfides exist. The precise elucidation of the biological roles of native small molecule persulfides is hampered by their inherent instability and cross reactivity. An increased chemical and biological understanding of persulfide speciation, redox chemistry, and signaling mechanisms of native persulfides will aid in the elucidation of their (patho)physiological

roles. Carefully designed probes that respond specifically to persulfides and donor compounds that release persulfides in response to a variety of stimuli with a range of release rates are required to better characterize these biological interactions.

Beyond chemical biology, comparison studies between persulfide donors and similar H_2S donors may offer guidance on RSS-based drug design for specific disease indications. Macromolecular and supramolecular persulfide donors may enable tissue targeting and extended release. In addition to persulfide delivery alone, persulfide donor compounds that also release a drug may be therapeutically useful. Several H_2S donor-NSAID hybrids have already shown therapeutic promise, a couple of which have participated in clinical trials.[97-98] Because persulfides are stronger bioreductants than H_2S, one could imagine accessing more potent variants of donor/drug hybrids simply by attaching analogous persulfide donors in the place of H_2S donors. The potential for the synthesis and evaluation of these persulfide donor/drug hybrids may lead to rapid innovation in the near future. The field of persulfide donor chemistry is young, but through collaboration among chemists, biologists, pharmacologists, and clinicians, a thorough understanding of persulfide biology may be realized, transitioning the field from an area of academic inquiry to potentially finding uses for these donors as "real world" therapeutics.

1.9. Acknowledgements

We are grateful to the National Science Foundation (DMR-1454754) and the National Institutes of Health (R01GM123508) for support of our work in this area.

1.10. References

1. Kabil, O.; Vitvitsky, V.; Banerjee, R., Sulfur as a signaling nutrient through hydrogen sulfide. *Annu. Rev. Nutr.* **2014,** *34*, 171–205.

2. Abe, K.; Kimura, H., The possible role of hydrogen sulfide as an endogenous neuromodulator. *J. Neurosci* **1996,** *16* (3), 1066–1071.

3. Ida, T.; Sawa, T.; Ihara, H.; Tsuchiya, Y.; Watanabe, Y.; Kumagai, Y.; Suematsu, M.; Motohashi, H.; Fujii, S.; Matsunaga, T.; Yamamoto, M.; Ono, K.; Devarie-Baez, N. O.; Xian, M.; Fukuto, J. M.; Akaike, T., Reactive cysteine persulfides and *S*-polythiolation regulate oxidative stress and redox signaling. *Proc. Natl. Acad. Sci.* **2014,** *111* (21), 7606–7611.

4. DeLeon, E. R.; Gao, Y.; Huang, E.; Olson, K. R., Garlic oil polysulfides: H_2S- and O_2-independent prooxidants in buffer and antioxidants in cells. *Am. J. Physiol. Regul.* **2016,** *310* (11), R1212–R1225.

5. Wang, X.-B.; Jin, H.-F.; Tang, C.-S.; Du, J.-B., The biological effect of endogenous sulfur dioxide in the cardiovascular system. *Eur. J. Pharmacol.* **2011,** *670* (1), 1–6.

6. Steiger, A. K.; Zhao, Y.; Pluth, M. D., Emerging Roles of Carbonyl Sulfide in Chemical Biology: Sulfide Transporter or Gasotransmitter? *Antioxid. Redox. Signal.* **2017,** *28* (16), 1516–1532.

7. DeMartino, A. W.; Zigler, D. F.; Fukuto, J. M.; Ford, P. C., Carbon disulfide. Just toxic or also bioregulatory and/or therapeutic? *Chem. Soc. Rev.* **2017,** *46* (1), 21–39.

8. Wang, R., The Gasotransmitter Role of Hydrogen Sulfide. *Antioxid. Redox. Signal.* **2003,** *5* (4), 493–501.

9. Wang, R., Two's company, three's a crowd: can H_2S be the third endogenous gaseous transmitter? *FASEB J.* **2002,** *16* (13), 1792–1798.

10. Siracusa, R.; Schaufler, A.; Calabrese, V.; Fuller, P. M.; Otterbein, L. E., Carbon Monoxide: from Poison to Clinical Trials. *Trends Pharmacol. Sci.* **2021,** *42* (5), 329–339.

11. Mustafa, A. K.; Gadalla, M. M.; Snyder, S. H., Signaling by Gasotransmitters. *Sci. Signal* **2009,** *2* (68), 1–8.

12. Kolluru, G. K.; Shen, X.; Bir, S. C.; Kevil, C. G., Hydrogen sulfide chemical biology: Pathophysiological roles and detection. *Nitric Oxide* **2013,** *35*, 5–20.

13. Wang, R., Physiological Implications of Hydrogen Sulfide: A Whiff Exploration That Blossomed. *Physiol. Rev.* **2012,** *92* (2), 791–896.

14. Giovinazzo, D.; Bursac, B.; Sbodio, J. I.; Nalluru, S.; Vignane, T.; Snowman, A. M.; Albacarys, L. M.; Sedlak, T. W.; Torregrossa, R.; Whiteman, M.; Filipovic, M. R.; Snyder, S. H.; Paul, B. D., Hydrogen sulfide is neuroprotective in Alzheimer's disease by sulfhydrating GSK3β and inhibiting Tau hyperphosphorylation. *Proc. Natl. Acad. Sci.* **2021,** *118* (4), e2017225118.

15. Powell, C. R.; Dillon, K. M.; Matson, J. B., A review of hydrogen sulfide (H_2S) donors: Chemistry and potential therapeutic applications. *Biochem. Pharmacol.* **2018,** *149*, 110–123.

16. Wallace, J. L.; Wang, R., Hydrogen sulfide-based therapeutics: exploiting a unique but ubiquitous gasotransmitter. *Nat. Rev. Drug Discov.* **2015,** *14* (5), 329–345.

17. Kasamatsu, S.; Nishimura, A.; Morita, M.; Matsunaga, T.; Abdul Hamid, H.; Akaike, T., Redox Signaling Regulated by Cysteine Persulfide and Protein Polysulfidation. *Molecules* **2016,** *21* (12), 1721.

18. Galardon, E.; Huguet, F.; Herrero, C.; Ricoux, R.; Artaud, I.; Padovani, D., Reactions of persulfides with the heme cofactor of oxidized myoglobin and microperoxidase 11: reduction or coordination. *Dalton Trans.* **2017,** *46* (24), 7939–7946.

19. Hidese, R.; Mihara, H.; Esaki, N., Bacterial cysteine desulfurases: versatile key players in biosynthetic pathways of sulfur-containing biofactors. *Appl. Microbiol. Biotechnol.* **2011,** *91* (1), 47–61.

20. Zhang, B.; Crack, J. C.; Subramanian, S.; Green, J.; Thomson, A. J.; Le Brun, N. E.; Johnson, M. K., Reversible cycling between cysteine persulfide-ligated [2Fe-2S] and cysteine-ligated [4Fe-4S] clusters in the FNR regulatory protein. *Proc. Natl. Acad. Sci.* **2012,** *109* (39), 15734.

21. Cortese-Krott, M. M.; Koning, A.; Kuhnle, G. G. C.; Nagy, P.; Bianco, C. L.; Pasch, A.; Wink, D. A.; Fukuto, J. M.; Jackson, A. A.; van Goor, H.; Olson, K. R.; Feelisch, M., The Reactive Species Interactome: Evolutionary Emergence, Biological Significance, and Opportunities for Redox Metabolomics and Personalized Medicine. *Antioxid. Redox. Signal.* **2017,** *27* (10), 684–712.

22. Filipovic, M. R.; Zivanovic, J.; Alvarez, B.; Banerjee, R., Chemical Biology of H_2S Signaling through Persulfidation. *Chem. Rev.* **2018,** *118* (3), 1253–1337.

23. Cuevasanta, E.; Lange, M.; Bonanata, J.; Coitiño, E. L.; Ferrer-Sueta, G.; Filipovic, M. R.; Alvarez, B., Reaction of Hydrogen Sulfide with Disulfide and Sulfenic Acid to Form the Strongly Nucleophilic Persulfide. *J. Biol. Chem.* **2015,** *290* (45), 26866–26880.

24. Portillo-Ledesma, S.; Sardi, F.; Manta, B.; Tourn, M. V.; Clippe, A.; Knoops, B.; Alvarez, B.; Coitiño, E. L.; Ferrer-Sueta, G., Deconstructing the Catalytic Efficiency of Peroxiredoxin-5 Peroxidatic Cysteine. *Biochemistry* **2014,** *53* (38), 6113–6125.

25. Li, Q.; Lancaster, J. R., Chemical foundations of hydrogen sulfide biology. *Nitric Oxide* **2013,** *35* (1), 21–34.

26. Benchoam, D.; Cuevasanta, E.; Möller, Matías N.; Alvarez, B., Persulfides, at the crossroads between hydrogen sulfide and thiols. *Essays Biochem.* **2020,** *64* (1), 155–168.

27. Nishida, M.; Toyama, T.; Akaike, T., Role of 8-nitro-cGMP and its redox regulation in cardiovascular electrophilic signaling. *J. Mol. Cell. Cardiol.* **2014,** *73*, 10–17.

28. Sawa, T.; Zaki, M. H.; Okamoto, T.; Akuta, T.; Tokutomi, Y.; Kim-Mitsuyama, S.; Ihara, H.; Kobayashi, A.; Yamamoto, M.; Fujii, S.; Arimoto, H.; Akaike, T., Protein *S*-guanylation by the biological signal 8-nitroguanosine 3′,5′-cyclic monophosphate. *Nat. Chem. Biol.* **2007,** *3* (11), 727–735.

29. Saund, S. S.; Sosa, V.; Henriquez, S.; Nguyen, Q. N. N.; Bianco, C. L.; Soeda, S.; Millikin, R.; White, C.; Le, H.; Ono, K.; Tantillo, D. J.; Kumagai, Y.; Akaike, T.; Lin, J.; Fukuto, J. M., The chemical biology of hydropersulfides (RSSH): Chemical stability, reactivity and redox roles. *Arch. Biochem. Biophys.* **2015,** *588*, 15–24.

30. Everett, S. A.; Wardman, P., Perthiols as antioxidants: Radical-scavenging and prooxidative mechanisms. In *Methods Enzymol.*, Academic Press: 1995; Vol. 251, pp 55–69.

31. Ono, K.; Akaike, T.; Sawa, T.; Kumagai, Y.; Wink, D. A.; Tantillo, D. J.; Hobbs, A. J.; Nagy, P.; Xian, M.; Lin, J.; Fukuto, J. M., Redox chemistry and chemical biology of H_2S, hydropersulfides, and derived species: Implications of their possible biological activity and utility. *Free Radical Biol. Med.* **2014,** *77*, 82–94.

32. Chauvin, J.-P. R.; Griesser, M.; Pratt, D. A., Hydropersulfides: H-Atom Transfer Agents Par Excellence. *J. Am. Chem. Soc.* **2017,** *139* (18), 6484–6493.

33. Bianco, C. L.; Chavez, T. A.; Sosa, V.; Saund, S. S.; Nguyen, Q. N. N.; Tantillo, D. J.; Ichimura, A. S.; Toscano, J. P.; Fukuto, J. M., The chemical biology of the persulfide (RSSH)/perthiyl (RSS·) redox couple and possible role in biological redox signaling. *Free Radical Biol. Med.* **2016,** *101*, 20–31.

34. Koppenol, W. H.; Bounds, P. L., Signaling by sulfur-containing molecules. Quantitative aspects. *Arch. Biochem. Biophys.* **2017,** *617*, 3–8.

35. Kabil, O.; Banerjee, R., Characterization of Patient Mutations in Human Persulfide Dioxygenase (ETHE1) Involved in H_2S Catabolism. *J. Biol. Chem.* **2012,** *287* (53), 44561-44567.

36. Kasamatsu, S., Persulfide-Dependent Regulation of Electrophilic Redox Signaling in Neural Cells. *Antioxid. Redox. Signal.* **2020,** *33* (18), 1320–1331.

37. Akaike, T.; Ida, T.; Wei, F.-Y.; Nishida, M.; Kumagai, Y.; Alam, M. M.; Ihara, H.; Sawa, T.; Matsunaga, T.; Kasamatsu, S.; Nishimura, A.; Morita, M.; Tomizawa, K.; Nishimura, A.; Watanabe, S.; Inaba, K.; Shima, H.; Tanuma, N.; Jung, M.; Fujii, S.; Watanabe, Y.; Ohmuraya, M.; Nagy, P.; Feelisch, M.; Fukuto, J. M.; Motohashi, H., Cysteinyl-tRNA synthetase governs cysteine polysulfidation and mitochondrial bioenergetics. *Nat. Commun.* **2017,** *8* (1), 1177.

38. Nishida, M.; Sawa, T.; Kitajima, N.; Ono, K.; Inoue, H.; Ihara, H.; Motohashi, H.; Yamamoto, M.; Suematsu, M.; Kurose, H.; van der Vliet, A.; Freeman, B. A.; Shibata, T.; Uchida, K.; Kumagai, Y.; Akaike, T., Hydrogen sulfide anion regulates redox signaling via electrophile sulfhydration. *Nat. Chem. Biol.* **2012,** *8* (8), 714–724.

39. Vandiver, M. S.; Paul, B. D.; Xu, R.; Karuppagounder, S.; Rao, F.; Snowman, A. M.; Seok Ko, H.; Il Lee, Y.; Dawson, V. L.; Dawson, T. M.; Sen, N.; Snyder, S. H., Sulfhydration mediates neuroprotective actions of parkin. *Nat. Commun.* **2013,** *4* (1), 1626.

40. Sawa, T.; Motohashi, H.; Ihara, H.; Akaike, T., Enzymatic Regulation and Biological Functions of Reactive Cysteine Persulfides and Polysulfides. *Biomolecules* **2020,** *10* (9), 1245.

41. Benchoam, D.; Cuevasanta, E.; Möller, M. N.; Alvarez, B., Hydrogen Sulfide and Persulfides Oxidation by Biologically Relevant Oxidizing Species. *Antioxidants* **2019,** *8* (2), 48.

42. Li, H.; Liu, H.; Chen, Z.; Zhao, R.; Wang, Q.; Ran, M.; Xia, Y.; Hu, X.; Liu, J.; Xian, M.; Xun, L., Using resonance synchronous spectroscopy to characterize the reactivity and electrophilicity of biologically relevant sulfane sulfur. *Redox Biol.* **2019,** *24*, 101179.

43. Heppner, D. E.; Hristova, M.; Ida, T.; Mijuskovic, A.; Dustin, C. M.; Bogdándi, V.; Fukuto, J. M.; Dick, T. P.; Nagy, P.; Li, J.; Akaike, T.; van der Vliet, A., Cysteine perthiosulfenic acid (Cys-SSOH): A novel intermediate in thiol-based redox signaling? *Redox Biol.* **2018,** *14*, 379–385.

44. Francoleon, N. E.; Carrington, S. J.; Fukuto, J. M., The reaction of H_2S with oxidized thiols: Generation of persulfides and implications to H_2S biology. *Arch. Biochem. Biophys.* **2011,** *516* (2), 146–153.

45. Fukuto, J. M.; Hobbs, A. J., A comparison of the chemical biology of hydropersulfides (RSSH) with other protective biological antioxidants and nucleophiles. *Nitric Oxide* **2021,** *107*, 46–57.

46. Venkatesh, Y.; Kiran, K. S.; Shah, S. S.; Chaudhuri, A.; Dey, S.; Singh, N. D. P., One- and two-photon responsive sulfur dioxide (SO_2) donors: a combinatorial drug delivery for improved antibiotic therapy. *Org. Biomol. Chem.* **2019,** *17* (10), 2640–2645.

47. Khodade, V. S.; Toscano, J. P., Development of S-Substituted Thioisothioureas as Efficient Hydropersulfide Precursors. *J. Am. Chem. Soc.* **2018,** *140* (50), 17333–17337.

48. Yadav, P. K.; Martinov, M.; Vitvitsky, V.; Seravalli, J.; Wedmann, R.; Filipovic, M. R.; Banerjee, R., Biosynthesis and Reactivity of Cysteine Persulfides in Signaling. *J. Am. Chem. Soc.* **2016,** *138* (1), 289–299.

49. Zheng, Y.; Yu, B.; Li, Z.; Yuan, Z.; Organ, C. L.; Trivedi, R. K.; Wang, S.; Lefer, D. J.; Wang, B., An Esterase-Sensitive Prodrug Approach for Controllable Delivery of Persulfide Species. *Angew. Chem. Int. Ed.* **2017,** *56* (39), 11749–11753.

50. Park, C.-M.; Johnson, B. A.; Duan, J.; Park, J.-J.; Day, J. J.; Gang, D.; Qian, W.-J.; Xian, M., 9-Fluorenylmethyl (Fm) Disulfides: Biomimetic Precursors for Persulfides. *Org. Lett.* **2016,** *18* (5), 904–907.

51. Zhang, D.; Macinkovic, I.; Devarie-Baez, N. O.; Pan, J.; Park, C.-M.; Carroll, K. S.; Filipovic, M. R.; Xian, M., Detection of Protein S-Sulfhydration by a Tag-Switch Technique. *Angew. Chem. Int. Ed.* **2014,** *53* (2), 575–581.

52. Khodade, V. S.; Pharoah, B. M.; Paolocci, N.; Toscano, J. P., Alkylamine-Substituted Perthiocarbamates: Dual Precursors to Hydropersulfide and Carbonyl Sulfide with Cardioprotective Actions. *J. Am. Chem. Soc.* **2020,** *142* (9), 4309–4316.

53. Chen, W.; Liu, C.; Peng, B.; Zhao, Y.; Pacheco, A.; Xian, M., New fluorescent probes for sulfane sulfurs and the application in bioimaging. *Chem.* **2013,** *4* (7), 2892–2896.

54. Takano, Y.; Hanaoka, K.; Shimamoto, K.; Miyamoto, R.; Komatsu, T.; Ueno, T.; Terai, T.; Kimura, H.; Nagano, T.; Urano, Y., Development of a reversible fluorescent probe for reactive sulfur species, sulfane sulfur, and its biological application. *Chem. Commun.* **2017,** *53* (6), 1064–1067.

55. Hou, Y.; Yang, X.-F.; Zhong, Y.; Li, Z., Development of fluorescent probes for hydrogen polysulfides by using cinnamate ester as the recognition unit. *Sens. Actuators B Chem.* **2016,** *232*, 531–537.

56. Li, K.-B.; Chen, F.-Z.; Zhang, S.; Shi, W.; Han, D.-M.; Cai, C.; Chen, C.-X., A nile red-based near-infrared fluorescent probe for endogenous hydrogen polysulfides in living cells. *Anal. Methods* **2017,** *9* (45), 6443–6447.

57. Gupta, N.; Reja, S. I.; Bhalla, V.; Kumar, M., Fluorescent probes for hydrogen polysulfides: From design rationale to applications. *Org. Biomol. Chem.* **2017,** *15* (32), 6692–6701.

58. Kawagoe, R.; Takashima, I.; Uchinomiya, S.; Ojida, A., Reversible ratiometric detection of highly reactive hydropersulfides using a FRET-based dual emission fluorescent probe. *Chem.* **2017,** *8* (2), 1134–1140.

59. Umezawa, K.; Kamiya, M.; Urano, Y., A Reversible Fluorescent Probe for Real-Time Live-Cell Imaging and Quantification of Endogenous Hydropolysulfides. *Angew. Chem. Int. Ed.* **2018,** *57* (30), 9346–9350.

60. Roger, T.; Raynaud, F.; Bouillaud, F.; Ransy, C.; Simonet, S.; Crespo, C.; Bourguignon, M.-P.; Villeneuve, N.; Vilaine, J.-P.; Artaud, I.; Galardon, E., New Biologically Active Hydrogen Sulfide Donors. *Chembiochem* **2013,** *14* (17), 2268–2271.

61. Zhao, Y.; Bhushan, S.; Yang, C.; Otsuka, H.; Stein, J. D.; Pacheco, A.; Peng, B.; Devarie-Baez, N. O.; Aguilar, H. C.; Lefer, D. J.; Xian, M., Controllable Hydrogen Sulfide Donors and Their Activity against Myocardial Ischemia-Reperfusion Injury. *ACS Chem. Biol.* **2013,** *8* (6), 1283–1290.

62. Artaud, I.; Galardon, E., A Persulfide Analogue of the Nitrosothiol SNAP: Formation, Characterization and Reactivity. *Chembiochem* **2014,** *15* (16), 2361–2364.

63. Dawson, P. E.; Muir, T. W.; Clark-Lewis, I.; Kent, S. B., Synthesis of proteins by native chemical ligation. *Science* **1994,** *266* (5186), 776–779.

64. Xu, S.; Hamsath, A.; Neill, D. L.; Wang, Y.; Yang, C.; Xian, M., Strategies for the Design of Donors and Precursors of Reactive Sulfur Species. *Chem. Eur. J.* **2019,** *25* (16), 4005–4016.

65. Xu, S.; Wang, Y.; Parent, Z.; Xian, M., Diacyl disulfides as the precursors for hydrogen persulfide (H_2S_2). *Bioorg. Med. Chem. Lett.* **2020,** *30* (4), 126903.

66. Peng, B.; Chen, W.; Liu, C.; Rosser, E. W.; Pacheco, A.; Zhao, Y.; Aguilar, H. C.; Xian, M., Fluorescent Probes Based on Nucleophilic Substitution–Cyclization for Hydrogen Sulfide Detection and Bioimaging. *Chem. Eur. J.* **2014,** *20* (4), 1010–1016.

67. Liu, C.; Chen, W.; Shi, W.; Peng, B.; Zhao, Y.; Ma, H.; Xian, M., Rational Design and Bioimaging Applications of Highly Selective Fluorescence Probes for Hydrogen Polysulfides. *J. Am. Chem. Soc.* **2014,** *136* (20), 7257–7260.

68. Bibli, S.-I.; Luck, B.; Zukunft, S.; Wittig, J.; Chen, W.; Xian, M.; Papapetropoulos, A.; Hu, J.; Fleming, I., A selective and sensitive method for quantification of endogenous polysulfide production in biological samples. *Redox Biol.* **2018,** *18*, 295–304.

69. Saeed, S.; Rashid, N.; Jones, P. G.; Ali, M.; Hussain, R., Synthesis, characterization and biological evaluation of some thiourea derivatives bearing benzothiazole moiety as potential antimicrobial and anticancer agents. *Eur. J. Med. Chem.* **2010,** *45* (4), 1323–1331.

70. Baig, M. H.; Adil, M.; Khan, R.; Dhadi, S.; Ahmad, K.; Rabbani, G.; Bashir, T.; Imran, M. A.; Husain, F. M.; Lee, E. J.; Kamal, M. A.; Choi, I., Enzyme targeting strategies for prevention and treatment of cancer: Implications for cancer therapy. *Semin. Cancer Biol.* **2019,** *56*, 1–11.

71. Yu, B.; Zheng, Y.; Yuan, Z.; Li, S.; Zhu, H.; De La Cruz, L. K.; Zhang, J.; Ji, K.; Wang, S.; Wang, B., Toward Direct Protein S-Persulfidation: A Prodrug Approach That Directly Delivers Hydrogen Persulfide. *J. Am. Chem. Soc.* **2018,** *140* (1), 30–33.

72. Amsberry, K. L.; Borchardt, R. T., The lactonization of 2'-hydroxyhydrocinnamic acid amides: a potential prodrug for amines. *J. Org. Chem.* **1990,** *55* (23), 5867–5877.

73. Yuan, Z.; Zheng, Y.; Yu, B.; Wang, S.; Yang, X.; Wang, B., Esterase-Sensitive Glutathione Persulfide Donor. *Org. Lett.* **2018,** *20* (20), 6364–6367.

74. Dillon, K. M.; Carrazzone, R. J.; Wang, Y.; Powell, C. R.; Matson, J. B., Polymeric Persulfide Prodrugs: Mitigating Oxidative Stress through Controlled Delivery of Reactive Sulfur Species. *ACS Macro Lett.* **2020**, 606–612.

75. Walsh, B. J. C.; Giedroc, D. P., H_2S and reactive sulfur signaling at the host-bacterial pathogen interface. *J. Biol. Chem.* **2020,** *295* (38), 13150–13168.

76. Dillon, K. M.; Morrison, H. A.; Powell, C. R.; Carrazzone, R. J.; Ringel-Scaia, V. M.; Winckler, E. W.; Council-Troche, R. M.; Allen, I. C.; Matson, J. B., Targeted Delivery of Persulfides to the Gut: Effects on the Microbiome. *Angew. Chem. Int. Ed.* **2021,** *60* (11), 6061–6067.

77. Miller, A.-F.; Park, T. J.; Ferguson, L. K.; Pitsawong, W.; Bommarius, S. A., Informing Efforts to Develop Nitroreductase for Amine Production. *Molecules* **2018,** *23* (2), 211.

78. Gonzaga, R. V.; do Nascimento, L. A.; Santos, S. S.; Machado Sanches, B. A.; Giarolla, J.; Ferreira, E. I., Perspectives About Self-Immolative Drug Delivery Systems. *J. Pharm. Sci.* **2020,** *109* (11), 3262–3281.

79. De Preter, V.; Machiels, K.; Joossens, M.; Arijs, I.; Matthys, C.; Vermeire, S.; Rutgeerts, P.; Verbeke, K., Faecal metabolite profiling identifies medium-chain fatty acids as discriminating compounds in IBD. *Gut* **2015,** *64* (3), 447–458.

80. Powell, C. R.; Dillon, K. M.; Wang, Y.; Carrazzone, R. J.; Matson, J. B., A Persulfide Donor Responsive to Reactive Oxygen Species: Insights into Reactivity and Therapeutic Potential. *Angew. Chem. Int. Ed.* **2018,** *57* (21), 6324–6328.

81. Zhao, Y.; Henthorn, H. A.; Pluth, M. D., Kinetic Insights into Hydrogen Sulfide Delivery from Caged-Carbonyl Sulfide Isomeric Donor Platforms. *J. Am. Chem. Soc.* **2017,** *139* (45), 16365–16376.

82. Bora, P.; Chauhan, P.; Manna, S.; Chakrapani, H., A Vinyl-Boronate Ester-Based Persulfide Donor Controllable by Hydrogen Peroxide, a Reactive Oxygen Species (ROS). *Org. Lett.* **2018,** *20* (24), 7916–7920.

83. Hankins, R. A.; Suarez, S. I.; Kalk, M. A.; Green, N. M.; Harty, M. N.; Lukesh Iii, J. C., An Innovative Hydrogen Peroxide-Sensing Scaffold and Insight Towards its Potential as an ROS-Activated Persulfide Donor. *Angew. Chem. Int. Ed.* **2020,** *59* (49), 22238–22245.

84. Wang, Y.; Dillon, K. M.; Li, Z.; Winckler, E. W.; Matson, J. B., Alleviating Cellular Oxidative Stress through Treatment with Superoxide-Triggered Persulfide Prodrugs. *Angew. Chem. Int. Ed.* **2020,** *59* (38), 16698–16704.

85. Loschen, G.; Azzi, A.; Richter, C.; Flohé, L., Superoxide radicals as precursors of mitochondrial hydrogen peroxide. *FEBS Lett.* **1974,** *42* (1), 68–72.

86. Lim, S. C.; Kim, Y. H., Evidence for formation of diphenylphosphinic peroxy radical intermediate: Spin trapping and chemical reactivity of the new phosphorus radical generated from diphenylphosphinic chloride and superoxide. *Heteroat. Chem* **1990,** *1* (3), 261–265.

87. Chaudhuri, A.; Venkatesh, Y.; Das, J.; Gangopadhyay, M.; Maiti, T. K.; Singh, N. D. P., One- and Two-Photon-Activated Cysteine Persulfide Donors for Biological Targeting. *J. Org. Chem.* **2019,** *84* (18), 11441–11449.

88. Kaur, K.; Carrazzone, R. J.; Matson, J. B., The Benefits of Macromolecular/Supramolecular Approaches in Hydrogen Sulfide Delivery: A Review of

Polymeric and Self-Assembled Hydrogen Sulfide Donors. *Antioxid. Redox. Signal.* **2020,** *32* (2), 79–95.

89. Yang, J.; An, H.-W.; Wang, H., Self-Assembled Peptide Drug Delivery Systems. *ACS Appl. Bio Mater.* **2021,** *4* (1), 24–46.

90. Sung, Y. K.; Kim, S. W., Recent advances in polymeric drug delivery systems. *Biomater. Res.* **2020,** *24* (1), 1–12.

91. Liechty, W. B.; Kryscio, D. R.; Slaughter, B. V.; Peppas, N. A., Polymers for drug delivery systems. *Annu. Rev. Chem. Biomol. Eng.* **2010,** *1*, 149–173.

92. Chiefari, J.; Chong, Y. K.; Ercole, F.; Krstina, J.; Jeffery, J.; Le, T. P. T.; Mayadunne, R. T. A.; Meijs, G. F.; Moad, C. L.; Moad, G.; Rizzardo, E.; Thang, S. H., Living Free-Radical Polymerization by Reversible Addition−Fragmentation Chain Transfer: The RAFT Process. *Macromolecules* **1998,** *31* (16), 5559–5562.

93. Saif, M. W.; Choma, A.; Salamone, S. J.; Chu, E., Pharmacokinetically Guided Dose Adjustment of 5-Fluorouracil: A Rational Approach to Improving Therapeutic Outcomes. *J. Natl. Cancer Inst.* **2009,** *101* (22), 1543–1552.

94. Adams, D. J.; Boskovic, Z. V.; Theriault, J. R.; Wang, A. J.; Stern, A. M.; Wagner, B. K.; Shamji, A. F.; Schreiber, S. L., Discovery of Small-Molecule Enhancers of Reactive Oxygen Species That are Nontoxic or Cause Genotype-Selective Cell Death. *ACS Chem. Biol.* **2013,** *8* (5), 923–929.

95. Reliene, R.; Schiestl, R. H., Glutathione depletion by buthionine sulfoximine induces DNA deletions in mice. *Carcinogenesis* **2006,** *27* (2), 240-244.

96. Zhan, J.; Cai, Y.; He, S.; Wang, L.; Yang, Z., Tandem Molecular Self-Assembly in Liver Cancer Cells. *Angew. Chem. Int. Ed.* **2018,** *57* (7), 1813–1816.

97. Kashfi, K., Development and therapeutic potential of NOSH-NSAIDs: A new class of anti-inflammatory pharmaceuticals. *FASEB J.* **2016,** *30* (S1), 1272.8.

98. Wallace, J. L.; Nagy, P.; Feener, T. D.; Allain, T.; Ditrói, T.; Vaughan, D. J.; Muscara, M. N.; de Nucci, G.; Buret, A. G., A proof-of-concept, Phase 2 clinical trial of the gastrointestinal safety of a hydrogen sulfide-releasing anti-inflammatory drug. *Br. J. Pharmacol.* **2020,** *177* (4), 769–777.

Chapter 2: A Reactive Species (ROS)-Responsive Persulfide Donor: Insights into Reactivity and Therapeutic Potential

Adapted with permission from: Powell, C. R., Dillon, K. M., et al. "A Reactive Oxygen Species (ROS)-Responsive Persulfide Donor: Insights into Reactivity and Therapeutic Potential" Angewandte Chemie **130**: 6432-6436.

2.1. Authors

Chadwick R. Powell,[§,†] Kearsley M. Dillon,[§,†] Yin Wang, [§,†] Ryan J. Carrazzone, [§,†] and John B. Matson*[§,†]

§Department of Chemistry, Virginia Tech, Blacksburg, Virginia 24061, United States

†Virginia Tech Center for Drug Discovery, Virginia Tech, Blacksburg, Virginia 24061, United States

2.2. Abstract

Persulfides (R–SSH) have been hypothesized as critical components in sulfur-mediated redox cycles and as potential signaling compounds, similar to hydrogen sulfide (H_2S). Hindering the study of persulfides is a lack of persulfide donor compounds with selective triggers that release discrete persulfide species. Herein we report the synthesis and characterization of an ROS-responsive, self-immolative persulfide donor. The donor, termed BDP-NAC, showed selectivity towards H_2O_2 over other potential oxidative or nucleophilic triggers, resulting in the sustained release of the persulfide of *N*-acetyl cysteine (NAC) over the course of 2 h, as measured by LCMS. Exposure of H9C2 cardiomyocytes to H_2O_2 revealed that BDP-NAC mitigated the effects of a highly oxidative environment in a dose-dependent manner over relevant controls and to a greater degree than common H_2S donors sodium sulfide (Na_2S) and GYY4137. BDP-NAC also rescued

cells more effectively than a non-persulfide releasing control compound with a Bpin moiety in concert with common H_2S donors and thiols.

2.3. Introduction

Hydrogen sulfide (H_2S) plays a key signaling role in mammalian biology and has been under investigation as a potential therapeutic via exogenous delivery.[1-4] To help elucidate its biological roles, chemists have synthesized several types of H_2S releasing compounds (termed H_2S donors) with a variety of biologically relevant triggers, including water,[5-8] nucleophiles (e.g., thiols, amines),[9-10] enzymes,[11-13] and light.[14-15] Additionally, compounds that release carbonyl sulfide (COS),[16-17] and sulfur dioxide (SO_2),[18-19] have recently been reported, allowing for the study of other small molecule sulfur species as potential signaling compounds. These donors aid in our understanding of the physiological roles of H_2S and related compounds, and hold potential therapeutic value via exogenous H_2S delivery.[20-22] Interestingly, recent studies into the redox chemistry of sulfur species in the body indicate that persulfides (R–SSH) may have physiological roles similar to H_2S, insinuating that some of the physiological effects ascribed to delivery of H_2S may actually be derived from persulfides.[23-26] Further study of persulfides is needed to differentiate between the roles of H_2S itself and its biological products. Moreover, a clear description of sulfur redox chemistry in a biological context will allow further development of therapeutics that exploit pathways involved in H_2S signaling.

Dean and coworkers first identified persulfides in a biological context in their 1994 report on a protein persulfide intermediate of the cysteine desulfurase NifS.[27] Persulfides are prevalent in mammalian biology, generated via reaction of an oxidized thiol (e.g., a sulfenic acid, R–SOH)

with H_2S in a process called S-persulfidation.[28] More nucleophilic than thiols, persulfides have pK_a values a few units lower than their corresponding thiols,[29] as well as greater reduction potentials,[30] making them highly reactive, transiently stable species. In a biological context, persulfides protect thiols from irreversible oxidation, serve as reactive intermediates in sulfur shuttling,[31] and alter enzymatic activity.[32-33] Some examples of protein persulfidation and the resulting changes in protein activity include: an increased parkin activity upon *S*-persulfidation resulting in a decrease in Parkinson's symptoms,[34] an increase in activity of GAPDH, protecting cells from apoptosis,[35] and H-Ras activation in cardiac tissue, regulating cellular redox signaling.[36] More recently, studies have confirmed the presence of endogenously produced small molecule persulfides (e.g., cysteine persulfide and glutathione persulfide) with reported concentrations as high as 150 μM in human and mouse tissue.[23] Small molecule persulfides likely play a role in regulating cellular redox balance and mediating cellular signaling.[25] A major barrier in the study of the biological roles of persulfides is a lack of chemical tools capable of generating well-defined persulfide species in response to specific, biologically relevant triggers. Our understanding of H_2S biology has been aided immensely by the synthesis of organic H_2S donors; analogous to H_2S, persulfide donors will be vital tools for understanding how persulfides fit into the overall web of redox signaling.

Polysulfides ($RS–(S)_n–SR$), such as naturally occurring diallyl trisulfide (DATS), are perhaps the best known type of persulfide donor, but their reactivity in biological systems is complex, leading to generation of other redox-active species, including H_2S.[37-39] As a result, polysulfides are not ideal persulfide donors for use in studying persulfide biology, and the complex product mixture may limit their therapeutic potential. Free persulfides (i.e., R–SSH) have been isolated, but they

suffer from poor stability under storage conditions and poor water solubility, and thus have relatively low utility in a practical sense.[39] Persulfides are also proposed intermediates in several types of H_2S donors,[9-10] but these compounds all require conditions that cause rapid conversion of the persulfide into H_2S. To date there exist only two families of compounds capable of generating discrete persulfides: Wang and coworkers developed esterase-triggered persulfide prodrugs capable of releasing either a persulfide or hydrogen persulfide (HSSH) and Galardon and coworkers developed a pH-triggered persulfide analog of the nitrosothiol SNAP.[40-42] These donors generate persulfides without concomitant generation of H_2S and can be viewed as spontaneous persulfide donors due to the ubiquity of esterases *in vitro* and *in vivo*.

We sought to synthesize a discrete persulfide donor scaffold, inert under normal physiological conditions but capable of self-immolation in response to a specific trigger, revealing a discrete persulfide species (Figure 1). As the triggering moiety and persulfide could be readily tuned, this system would enable persulfide generation in response to many types of triggers, providing a valuable set of laboratory tools similar to the self-immolative COS donors recently reported by Pluth and coworkers.[43]

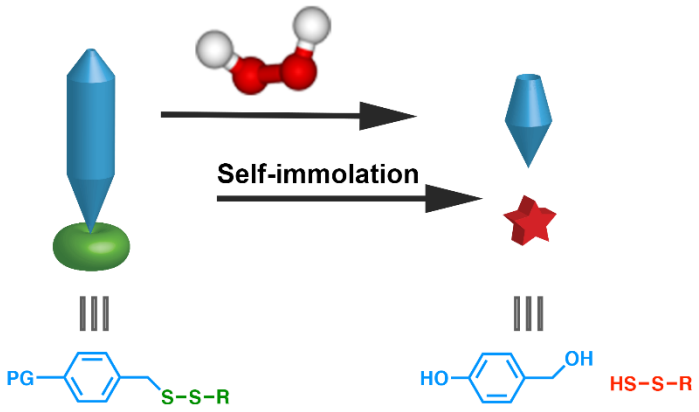

Figure 1. Cartoon schematic representing the proposed release of a discrete persulfide species from a generalized self-immolative prodrug (PG = protecting group) in the presence of a trigger (H_2O_2 shown here).

In addition to their use as biological tools to study persulfide reactivity, persulfide prodrugs are exciting from a therapeutic standpoint because the reduction potential of persulfides is higher than that of thiols or H_2S, making them prime candidates for scavenging and reducing the harmful effects resulting from high levels of reactive oxygen species (ROS). Therefore, we aimed to synthesize an ROS-responsive persulfide prodrug as a proof of concept. This would allow for a two-stage quenching of ROS: the initial reaction of the ROS with the prodrug to trigger release, followed by the release of the persulfide. We envisioned that such an ROS-triggered persulfide prodrug would be ideal for cytoprotection against harmful levels of ROS.

2.4. Results and Discussion

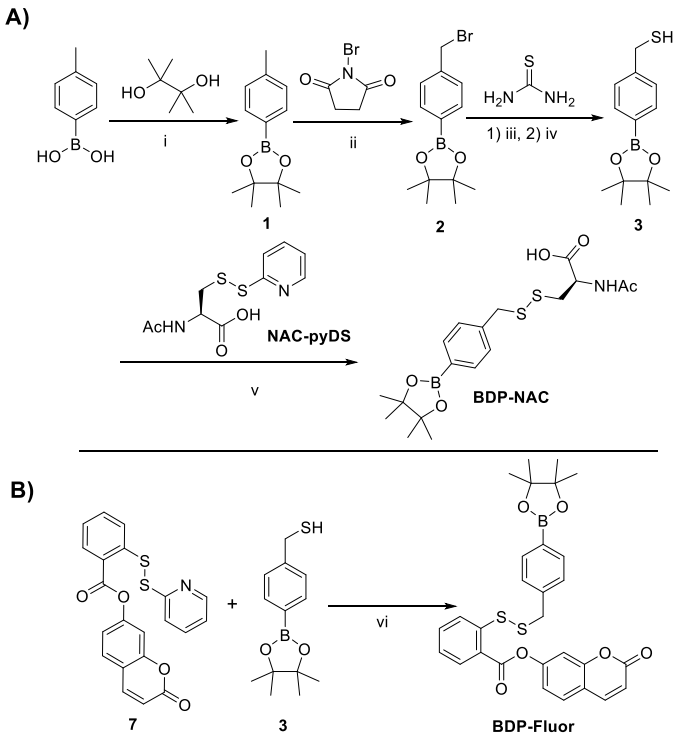

Scheme 1. A) Synthetic route to BDP-NAC. ConditionL i) $MgSO_4$, Et_2O, rt, 16 h; ii) AIBN, C_6H_{12}, reflux, 16 h; iii) EtOH, rt, 4 h; iv) 1 N NaOH, reflux, 45 min; v) NEt_3, $CHCl_3$, rt, 3 h; B) Synthetic route to **BDP-Fluor**. Conditions: vi) $CHCl_3$:MeOH (1:1 v/v), rt, 40 h

Aryl boronic esters are relatively easy to synthesize, generally biocompatible, and react selectively with ROS in a B–C bond cleavage reaction to reveal the corresponding phenolate. Therefore, we set out to synthesize a self-immolative persulfide donor containing an aryl boronic ester as an ROS-sensitive trigger. The desired persulfide donor (termed **BDP-NAC** for Bpin-disulfide prodrug-*N*-acetyl cysteine) was synthesized from commercially available 4-tolylboronic acid in four steps (Scheme 1A). Theoretically, any thiol may be installed on the distal end of the disulfide bond from the trigger/self-immolation moiety. Our choice of *N*-acetyl cysteine (NAC) was

motivated by its biocompatibility as well as its ability to protect cells in vitro in highly oxidative environments.[44-45]

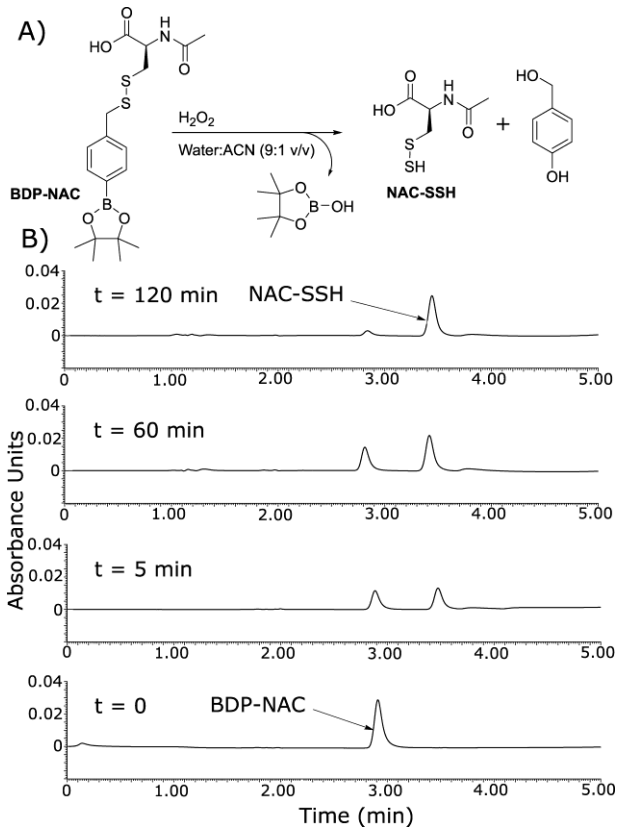

Figure 2. A) Proposed reaction of **BDP-NAC** in the presence of H_2O_2 leading to the release of **NAC–SSH**. B) LC chromatograms highlighting the conversion of **BDP-NAC** into NAC persulfide (**NAC-SSH**) in the presence of H_2O_2. Timepoints are noted above each LC chromatogram. The peak eluting at 2.9 min corresponds to **BDP-NAC**, and the peak at 3.4 min corresponds to **NAC-SSH** (see Figure S20 for corresponding mass spectrometry data).

The ability of **BDP-NAC** to mediate the release of the desired NAC persulfide (**NAC-SSH**) in response to ROS was analyzed by LCMS (Figure 2). Aliquots of the reaction mixture of **BDP-**

NAC with H_2O_2 were injected at various time points until the peak attributed to **BDP-NAC** (2.9 min) had subsided, revealing near complete decomposition of **BDP-NAC** within 2 h. A peak corresponding to **NAC–SSH** (3.4 min) increased in intensity over the course of the reaction, consistent with our proposed mechanism of persulfide generation. Mass spectrometry evidence also confirmed the presence of the other byproduct of the reaction, 4-hydroxybenzyl alcohol (a result of addition of water to the quinone methide), but the chromatogram peak was weak, likely due to low absorbance at the monitoring wavelength. In addition to LCMS, we also investigated the reaction of **BDP-NAC** with H_2O_2 utilizing ^{1}H NMR spectroscopy. Experiments were conducted in DMSO-d_6:D_2O (9:1 v/v) due to the hydrophobic nature of **BDP-NAC** and the increased concentration required in NMR spectroscopy compared with LCMS. Shortly after the addition of H_2O_2 to the **BDP-NAC** solution, two new sets of peaks in the aryl region of the ^{1}H NMR spectrum appeared. One was consistent with 4-hydroxybenzyl alcohol, and the other was attributed to the slow hydrolysis of the Bpin moiety of **BDP-NAC**, yielding a boronic acid; boronic acids react with H_2O_2 in a similar fashion as pinacol boronic esters.[46] The reaction was considerably slower under these conditions than in the LCMS experiments. This retardation in reaction rate is likely a result of the high organic solvent content in the reaction.[47]

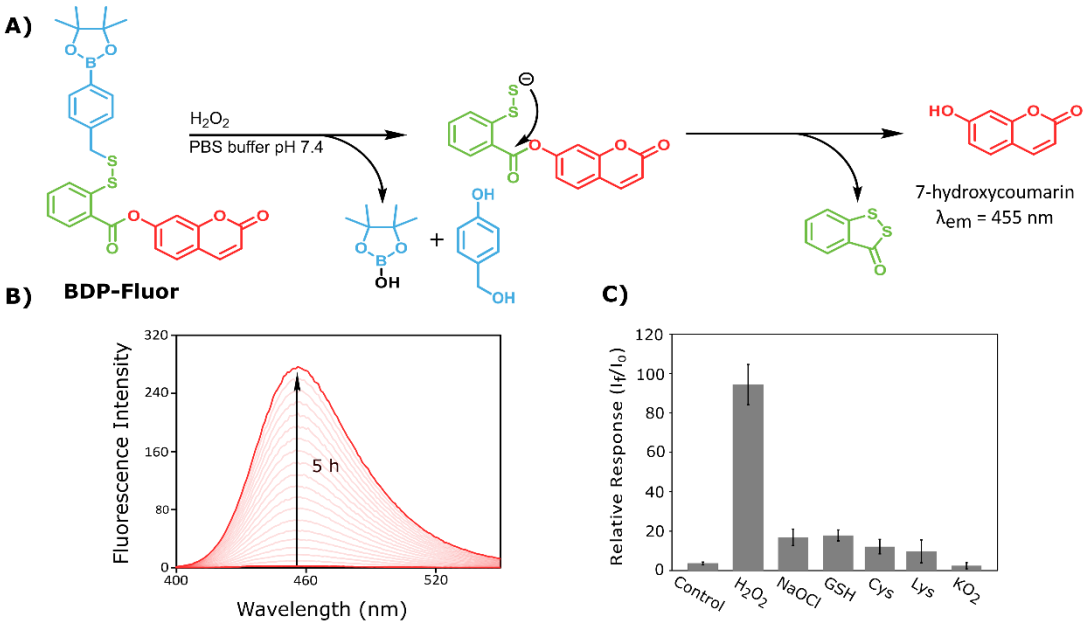

Figure 3. A) Proposed reaction mechanism for the release of 7-hydroxycoumarin from **BDP-Fluor** in the presence of H_2O_2. B) Representative overlay of the fluorescence spectra of **BDP-Fluor** in the presence of 100-fold excess H_2O_2 resulting from the release of 7-hydroxycoumarin over the course of 5 h. C) Relative response of **BDP-Fluor** (3.3 μM) to each potential trigger (330 μM) or control (no trigger added) represented as the ratio of the final fluorescence (I_f) intensity after 5 h to the initial fluorescence intensity (I_0), showing an increased selectivity for H_2O_2 over other potential triggers.

To further evaluate the reactivity and trigger selectivity of **BDP-NAC**, a profluorophore (**BDP-Fluor**, Scheme 1B) was synthesized. Drawing inspiration from Xian and coworkers' turn-on fluorescence probe (compound **7**) used for detection of sulfane sulfur species (HSSH, RS–$(S)_n$–SR, or S_8), the self-immolative **BDP-Fluor** has the same general structure as **BDP-NAC**, but with a coumarin-based fluorophore as the distal thiol species.[48] As shown in Figure 3A, we expected

self-immolation to trigger release of a discrete persulfide, which would then cyclize to form a 5-membered benzodithiolone species, resulting in the release of 7-hydroxycoumarin. Because **BDP-Fluor** itself is not fluorescent, an increase in fluorescence at the characteristic emission wavelength of 7-hydroxycoumarin should only result from persulfide release and subsequent intramolecular cyclization, providing secondary confirmation of persulfide release from these self-immolative prodrug systems.

We tested this design by exposing **BDP-Fluor** to a variety of potential triggers. **BDP-Fluor** showed no evidence of self-immolative behavior (i.e., no fluorescence signal) in the absence of a trigger, but addition of H_2O_2 (100-fold excess) led to a 90-fold increase in fluorescence intensity at the characteristic wavelength of 7-hydroxycoumarin after incubation for 5 h in PBS buffer (Figure 3B and C). When **BDP-Fluor** was treated with other potential triggers, including sodium hypochlorite (NaOCl), cysteine (Cys), glutathione (GSH), lysine (Lys), and potassium superoxide (KO_2), the response was significantly lower, with H_2O_2 showing a greater than 20-fold response over all of these potential triggers, and a greater than 90-fold response over Lys and KO_2. As the increase in fluorescence response to thiols was unexpected, further investigation indicated that the fluorescence increase may be attributed to nucleophilic attack by cysteine at the aryl ester position, resulting in the release of 7-hydroxycoumarin. Taken together, these results confirm release of the desired persulfide species and demonstrate the selectivity of H_2O_2 as a trigger.

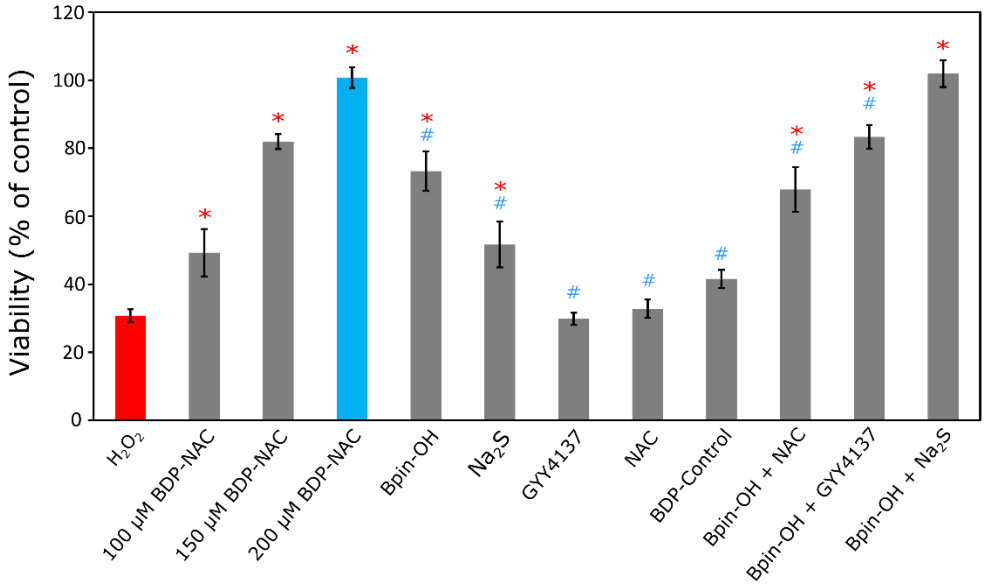

Figure 4. Viability of H9C2 cardiomyoctyes treated with BDP-NAC or various controls and related compounds concurrent with exposure to H_2O_2 (100 µM) for 1 h. Each control compound was applied at a concentration of 200 µM (except for Na_2S (100 µM) in the Bpin-OH + Na_2S treatment group). Quantification of viability was carried out using Cell Counting Kit-8 (CCK-8). Results are expressed as the mean ± SEM (n = 10–15 for each treatment group) with 2–3 independent experiments. *P<0.01 for comparisons with the H_2O_2 treatment group and #P<0.01 for comparisons with the BDP-NAC (200 µM) treatment group. Group comparisons are indicated as determined by a one-way analysis of variance (ANOVA) with a Student-Newman-Keuls comparisons post-hoc test.

We next aimed to analyze **BDP-NAC** in a biological context. In vitro cytotoxicity studies on H9C2 cardiomyocytes showed that **BDP-NAC** is non-toxic up to 200 µM (Figure S27). As mentioned previously, persulfides have greater reducing potential than their corresponding thiols as well as H_2S. Thus, we envisioned that **BDP-NAC** might be effective in rescuing cells under oxidative stress, either via direct reduction of H_2O_2 or via upregulation of antioxidant pathways mediated by

persulfide signaling.[23, 32] To this end, we evaluated the protective effects of **BDP-NAC** on H9C2 cells in culture via exogenous delivery of H_2O_2, which stresses the cells and promotes apoptosis (Figure 4). In the absence of **BDP-NAC**, cell viability drastically decreased after exposure to H_2O_2 (100 μM) for 1 h. However, simultaneous application of **BDP-NAC** (100–200 μM) with H_2O_2 showed a dose-dependent increase in cell viability, with no cytotoxicity observed after treatment with 200 μM **BDP-NAC**. At longer treatment times (2 h), **BDP-NAC** rescued a similar percentage of cells compared to H_2O_2-only controls (Figure S29). These results indicate that **BDP-NAC** can successfully mitigate the deleterious effects of a hyperoxidative environment in culture.

To further ensure that persulfide release imparts protection to the cardiomyocytes in the presence of H_2O_2, several control studies were carried out. Exposure of the cells to H_2O_2 with added 4-(hydroxymethyl)benzeneboronic acid pinacol ester (Bpin-OH), a non-persulfide releasing compound with a Bpin moiety, showed an increase in viability compared to H_2O_2 alone but did not rescue cells to the same extent as **BDP-NAC**. We also compared **BDP-NAC** to sodium sulfide (Na_2S), a fast-releasing H_2S donor, and GYY4137, a slow-releasing H_2S donor, under the same experimental conditions. Na_2S had a limited ability to rescue cells while GYY4137 had no effect on viability. Interestingly, **BDP-NAC** was more effective at rescuing cells than Na_2S, even while Na_2S enhanced H9C2 proliferation in the absence of H_2O_2 (Figure S28). This provides further evidence that persulfides may serve to maintain redox homeostasis in cells to a greater extent than H_2S. NAC, a potential thiol byproduct after reaction of **BDP-NAC**, also had no effect on viability. To confirm that **BDP-NAC** derives its activity from ROS-triggered persulfide release, the cardiomyocytes were treated with **BDP-Control**, which has an identical structure to **BDP-NAC**, but without the Bpin triggering moiety. **BDP-Control** also did not rescue cells exposed to H_2O_2

under identical conditions to the previous experiments. Finally, to recreate the synergistic effects of the Bpin moiety of **BDP-NAC** and the resultant persulfide release, cells were treated with Bpin-OH simultaneously with either NAC, GYY4137, or Na_2S. Each of these combinations was able to mitigate the effects of H_2O_2 on cell viability, but not to the same degree as **BDP-NAC**, with the exception of Bpin-OH + Na_2S. We suspect that simultaneous treatment of the cardiomyocytes with Bpin-OH and Na_2S gives a greater instantaneous concentration of potential antioxidants than **BDP-NAC**, considering its sustained release. In a system with continuous generation of ROS, delivery of Bpin-OH and Na_2S would likely have a diminished ability to rescue cells compared to sustained release from **BDP-NAC**.

2.5. Conclusions

In summary, we have synthesized a self-immolative prodrug that releases a discrete persulfide species (**BDP-NAC**) in the presence of H_2O_2. Persulfide release and trigger specificity were characterized by LCMS, NMR, and fluorescence spectroscopy, demonstrating that sustained release of the persulfide is selectively triggered by H_2O_2. In vitro studies using H9C2 cardiomyocytes under oxidative stress showed that **BDP-NAC** mitigates the harmful effects of highly oxidative environments with greater potency than commonly used H_2S donors Na_2S and GYY4137 as well as relevant controls. **BDP-NAC** not only shows promise therapeutically, but it also provides a modular system for persulfide donors that may be triggered under a variety of conditions. We envision that a library of persulfide donors based on the **BDP-NAC** template will enable the study of persulfide biology in greater depth than is currently possible, providing insight into sulfur redox cycles and sulfur-mediated cell signaling.

2.6. Acknowledgements

This work was supported by the National Science Foundation (DMR-1454754) and the National Institutes of Health (R01GM123508). We also thank 3M for support of this work through a Non-Tenured Faculty Award to JBM. We thank Dr. Tijana Grove and Dr. Webster Santos and their students for experimental assistance as well as Dr. Mehdi Ashraf-Khorassani for help with the LCMS

2.7. References

1. Wang, R., Two's company, three's a crowd: can H_2S be the third endogenous gaseous transmitter? *FASEB J.* **2002,** *16* (13), 1792-1798.

2. Papapetropoulos, A.; Pyriochou, A.; Altaany, Z.; Yang, G.; Marazioti, A.; Zhou, Z.; Jeschke, M. G.; Branski, L. K.; Herndon, D. N.; Wang, R.; Szabó, C., Hydrogen sulfide is an endogenous stimulator of angiogenesis. *Proc. Natl. Acad. Sci. U. S. A.* **2009,** *106* (51), 21972-21977.

3. Mustafa, A. K.; Gadalla, M. M.; Snyder, S. H., Signaling by Gasotransmitters. *Sci. Signal* **2009,** *2* (68), 1-8.

4. Predmore, B. L.; Lefer, D. J.; Gojon, G., Hydrogen sulfide in biochemistry and medicine. *Antioxid. Redox. Signal.* **2012,** *17* (1), 119-140.

5. Zhao, W.; Zhang, J.; Lu, Y.; Wang, R., The vasorelaxant effect of H_2S as a novel endogenous gaseous K(ATP) channel opener. *EMBO J.* **2001,** *20* (21), 6008-6016.

6. Nicolau, L. A. D.; Silva, R. O.; Damasceno, S. R. B.; Carvalho, N. S.; Costa, N. R. D.; Aragão, K. S.; Barbosa, A. L. R.; Soares, P. M. G.; Souza, M. H. L. P.; Medeiros, J. V. R., The

hydrogen sulfide donor, Lawesson's reagent, prevents alendronate-induced gastric damage in rats. *Braz. J. Med. Biol. Res.* **2013,** *46*, 708-714.

7. Li, L.; Whiteman, M.; Guan, Y. Y.; Neo, K. L.; Cheng, Y.; Lee, S. W.; Zhao, Y.; Baskar, R.; Tan, C.-H.; Moore, P. K., Characterization of a Novel, Water-Soluble Hydrogen Sulfide–Releasing Molecule (GYY4137). *Circulation* **2008,** *117* (18), 2351.

8. Zanatta, S. D.; Jarrott, B.; Williams, S. J., Synthesis and Preliminary Pharmacological Evaluation of Aryl Dithiolethiones with Cyclooxygenase-2-Selective Inhibitory Activity and Hydrogen Sulfide-Releasing Properties. *Aust. J. Chem.* **2010,** *63* (6), 946-957.

9. Zhao, Y.; Wang, H.; Xian, M., Cysteine-Activated Hydrogen Sulfide (H_2S) Donors. *J. Am. Chem. Soc.* **2011,** *133* (1), 15-17.

10. Foster, J. C.; Powell, C. R.; Radzinski, S. C.; Matson, J. B., *S*-Aroylthiooximes: A Facile Route to Hydrogen Sulfide Releasing Compounds with Structure-Dependent Release Kinetics. *Org. Lett.* **2014,** *16* (6), 1558-1561.

11. Zheng, Y.; Yu, B.; Ji, K.; Pan, Z.; Chittavong, V.; Wang, B., Esterase-Sensitive Prodrugs with Tunable Release Rates and Direct Generation of Hydrogen Sulfide. *Angew. Chem. Int. Ed. Engl.* **2016,** *55* (14), 4514-4518.

12. Li, Z.; Organ, C. L.; Zheng, Y.; Wang, B.; Lefer, D. J., Novel Esterase-Activated Hydrogen Sulfide Donors Attenuate Myocardial Ischemia/Reperfusion Injury. *Circulation* **2016,** *134*, 17903.

13. Chauhan, P.; Bora, P.; Ravikumar, G.; Jos, S.; Chakrapani, H., Esterase Activated Carbonyl Sulfide/Hydrogen Sulfide (H_2S) Donors. *Org. Lett.* **2017,** *19* (1), 62-65.

14. Devarie-Baez, N. O.; Bagdon, P. E.; Peng, B.; Zhao, Y.; Park, C.-M.; Xian, M., Light-Induced Hydrogen Sulfide Release from "Caged" gem-Dithiols. *Org. Lett.* **2013,** *15* (11), 2786-2789.

15. Fukushima, N.; Ieda, N.; Sasakura, K.; Nagano, T.; Hanaoka, K.; Suzuki, T.; Miyata, N.; Nakagawa, H., Synthesis of a photocontrollable hydrogen sulfide donor using ketoprofenate photocages. *Chem. Commun.* **2014,** *50* (5), 587-589.

16. Powell, C. R.; Foster, J. C.; Okyere, B.; Theus, M. H.; Matson, J. B., Therapeutic Delivery of H_2S via COS: Small Molecule and Polymeric Donors with Benign Byproducts. *J. Am. Chem. Soc.* **2016,** *138* (41), 13477-13480.

17. Steiger, A. K.; Pardue, S.; Kevil, C. G.; Pluth, M. D., Self-Immolative Thiocarbamates Provide Access to Triggered H_2S Donors and Analyte Replacement Fluorescent Probes. *J. Am. Chem. Soc.* **2016,** *138* (23), 7256-7259.

18. Wang, W.; Ji, X.; Du, Z.; Wang, B., Sulfur dioxide prodrugs: triggered release of SO_2 via a click reaction. *Chem. Commun.* **2017,** *53* (8), 1370-1373.

19. Day, J. J.; Yang, Z.; Chen, W.; Pacheco, A.; Xian, M., Benzothiazole Sulfinate: a Water-Soluble and Slow-Releasing Sulfur Dioxide Donor. *ACS Chem. Biol.* **2016,** *11* (6), 1647–1651.

20. Zheng, Y.; Yu, B.; De La Cruz, L. K.; Roy Choudhury, M.; Anifowose, A.; Wang, B., Toward Hydrogen Sulfide Based Therapeutics: Critical Drug Delivery and Developability Issues. *Med. Res. Rev.* **2018,** *38* (1), 57-100.

21. Powell, C. R.; Dillon, K. M.; Matson, J. B., A review of hydrogen sulfide (H_2S) donors: Chemistry and potential therapeutic applications. *Biochem. Pharmacol.* **2018,** *149* (1) 110-123.

22. Zhao, Y.; Biggs, T. D.; Xian, M., Hydrogen sulfide (H_2S) releasing agents: chemistry and biological applications. *Chem. Commun.* **2014,** *50* (80), 11788-11805.

23. Ida, T.; Sawa, T.; Ihara, H.; Tsuchiya, Y.; Watanabe, Y.; Kumagai, Y.; Suematsu, M.; Motohashi, H.; Fujii, S.; Matsunaga, T.; Yamamoto, M.; Ono, K.; Devarie-Baez, N. O.; Xian, M.; Fukuto, J. M.; Akaike, T., Reactive cysteine persulfides and S-polythiolation regulate oxidative stress and redox signaling. *Proc. Natl. Acad. Sci. U. S. A.* **2014,** *111* (21), 7606-7611.

24. Yadav, P. K.; Martinov, M.; Vitvitsky, V.; Seravalli, J.; Wedmann, R.; Filipovic, M. R.; Banerjee, R., Biosynthesis and Reactivity of Cysteine Persulfides in Signaling. *J. Am. Chem. Soc.* **2016,** *138* (1), 289-99.

25. Cuevasanta, E.; Möller, M. N.; Alvarez, B., Biological chemistry of hydrogen sulfide and persulfides. *Arch. Biochem. Biophys.* **2017,** *617* (Supplement C), 9-25.

26. Filipovic, M. R.; Zivanovic, J.; Alvarez, B.; Banerjee, R., Chemical Biology of H_2S Signaling through Persulfidation. *Chem. Rev.* **2018,** *118* (3), 1253-1337.

27. Zheng, L.; White, R. H.; Cash, V. L.; Dean, D. R., Mechanism for the Desulfurization of L-Cysteine Catalyzed by the nifS Gene Product. *Biochemistry* **1994,** *33* (15), 4714-4720.

28. Filipovic, M. R., Persulfidation (S-sulfhydration) and H_2S. In *Chemistry, Biochemistry and Pharmacology of Hydrogen Sulfide*, Moore, P. K.; Whiteman, M., Eds. Springer International Publishing: Cham, 2015; pp 29-59.

29. Cai, Y.-R.; Hu, C.-H., Computational Study of H_2S Release in Reactions of Diallyl Polysulfides with Thiols. *J. Phys. Chem. B* **2017,** *121* (26), 6359-6366.

30. Francoleon, N. E.; Carrington, S. J.; Fukuto, J. M., The reaction of H_2S with oxidized thiols: Generation of persulfides and implications to H2S biology. *Arch. Biochem. Biophys.* **2011,** *516* (2), 146-153.

31. Flint, D. H., Escherichia coli contains a protein that is homologous in function and N-terminal sequence to the protein encoded by the nifS gene of Azotobacter vinelandii and that can

participate in the synthesis of the Fe-S cluster of dihydroxy-acid dehydratase. *J. Biol. Chem.* **1996,** *271* (27), 16068-74.

32. Millikin, R.; Bianco, C. L.; White, C.; Saund, S. S.; Henriquez, S.; Sosa, V.; Akaike, T.; Kumagai, Y.; Soeda, S.; Toscano, J. P.; Lin, J.; Fukuto, J. M., The chemical biology of protein hydropersulfides: Studies of a possible protective function of biological hydropersulfide generation. *Free Radic. Biol. Med.* **2016,** *97* (Supplement C), 136-147.

33. Mueller, E. G., Trafficking in persulfides: delivering sulfur in biosynthetic pathways. *Nat. Chem. Biol.* **2006,** *2* (4), 185-194.

34. Vandiver, M. S.; Paul, B. D.; Xu, R.; Karuppagounder, S.; Rao, F.; Snowman, A. M.; Ko, H. S.; Lee, Y. I.; Dawson, V. L.; Dawson, T. M.; Sen, N.; Snyder, S. H., Sulfhydration mediates neuroprotective actions of parkin. *Nat. Commun.* **2013,** *4*, 1626.

35. Mustafa, A. K.; Gadalla, M. M.; Sen, N.; Kim, S.; Mu, W.; Gazi, S. K.; Barrow, R. K.; Yang, G.; Wang, R.; Snyder, S. H., H_2S Signals Through Protein S-Sulfhydration. *Sci. Signal* **2009,** *2* (96), 1-8.

36. Nishida, M.; Sawa, T.; Kitajima, N.; Ono, K.; Inoue, H.; Ihara, H.; Motohashi, H.; Yamamoto, M.; Suematsu, M.; Kurose, H.; van der Vliet, A.; Freeman, B. A.; Shibata, T.; Uchida, K.; Kumagai, Y.; Akaike, T., Hydrogen sulfide anion regulates redox signaling via electrophile sulfhydration. *Nat. Chem. Biol.* **2012,** *8* (8), 714-24.

37. Benavides, G. A.; Squadrito, G. L.; Mills, R. W.; Patel, H. D.; Isbell, T. S.; Patel, R. P.; Darley-Usmar, V. M.; Doeller, J. E.; Kraus, D. W., Hydrogen sulfide mediates the vasoactivity of garlic. *Proc. Natl. Acad. Sci.* **2007,** *104* (46), 17977-17982.

38. Cerda, M. M.; Hammers, M. D.; Earp, M. S.; Zakharov, L. N.; Pluth, M. D., Applications of Synthetic Organic Tetrasulfides as H2S Donors. *Org. Lett.* **2017,** *19* (9), 2314-2317.

39. Park, C.-M.; Weerasinghe, L.; Day, J. J.; Fukuto, J. M.; Xian, M., Persulfides: current knowledge and challenges in chemistry and chemical biology. *Mol. Biosyst.* **2015,** *11* (7), 1775-1785.

40. Zheng, Y.; Yu, B.; Li, Z.; Yuan, Z.; Organ, C. L.; Trivedi, R. K.; Wang, S.; Lefer, D. J.; Wang, B., An Esterase-Sensitive Prodrug Approach for Controllable Delivery of Persulfide Species. *Angew. Chem. Int. Ed.* **2017,** *56* (39), 11749-11753.

41. Yu, B.; Zheng, Y.; Yuan, Z.; Li, S.; Zhu, H.; De La Cruz, L. K.; Zhang, J.; Ji, K.; Wang, S.; Wang, B., Toward Direct Protein S-Persulfidation: A Prodrug Approach That Directly Delivers Hydrogen Persulfide. *J. Am. Chem. Soc.* **2017,** *140* (1), 30-33.

42. Artaud, I.; Galardon, E., A persulfide analogue of the nitrosothiol SNAP: formation, characterization and reactivity. *ChemBioChem* **2014,** *15* (16), 2361-4.

43. Zhao, Y.; Henthorn, H. A.; Pluth, M. D., Kinetic Insights into Hydrogen Sulfide Delivery from Caged-Carbonyl Sulfide Isomeric Donor Platforms. *J. Am. Chem. Soc.* **2017,** *139* (45), 16365-16376.

44. Zafarullah, M.; Li, W.; Sylvester, J.; Ahmad, M., Molecular mechanisms of N-acetylcysteine actions. *Cell. Mol. Life Sci.* **2003,** *60* (1), 6-20.

45. Murphy, N. P.; Lampe, K. J., Fabricating PLGA microparticles with high loads of the small molecule antioxidant N-acetylcysteine that rescue oligodendrocyte progenitor cells from oxidative stress. *Biotechnol. Bioeng.* **2018,** *115* (1), 246-256.

46. Kuivila, H. G., Electrophilic Displacement Reactions. III. Kinetics of the Reaction between Hydrogen Peroxide and Benzeneboronic Acid1. *J. Am. Chem. Soc.* **1954,** *76* (3), 870-874.

47. Schmid, K. M.; Jensen, L.; Phillips, S. T., A Self-Immolative Spacer That Enables Tunable Controlled Release of Phenols under Neutral Conditions. *J. Org. Chem.* **2012,** *77* (9), 4363-4374.

48. Chen, W.; Liu, C.; Peng, B.; Zhao, Y.; Pacheco, A.; Xian, M., New fluorescent probes for sulfane sulfurs and the application in bioimaging. *Chem.* **2013,** *4* (7), 2892-2896.

2.8. Experimental

Materials and Methods

All reagents were obtained from commercial vendors and used as received unless otherwise stated. NMR spectra were measured on Agilent 400 MHz or Bruker 500 MHz spectrometers. ^{1}H and ^{13}C NMR chemical shifts are reported in ppm relative to internal solvent resonances. CH_2Cl_2 was dried and degassed on solvent columns (MBraun) containing alumina absorbent and stored in a Strauss flask under N_2 before use. Other solvents were used as received unless otherwise noted. Yields refer to chromatographically and spectroscopically pure compounds unless otherwise stated. Thin-layer chromatography (TLC) was performed on glass-backed silica plates and visualized by UV unless otherwise stated. LCMS experiments were performed on a Waters Acquity UPLC system equipped with a Waters Polarity C_{18}-functionalized silica column, diode array detector, and ESI mass spectrometer. Fluorescence spectra were recorded in a 1 cm quartz cuvette on a Cary Eclipse fluorescence spectrophotometer equipped with a PMT detector (600 V), excitation and emission slit widths of 5 nm, 600 nm/min scan speed, and 1.00 nm step. High-resolution mass spectra were taken on an Agilent Technologies 6230 TOF LC/MS mass spectrometer.

Cell studies were conducted on an adherent H9C2 line of rat embryonic cardiomyocytes (ATCC, Manassas, VA, USA). Cultures were grown in Dulbecco's Modified Eagle Medium (DMEM, VWR, Radnor, PA), supplemented with 10 % fetal bovine serum (FBS, VWR, Radnor, PA). Cells were cultured at 37 °C in 5 % CO_2-air. The cultures were passaged after 70–80 % confluence was achieved. Cells were rinsed with PBS solution, and then released with trypsin and EDTA solution (VWR, Radnor, PA). The suspension of released cells was centrifuged at 1000 rpm for 5 min

Synthesis of *p*-Tolylboronic Acid Pinacol Ester **(1)**

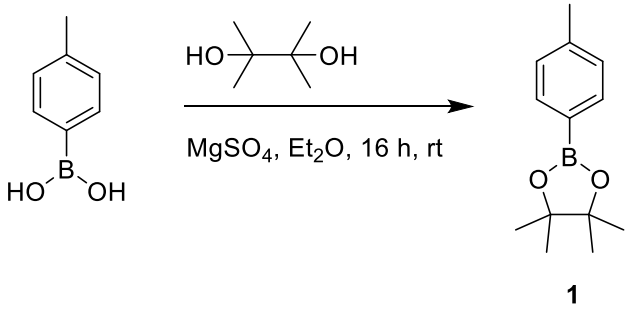

1

A round bottom flask equipped with a septum was charged with diethyl ether (300 mL), *p*-tolylboronic acid (10 g, 74 mmol), and a stir bar. The white suspension was stirred until all solids dissolved (30 min – 1 h). $MgSO_4$ (15 g, 125 mmol) and pinacol (8.9 g, 75 mmol) were then added sequentially to the solution while stirring. The reaction mixture was stirred at rt for 16 h, at which point the reaction was complete by TLC (50:50 hexanes:EtOAc). The resulting white suspension was then filtered, rinsed with diethyl ether (250 mL), and concentrated via rotary evaporation, yielding compound **1** (12.9 g, 87% yield) as white crystals. This product was used in the next reaction step without further purification. ^{1}H-NMR ($CDCl_3$): δ 7.70 (m, 2H), 7.19 (m, 2H), 2.37 (s, 3H), 1.34 (s, 12H). ^{13}C-NMR ($CDCl_3$): δ 141.48, 134.92, 128.63, 83.70, 24.97, 21.85.

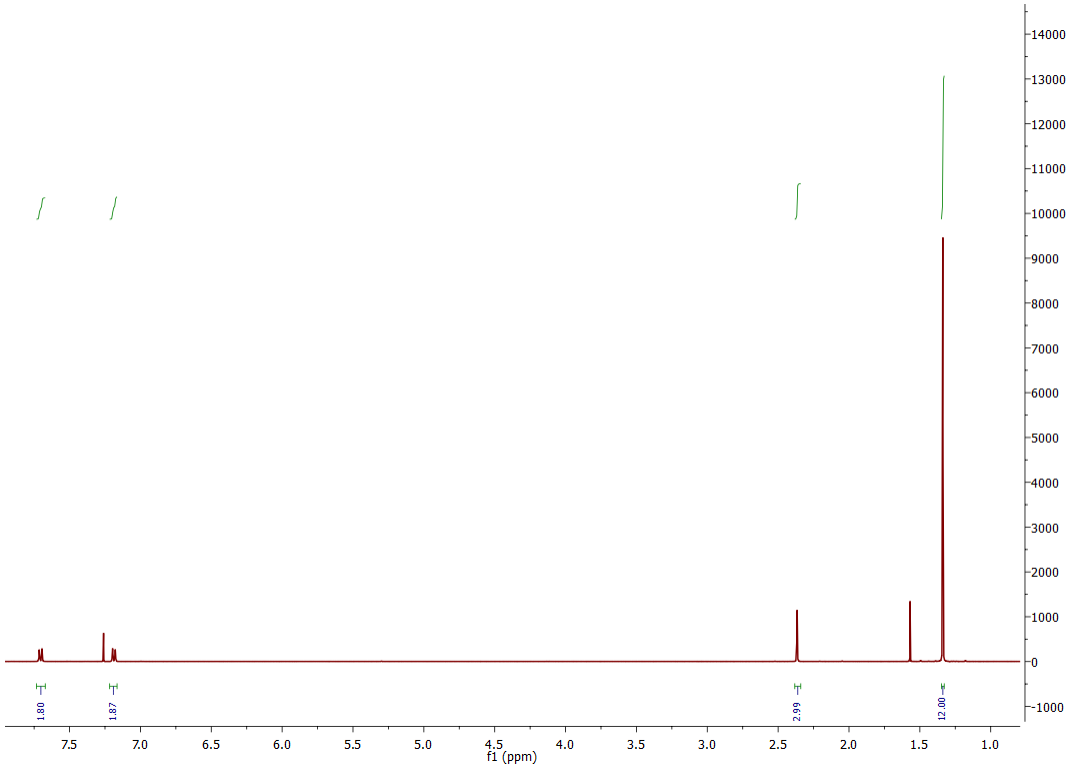

Figure S1. ^{1}H NMR of **1**.

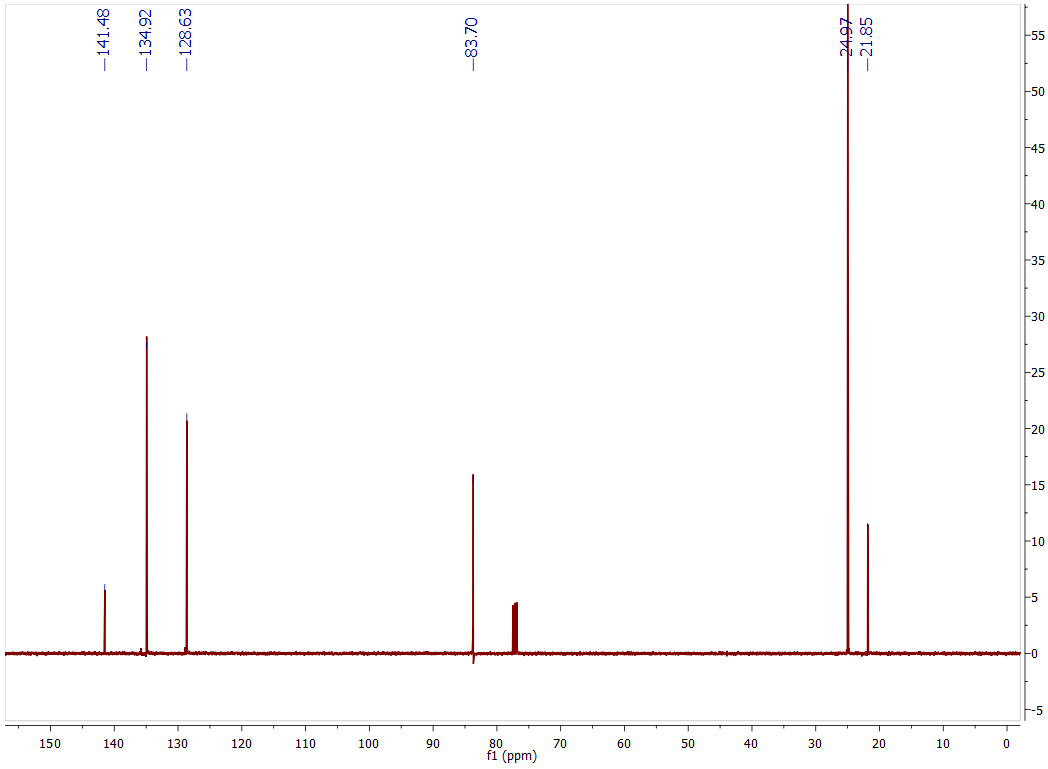

Figure S2. ^{13}C NMR of **1**.

Synthesis of *p*-Benzylboronic Acid Pinacol Ester Bromide **(2)**

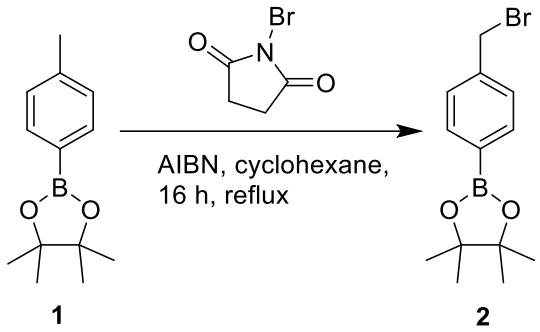

1 **2**

A flame-dried, 2-neck round bottom flask equipped with a septum and condenser was charged with compound **1** (7.87 g, 36.1 mmol), dry, degassed (stored over activated molecular sieves overnight, bubbled with N_2 for 1 h) cyclohexane (120 mL), and *N*-bromosuccinimide (7.07 g, 39.7 mmol) under N_2 flow. The mixture was stirred until the solids fully dissolved to give a clear, light brown solution. Azobisisobutyronitrile (AIBN) (0.593 g, 3.61 mmol) was added in one portion under N_2 flow, and the reaction mixture was heated to reflux. The reaction was monitored by TLC (50:50 hexanes:EtOAc) until starting material was consumed (16 h). The reaction mixture was cooled to rt and washed successively with saturated $NaHCO_3$ (2 x 30 mL), ice water (2 x 30 mL), and brine (30 mL). The organic layer was separated, dried over Na_2SO_4, and then concentrated via rotary evaporation to yield a pale yellow powder. This crude product was then recrystallized from cyclohexane to yield product **2** (6.04 g, 73 % yield) as an off white solid. ^{1}H NMR ($CDCl_3$): δ 7.80 (m, 2H) 7.39 (m, 2H), 4.49 (s, 2H), 1.35 (s, 12H). ^{13}C NMR ($CDCl_3$): δ 140.76, 135.32, 128.40, 83.99, 33.43, 24.97.

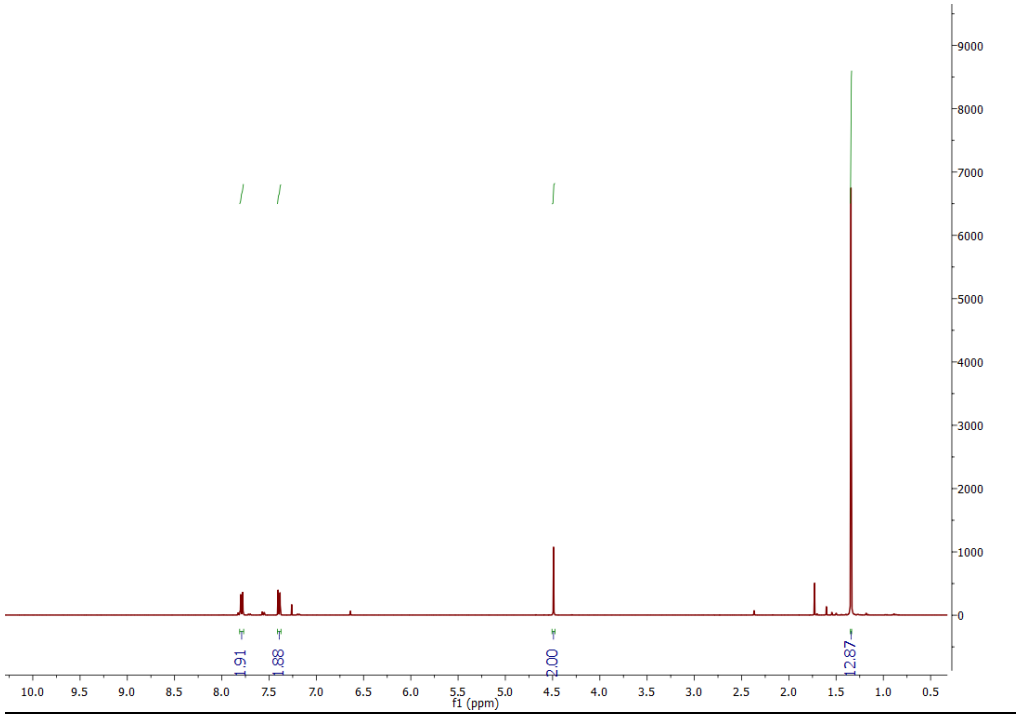

Figure S3. ^{1}H NMR of **2**.

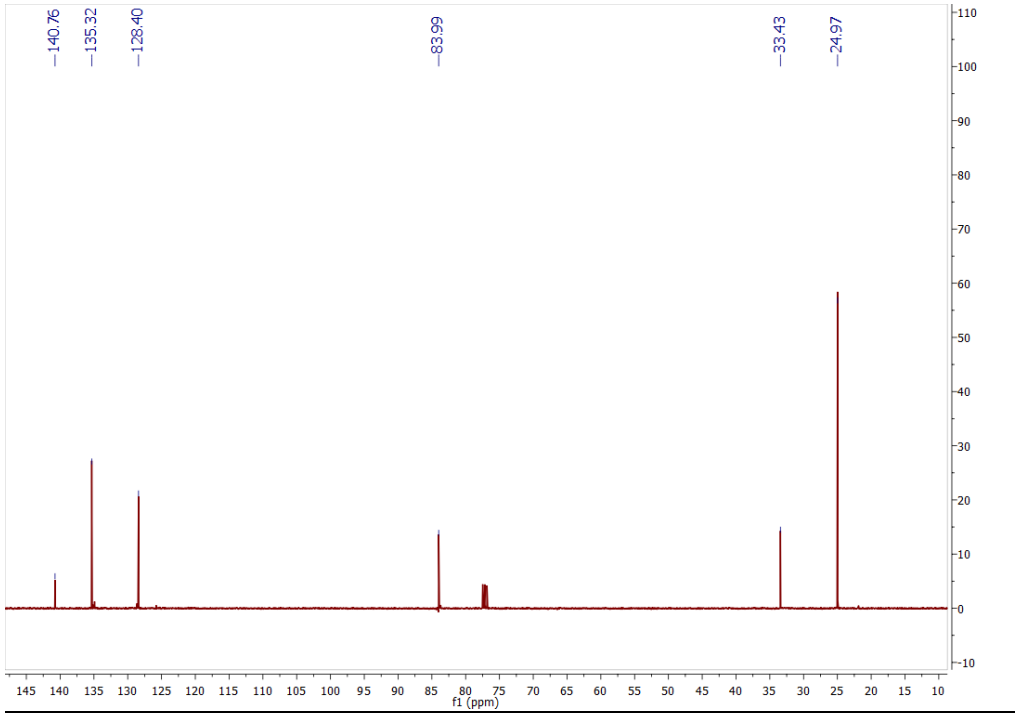

Figure S4. ^{13}C NMR of **2**.

Synthesis of *p*-Benzylboronic Acid Pinacol Ester Thiol **(3)**

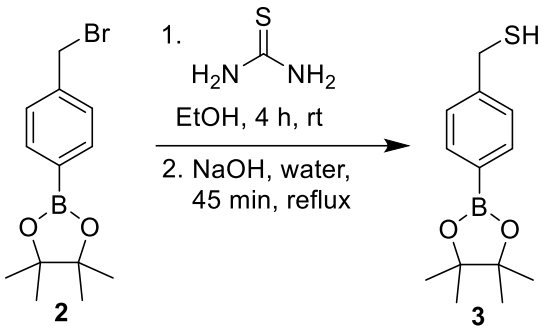

A two-neck round bottom flask equipped with a vacuum adaptor, and a septum was charged with compound **2** (3.47 g, 11.7 mmol), EtOH (30 mL), and a stirbar. The resulting suspension was bubbled with N_2 for 30 min. Thiourea (0.940 g, 12.3 mmol) was then added in one portion under N_2, and the reaction mixture was stirred at rt. The solids dissolved slowly over the course of 1 h to give a clear, colorless solution. Reaction progress was monitored by TLC (50:50 hexanes:EtOAc) until starting material was consumed (4 h). The reaction mixture was then concentrated via rotary evaporation, and the thiouronium intermediate was subsequently dissolved in DI H_2O (20 mL). A reflux condenser was added to the flask, and the suspension was bubbled with N_2 for 30 min. NaOH pellets (1.90 g, 46.7 mmol) were then added under N_2, and the resulting yellow solution was refluxed for 45 min. The reaction mixture was cooled to rt and then placed in an ice bath. HCl (1 N) was added dropwise at 0 °C, resulting in the formation of a white precipitate. HCl addition was continued until the pH of the solution was ~2. The aqueous suspension was then extracted with $CHCl_3$ (5 x 20 mL), and the organic layer was separated and dried over Na_2SO_4. The product was then further purified by silica gel chromatography, eluting with 30 % EtOAc in hexanes, yielding an off-white solid (2.15 g, 74 % yield). ^{1}H NMR ($CDCl_3$): δ 7.77 (m, 2H) 7.34 (m, 2H), 3.74 (d, *J* = 7.8 Hz, 2H), 1.74 (t, *J* = 1.7 Hz, 1H), 1.34 (s, 12H). ^{13}C NMR ($CDCl_3$): δ 144.43, 135.31, 127.50, 83.90, 29.18, 24.98.

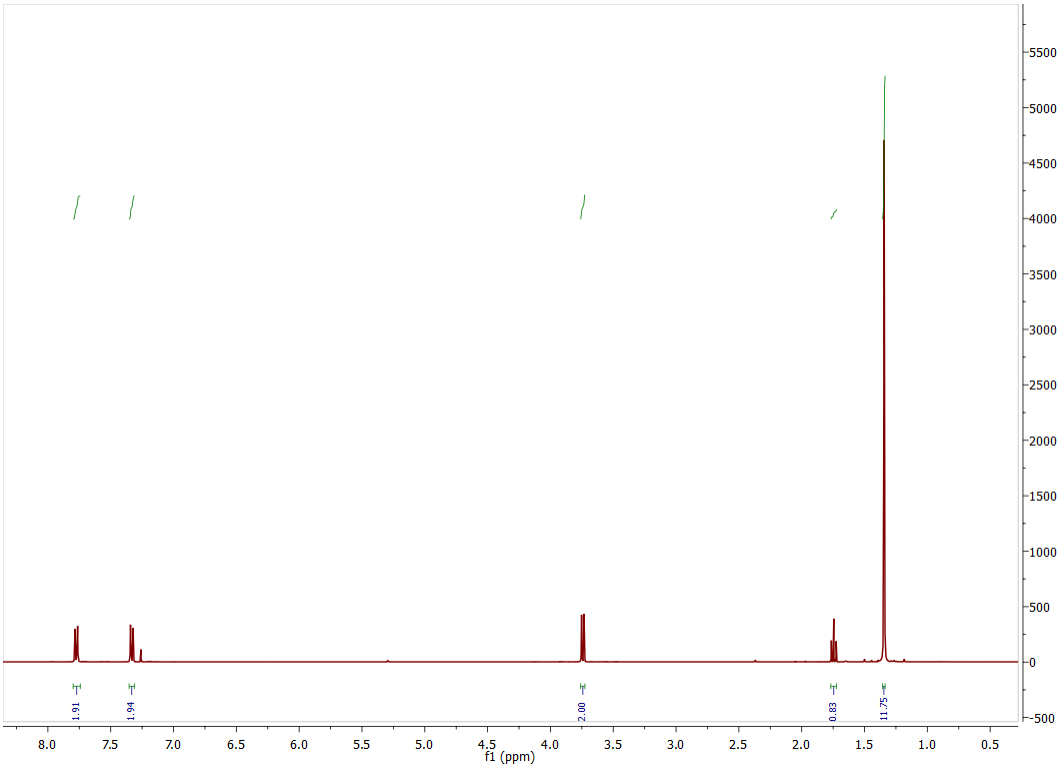

Figure S5. ^{1}H NMR of **3**.

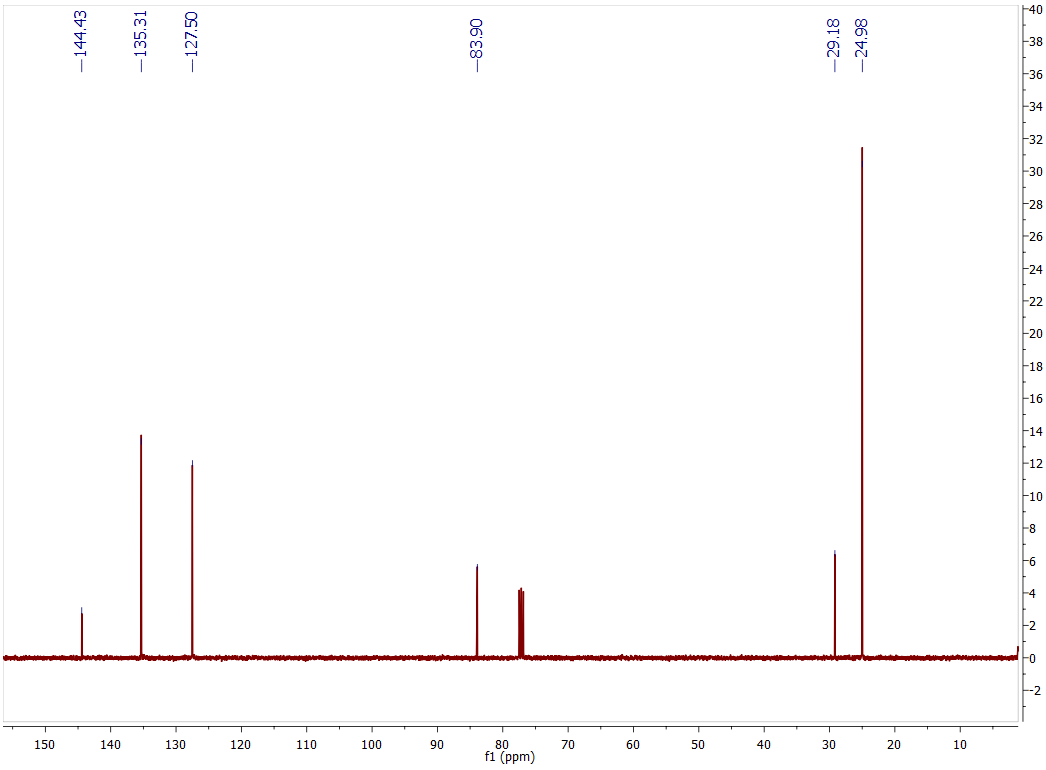

Figure S6. ^{13}C NMR of **3**.

Synthesis of Activated N-Acetylcysteine Disulfide **(NAC-pyDS)**

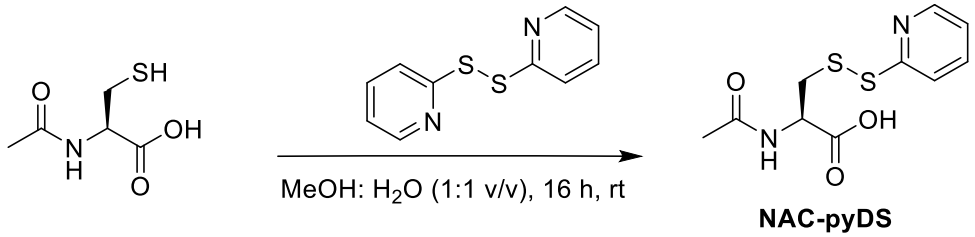

NAC-pyDS

A round bottom flask was charged with *N*-acetylcysteine (2.0 g, 12.3 mmol), H_2O (17 mL), and a stirbar to give a clear solution. A solution of 2,2'-dipyridyl disulfide (5.40 g, 24.5 mmol) in MeOH (17 mL) was added in one portion resulting in a clear, yellow solution. The reaction mixture was stirred at rt (16 h). Reaction progress was monitored by TLC (EtOAc), showing complete consumption of starting material. The resulting yellow solution was concentrated via rotary evaporation and extracted with DCM (3 x 30 mL). The organic layers were combined, dried over Na_2SO_4, and concentrated by rotary evaporation. The crude product, obtained as a yellow solid, was then purified by silica gel chromatography eluting with 5 % to 15 % MeOH in CH_2Cl_2, yielding a light yellow powder (2.30 g, 69% yield). ^{1}H NMR (DMSO-d_6): δ 12.97 (s, 1H), 8.46 (m, 1H), 8.42 (d, *J* = 7.89 Hz, 1H), 7.81 (m, 1H), 7.75 (m, 1H), 7.24 (m, 1H), 4.47 (m, 1H), 3.15 (m, 2H), 1.86 (s, 3H). ^{13}C NMR (DMSO-d_6): δ 171.88, 169.49, 158.77, 149.69, 137.86, 121.33, 119.34, 51.39, 39.93, 22.44.

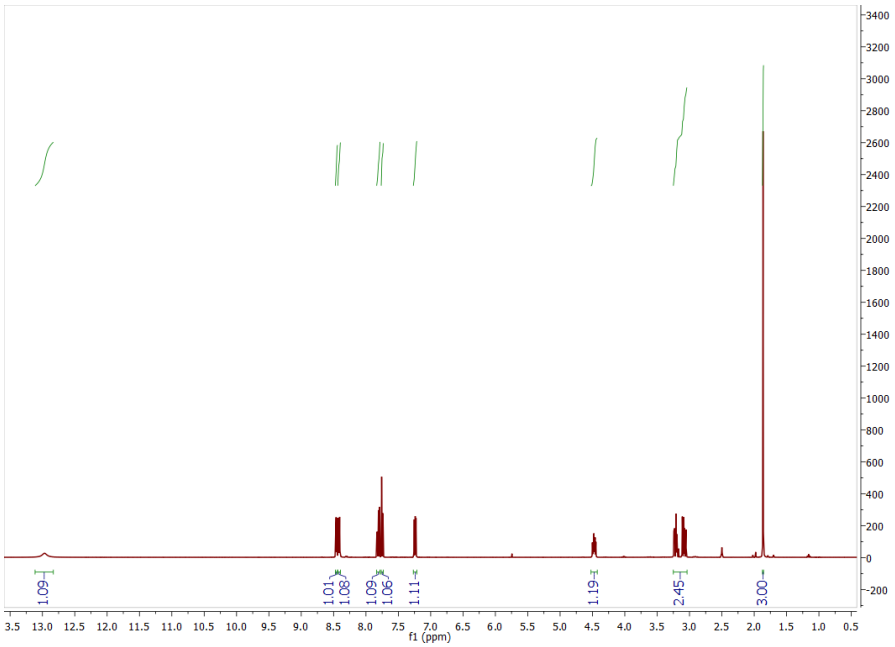

Figure S7. ^{1}H NMR of **NAC-pyDS**.

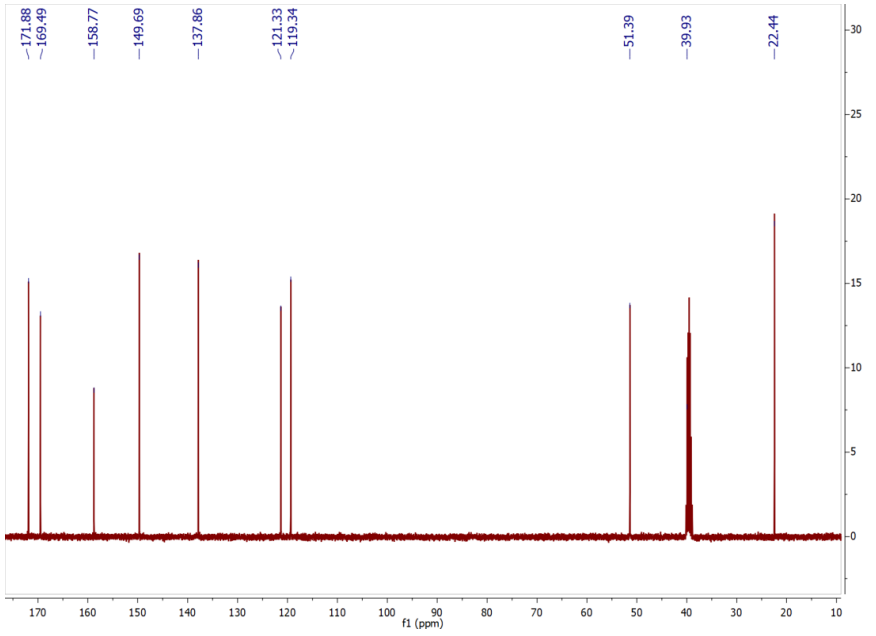

Figure S8. ^{13}C NMR of **NAC-pyDS**.

Synthesis of *p*-Benzylboronic Acid Pinacol Ester *N*-Acetalcysteine Disulfide **(BDP-NAC)**

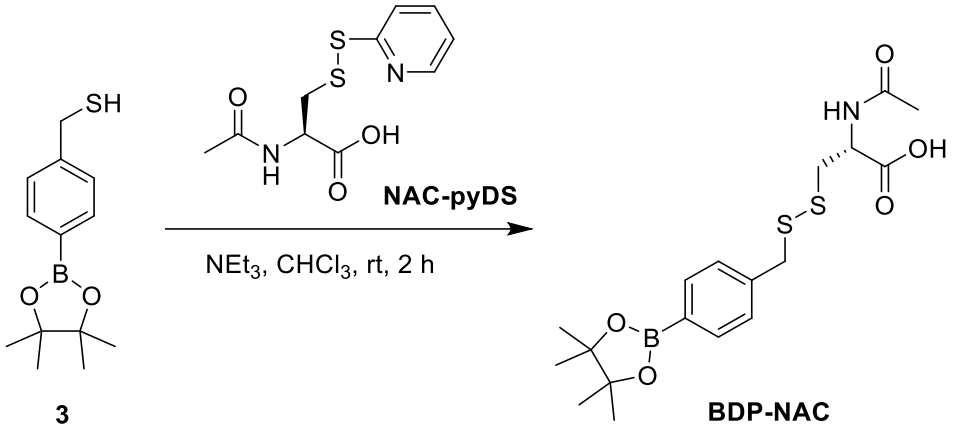

A single-neck roundbottom flask was charged with compound **3** (0.412 g, 1.65 mmol), $CHCl_3$ (8 mL), and a stirbar, resulting in a light yellow solution. **NAC-pyDS** (0.900 g, 3.29 mmol), and triethylamine (NEt_3) (0.460 mL, 3.30 mmol) were added sequentially, resulting in a yellow solution. The reaction mixture was stirred for 2 h at rt, monitoring reaction progress with TLC (50:50 hexanes:EtOAc). Once complete, the reaction mixture was diluted with $CHCl_3$ (10 mL) and washed sequentially with 1 N HCl (2 x 5 mL) and brine (5 mL). The organic layer was then dried over Na_2SO_4, concentrated via rotary evaporation, and purified by silica gel chromatography (30% EtOAc in hexanes), yielding a yellow solid (0.375 g, 56 % yield). ^{1}H NMR (DMSO-d_6): δ 12.89 (s, 1H), 8.30 (d, *J* = 8.1, 1H), 7.62 (m, 2H), 7.33 (m, 2H), 4.47 (m, 1H), 3.98 (d, *J* = 2.6 Hz, 2H), 3.02-2.94 (m, 1H), 2.81-2.74 (m, 1H), 1.86 (s, 3H), 1.28 (s, 12H). ^{13}C NMR (DMSO-d_6): δ 172.06, 169.40, 140.88, 134.55, 128.81, 83.66, 51.16, 41.79, 39.35, 24.71, 22.43. HRMS (ESI-TOF) calcd. for $C_{18}H_{27}BNO_5S_2$ $[M+H]^+$ 412.1429, found 412.1422. Calcd. for $C_{18}H_{26}BKNO_5S_2$ $[M+K]^+$ 450.0946, found 450.0980.

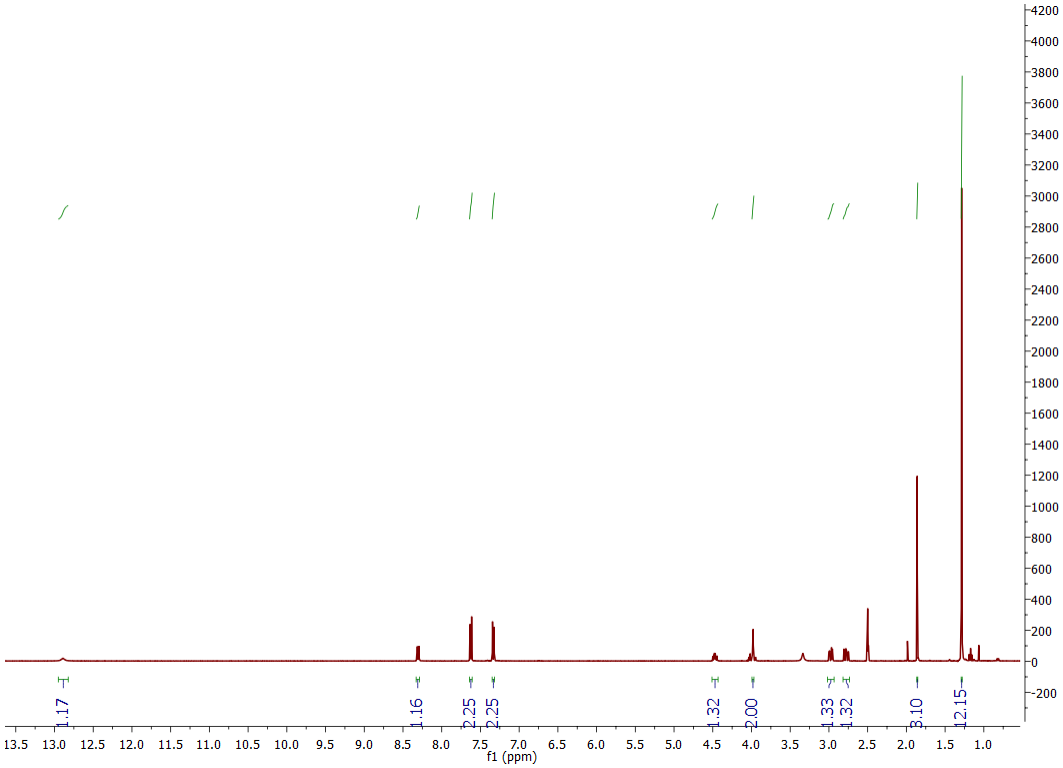

Figure S9. ^{1}H NMR of **BDP-NAC**.

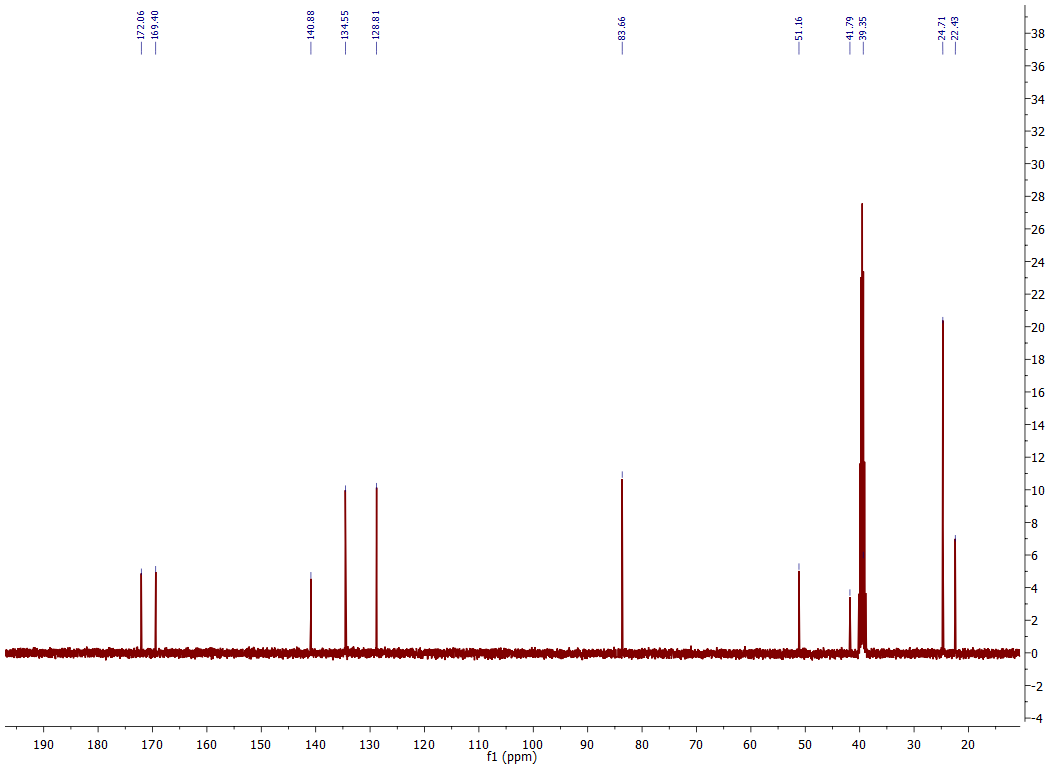

Figure S10. ^{13}C NMR of **BDP-NAC**.

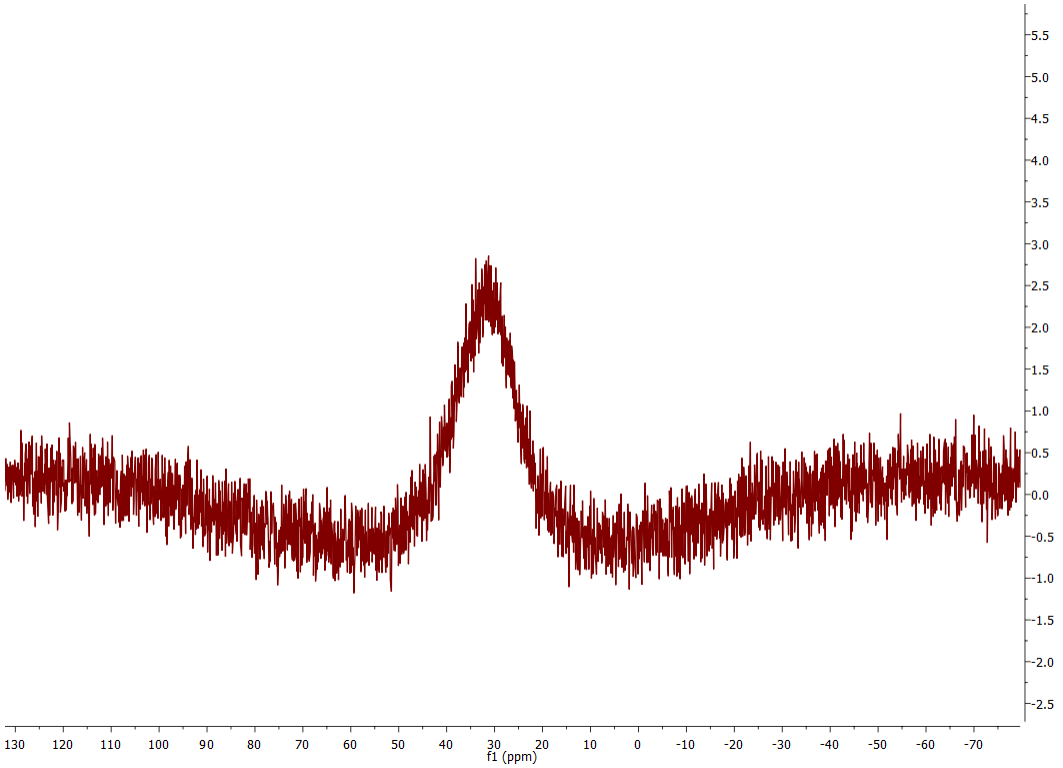

Figure S11. ^{11}B NMR spectra of **BDP-NAC** in 90 % (v/v) DMSO-d_6:D_2O.

Synthesis of Benzyl *N*-Acetylcysteine Disulfide **(BDP-Control)**

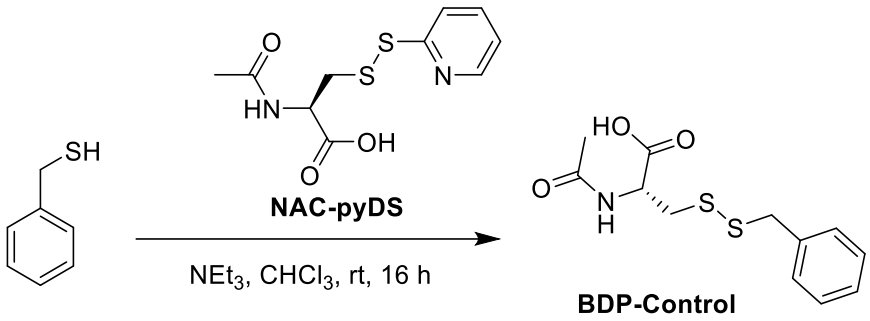

A single neck round bottom flask was charged with **NAC-pyDS** (1.3 g, 4.8 mmol) and $CHCl_3$ (10 mL) to form a suspension. Benzyl mercaptan (0.52 mL, 4.0 mmol) and NET_3 (0.83 mL, 6.0 mmol) were added sequentially. Upon addition of NET_3, a clear, yellow solution formed. The reaction mixture was stirred for 4 h at rt, monitoring reaction progress by TLC (30 % EtOAc in hexanes). Once complete, the reaction mixture was diluted with $CHCl_3$ (10 mL), washed successively with

1 N HCl (2 x 5 mL) and brine (5 mL), dried over Na_2SO_4, and concentrated by rotary evaporation. The resulting yellow powder was purified by silica gel chromatography eluting with a gradient of 0% to 10 % MeOH in EtOAc, yielding a light brown solid (0.688 g, 60 % yield). ^{1}H NMR (DMSO-d_6): δ 12.94 (s, 1H), 8.30 (d, *J* = 4.7, 1H), 7.37-7.23 (m, 5H), 4.46 (m, 1H), 3.97 (m, 2H), 2.99-2.71 (m, 2H), 1.86 (s, 3H). ^{13}C NMR (DMSO-d_6): δ 172.10, 169.39, 137.37, 129.30, 128.44, 127.31, 51.25, 41.92, 39.45, 22.45. HRMS (ESI-TOF) calcd. for $C_{12}H_{16}NO_3S_2$ $[M+H]^+$ 286.0571, found 286.0566. Calcd. for $C_{12}H_{15}NNaO_3S_2$ $[M+Na]^+$ 309.0414, found 309.0414.

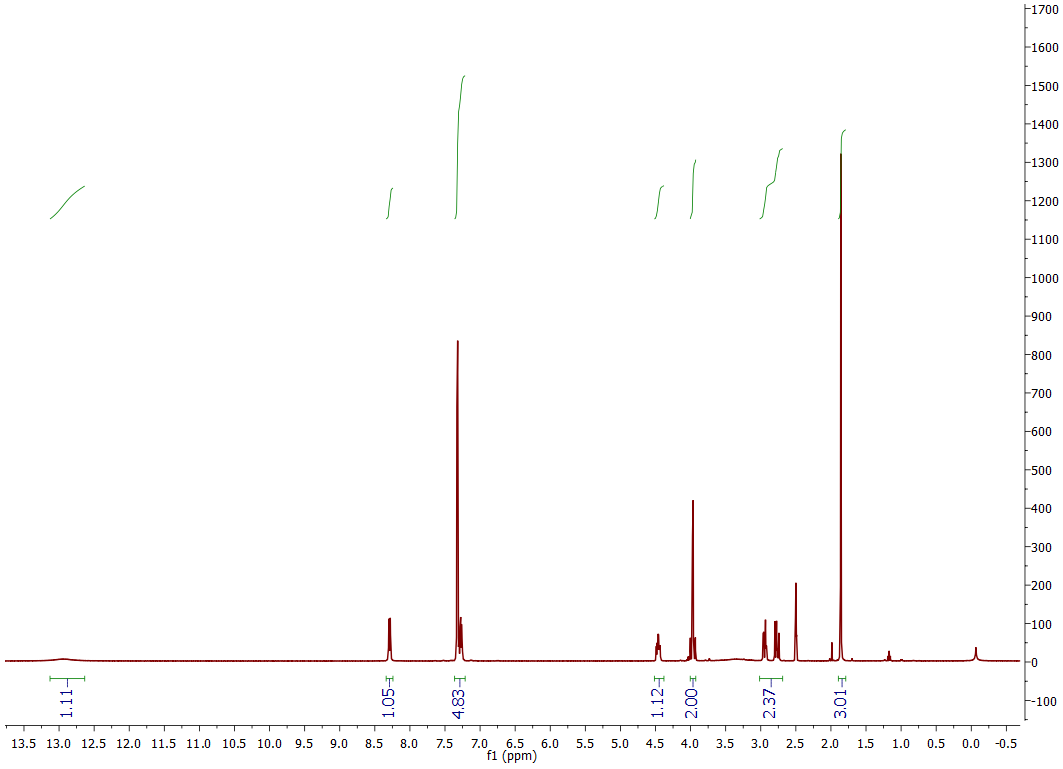

Figure S12. ^{1}H NMR of **BDP-Control**.

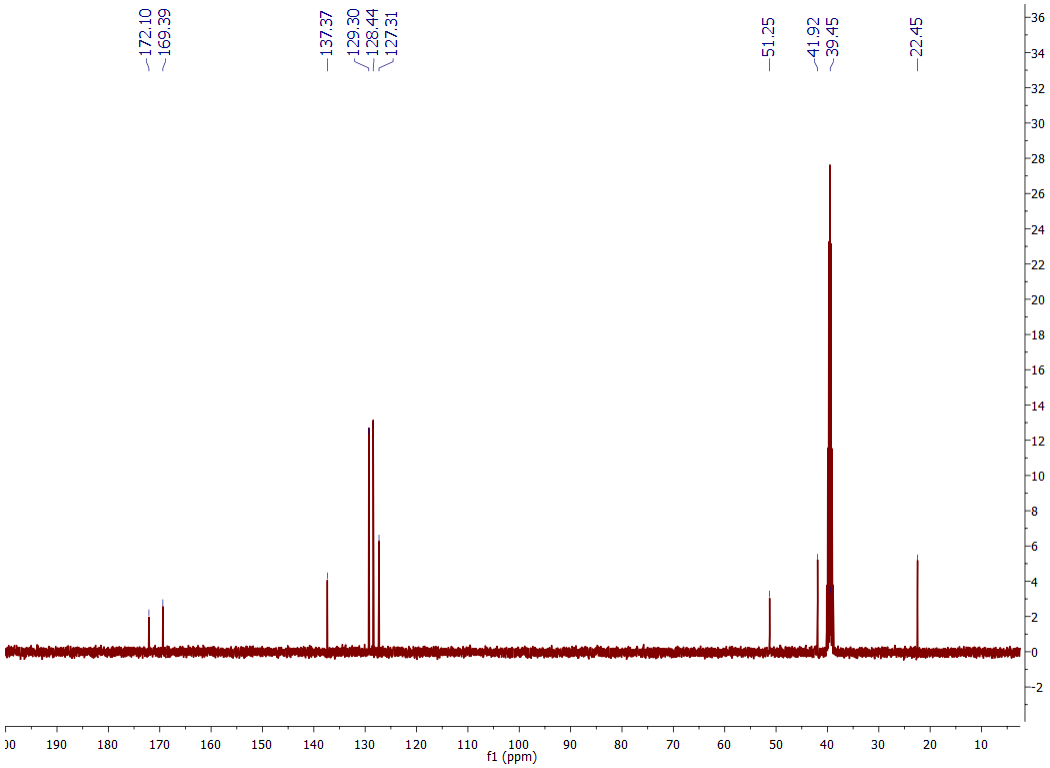

Figure S13. ^{13}C NMR of **BDP-Control**.

Synthesis of Activated Persulfide Probe **(4)**

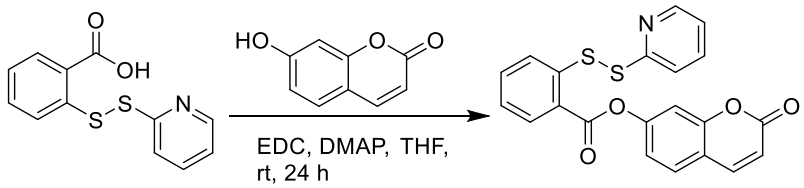

Thiosalicylic acid-pyDS **4**

A single neck round bottom flask was charged with **Thiosalicylic acid-pyDS** (4.0 g, 15 mmol) and THF (150 mL) to give a light yellow solution. To this solution, EDC (4.7 g, 30 mmol), and DMAP (122 mg, 1 mmol) were added sequentially and stirred until the solution was homogeneous. Next, 7-hydroxycoumarin (2.6 g, 17 mmol) was added, and the reaction mixture was stirred at rt (16 h). Reaction progress monitored by TLC (EtOAc) until starting material was consumed. The resulting amber solution was concentrated via rotary evaporation, and the residue was dissolved

in $CHCl_3$ (200 mL). This solution was washed successively with saturated $NaHCO_3$ (2 x 50 mL), DI H_2O (100 mL), and brine (100 mL), and then separated and dried over Na_2SO_4. The resulting crude product was purified by silica gel chromatography eluting with 20 % EtOAc in CH_2Cl_2 to yield an off-white solid (2.9 g, 47% yield). Spectroscopic data agree with literature precedent.[48] ^{1}H NMR ($CDCl_3$) δ 8.46 (m, 1H), 8.29 (m, 1H), 7.98 (m, 1H), 7.73 (d, *J* = 9.5 Hz, 1H), 7.60-7.50 (m, 4H), 7.35 (m, 1H), 7.29-7.21 (m, 2H), 7.10 (m, 1H), 6.42 (d, *J* = 9.6 Hz, 1H). ^{13}C NMR ($CDCl_3$) δ 164.14, 160.25, 158.93, 158.70, 154.76, 153.02, 149.55, 142.81, 141.94, 137.36, 134.20, 132.12, 128.68, 126.27, 125.94, 121.11, 119.64, 118.58, 116.96, 116.31, 110.65.

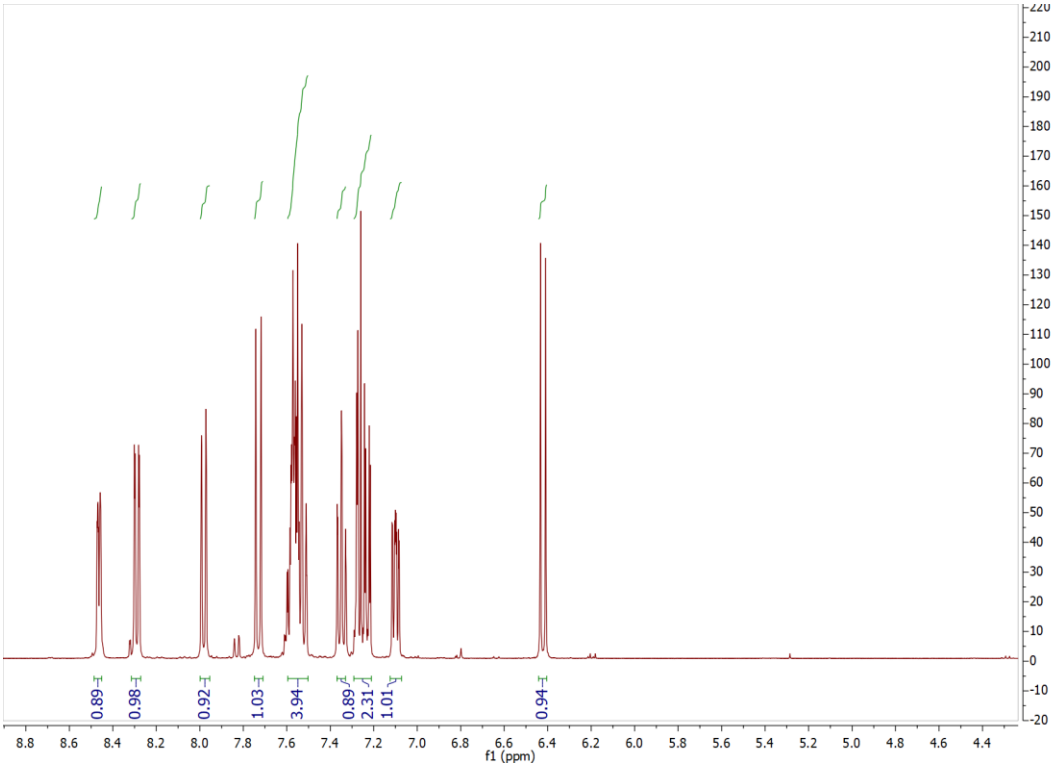

Figure S14. ^{1}H NMR of **7**.

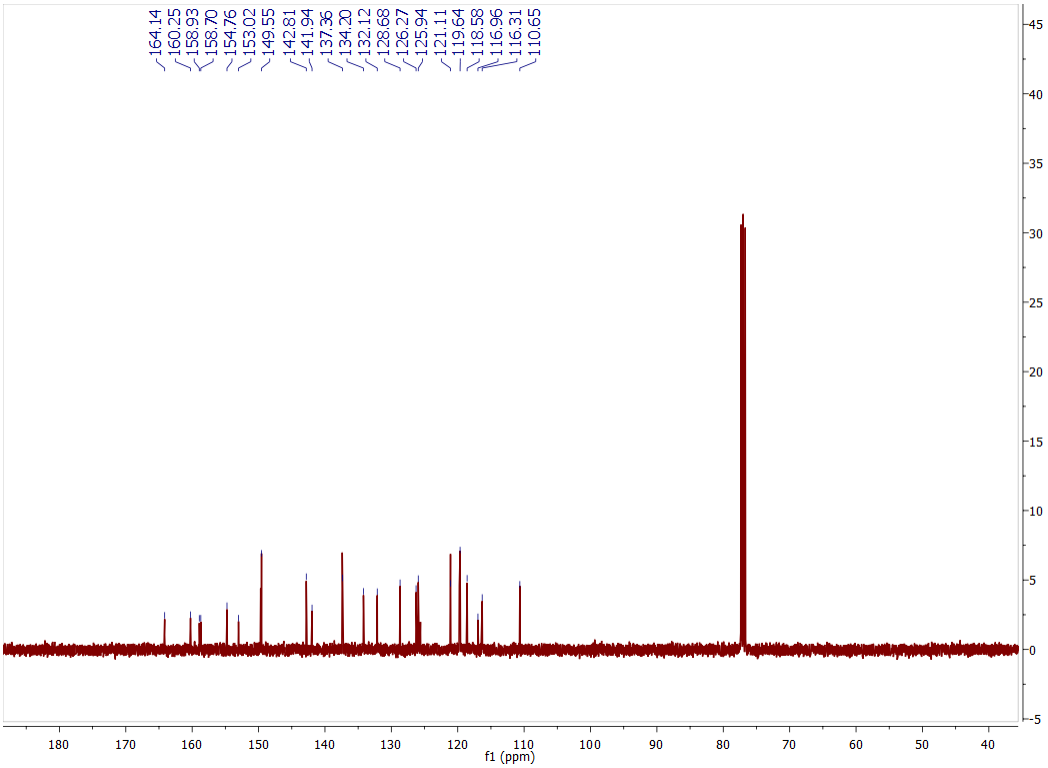

Figure S15. ^{13}C NMR of **7**.

Synthesis of Probe-Bpin Disulfide **(BDP-Fluor)**

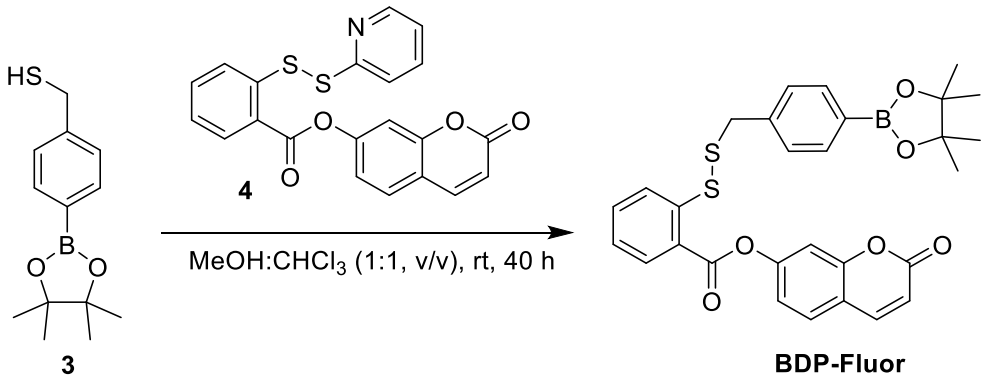

A round bottom flask was charged with compound **4** (538 mg, 1.32 mmol), MeOH (5 mL) and a stir bar to give a clear suspension. Thiol **3** (300 mg, 1.20 mmol) was added as a solution in $CHCl_3$ (5 mL), and the resultant yellow suspension was stirred for 40 h at rt. Reaction progress monitored by TLC (70 % EtOAc in hexanes). Once complete, the reaction mixture was concentrated via

rotary evaporation and purified on a silica column eluting with 30% EtOAc:hexanes, yielding **BDP-Fluor** as a waxy off-white solid (34 mg, 5.4% yield). ^{1}H NMR ($CDCl_3$) δ 8.19 (m, 1H), 8.07 (m, 1H), 7.72 (m, 1H), 7.69 (m, 2H), 7.57-7.51 (m, 2H), 7.31-7.25 (m, 5H), 7.21 (m, 1H), 6.42 (d, *J* = 9.6, 1H) 3.95 (s, 2H), 1.34 (s, 12H). ^{13}C NMR ($CDCl_3$): δ 164.06, 160.45, 154.88, 153.27, 143.17, 142.98, 139.38, 137.55, 135.14, 133.75, 132.09, 126.36, 125.64, 125.44, 121.25, 119.82, 118.79, 116.97, 116.33, 110.78, 83.95, 43.51, 24.98. HRMS (ESI-TOF) calcd. for $C_{29}H_{28}{}^{11}BO_6S_2$ $[M+H]^+$ 547.1415, found 547.1452. Calcd. for $C_{29}H_{31}{}^{11}BNO_6S_2$ $[M+NH_4]^+$ 564.168, found 564.1705. Calcd. for $C_{29}H_{27}{}^{11}BNaO_6S_2$ $[M+Na]^+$ 569.1234, found 569.1267. Calcd. for $C_{29}H_{27}{}^{11}BKO_6S_2$ $[M+K]^+$ 585.0974, found 585.1059.

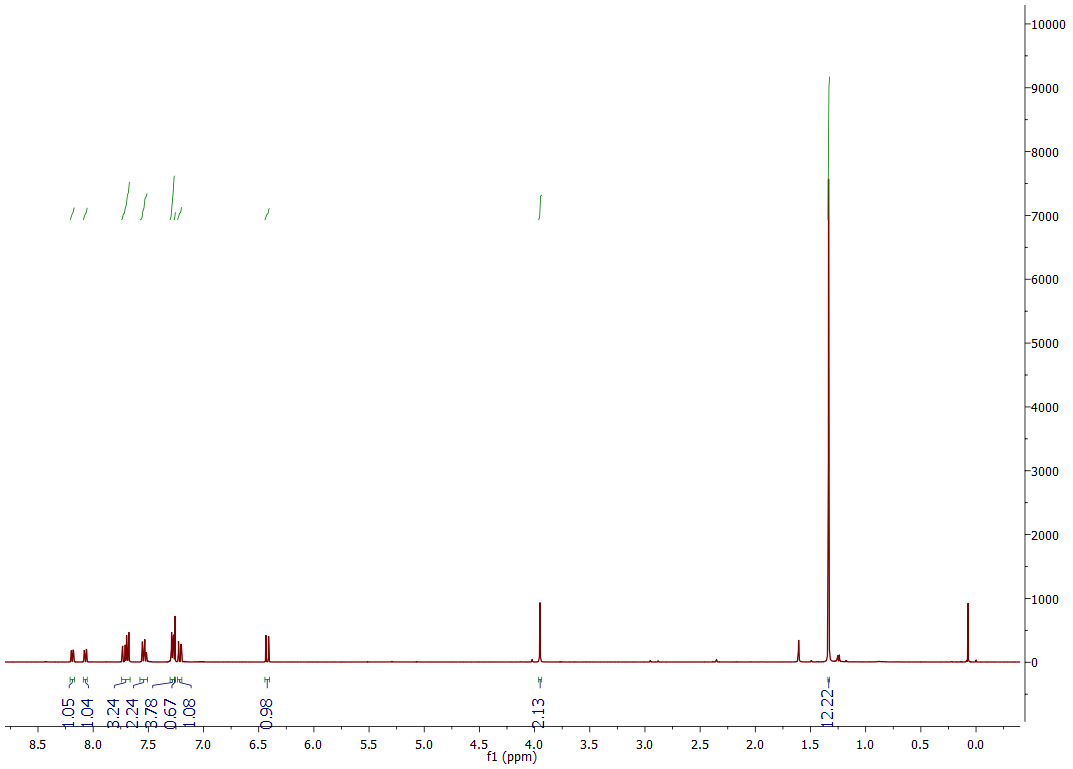

Figure S16. ^{1}H NMR of **BDP-Fluor.**

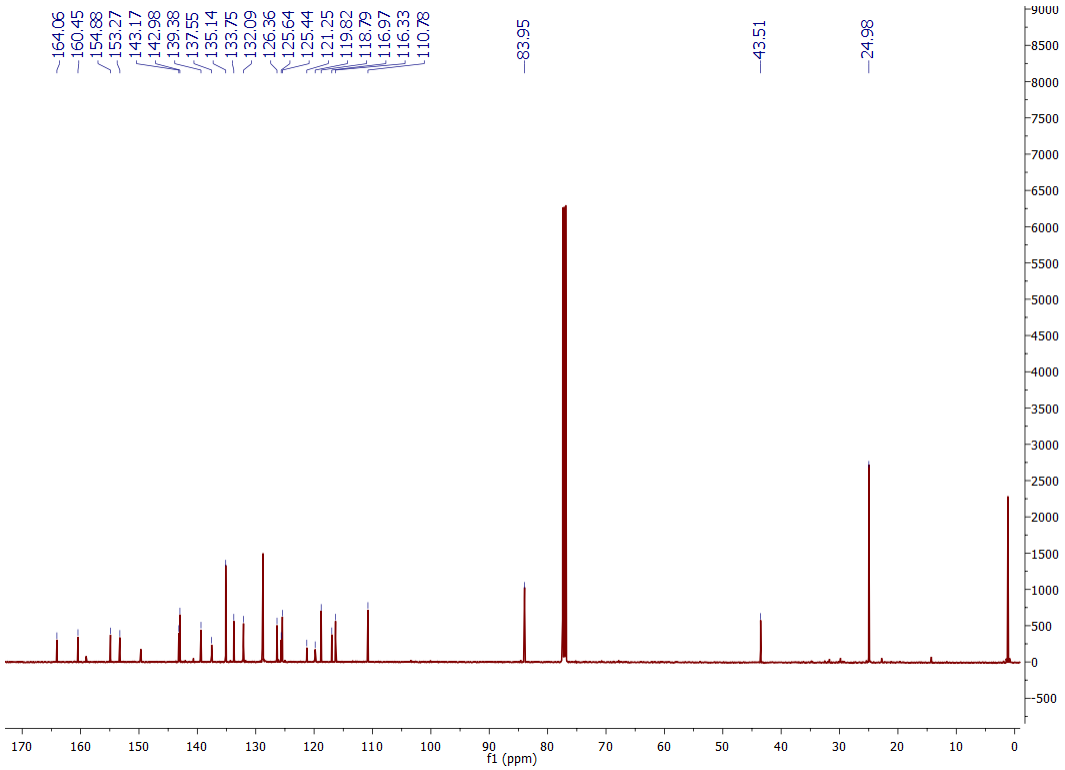

Figure S17. ^{13}C NMR of **BDP-Fluor.**

Synthesis of Probe-Control Disulfide **(5)**

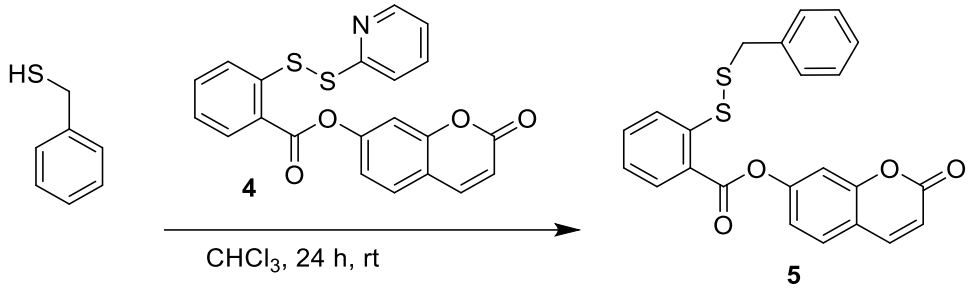

A single-neck roundbottom flask was charged with benzyl mercaptan (0.075 mL, 0.64 mmol) and **4** (248 mg, 0.590 mmol), $CHCl_3$ (1 mL), and MeOH (1 mL). The resulting clear, yellow reaction mixture was stirred for 24 h at rt, reaction progress monitored by TLC (CH_2Cl_2). The reaction mixture was then concentrated by rotary evaporation, and the resultant yellow solid was purified by silica gel chromatography eluting with 30% EtOAc:hexanes, yielding **5** as a yellow solid (64

mg, 23 % yield). ^{1}H NMR ($CDCl_3$): δ 8.21 (m, 1H), 8.07 (m, 1H), 7.73 (d, 1H), 7.54 (m, 2H), 7.32-7.27 (m, 5H), 7.25-7.19 (m, 3H), 6.43 (d, *J* = 9.6, 1H), 3.96 (s, 2H). ^{13}C NMR ($CDCl_3$): δ 164.14, 160.45, 154.88, 153.25, 143.18, 142.98, 136.43, 133.76, 132.13, 129.36, 128.75, 127.83, 126.23, 125.60, 125.47, 118.76, 117.00, 116.37, 110.79, 43.52. HRMS (ESI-TOF) calcd. for $C_{23}H_{17}O_4S_2$ $[M+H]^+$ 421.0563, found 421.0585. Calcd. for $C_{29}H_{27}{}^{11}BNaO_6S_2$ $[M+Na]^+$ 443.0382, found 443.0416.

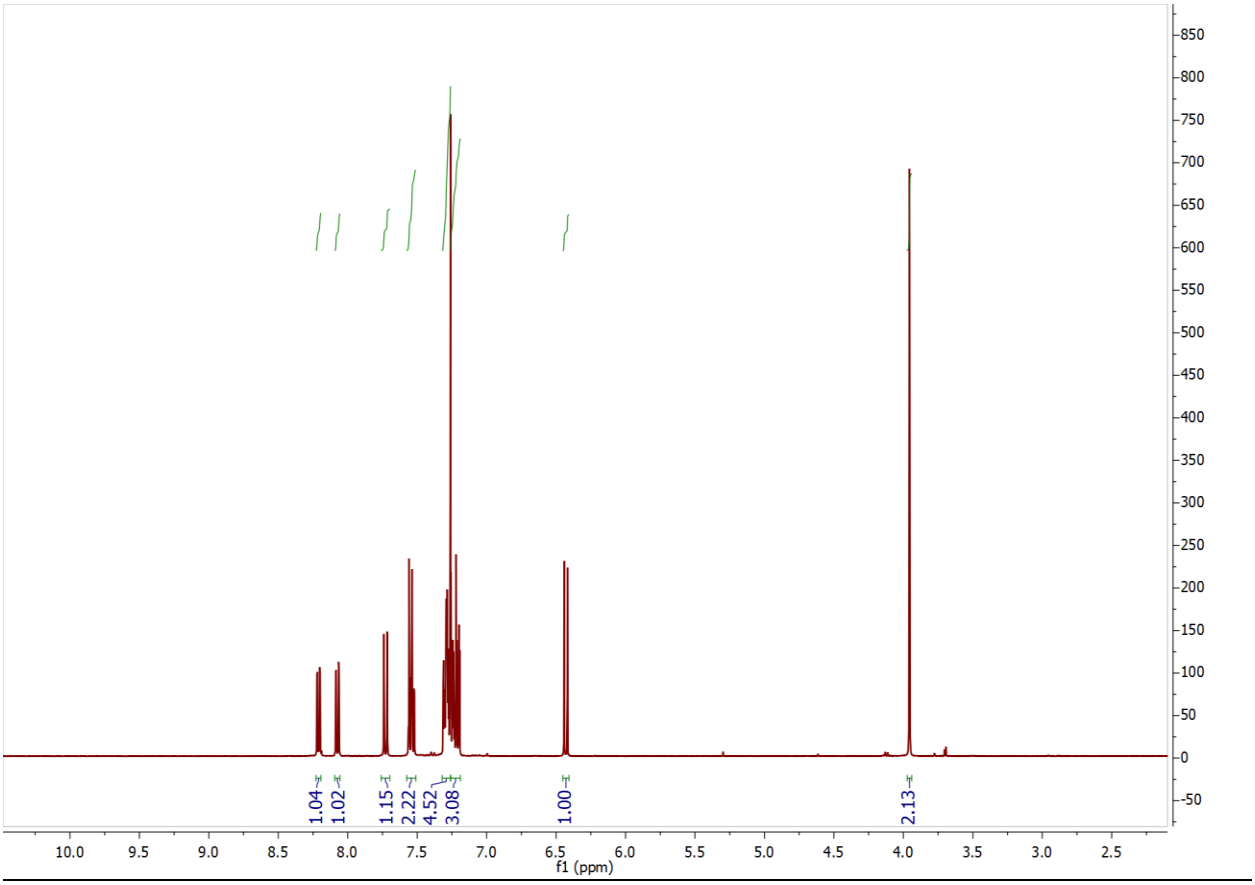

Figure S18. ^{1}H NMR of compound **5**.

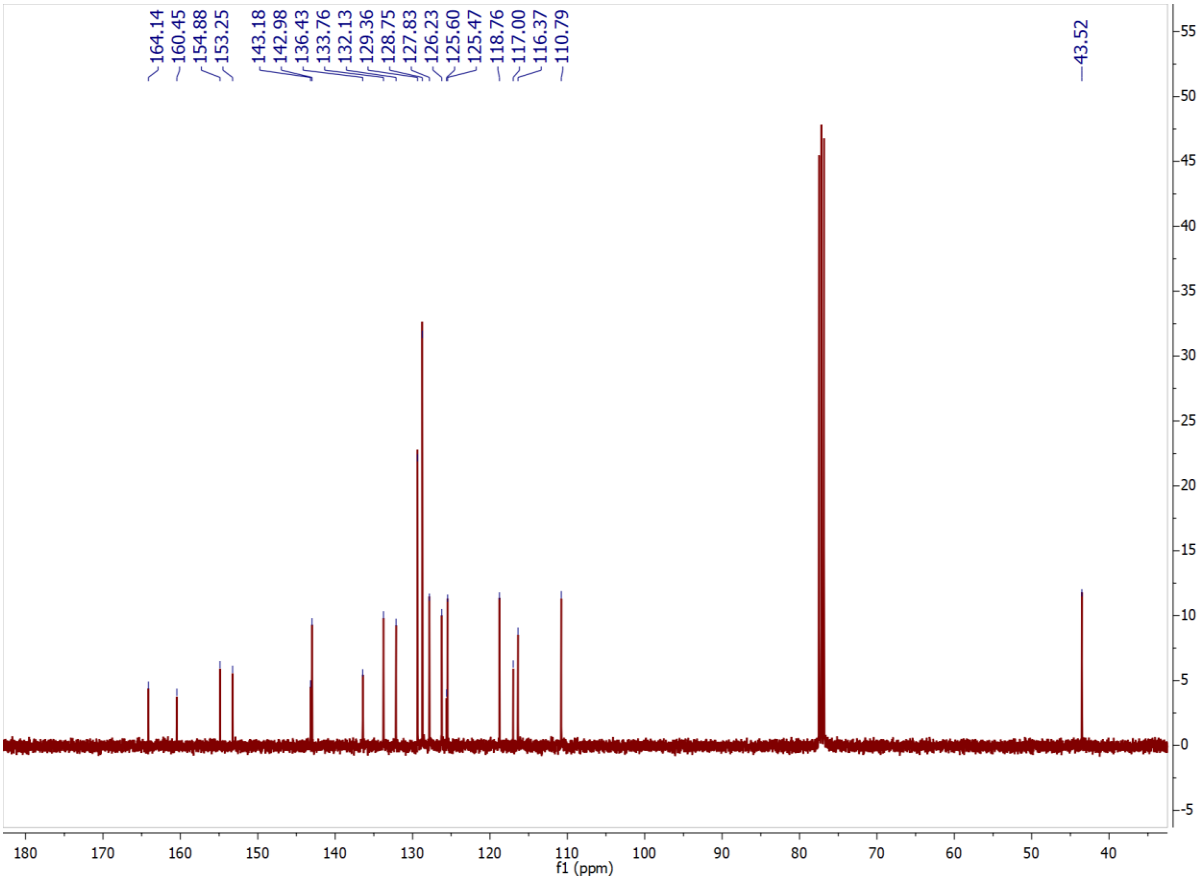

Figure S19. ^{13}C NMR of compound **5**.

Analysis of persulfide release by LCMS

A one-dram vial was charged with a solution of **BDP-NAC** (100 µL; 20 mM in ACN) and diluted with water (0.9 mL) to give a clear, colorless solution. An aliquot (50 µL) was removed and diluted into water (0.4 mL) in a vial equipped with a screw cap lid with a rubber septum, which served as the "zero" time point. The aliquot was then analyzed by LCMS. LCMS method is as follows: 2 µL injection volume eluting 5 to 90 % ACN in water with 10 mM NH_4OH over the course of 6 min, followed by a 4-min column equilibration in 5 % ACN in water with 10 mM NH_4OH. After acquisition of the zero time point H_2O_2 (30 µL, 3.5 wt %) was added to the reaction mixture. The vial was shaken thoroughly, and after 1 min the first aliquot was removed and diluted into water

and injected into the LCMS in the same fashion as the zero min time point (we estimate 5 min for total reaction time based on sample prep and autosampler time). Aliquots were then taken at the 60 and 120 min mark until the peak attributed to **BDP-NAC** subsided. The UV detector readout was set to 220 nm, and mass spectra were collected by direct infusion into the mass spectrometer in ESI negative mode.

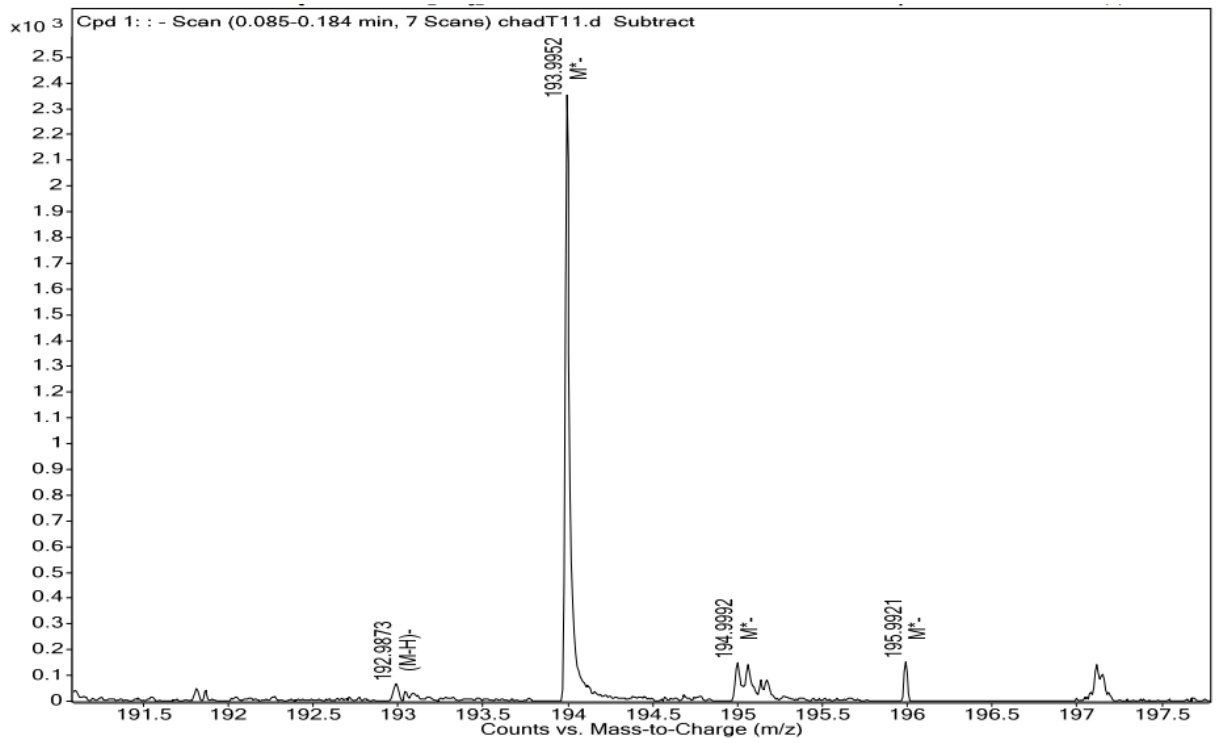

Figure S20. HRMS of the peak eluting at 3.4 min (Figure 2) corresponding to the persulfide of NAC (exact mass calculated to be 193.9551).

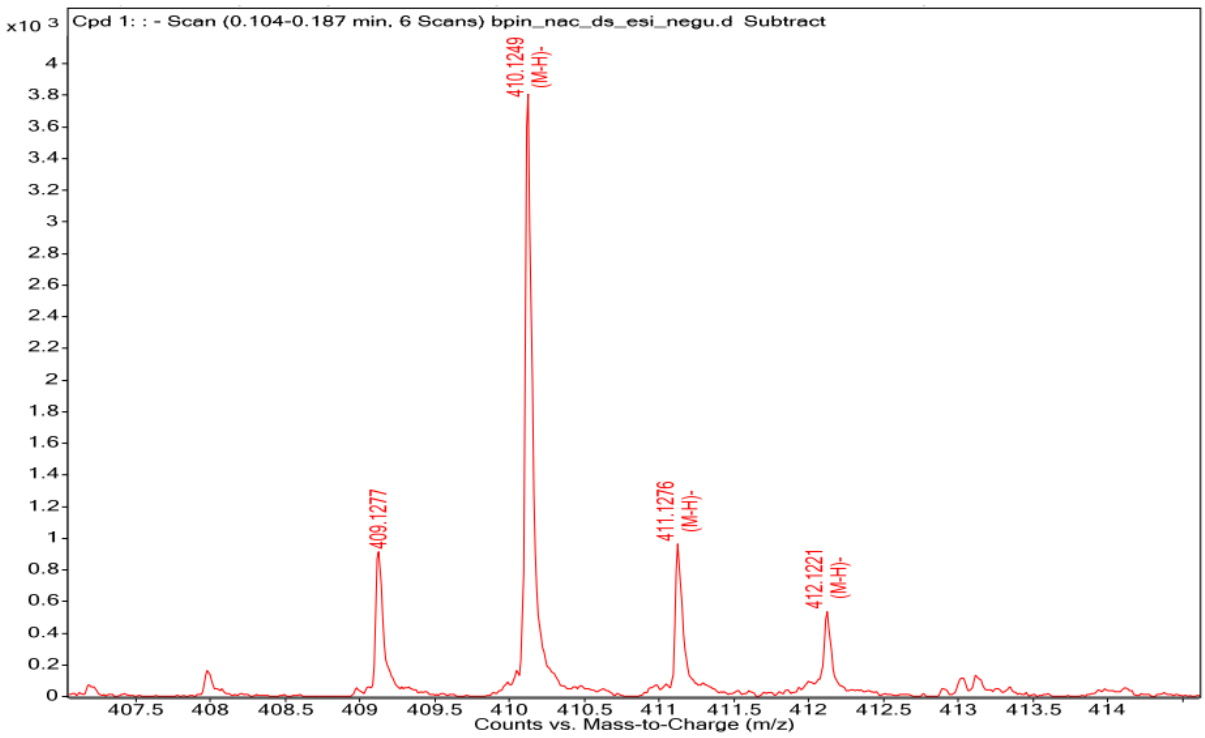

Figure S21. HRMS of **BDP-NAC** (exact mass calculated to be 411.1345).

Analysis of persulfide release by Fluorescence spectroscopy

Fluorescence assays were prepared in a 3 mL quartz cuvette with a threaded lid containing 1.98 mL 1X PBS buffer (pH 7.4), 1.0 mL cetyltrimethylammonium bromide solution (CTAB) (3 mM in PBS buffer), and 0.020 mL **BDP-Fluor** or **5** probe solution (0.50 mM in DMSO). The fluorescence spectrum of this mixture was collected from 400 to 600 nm (λ_{ex} = 380 nm) as the t = 0 timepoint. To this solution was added 5 µL of trigger solution (200 mM in PBS buffer). The cuvette was capped and shaken to mix the solution. The cuvette was then placed in the fluorimeter, and fluorescence spectra were collected every 10 min from 400 to 600 nm. Analysis was completed by comparing the fluorescence intensity at the 5 h timepoint (I_f) to the fluorescence intensity at t_0 (I_0)

at 460 nm. Each measurement was run in triplicate and reported values are the average of these runs, error bars are represented by the standard error of the mean.

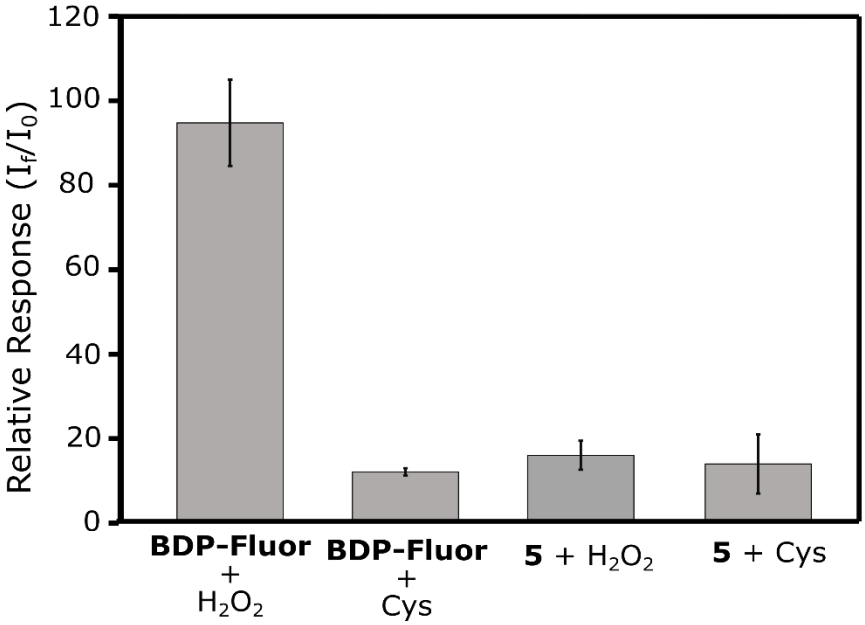

Figure S22. Relative response (I_f / I_0) of **BDP-Fluor** and control fluorescent compound **5** (3.3 μM) to H_2O_2 and Cys (both 330 μM) measured at 460 nm. The increased response of **BDP-Fluor** relative to other potential triggers (Figure 3) is a result of nucleophilic attack of the Cys thiol on the aryl ester bond, liberating 7-hydroxycoumarin. As compound **5** does not have the oxidative-labile Bpin moiety, it does not respond to H_2O_2 to the same degree as **BDP-Fluor**, but it shows an equal response to Cys. These results indicate that nucleophilic attack by cysteine likely causes release of the 7-hydroxycoumarin, leading to a slightly increased response of **BDP-Fluor** to Cys.

NMR kinetics analysis of **BDP-NAC**

For ^{1}H NMR experiments, **BDP-NAC** (10 mg, 0.024 mmol) or **BDP-Control** (10 mg, 0.036 mmol) was added to a vial and dissolved in DMSO-d_6 (900 µL). Upon full dissolution, D_2O (100 µL) was added to the vial, and the solution was transferred to an NMR tube. A ^{1}H NMR spectrum was collected at this time, which served as the zero time point (t_0). After the addition of H_2O_2 solution (20 µL, 30 wt.% in H_2O), ^{1}H NMR spectra were recorded at various time intervals. The kinetics of **BDP-NAC** oxidation by H_2O_2 is displayed as a pseudo first-order kinetics plot, where p represents the disappearance of the aryl peaks attributed to **BDP-NAC** (a, a'). Concentration of BDP-NAC (relative to concentration at t_0) was obtained by normalizing the integral values of a + a' to the integral values at t_0, relative to the NAC methyl peak. The data were then fitted to a first-order kinetics equation given by $y = 1 - e^{-kt}$, where k is the slope and t is time.

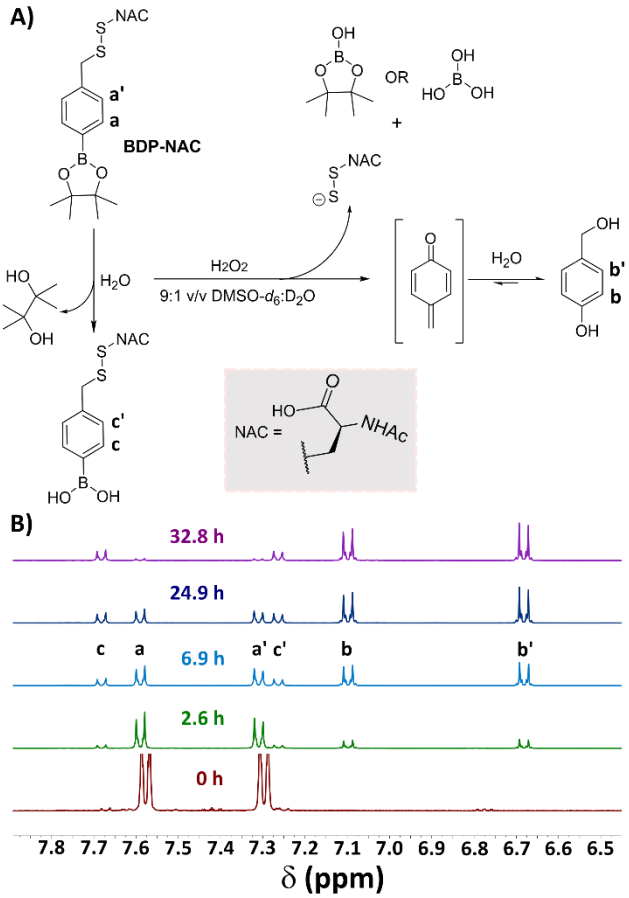

Figure S23. A) Proposed reaction scheme for persulfide release from **BDP-NAC**. B) Stacked ^{1}H NMR spectra showing the formation of *p*-hydroxybenzyl alcohol. Conditions: **BDP-NAC** (10 mg/mL) in 90% (v/v) DMSO-d_6/D_2O with 10-fold molar excess of H_2O_2.

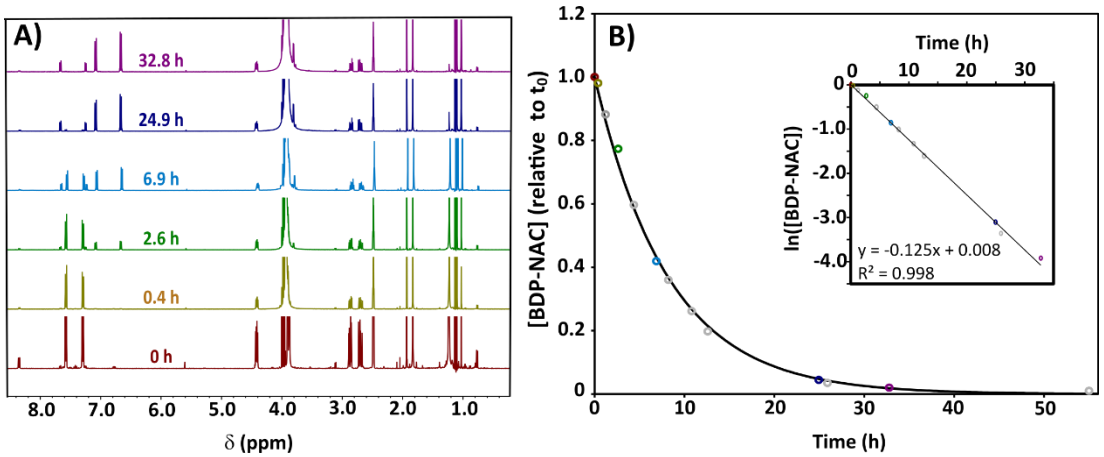

Figure S24. (A) Expanded time dependent ^{1}H NMR spectra and (B) pseudo first-order kinetics plot of **BDP-NAC** (24.3 mM) in 90% (v/v) DMSO-d_6/D_2O with 10-fold excess of H_2O_2. Data points denoted in gray do not have a representative NMR spectrum shown. Inset shows pseudo-first order kinetics plot where [BDP-NAC] was determined by normalizing the data from each time point to the integral value of the BDP-NAC aryl peaks (a, a') of the t_0 time point. The half-life for this reaction was calculated to be 7.5 ± 0.3 h based on the slope of the pseudo-first order kinetics plot ($t_{1/2} = \ln(2)/k_{obs}$).

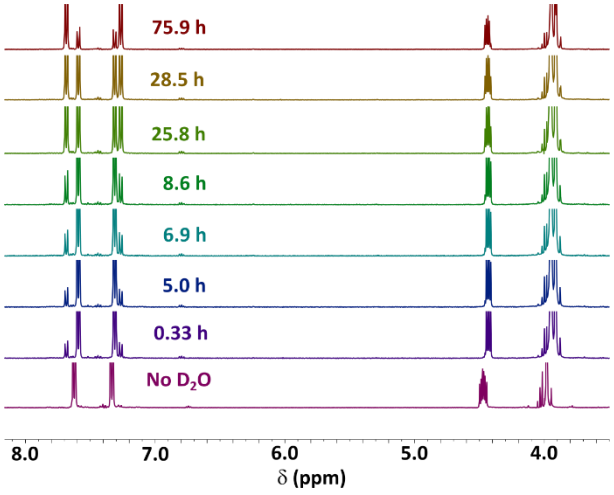

Figure S25. Time dependent ^{1}H NMR spectra of **BDP-NAC** in 90% (v/v) DMSO-d_6/D_2O without addition of H_2O_2. Hydrolysis of the Bpin moiety was followed by monitoring the change in peaks

in the aryl region (7.6-7.2 ppm) and the alkyl region (1.1-0.9 ppm). A half-life of hydrolysis was calculated to be 33 h by following the disappearance of the **BDP-NAC** aryl peaks and fitting these data to a pseudo-first order kinetic equation.

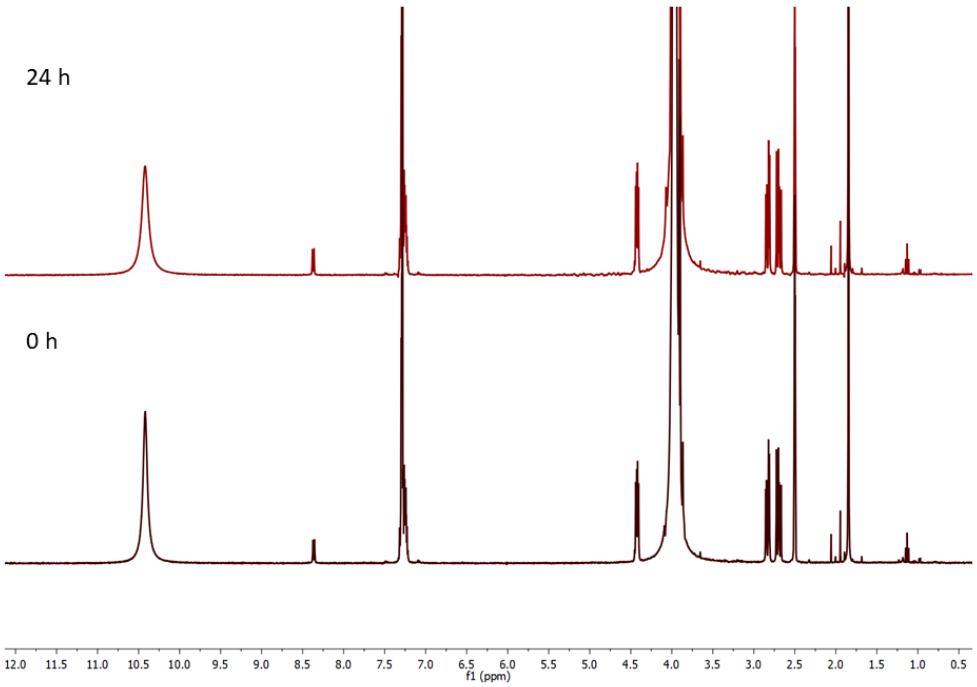

Figure S26. Time dependent ^{1}H NMR spectra of **BDP-Control** in 90% (v/v) DMSO-d_6/D_2O immediately following the addition of H_2O_2 (10-fold excess) (black spectrum), and 24 h after addition of H_2O_2 (red spectrum). No changes in the NMR spectra were observed, indicating that H_2O_2 does not cause persulfide release without the Bpin triggering moiety.

Cell Viability Assays

For experiments, H9C2 cells were plated at a density of 5000 cells per well in a volume of 180 µL serum-containing media per well in a 96-well plate and cultured for 24 h before treatment. Cell viability data was analyzed using a BioTek Synergy Mx plate reader (BioTek, Winooski, VT).

Cell viability assays were performed by using Cell counting kit 8 (CCK-8, Dojindo, Rockville, Md.). H9C2 cardiomyocytes in a 96-well plate (n = 5 for each group) were treated with various concentrations of **BDP-NAC**, GYY4137, Na_2S, **BDP-Control**, 4-(hydroxymethyl)benzeneboronic acid pinacol ester, *N*-acetylcysteine, or any combination indicated (20 μL) with or without H_2O_2 (200 μM) for 1 h in serum-containing media. For treatment groups containing **BDP-NAC**, **BDP-Control**, 4-(hydroxymethyl)benzeneboronic acid pinacol ester, or NAC, DMSO was used as a vehicle to enable full solubility of these compounds in the stock solutions. Final concentration of DMSO in these treatment groups is 0.2 v/v % in DMEM. After incubation with the aforementioned compounds for 1 h, the cardiomyocytes were then washed with 1X PBS buffer three times. After washing, fresh DMEM (100 μL) without FBS and 10 v/v % CCK-8 solution was added, and the cells were incubated for 3 h. Absorbance was recorded then at 450 and 750 nm. Data were graphed using GraphPad InStat, version 3 (GraphPad Software, Inc., San Diego, CA). For data analysis, multiple comparisons were done using one-way ANOVA followed by Student-Newman-Keuls post-hoc tests for multiple pairwise examinations. Changes were identified as significant if p was less than 0.05. Mean values are reported together with the standard error of mean (SEM) representing the combination of 2–3 different experimental runs (n = 10–15 for each treatment group).

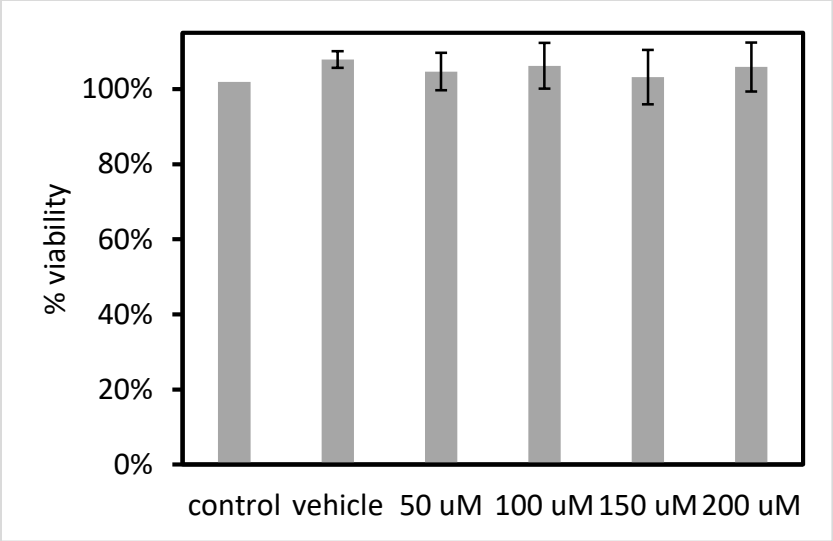

Figure S27. H9C2 cardiomyocyte viability after treatment with **BDP-NAC** (50-200 μM) without H_2O_2.

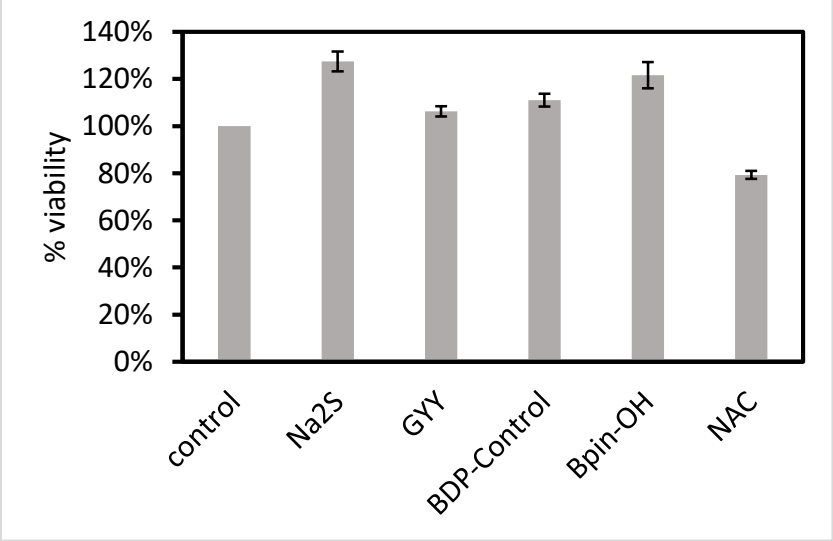

Figure S28. H9C2 cardiomyocyte viability after treatment with compound Na_2S, GYY4137, **BDP-Control**, Bpin-OH, and NAC (200 μm) without H_2O_2.

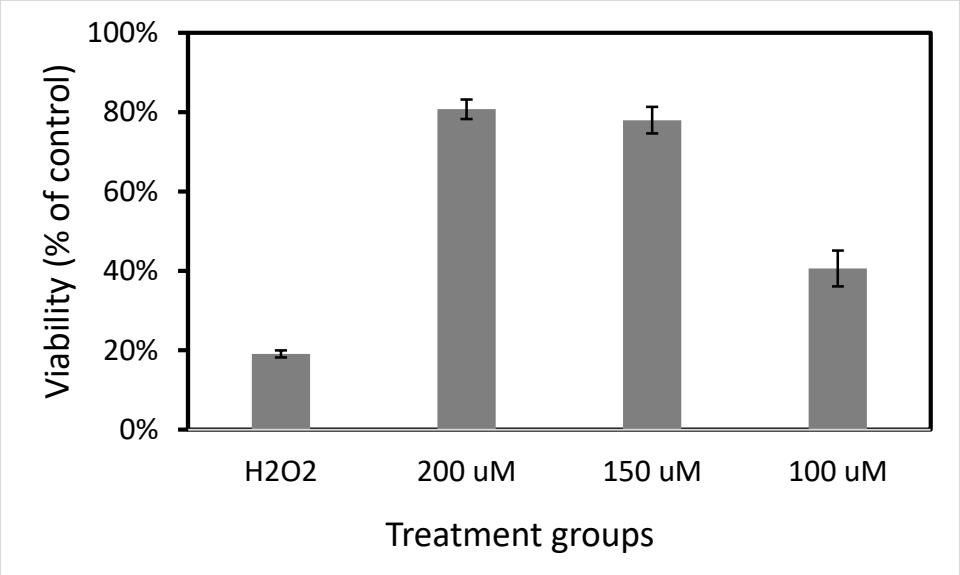

Figure S29. H9C2 cardiomyocyte viability after treatment with **BDP-NAC** (100-200 μM) concurrently with 100 μM H_2O_2 for 2 h.

Chapter 3: Alleviating cellular oxidative stress through treatment with superoxide-triggered persulfide prodrugs

Adapted with permission from: Wang, Y., Dillon, K. M., et al. "Alleviating cellular oxidative stress through treatment with superoxide-triggered persulfide prodrugs" Angewandte Chemie **59**: 16698-16704.

3.1. Authors

Yin Wang[#,§], Kearsley M. Dillon[#,§], Zhao Li[§], Ethan W. Winckler[§], and John B. Matson*[§]

§Department of Chemistry, Virginia Tech Center for Drug Discovery, and Macromolecules Innovation Institute, Virginia Tech, Blacksburg, Virginia 24061, United States

#These authors contributed to this work equally

3.2. Abstract

Overproduction of superoxide anion ($O_2^{\cdot -}$), the primary cellular reactive oxygen species (ROS), is implicated in various human diseases. To reduce cellular oxidative stress caused by overproduction of superoxide, we developed a compound that reacts with $O_2^{\cdot -}$ to release a persulfide (RSSH), a type of reactive sulfur species related to the gasotransmitter hydrogen sulfide (H_2S). Termed SOPD-NAC, this persulfide donor reacts specifically with $O_2^{\cdot -}$, decomposing to generate *N*-acetyl cysteine (NAC) persulfide. To enhance persulfide delivery to cells, we conjugated the SOPD motif to a short, self-assembling peptide (Bz-CFFE-NH_2) to make a superoxide-responsive, persulfide-donating peptide (SOPD-Pep). Both SOPD-NAC and SOPD-Pep delivered persulfides/H_2S to H9C2 cardiomyocytes and lowered ROS levels as confirmed by quantitative *in vitro* fluorescence imaging studies. Additional *in vitro* studies on RAW 264.7 macrophages showed that SOPD-Pep

mitigated toxicity induced by phorbol 12-myristate 13-acetate (PMA) more effectively than SOPD-NAC and several control compounds, including common H_2S donors.

3.3. Introduction

Superoxide anion ($O_2^{\bullet-}$), the product of a one-electron reduction of O_2 generated primarily in mitochondria during cellular respiration, is a reactive oxygen species (ROS) implicated in various diseases related to mitochondrial dysfunction.[1] While a minimum level of $O_2^{\bullet-}$ is essential for cell survival, excessive production leads to damage to proteins, lipids, and nucleic acids.[2] Beyond the harm that superoxide can inflict directly, it is also a key precursor for other even more damaging ROS; for example, it reacts with nitric oxide (NO) to produce peroxynitrite ($ONOO^-$), a powerful and destructive oxidant.[3] Superoxide dismutases, enzymes that deactivate $O_2^{\bullet-}$, exist in nearly all cells and have evolved over 2 billion years to limit the extent of cell damage from $O_2^{\bullet-}$.[4] Despite this cellular defense against $O_2^{\bullet-}$, its overproduction is ascribed to many oxidative stress-induced diseases, including degenerative disorders, ischemia-reperfusion (IR) injury resulting from surgery, cardiovascular disease, and some cancers (e.g., prostate cancer).[5] Given the roles of $O_2^{\bullet-}$ in both cell signaling and disease, turn-on fluorescence probes capable of detecting $O_2^{\bullet-}$ have been developed.[6-7] Surprisingly, no compounds exist that react specifically with $O_2^{\bullet-}$ to both reduce $O_2^{\bullet-}$ levels and release a molecule capable of further alleviating oxidative stress.

One signaling species that may be capable of regulating redox balance in cells with high levels of $O_2^{\bullet-}$ is a persulfide (RSSH).[8] Persulfides are related to the signaling gas (gasotransmitter) hydrogen sulfide (H_2S), a reactive sulfur species crucial to many (patho)physiological processes.[9] Because of their potentially dominant roles in H_2S-related signaling pathways, combined with their ability to persulfidate biological targets (conversion of RSH into RSSH)

under conditions where H_2S cannot, persulfides have recently gained attention.[10] Key reactivities of persulfides are their nucleophilicity and reducing abilities; both small molecule and protein-bound persulfides regulate redox signaling through direct and indirect routes.[11] For example, glutathione persulfide quickly scavenges the biological oxidant H_2O_2,[12] and persulfidation of p66Shc, a protein involved in mitochondrial redox signaling, inhibits mitochondrial ROS production.[13] Therefore, we envisioned that a persulfide donor that could be triggered by $O_2^{\bullet-}$ might be a powerful tool for reducing its deleterious effects. Beyond decreasing $O_2^{\bullet-}$ levels, a superoxide-triggered persulfide donor might help uncover the roles and connections among $O_2^{\bullet-}$ and persulfides in the reactive species interactome.[4]

The difficulty in developing persulfide donors comes from the instability of persulfides, which react quickly with various species, including themselves, oxidants, and free thiol groups.[14] Therefore, protected persulfides (i.e., prodrugs), in which a specific stimulus activates the removal of the protecting group to release the persulfide, are needed to achieve controlled delivery. Accordingly, persulfide donors exist that respond to biologically relevant stimuli, including enzymes,[15-17] light,[18] and H_2O_2.[19-20] We envisioned that a superoxide-triggered persulfide donor could be constructed by linking a diphenylphosphinate ester, which can be oxidized by $O_2^{\bullet-}$ in a bond cleaving reaction,[21] to a 4-($RSSCH_2$)phenoxy group. In a cascade of reactions, $O_2^{\bullet-}$ should react at phosphorous to cleave the 4-($RSSCH_2$)phenoxy group, which would then undergo a 1,6-elimination reaction to reveal a persulfide anion (RSS^-). Such a persulfide donor would serve two functions—capturing $O_2^{\bullet-}$ and releasing a persulfide. Additionally, we aimed to develop a delivery system for this donor that would enhance its water solubility, bioavailability, and provide a potential mechanism for eventual targeting to specific cells or tissues. Therefore, we detail here our efforts to develop a small molecule superoxide-triggered persulfide donor that could be used

on its own and could also be easily conjugated to a self-assembling peptide-based delivery vehicle to improve solubility and bioactivity.

3.4. Results and Discussion

We chose the diphenylphosphinate group as the stimuli-responsive unit because of its ability to selectively react with $O_2^{\bullet -}$.[21] We conjugated this group to *N*-acetyl cysteine (NAC), which we selected because of its powerful antioxidant capability[20, 22-24] and its free thiol group for conjugation to a thiol-containing diphenylphosphinate. Synthesis was carried out as shown in Scheme 1A. Briefly, diphenylphosphinic chloride was treated with *p*-cresol under basic conditions. The resulting tolyl diphenylphosphinate (**1**) was then brominated by using NBS to generate a benzyl bromide (**2**). Bromide displacement was achieved by treating compound **2** with thiourea followed by hexylamine, resulting in a benzyl thiol (**3**). Finally, we treated thiol **3** with the activated disulfide of NAC (**NACpyDS**) in a disulfide exchange reaction to afford the target persulfide donor termed **SOPD-NAC** (SOPD = **s**uper**o**xide-triggered **p**ersulfide **d**onor). A proposed mechanism for persulfide release is shown in Scheme 1B.

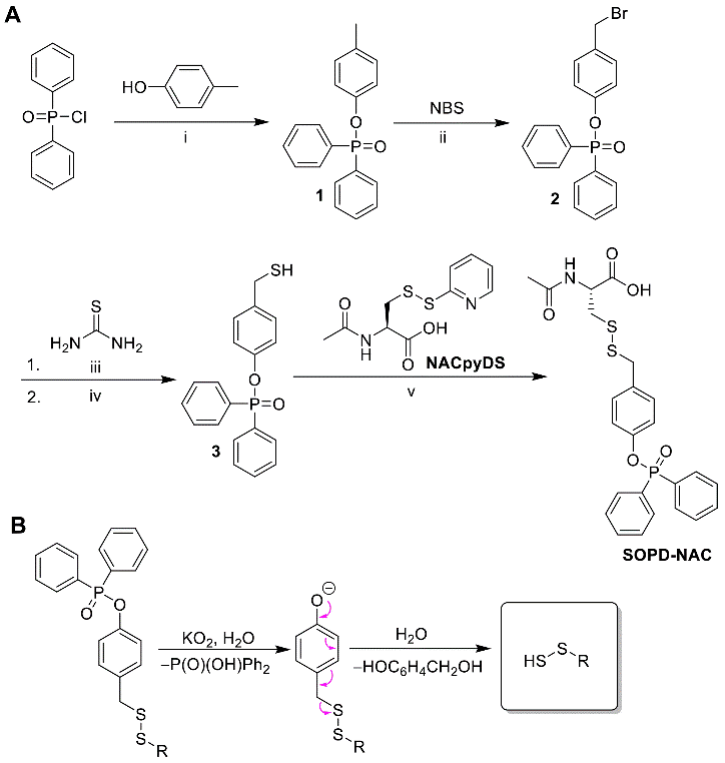

Scheme 1. A) Synthesis of **SOPD-NAC**. Reaction conditions: i) NEt_3, DMAP, THF, 16 h, rt, 82% yield; ii) AIBN, C_6H_6, 16 h, reflux, 91% yield; iii) CH_3OH, 16 h, rt; iv) hexylamine, $CHCl_3$, 24 h, rt, 90% yield; v) CH_2Cl_2, 24 h, rt, 56% yield. B) Proposed mechanism of superoxide-triggered persulfide release from **SOPD-NAC** (R=NAC).

One promising strategy to address limitations in prodrug solubility and bioavailability is appending drugs or prodrugs to self-assembling peptides. Due to their inherent biodegradability and biocompatibility in most contexts, peptides capable of self-assembly into nanostructures and/or hydrogels are powerful materials for biomedical applications.[25] Previously, we have shown that conjugation of H_2S-donating *S*-aroylthiooximes (SATOs) to short peptides not only extended H_2S release profiles, but also modulated release behaviors as a result of their different self-assembled

morphologies.[26-30] In this regard, conjugating SOPD to a self-assembling peptide scaffold would endow the resultant conjugate with new properties, including improved water solubility and the potential for cell targeting.

Therefore, we conjugated 4-(mercaptomethyl)phenyl diphenylphosphinate to a tetrapeptide Bz-Cys-Phe-Phe-Glu (Bz-CFFE) (Bz = benzoyl) through a disulfide linkage (Scheme 2A). In this two-step synthesis, the 2-thiopyridyl-activated disulfide of Bz-CFFE was prepared and then treated with 4-(mercaptomethyl)phenyl diphenylphosphinate to afford the target superoxide responsive peptide (**SOPD-Pep**). We also synthesized a control peptide termed **SOPD-Pep-Cont**, which included the same peptide sequence conjugated to the diphenylphosphinate group through a thioether linkage instead of a disulfide. **SOPD-Pep-Cont** was synthesized in one step by reacting Bz-CFFE with 4-(bromomethyl)phenyl diphenylphosphinate (Scheme 2B). We chose Bz-CFFE not only because of the free thiol group in the sequence, but also because of its propensity to form discrete one-dimensional nanostructures.[31-32]

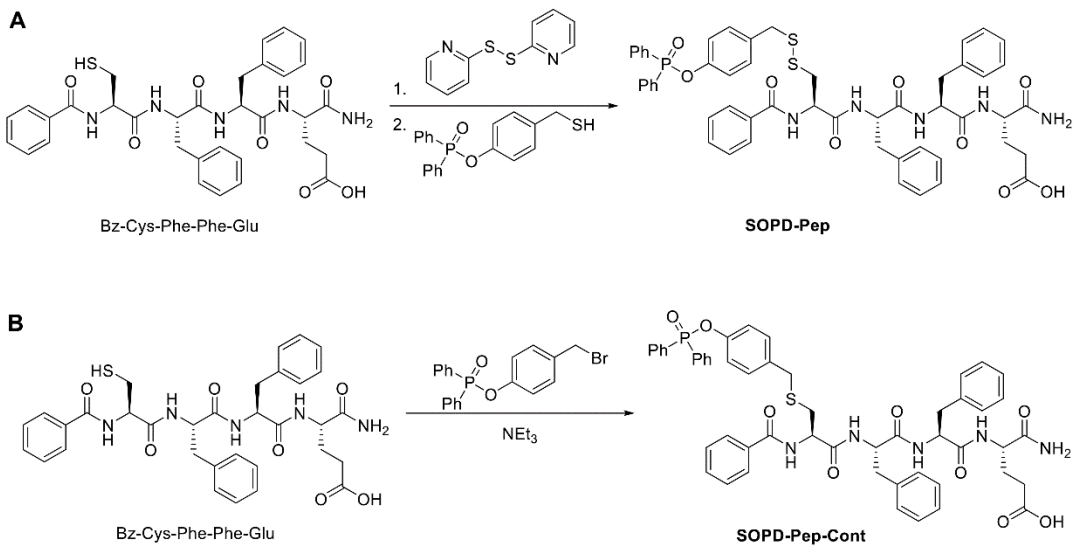

Scheme 2. A) Synthesis of **SOPD-Pep** and B) **SOPD-Pep-Cont**

Next, we investigated whether **SOPD-NAC** and **SOPD-Pep** could specifically react with $O_2^{\bullet-}$ to release persulfides by 1,6-elimination (self-immolation), a strategy used in several ROS-triggered H_2S donors.[33-37] Because very few persulfide-specific chemical probes exist, we first evaluated persulfide release by relying on the ability of persulfides to rapidly react with cysteine (Cys) to generate H_2S.[10] To this end, we evaluated the reactivity of **SOPD-NAC** and **SOPD-Pep** with several potential triggers by monitoring the fluorescence increase of an H_2S-selective fluorescent probe WSP-2 reported previously[38] (Figures S10 and 1A). The experiment probed whether persulfide donors react with the triggers by monitoring the fluorescence intensity at λ_{em}=455 nm, the characteristic wavelength of 7-hydroxycoumarin (Figure 1B).

The results revealed that neither **SOPD-NAC** nor **SOPD-Pep** alone showed any fluorescence increase in the absence of a trigger (control groups in Figures 1A (**SOPD-Pep**) and S10 (**SOPD-NAC**)). However, adding excess Cys and $O_2^{\bullet-}$ led to a 16-fold and 12-fold increase in fluorescence intensity for **SOPD-Pep** and **SOPD-NAC**, respectively (red bars, Figures 1A and S10). Incubating **SOPD-NAC** or **SOPD-Pep** with either Cys alone or $O_2^{\bullet-}$ alone generated a limited increase in fluorescence intensity, significantly lower than that of the treatment group containing both triggers. These results implied that H_2S liberation from **SOPD-NAC** or **SOPD-Pep** requires both Cys and $O_2^{\bullet-}$. Consistent with previous reports on superoxide-responsive probes,[6] other common reactive sulfur, oxygen, and nitrogen species (RSONS)—hypochlorite (ClO^-), peroxynitrite ($ONOO^-$), sulfate (SO_4^{2-}), and glutathione (GSH)—failed to trigger release of H_2S. More importantly, H_2O_2 did not enhance the fluorescence intensity, suggesting that **SOPD-NAC** and **SOPD-Pep** are selective to $O_2^{\bullet-}$. In summary, this screening assay validated that **SOPD-NAC** and **SOPD-Pep** possess good selectivity for $O_2^{\bullet-}$ and that both persulfide

donors could release H_2S in the presence of Cys (Figure 1B). For direct verification, we also confirmed persulfide release through mass spectrometry (Figure S11).

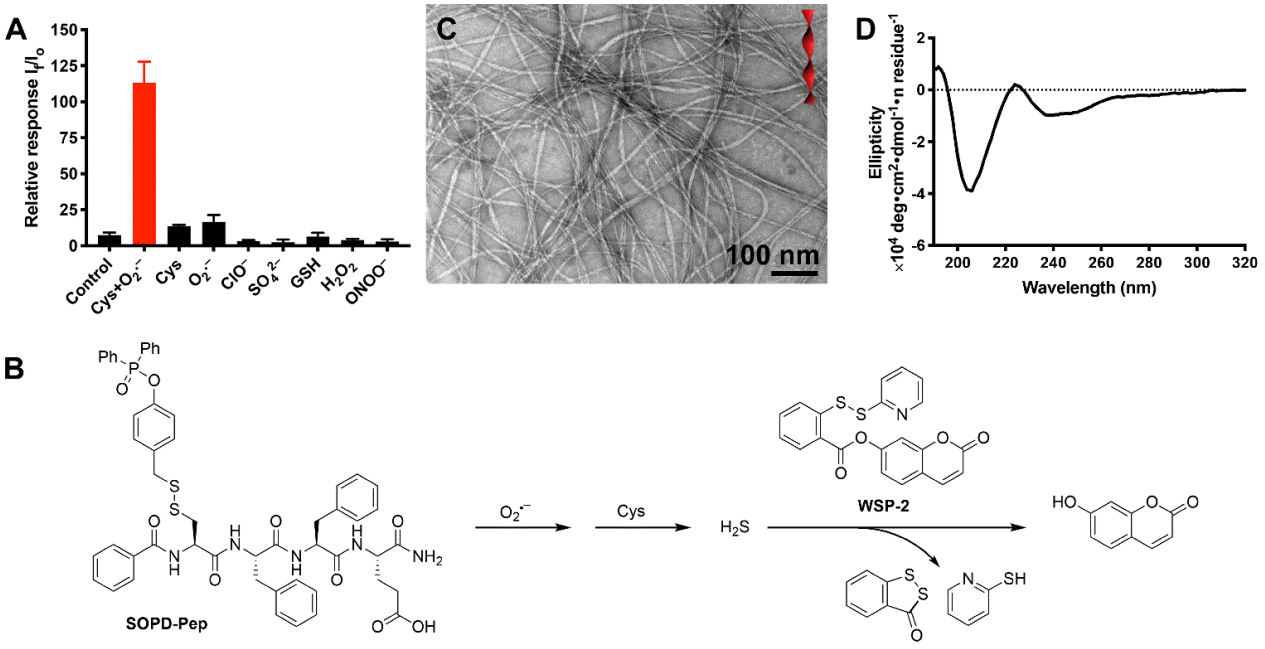

Figure 1. (A) Relative response of 1 mM **SOPD-Pep** and 50 μM WSP-2 to each potential trigger (4 mM) or combination of triggers or control (no trigger added) represented as the ratio of the final fluorescence intensity (I_f) after 30 min to the initial fluorescence intensity (I_0), showing an increased selectivity for Cys + $O_2^{\bullet -}$ over other potential triggers (KO_2 was used as the superoxide source). The results were expressed as the mean ± SD (n = 3). (B) Proposed mechanism for fluorescence turn-on of WSP-2 by H_2S released from **SOPD-Pep** in the presence of Cys and $O_2^{\bullet -}$. (C) Conventional TEM characterization of twisted nanoribbons formed by **SOPD-Pep** in 10 mM phosphate buffer (pH=7.4). The concentration was 100 μM, diluted from 1 mM pre-assembled stock solution. The TEM grid was stained with 2 wt % uranyl acetate prior to imaging. (D) CD spectrum of **SOPD-Pep** in 10 mM phosphate buffer (pH=7.4) at 100 μM.

Given the amphiphilic nature of **SOPD-Pep**, we next studied the morphology of **SOPD-Pep** after dissolution in 10 mM phosphate buffer (pH 7.4) by conventional transmission electron microscopy (TEM). TEM imaging showed that **SOPD-Pep** self-assembled into twisted nanoribbons as indicated by the varying thickness and grayscale intensity (Figure 1C). Average widths were 10 ± 2 nm, and lengths were on the scale of a few micrometers. The molecular packing within these nanoribbons was then assessed by circular dichroism (CD) spectroscopy (Figure 1D). CD revealed that **SOPD-Pep** had a primarily random coil structure with some β-sheet contribution. The minimum at 206 nm may result from π−π interactions of the aromatic side chains in nanostructures and the distortion of β-sheets, which have been previously observed in aromatic peptide amphiphile systems.[39-40] The negative peak near 250 nm was attributed to the absorption of diphenylphosphinate group.

We then focused on biological applications of **SOPD-NAC** and **SOPD-Pep**. Cell viability assays indicated that both **SOPD-NAC** and **SOPD-Pep** were nontoxic to H9C2 cardiomyocytes, a widely used cell line for testing how compounds may affect heart function, at concentrations up to 200 μM (Figure S15). Fluorescence microscopy was then used to investigate whether H_2S could be liberated from **SOPD-NAC** and **SOPD-Pep** and delivered to cells in the presence of $O_2^{\bullet -}$. We used L-buthionine-(*S*,*R*)-sulfoximine (BSO), which induces oxidative stress in cells by depleting glutathione (GSH),[41] to generate superoxide *in vitro*.[42] WSP-5,[38] an H_2S-selective fluorescent probe, was used to monitor H_2S accumulation in H9C2 cells. No additional Cys was added, relying instead on endogenous thiols to convert persulfides into detectable H_2S.

As expected, BSO alone provided a negligible fluorescent signal (Figure 2, first row). Treating cells with **SOPD-NAC** or **SOPD-Pep** without BSO generated a weak fluorescent signal. This most likely resulted from a small amount of H_2S liberated from **SOPD-NAC** or **SOPD-Pep** triggered by endogenous $O_2^{\bullet -}$ within cells (Figure 2, second and third rows). Co-incubation of **SOPD-NAC** with BSO generated a slightly stronger signal compared to **SOPD-NAC** alone (Figure 2, fourth row), indicating some amount of H_2S production from this small molecule persulfide donor. In sharp contrast, co-incubation of **SOPD-Pep** nanoribbons and BSO produced a significant increase in WSP-5 fluorescence (Figure 2, fifth row), demonstrating that **SOPD-Pep** can be successfully activated to release H_2S *in vitro*. Given the identical conditions and equimolar amounts of **SOPD-NAC** and **SOPD-Pep**, the difference in H_2S-release levels likely stems from different cellular accumulations of these two persulfide donors. We speculate that **SOPD-Pep** enters and remains in cells to a greater extent than **SOPD-NAC** due to its nanoscale size, a phenomenon that has been observed for other self-assembled peptide drug-delivery vehicles.[43-45]

Given that both **SOPD-NAC** and **SOPD-Pep** are triggered by $O_2^{\bullet -}$ *in vitro*, we then asked whether these persulfide donors could decrease ROS production. BSO was used as a superoxide inducer with dihydroethidium (DHE) as an ROS-sensing fluorescent probe.[46] As shown in row 1 of Figure 3, the control group (H9C2 cells without any treatments) showed a dim red fluorescent signal, indicating that a certain amount of ROS was naturally generated within H9C2 cells as a product of normal metabolism of oxygen, consistent with previous reports.[47] However, after treatment with BSO, the red fluorescent signal from DHE increased, implying that ROS had accumulated in cells (Figure 3, second row). We found that H9C2 cells co-incubated with BSO and **SOPD-Pep-Cont** showed a lower red fluorescence compared to those treated only with BSO

because **SOPD-Pep-Cont** possesses a diphenylphosphinate group that scavenges $O_2^{\bullet -}$, but it lacks the capacity to release a persulfide (Figure 3, third row). Co-incubation of BSO with persulfide donors **SOPD-NAC** or **SOPD-Pep** decreased the red fluorescence signal (Figure 3 fourth and fifth rows), with **SOPD-Pep** showing a similar fluorescence intensity to the control group. These results agree with the H_2S production studies (Figure 2), indicating that persulfides released from **SOPD-NAC** and **SOPD-Pep** suppress the production of ROS, and that **SOPD-Pep** suppresses more effectively than **SOPD-NAC**.

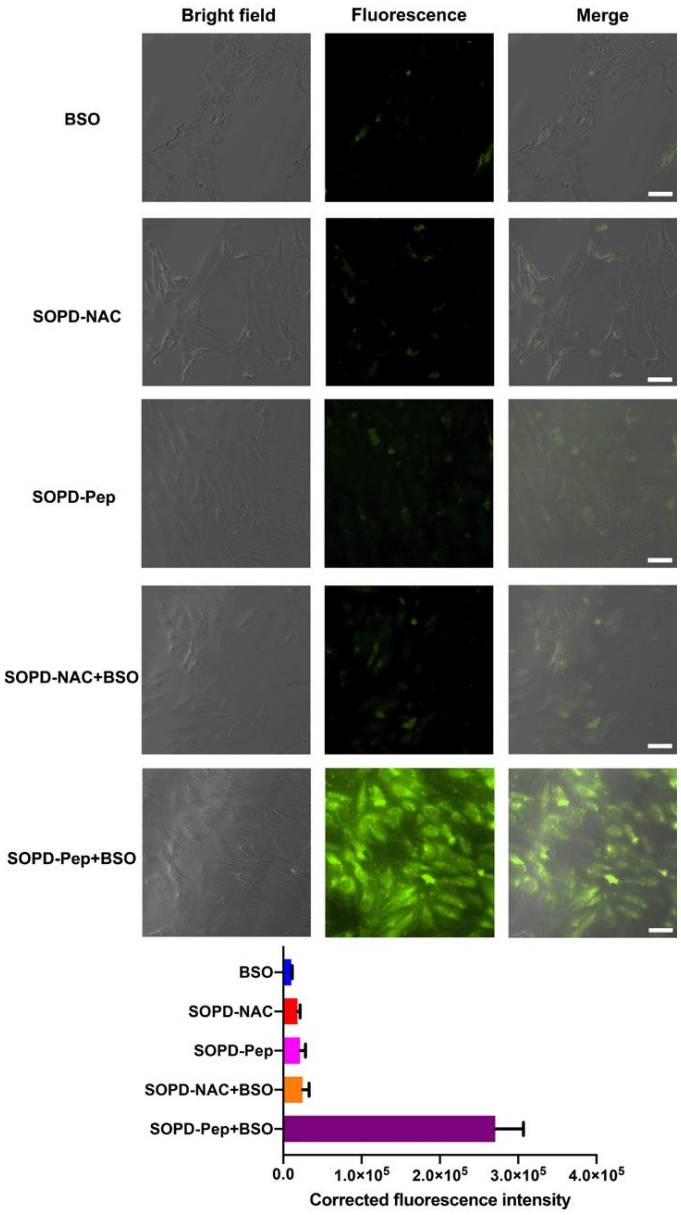

Figure 2. Bright field, fluorescence, and merged images showing fluorescence in H9C2 cells pre-incubated with **SOPD-NAC** or **SOPD-Pep** (200 μM) for 6 h, and subsequently treated with WSP-5 (50 μM) and BSO (5 mM) or an equal volume of PBS for 30 min. Cells were then washed, and fluorescence images were taken in PBS. Scale bars are 50 μm. Averaged fluorescence intensities of these five respective treatment groups were quantified by ImageJ (cell counts are > 30 for each group from three separate wells).

As **SOPD-NAC** and **SOPD-Pep** both deliver persulfides/H_2S into cells and further quench ROS production, we next explored their anti-inflammatory activities on RAW 264.7 macrophages. RAW 264.7 cells were chosen as a model because they generate a considerable amount of $O_2{\cdot}^-$ when incubated with phorbol 12-myristate 13-acetate (PMA).[36, 48] H_2S alleviates inflammation caused by ROS,[49-50] but the protective capacity of persulfide donors has not been tested in cells treated with PMA. Thus, we envisioned that **SOPD-NAC** and **SOPD-Pep** might rescue RAW 264.7 macrophages from induced oxidative stress.

First, we demonstrated that both **SOPD-NAC** and **SOPD-Pep** were nontoxic to RAW 264.7 cells at concentrations up to 200 μM (Figure S16). In contrast, PMA induced significant cytotoxicity at concentrations as low as 1 μg/mL (Figure 4A). In treatment studies, RAW 264.7 cells were pretreated with PMA for 1 h, a period consistent with previous reports,[36] then **SOPD-Pep** was added without removing PMA solution, and cells were subsequently cultured for another 4 h before analyzing viability. Compared to the PMA-only treatment group, cell viability increased significantly when cells were co-incubated with **SOPD-Pep** and PMA (Figure 4A). For example, exposure of PMA to cells at 2 μg/mL decreased viability to 51% while viability increased to 81% when co-incubated with 100 μM **SOPD-Pep**.

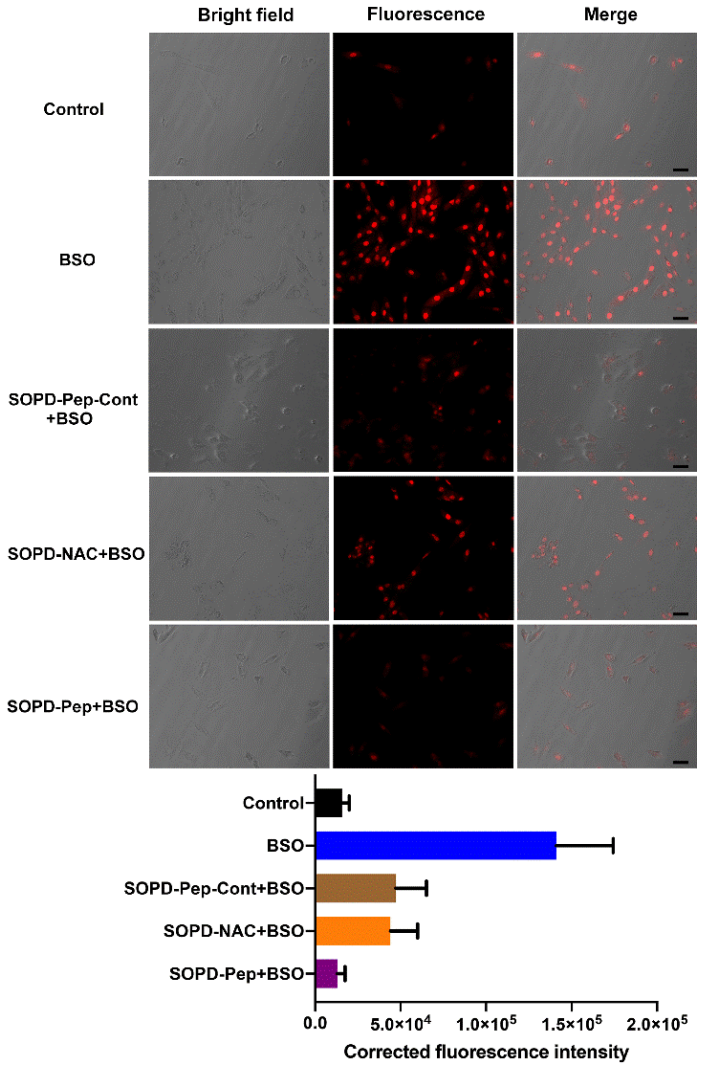

Figure 3. Bright field, fluorescence, and merged images showing fluorescence in H9C2 cells pre-incubated with **SOPD-Pep-Cont** or **SOPD-NAC** or **SOPD-Pep** (200 μM) for 6 h and then treated with DHE (10 μM) and BSO (5 mM) or an equal volume of DMSO for 30 min. Cells were then washed, and fluorescence images were taken in PBS. Scale bars are 50 μm. Averaged fluorescence intensities of these five respective treatment groups were quantified by ImageJ (cell counts are > 30 for each group from three separate wells).

To further ensure that persulfide release was responsible for imparting protection to the macrophages in the presence of PMA, several control studies were carried out (Figure 4B). **SOPD-NAC** showed a moderate ability to rescue cells; this result may be related to a small amount of persulfide/H_2S accumulated within cells, consistent with results shown in Figures 2 and 3. **SOPD-Pep-Cont** showed a similar cell protective ability to **SOPD-NAC**. This small but significant protective capacity likely resulted from the diphenylphosphinate group scavenging $O_2^{\bullet-}$ and, thus, lowering intracellular ROS levels. Under the same conditions, we also compared **SOPD-Pep** to sodium sulfide (Na_2S), a fast-releasing H_2S donor, and GYY4137,[51] a slow-releasing H_2S donor. Na_2S had limited ability to rescue cells, while GYY4137 had no effect. Therefore, **SOPD-Pep** more effectively rescued cells than did Na_2S and GYY4137.

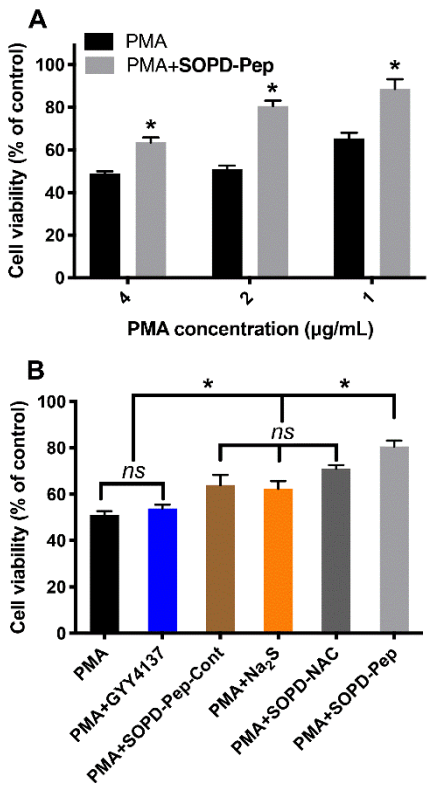

Figure 4. (A) Cell viability of RAW 264.7 macrophage cells pretreated with different concentrations of PMA for 1 h followed by exposure to **SOPD-Pep** (100 µM) for 4 h. * indicates $p < 0.01$ vs PMA-only groups. (B) Cell viability of RAW 264.7 macrophage cells pretreated with PMA (2 µg/mL) for 1 h followed by exposure to different groups (100 µM) for 4 h: GYY4137, **SOPD-Pep-Cont**, Na_2S, **SOPD-NAC**, and **SOPD-Pep**. * indicates $p < 0.01$. Error bars indicate standard deviation of three separate experiments with five replicates per experiment. Group comparisons are indicated as determined by a one-way analysis of variance (ANOVA) with a Student−Newman−Keuls comparisons *post-hoc* test.

3.5. Conclusion

In summary, we report a new dual-acting compound that scavenges $O_2^{\bullet -}$ and then decomposes to release a persulfide. This motif, based on a small molecule (**SOPD-NAC)**, was conjugated to a self-assembling peptide (**SOPD-Pep**). In the presence of $O_2^{\bullet -}$, both donors released persulfides, decreasing ROS levels in cells. Further, **SOPD-Pep** showed pronounced anti-inflammatory activity on macrophages, greater than **SOPD-NAC**, **SOPD-Pep-Cont** (a control peptide incapable of persulfide release), and common H_2S donors. These results highlight the potential of **SOPD-NAC** and **SOPD-Pep** for persulfide-based therapies and demonstrate their power to initiate complex changes in cell behavior. Broadly, this dual superoxide-scavenging–persulfide-donating scaffold could potentially find use to regulate the redox balance within cells, which may alleviate oxidative stress-induced diseases caused by upregulation of $O_2^{\bullet -}$.

3.6. Acknowledgements

This work was supported by the National Science Foundation (DMR-1454754) and the National Institutes of Health (R01GM123508). We also acknowledge the Dreyfus foundation for supporting these studies through a Camille Dreyfus Teacher-Scholar Award to J.B.M. We acknowledge Prof. Padmavathy Rajagopalan (Virginia Tech) for sharing RAW 264.7 macrophage cells, Prof. Mark Van Dyke (Virginia Tech) and Prof. Amanda J. Morris (Virginia Tech) for instrumental assistance, Dr. Chadwick R. Powell for synthesizing GYY4137, and Samantha J. Scannelli and Prof. Richard D. Gandour for careful readings of the manuscript. The authors also acknowledge use of facilities within the Nanoscale Characterization and Fabrication Laboratory at Virginia Tech.

3.7. References

1. Fridovich, I., Superoxide anion radical, superoxide dismutases, and related matters. *J. Biol. Chem.* **1997,** *272* (30), 18515-18517.

2. Bandyopadhyay, U.; Das, D.; Banerjee, R. K., Reactive oxygen species: Oxidative damage and pathogenesis. *Curr. Sci.* **1999,** *77* (5), 658-666.

3. Szabo, C.; Ischiropoulos, H.; Radi, R., Peroxynitrite: Biochemistry, pathophysiology and development of therapeutics. *Nat. Rev. Drug Discov.* **2007,** *6* (8), 662-680.

4. Cortese-Krott, M. M.; Koning, A.; Kuhnle, G. G. C.; Nagy, P.; Bianco, C. L.; Pasch, A.; Wink, D. A.; Fukuto, J. M.; Jackson, A. A.; van Goor, H.; Olson, K. R.; Feelisch, M., The reactive species interactome: evolutionary emergence, biological significance, and opportunities for redox metabolomics and personalized medicine. *Antioxid. Redox Signal.* **2017,** *27* (10), 684-712.

5. Pacher, P.; Beckman, J. S.; Liaudet, L., Nitric oxide and peroxynitrite in health and disease. *Physiol. Rev.* **2007,** *87* (1), 315-424.

6. Gao, X. Y.; Feng, G. X.; Manghnani, P. N.; Hu, F.; Jiang, N.; Liu, J. Z.; Liu, B.; Sun, J. Z.; Tang, B. Z., A two-channel responsive fluorescent probe with AIE characteristics and its application for selective imaging of superoxide anions in living cells. *Chem. Commun.* **2017,** *53* (10), 1653-1656.

7. Zhang, J. J.; Li, C. W.; Zhang, R.; Zhang, F. Y.; Liu, W.; Liu, X. Y.; Lee, S. M. Y.; Zhang, H. X., A phosphinate-based near-infrared fluorescence probe for imaging the superoxide radical anion in vitro and in vivo. *Chem. Commun.* **2016,** *52* (13), 2679-2682.

8. Cuevasanta, E.; Moller, M. N.; Alvarez, B., Biological chemistry of hydrogen sulfide and persulfides. *Arch. Biochem. Biophys.* **2017,** *617*, 9-25.

9. Wang, R., Physiological implications of hydrogen sulfide: A whiff exploration that blossomed. *Physiol. Rev.* **2012,** *92* (2), 791-896.

10. Filipovic, M. R.; Zivanovic, J.; Alvarez, B.; Banerjee, R., Chemical biology of H_2S signaling through persulfidation. *Chem. Rev.* **2018,** *118* (3), 377-461.

11. Kasamatsu, S.; Nishimura, A.; Morita, M.; Matsunaga, T.; Hamid, H. A.; Akaike, T., Redox signaling regulated by cysteine persulfide and protein polysulfidation. *Molecules* **2016,** *21* (12), 1721.

12. Ida, T.; Sawa, T.; Ihara, H.; Tsuchiya, Y.; Watanabe, Y.; Kumagai, Y.; Suematsu, M.; Motohashi, H.; Fujii, S.; Matsunaga, T.; Yamamoto, M.; Ono, K.; Devarie-Baez, N. O.; Xian, M.; Fukuto, J. M.; Akaike, T., Reactive cysteine persulfides and *S*-polythiolation regulate oxidative stress and redox signaling. *Proc. Natl. Acad. Sci. U. S. A.* **2014,** *111* (21), 7606-7611.

13. Xie, Z. Z.; Shi, M. M.; Xie, L.; Wu, Z. Y.; Li, G.; Hua, F.; Bian, J. S., Sulfhydration of p66Shc at cysteine59 mediates the antioxidant effect of hydrogen sulfide. *Antioxid. Redox Signal.* **2014,** *21* (18), 2531-2542.

14. Kawamura, S.; Horii, T.; Tsurugi, J., Aryl hydrodisulfides. *J. Org. Chem.* **1971,** *36* (24), 3677-3680.

15. Yuan, Z. N.; Zheng, Y. Q.; Yu, B. C.; Wang, S. M.; Yang, X. X.; Wang, B. H., Esterase-sensitive glutathione persulfide donor. *Org Lett* **2018,** *20* (20), 6364-6367.

16. Zheng, Y. Q.; Yu, B. C.; Li, Z.; Yuan, Z. N.; Organ, C. L.; Trivedi, R. K.; Wang, S. M.; Lefer, D. J.; Wang, B. H., An esterase-sensitive prodrug approach for controllable delivery of persulfide species. *Angew Chem Int Edit* **2017,** *56* (39), 11749-11753.

17. Dillon, K. M.; Carrazzone, R. J.; Wang, Y.; Powell, C. R.; Matson, J. B., Polymeric persulfide prodrugs: Mitigating oxidative stress through controlled delivery of reactive sulfur species. *ACS Macro Lett.* **2020**, 606-612.

18. Chaudhuri, A.; Venkatesh, Y.; Das, J.; Gangopadhyay, M.; Maiti, T. K.; Singh, N. D. P., One- and two-photon-activated cysteine persulfide donors for biological targeting. *J Org Chem* **2019,** *84* (18), 11441-11449.

19. Bora, P.; Chauhan, P.; Manna, S.; Chakrapani, H., A vinyl-boronate ester-based persulfide donor controllable by hydrogen peroxide, a reactive oxygen species (ROS). *Org Lett* **2018,** *20* (24), 7916-7920.

20. Powell, C. R.; Dillon, K. M.; Wang, Y.; Carrazzone, R. J.; Matson, J. B., A persulfide donor responsive to reactive oxygen species: Insights into reactivity and therapeutic potential. *Angew. Chem. Int. Edit.* **2018,** *57* (21), 6324-6328.

21. Lim, S. C.; Kim, Y. H., Evidence for formation of diphenylphosphinic peroxy radical intermediate: Spin trapping and chemical reactivity of the new phosphorus radical generated from diphenylphosphinic chloride and superoxide. *Heteroatom Chem.* **1990,** *1* (3), 261-265.

22. Ezerina, D.; Takano, Y.; Hanaoka, K.; Urano, Y.; Dick, T. P., N-Acetyl cysteine functions as a fast-acting antioxidant by triggering intracellular H_2S and sulfane sulfur production. *Cell Chem. Biol.* **2018,** *25* (4), 447-459.

23. Zafarullah, M.; Li, W. Q.; Sylvester, J.; Ahmad, M., Molecular mechanisms of *N*-acetylcysteine actions. *CMLS-Cell. Mol. Life Sci.* **2003,** *60* (1), 6-20.

24. Murphy, N. P.; Lampe, K. J., Fabricating PLGA microparticles with high loads of the small molecule antioxidant *N*-acetylcysteine that rescue oligodendrocyte progenitor cells from oxidative stress. *Biotechnol. Bioeng.* **2018,** *115* (1), 246-256.

25. Matson, J. B.; Stupp, S. I., Self-assembling peptide scaffolds for regenerative medicine. *Chem. Commun.* **2012,** *48* (1), 26-33.

26. Carter, J. M.; Qian, Y.; Foster, J. C.; Matson, J. B., Peptide-based hydrogen sulphide-releasing gels. *Chem. Commun.* **2015,** *51* (66), 13131-13134.

27. Longchamp, A.; Kaur, K.; Macabrey, D.; Dubuis, C.; Corpataux, J. M.; Deglise, S.; Matson, J. B.; Allagnat, F., Hydrogen sulfide-releasing peptide hydrogel limits the development of intimal hyperplasia in human vein segments. *Acta Biomater.* **2019,** *97*, 374-384.

28. Qian, Y.; Kaur, K.; Foster, J. C.; Matson, J. B., Supramolecular tuning of H_2S release from aromatic peptide amphiphile gels: effect of core unit substituents. *Biomacromolecules* **2019,** *20* (2), 1077-1086.

29. Wang, Y.; Kaur, K.; Scannelli, S. J.; Bitton, R.; Matson, J. B., Self-assembled nanostructures regulate H_2S release from constitutionally isomeric peptides. *J Am Chem Soc* **2018,** *140* (44), 14945-14951.

30. Wang, Y.; Matson, J. B., Supramolecular nanostructures with tunable donor loading for controlled H_2S release. *ACS Appl. Bio Mater.* **2019,** *2* (11), 5093-5098.

31. Fleming, S.; Ulijn, R. V., Design of nanostructures based on aromatic peptide amphiphiles. *Chem Soc Rev* **2014,** *43* (23), 8150-8177.

32. Reches, M.; Gazit, E., Casting metal nanowires within discrete self-assembled peptide nanotubes. *Science* **2003,** *300* (5619), 625-627.

33. Zhao, Y.; Pluth, M. D., Hydrogen sulfide donors activated by reactive oxygen species. *Angew. Chem. Int. Ed.* **2016,** *55* (47), 14638-14642.

34. Zhao, Y.; Henthorn, H. A.; Pluth, M. D., Kinetic insights into hydrogen sulfide delivery from caged-carbonyl sulfide isomeric donor platforms. *J. Am. Chem. Soc.* **2017,** *139* (45), 16365-16376.

35. Chauhan, P.; Jos, S.; Chakrapani, H., Reactive oxygen species-triggered tunable hydrogen sulfide release. *Org. Lett.* **2018,** *20* (13), 3766-3770.

36. Hu, Y. M.; Li, X. Y.; Fang, Y.; Shi, W.; Li, X. H.; Chen, W.; Xian, M.; Ma, H. M., Reactive oxygen species-triggered off-on fluorescence donor for imaging hydrogen sulfide delivery in living cells. *Chem. Sci.* **2019,** *10* (33), 7690-7694.

37. Zhang, N.; Hu, P.; Wang, Y. F.; Tang, Q.; Zheng, Q.; Wang, Z. L.; He, Y., A reactive oxygen species (ROS) activated hydrogen sulfide (H_2S) donor with self-reporting fluorescence. *ACS Sens.* **2020,** *5* (2), 319-326.

38. Peng, B.; Chen, W.; Liu, C. R.; Rosser, E. W.; Pacheco, A.; Zhao, Y.; Aguilar, H. C.; Xian, M., Fluorescent probes based on nucleophilic substitution-cyclization for hydrogen sulfide detection and bioimaging. *Chem.-Eur. J.* **2014,** *20* (4), 1010-1016.

39. Hu, Y.; Lin, R.; Zhang, P. C.; Fern, J.; Cheetham, A. G.; Patel, K.; Schulman, R.; Kan, C. Y.; Cui, H. G., Electrostatic-driven lamination and untwisting of beta-sheet assemblies. *Acs Nano* **2016,** *10* (1), 880-888.

40. Bakota, E. L.; Sensoy, O.; Ozgur, B.; Sayar, M.; Hartgerink, J. D., Self-assembling multidomain peptide fibers with aromatic cores. *Biomacromolecules* **2013,** *14* (5), 1370-1378.

41. Reliene, R.; Schiestl, R. H., Glutathione depletion by buthionine sulfoximine induces DNA deletions in mice. *Carcinogenesis* **2006,** *27* (2), 240-244.

42. Adams, D. J.; Boskovic, Z. V.; Theriault, J. R.; Wang, A. J.; Stern, A. M.; Wagner, B. K.; Shamji, A. F.; Schreiber, S. L., Discovery of small-molecule enhancers of reactive oxygen

species that are nontoxic or cause genotype-selective cell death. *Acs Chem Biol* **2013,** *8* (5), 923-929.

43. Zhan, J.; Cai, Y. B.; He, S. S.; Wang, L.; Yang, Z. M., Tandem molecular self-assembly in liver cancer cells. *Angew. Chem. Int. Ed.* **2018,** *57* (7), 1813-1816.

44. Liang, C. H.; Yan, X. R.; Zhang, R. S.; Xu, T. Y.; Zheng, D. B.; Tan, Z. Q.; Chen, Y. X.; Gao, Z. F.; Wang, L.; Li, X. Y.; Yang, Z. M., Enhanced cellular uptake and nuclear accumulation of drug-peptide nanomedicines prepared by enzyme-instructed self-assembly. *J. Control. Release* **2020,** *317*, 109-117.

45. Mumcuoglu, D.; Ekiz, M. S.; Gunay, G.; Tekinay, T.; Tekinay, A. B.; Guler, M. O., Cellular internalization of therapeutic oligonucleotides by peptide amphiphile nanofibers and nanospheres. *ACS Appl. Mater. Interfaces* **2016,** *8* (18), 11280-11287.

46. Robinson, K. M.; Janes, M. S.; Pehar, M.; Monette, J. S.; Ross, M. F.; Hagen, T. M.; Murphy, M. P.; Beckman, J. S., Selective fluorescent imaging of superoxide *in vivo* using ethidium-based probes. *P Natl Acad Sci USA* **2006,** *103* (41), 15038-15043.

47. Schieber, M.; Chandel, N. S., ROS function in redox signaling and oxidative stress. *Curr. Biol.* **2014,** *24* (10), R453-R462.

48. Xu, J.; Zhang, Y.; Yu, H.; Gao, X. D.; Shao, S. J., Mitochondria-targeted fluorescent probe for imaging hydrogen peroxide in living cells. *Anal. Chem.* **2016,** *88* (2), 1455-1461.

49. Han, Y. Y.; Shang, Q. W.; Yao, J.; Ji, Y., Hydrogen sulfide: A gaseous signaling molecule modulates tissue homeostasis: implications in ophthalmic diseases. *Cell Death Dis.* **2019,** *10*, 293.

50. Wallace, J. L., Hydrogen sulfide-releasing anti-inflammatory drugs. *Trends Pharmacol. Sci.* **2007,** *28* (10), 501-505.

51. Li, L.; Whiteman, M.; Guan, Y. Y.; Neo, K. L.; Cheng, Y.; Lee, S. W.; Zhao, Y.; Baskar, R.; Tan, C. H.; Moore, P. K., Characterization of a novel, water-soluble hydrogen sulfide - releasing molecule (GYY4137): New insights into the biology of hydrogen sulfide. *Circulation* **2008,** *117* (18), 2351-2360.

3.8. Experimental

Materials and Methods

All Fmoc amino acids and Rink amide MBHA resin were purchased from Peak Polypeptide Biosystems LLC (P3BioSystems, Louisville, KY, USA). Benzoic acid (BA) and potassium dioxide were purchased from Sigma-Aldrich (St. Louis, MO, USA). 2,2'-Dipyridyldisulfide (DPS) was purchase from Alfa Aesar (Haverhill, MA, USA). Dihydroethidium (DHE), L-buthionine-(*S*,*R*)-sulfoximine (BSO), and phorbol 12-myristate 13-acetate (PMA) were purchased from Cayman Chemical (Ann Arbor, MI, USA). All other reagents were sourced from Sigma-Aldrich (St. Louis, MO, USA) or VWR (Radnor, PA, USA) unless otherwise stated. H_2S selective probes WSP-2 and WSP-5 were synthesized according to a previous report.[1] NACpyDS was synthesized according to our recent report.[2]

Cell Culture

Cell studies were conducted on an adherent H9C2 line of rat embryonic cardiomyocytes (ATCC, Manassas, VA, USA; passage numbers 4-8) and RAW 264.7 macrophages (ATCC, Manassas, VA, USA; passage numbers 2-7). Cultures were grown in Dulbecco's Modified Eagle Medium (DMEM, VWR, Radnor, PA), supplemented with 10% fetal bovine serum (FBS, VWR, Radnor, PA), 50 IU/mL penicillin, and 50 μg/mL streptomycin (MP Biomedicals). Cells were cultured at

37 °C in 5% CO_2-air. The cultures were passaged after 70–80 % confluence was achieved. Cells were rinsed with 1X PBS solution three times, and then released with trypsin and 0.25% EDTA solution (VWR, Radnor, PA). The suspension of released cells was centrifuged at 1000 rpm (H9C2 cells) or 1500 rpm (RAW 264.7 cells) for 5 min before counting and plating for experiments.

Synthesis of 4-tolyl diphenylphosphinate (1)

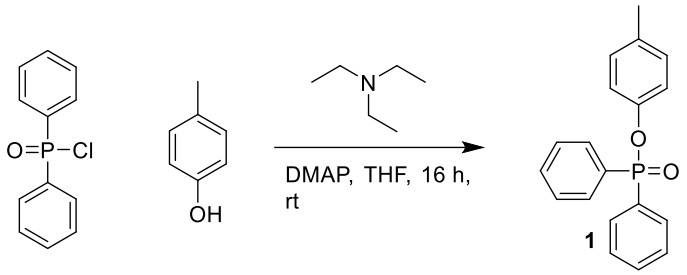

A round bottom flask was charged with *p*-cresol (3.8 g, 35 mmol), triethylamine (4.2 g, 42 mmol), DMAP (0.2 g, 1.6 mmol) and dry THF (100 mL). The resulting solution was then cooled to 0 °C in an ice bath. Diphenyl phosphinic chloride (10 g, 42 mmol) was then added dropwise via syringe over the course of 10 min. The reaction mixture was allowed to stir, warming to room temperature as the ice melted. After 16 h, the salts were filtered off, and the resulting organic phase was diluted with EtOAc (50 mL) and washed with saturated Na_2CO_3 (2 x 50 mL) and brine (50 mL). The organic layer was separated and dried over Na_2SO_4 and concentrated via rotary evaporation to yield compound **1** as a clear, colorless, viscous liquid. (8.9 g, 29 mmol, 82% yield). NMR spectra matched literature precedence.[3] ^{1}H NMR ($CDCl_3$): δ 7.89 (4H, m), 7.49 (6H, m), 7.04 (4H, m), 2.24 (3H, s). ^{13}C NMR ($CDCl_3$): δ 148.5, 134.1, 132.4, 132.3, 131.9, 131.8, 130.4, 130.0, 128.6, 128.5, 120.45, 120.41, 20.7.

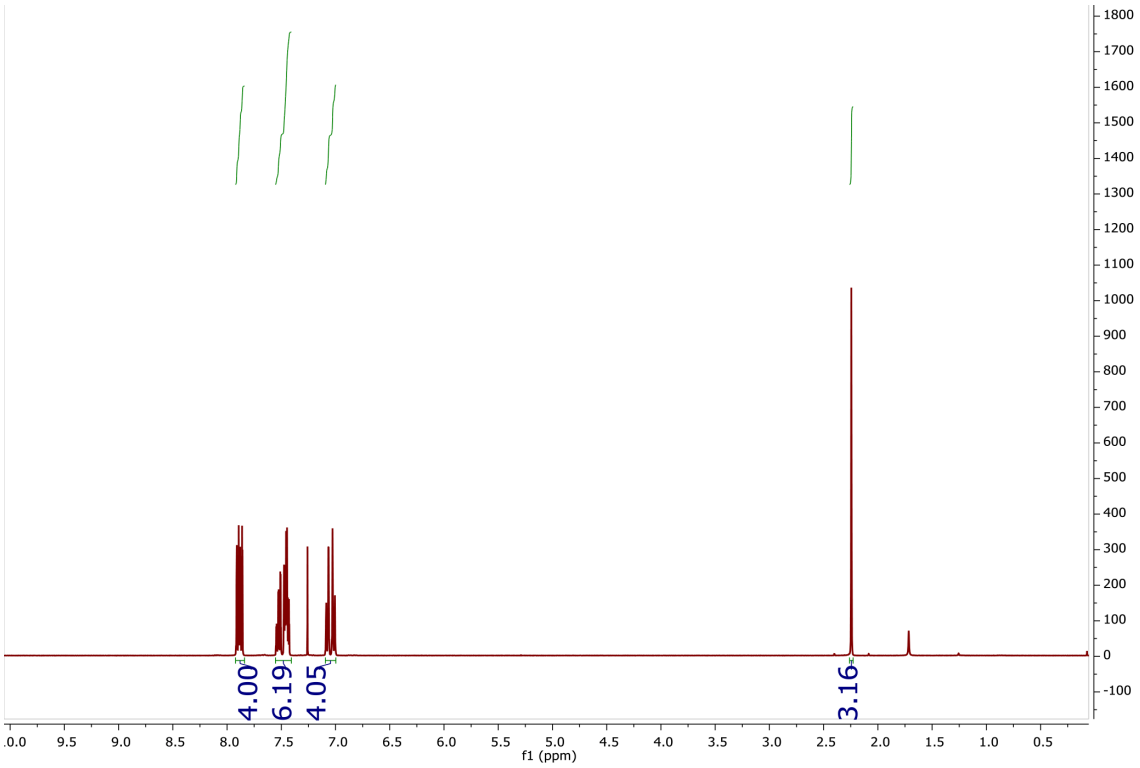

Figure S1. ^{1}H NMR of 4-tolyl diphenylphosphinate ($CDCl_3$).

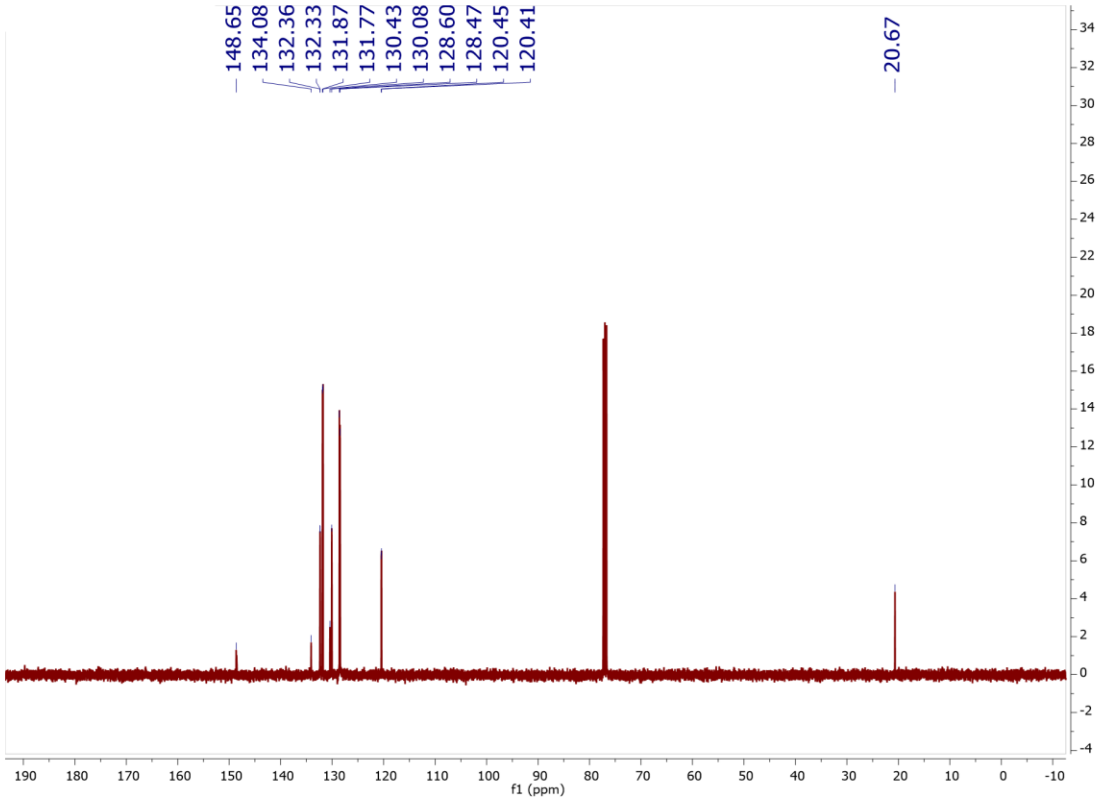

Figure S2. ^{13}C NMR of 4-tolyl diphenylphosphinate ($CDCl_3$).

Synthesis of 4-(bromomethyl)phenyl diphenylphosphinate (2)

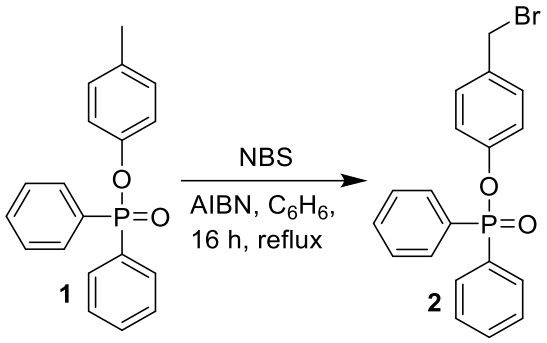

A flame-dried, 2-neck round bottom flask equipped with a septum and a condenser was charged with 4-tolyl diphenylphosphinate (Compound **1**, 7.3 g, 24 mmol), benzene (80 mL), and *N*-bromosuccinimide (4.6 g, 26 mmol) under N_2 flow. The mixture was stirred until solids dissolved, yielding a clear, light yellow solution. Azobisisobutyronitrile (AIBN) (0.38 g, 2.4 mmol) was added in one portion under N_2 flow, and the reaction mixture was heated to reflux. Reaction progress was monitored by TLC (CH_2Cl_2) until starting material was consumed (16 h). The reaction mixture was cooled to rt and washed successively with saturated $NaHCO_3$ (2 x 50 mL) and brine (50 mL). The organic layer was separated, dried over Na_2SO_4, and then concentrated via rotary evaporation to yield a brown, waxy solid. This crude product was then further purified via column chromatography, eluting with CH_2Cl_2 (R_f = 0.25, visualized with UV). The final product (Compound **2**) was isolated as a white solid and used in subsequent steps without further purification (8.3 g, 21 mmol, 91% yield), despite a small amount of an aromatic impurity. NMR spectra matched literature precedence.[4] ^{1}H NMR ($CDCl_3$): δ 7.89 (4H, m), 7.49 (6H, m), 7.22 (4H, m), 4.41 (2H, s). ^{13}C NMR ($CDCl_3$): δ 150.9, 134.0, 132.56, 132.53, 131.8, 131.7, 131.4, 130.5, 128.7, 128.6, 128.1, 121.0, 32.8.

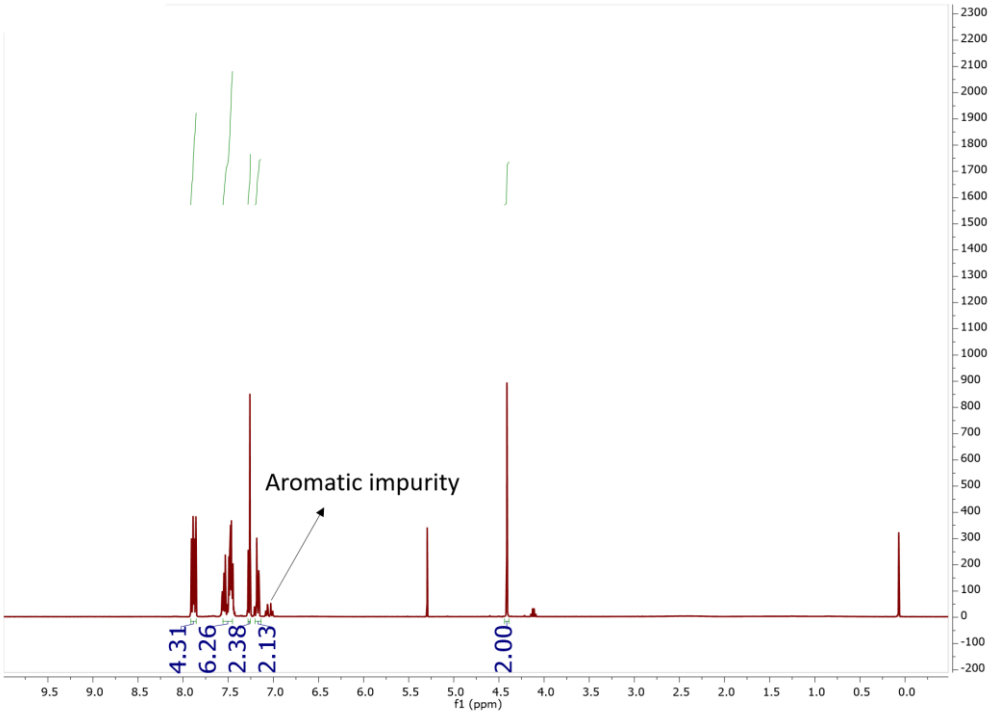

Figure S3. ^{1}H NMR of 4-(bromomethyl)phenyl diphenylphosphinate ($CDCl_3$).

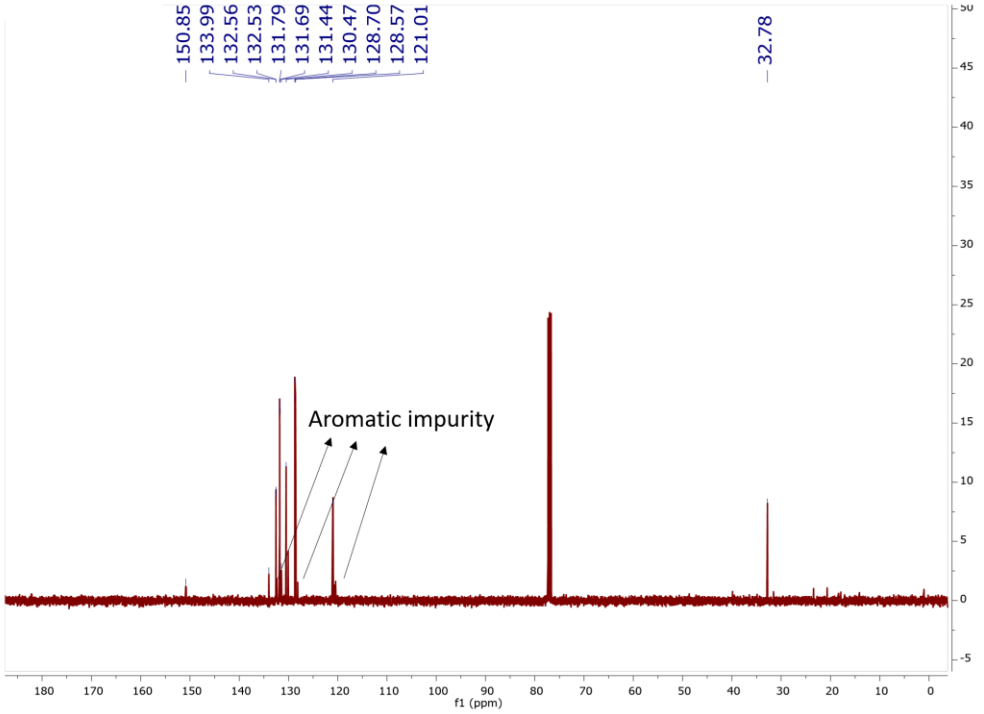

Figure S4. ^{13}C NMR of 4-(bromomethyl)phenyl diphenylphosphinate ($CDCl_3$).

Synthesis of 4-(mercaptomethyl)phenyl diphenylphosphinate (3)

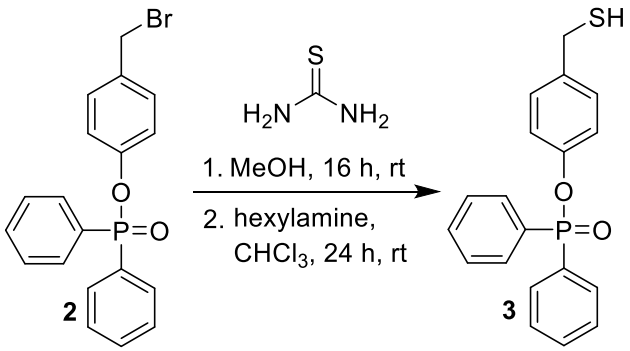

A two-neck round bottom flask equipped with a vacuum adaptor and a septum was charged with compound **2** (1.9 g, 4.9 mmol), MeOH (25 mL), and a stir bar. The resulting suspension was bubbled with N_2 for 15 min. Thiourea (0.41 g, 5.4 mmol) was then added in one portion under N_2 flow, and the reaction mixture was allow to stir at rt. The solids dissolved slowly over the course of several hours to give a clear, yellow solution. Reaction progress was monitored by TLC (CH_2Cl_2) until starting material was consumed (16 h). The reaction mixture was then concentrated via rotary evaporation, and the thiouronium bromide intermediate was subsequently suspended in $CHCl_3$ (25 mL) in a 2-neck round bottom flask. The suspension was degassed with N_2 for 15 min. Hexylamine (0.55 g, 0.71 mL, 5.4 mmol) was then injected via syringe. The resulting suspension slowly dissolved over the course of 24 h, yielding a bright yellow solution. This solution was washed with 1N HCl (25 mL) and brine (25 mL) in a separatory funnel. The organic layer was separated and dried over Na_2SO_4, then concentrated via rotary evaporation to yield a viscous, slightly yellow oil. The product (Compound **3**) was then further purified by silica gel chromatography, eluting with 1:1 EtOAc:hexanes, yielding a white, crystalline solid. (1.5 g, 90% yield) ^{1}H NMR ($CDCl_3$): δ 7.89 (4H, m), 7.44 (6H, m), 7.14 (4H, m), 3.69 (2H, *J* = 6.0 Hz d), 1.69 (1H, *J* = 6.0 Hz, t). ^{13}C NMR ($CDCl_3$): δ 137.3, 132.5, 132.4, 131.8, 131.7, 130.2, 129.28, 129.27, 128.7, 128.5, 120.9, 120.8, 28.3.

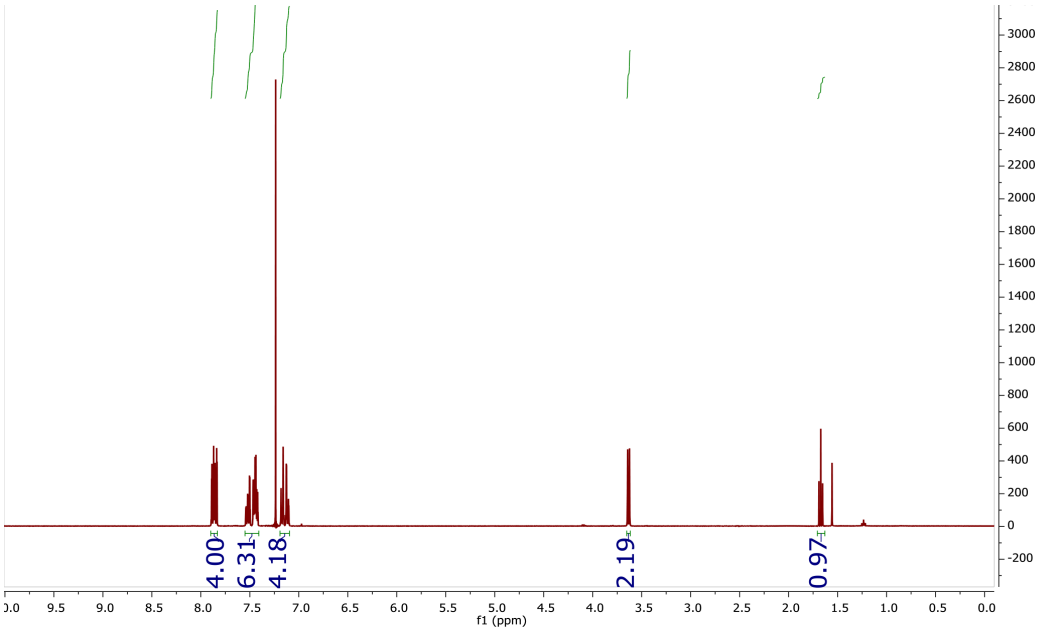

Figure S5. ^{1}H NMR of 4-(mercaptomethyl)phenyl diphenylphosphinate ($CDCl_3$).

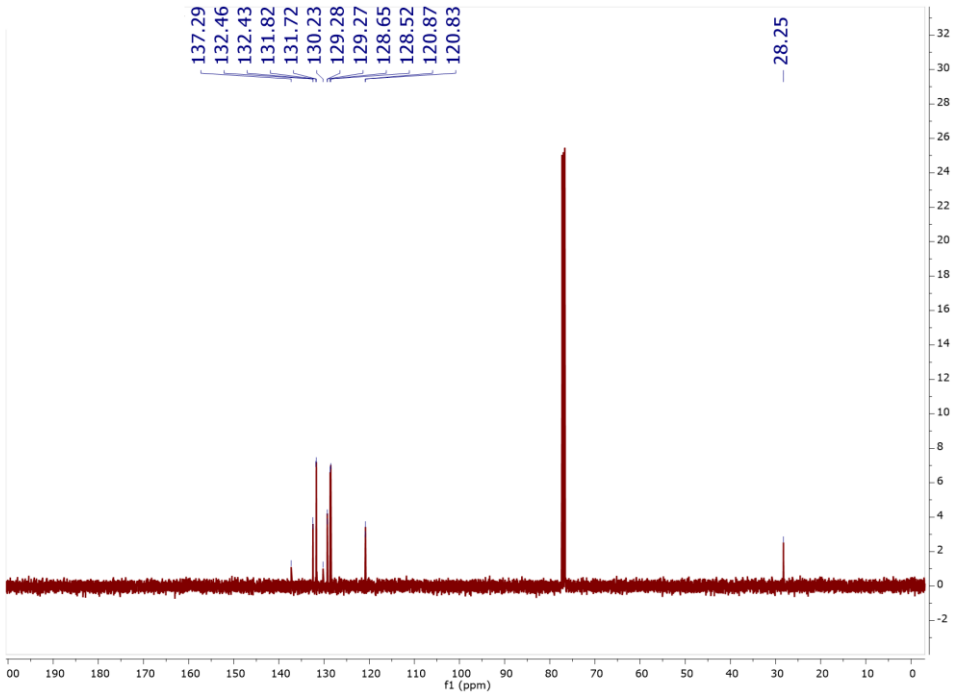

Figure S6. ^{13}C NMR of 4-(mercaptomethyl)phenyl phosphinate ($CDCl_3$).

Synthesis of SOPD-NAC

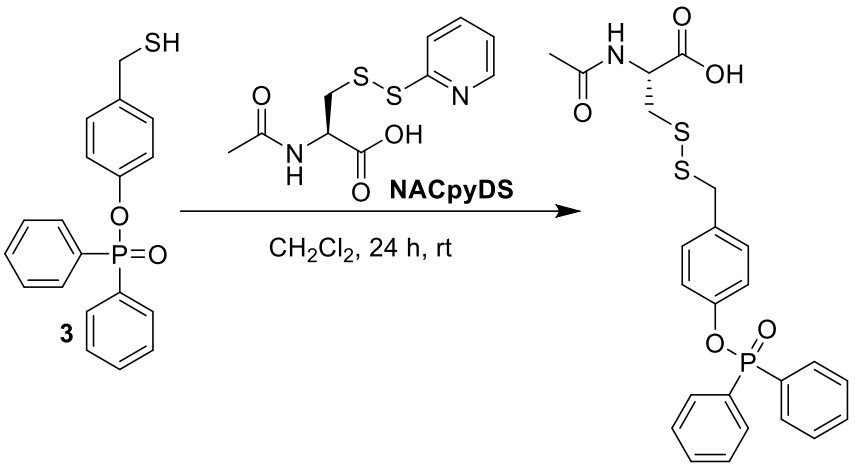

SOPD-NAC

A round bottom flask was charged with compound **3** (0.76 g, 2.2 mmol), CH_2Cl_2 (5 mL), and NACpyDS (0.61 g, 2.2 mmol). The reaction mixture was allowed to stir for 24 h, and then placed in the freezer at -4 °C for 4 h. The resulting white precipitate in a yellow solution was filtered and dried, yielding **SOPD-NAC** as a white, crystalline solid. (0.63 g, 56% yield) ^{1}H NMR (DMSO-d_6): δ 8.27, (1H, J = 7.4 Hz, d) 7.31 (14H, m), 4.45 (1H, m), 3.94 (2H, m), 2.99 (1H, m), 2.78 (1H, m) 1.84 (3H, s). ^{13}C NMR (DMSO-d_6): δ 172.5, 169.9, 150.3, 150.2, 149.5, 149.4, 135.7, 131.5, 130.72, 130.70, 126.4, 120.4, 120.33, 120.29, 51.6, 41.2, 39.8, 22.8. HRMS (ESI-TOF) calcd. for $C_{24}H_{23}NO_5S_2P$ $[M-H]^-$ 499.0677, found 499.0679.

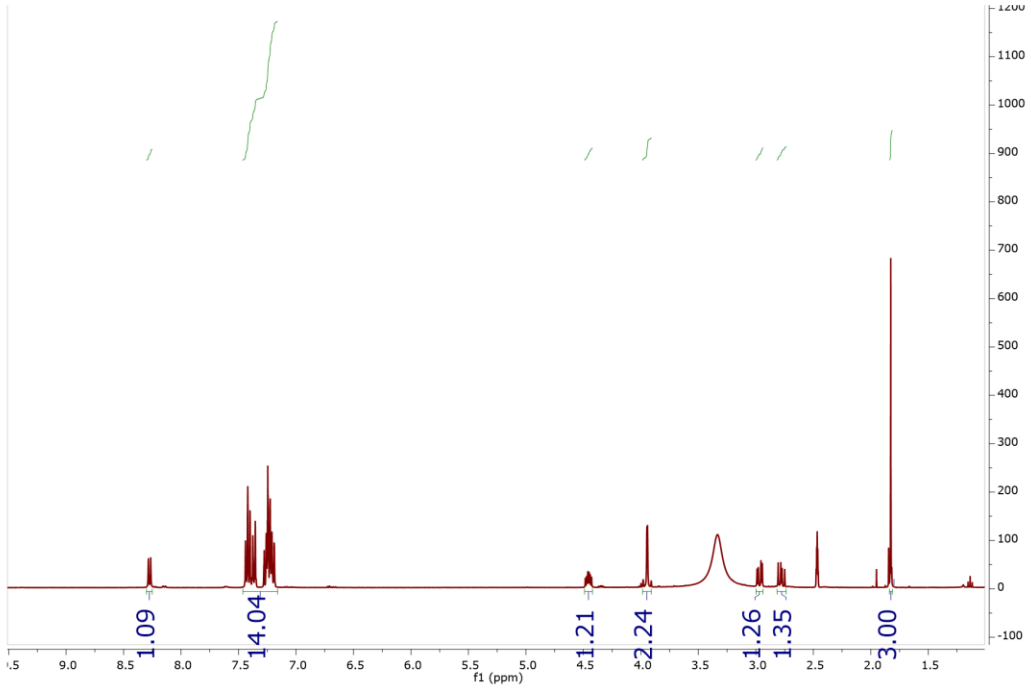

Figure S7. ^{1}H NMR of **SOPD-NAC** (DMSO-d_6).

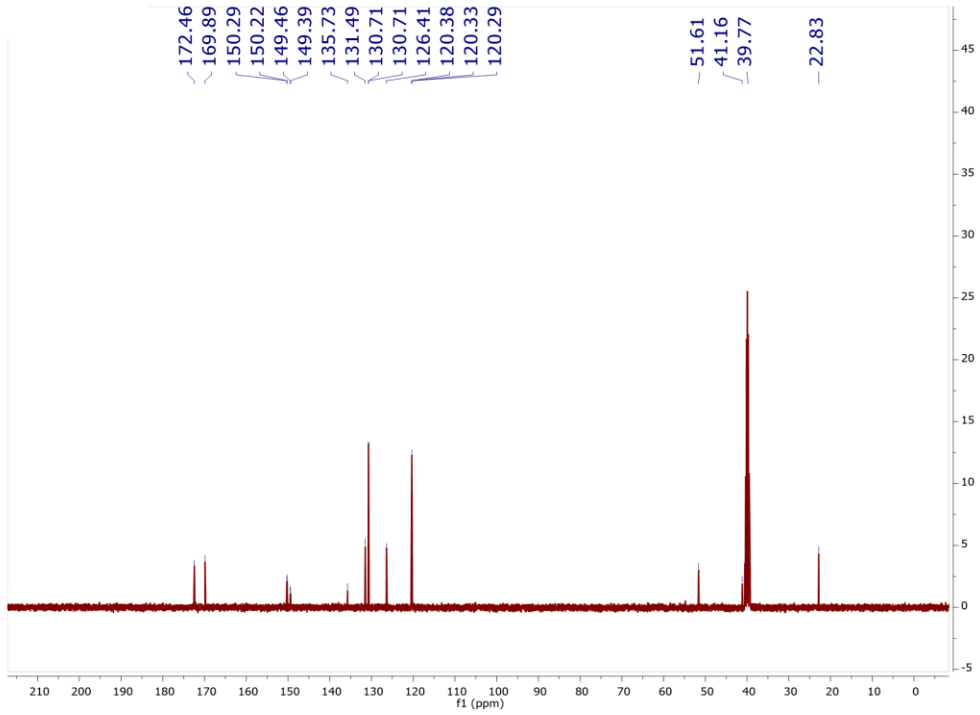

Figure S8. ^{13}C NMR of **SOPD-NAC** (DMSO-d_6).

General procedure for peptide synthesis

All peptides used in this study were manually synthesized using standard 9-fluorenylmethoxycarbonyl (Fmoc) solid phase synthesis techniques at a 0.5 mmol scale. Fmoc deprotection steps were carried out by treating the Rink amide MBHA resin with 4-methylpiperidine in dimethylformamide (DMF) (20% v/v). Amino acid coupling steps were performed following Fmoc deprotection by treating the resin with Fmoc-amino acid, *O*-benzotriazole-*N,N,N′,N′*-tetramethyluronium hexafluorophosphate (HBTU), and diisopropylethylamine (DIEA) (4:3.96:10 molar ratio to amine groups on resin) in DMF for 2 h. After coupling of the final amino acid, BA was then coupled to the N-terminus of the peptide using the same coupling conditions as noted above for Fmoc amino acids. Finally, peptides were cleaved from the resin by treatment with a TFA/TIS/H_2O (92.5:5:2.5) solution (15 mL) for 3 h. The solution was concentrated *in vacuo* and triturated with cold diethyl ether to precipitate the crude peptide. Following centrifugation to remove the supernatant liquid, the crude materials were dissolved in a mixture of water and acetonitrile containing 0.1% NH_4OH for purification. All peptides were purified by preparative RP-HPLC using an Agilent Technologies 1260 Infinity HPLC system (Agilent Technologies, Santa Clara, CA) equipped with a fraction collector. Separations were performed using an Agilent PLRP-S column (100 Å, 10 μm, 150 × 25 mm) monitoring at 220 nm. The expected mass was confirmed using ESI-MS (Advion ExpressIon Compact Mass Spectrometer). Fractions containing pure products were combined and lyophilized (FreeZone −105 °C, Labconco, Kansas City, MO), and then stored at −20 °C until needed.

Synthesis of superoxide anion responsive peptide (SOPD-Pep)

SOPD-Pep was synthesized in two steps as shown in Scheme S1. Specifically, Peptide Bz-Cys-Phe-Phe-Glu (100 mg, 155 μmol) and DPS (170 mg, 773 μmol) were dissolved in 2 mL of DMF.

After reaction for 48 h at rt in dark, the solution was diluted with HPLC grade water and acetonitrile, each containing 0.1% NH_4OH, (8 mL in total, 1:1 v/v) and purified by preparative RP-HPLC monitoring at 220 nm. Fractions containing pure products, as confirmed by ESI-MS (Advion ExpressIon CMS), were combined and lyophilized to afford peptide Bz-Cys(SPyr)-Phe-Phe-Glu.

Peptide Bz-Cys(SPyr)-Phe-Phe-Glu (50 mg, 66 μmol) and 4-(mercaptomethyl)phenyl diphenylphosphinate (34 mg, 100 μmol) were dissolved in 2 mL of DMF. The reaction mixture was allowed to stir at rt for 48 h in dark. The reaction mixture was then diluted with HPLC grade water and acetonitrile, each containing 0.1% NH_4OH, (8 mL in total, 1:1 v/v) and purified by preparative RP-HPLC monitoring at 220 nm. Fractions containing pure products, as confirmed by ESI-MS (Advion ExpressIon CMS), were combined and lyophilized to afford **SOPD-Pep**.

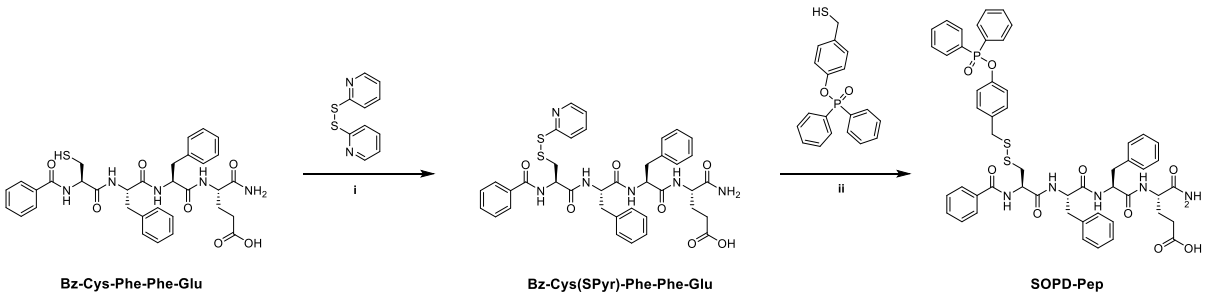

Scheme S1. Synthetic route to **SOPD-Pep**. Reaction conditions: i) DMF, rt, 48 h; ii) DMF, rt, 48 h.

Synthesis of control superoxide anion responsive peptide (SOPD-Pep-Cont)

SOPD-Pep-Cont was synthesized in one step as shown in Scheme S2. Peptide Bz-Cys-Phe-Phe-Glu (70 mg, 109 μmol) and 4-(bromomethyl)phenyl diphenylphosphinate (Compound **2**, 84 mg, 217 μmol) were dissolved in 2 mL of DMF. Triethylamine (46 μL) was added to the solution. The reaction mixture was heated at 75 ^oC in an oil bath with stirring for 48 h. The reaction mixture was

then diluted with HPLC grade water and acetonitrile, each containing 0.1% NH_4OH, (8 mL in total, 1:1 v/v) and purified by preparative RP-HPLC monitoring at 220 nm. Fractions containing pure products, as confirmed by ESI-MS (Advion ExpressIon CMS), were combined and lyophilized to afford **SOPD-Pep-Cont**.

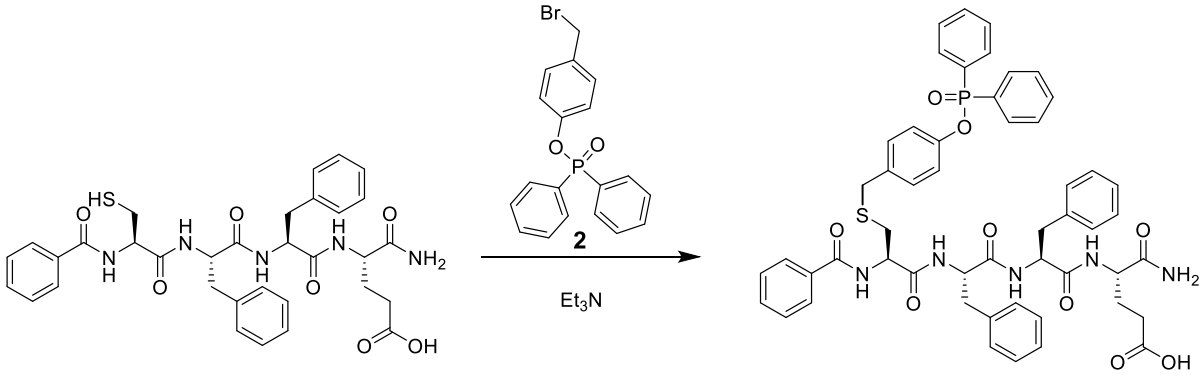

Scheme S2. Synthetic route to **SOPD-Pep-Cont**.

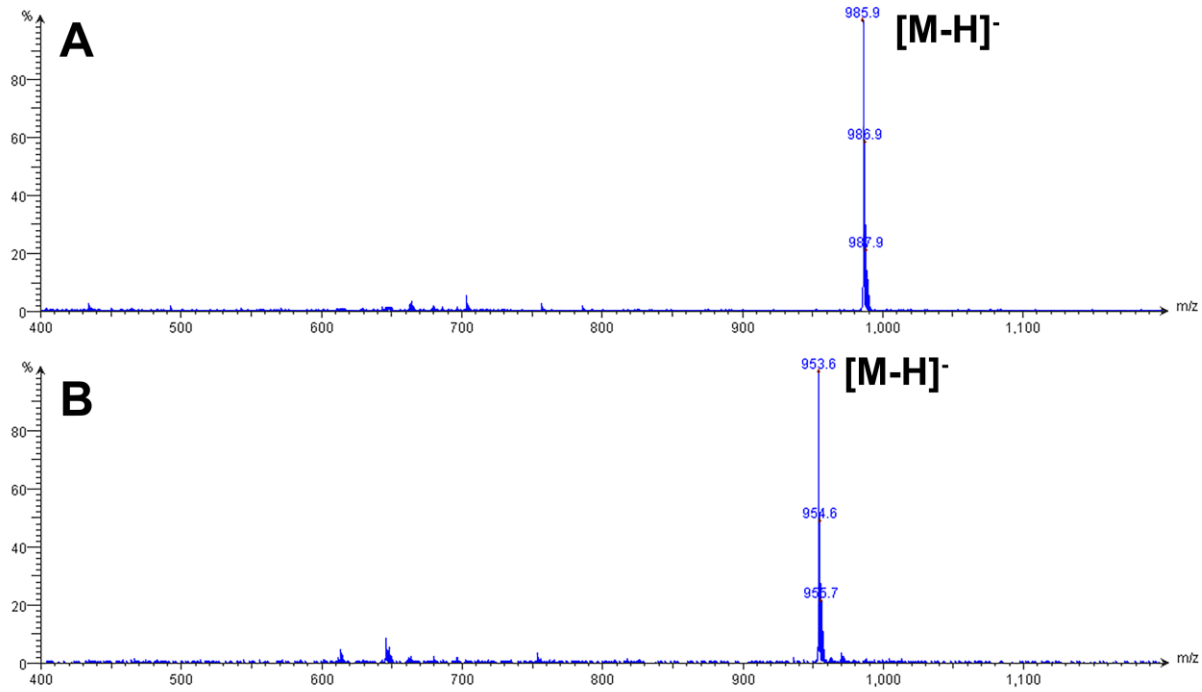

Figure S9. ESI mass spectra of (A) **SOPD-Pep** and (B) **SOPD-Pep-Cont**.

Preparation of $ONOO^-$

Solutions of $NaNO_2$ (5 mL, 0.6 M in H_2O) and H_2O_2 (5 mL, 0.7 M in H_2O) were prepared separately, mixed together, and then cooled to 0 °C. The reaction mixture was then acidified by addition of HCl (7 mL, 0.6 M in H_2O) over 1 min dropwise while stirring. Immediately after complete addition of the HCl solution, KOH solution (5 mL, 1.5 M in H_2O) was added to the reaction mixture all at once, causing the solution to turn faintly yellow. After stirring for 2 minutes, MnO_2 (200 mg, 2.3 mmol) was added, and the resulting gray/silver suspension was allowed to stir for 20 minutes to remove excess H_2O_2. The concentration of $ONOO^-$ was determined using the absorption peak at 302 nm ($\varepsilon = 1670\ M^{-1}\ cm^{-1}$).[5]

Fluorescence experiments with WSP-2

50 µL **SOPD-NAC** or **SOPD-Pep** solution (2 mM stock in 10% DMSO: pH 7.4 PBS) and 10 µL WSP-2 solution (500 µM stock in DMSO), 10 µL DMSO, and 10 µL pH 7.4 PBS were combined in a quartz cuvette. The instrument was zeroed, then 10 µL of the desired oxidant/reductant (40 mM stock in 1:1 DMSO:H_2O) and 10 µL Cys (40 mM in pH 7.4 PBS) were added in quick succession. Subsequent scans were taken every 5 min for 30 min (7 total scans), and experiments were repeated 3 times each (n =3). For experiments where Cys or oxidant wasn't added, 10 µL additional pH 7.4 PBS was added to keep the total assay volume constant at 100 µL.

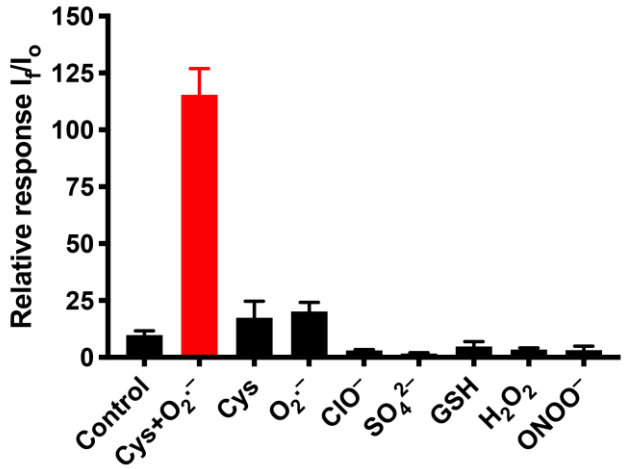

Figure S10. Relative response of 1 mM **SOPD-NAC** and 50 µM WSP-2 to each potential trigger (4 mM) or combination of triggers or control (no trigger added) represented as the ratio of the final fluorescence intensity (I_f) after 30 min to the initial fluorescence intensity (I_0), showing an increased selectivity for Cys + superoxide (KO_2 was used as the superoxide source) over other potential triggers. The results are expressed as the mean ± SD (n = 3).

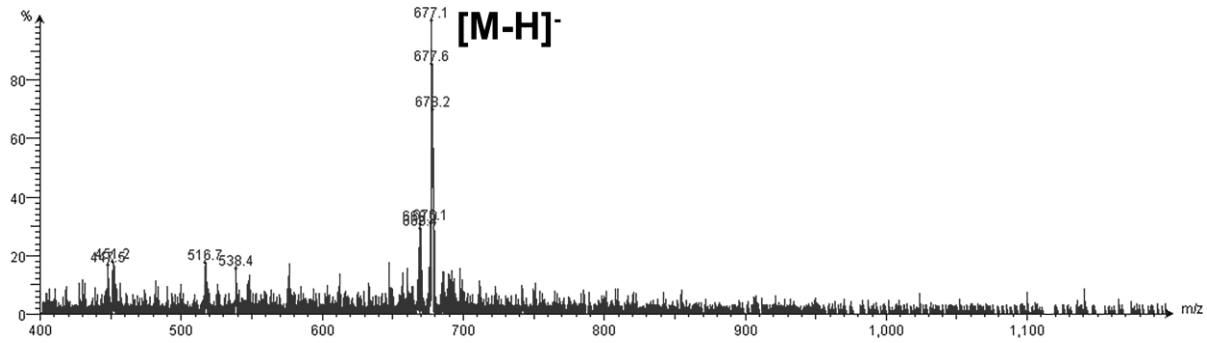

Figure S11. ESI mass spectrum of Bz-C(SS⁻)FFE released from 100 μM **SOPD-Pep** in phosphate buffer (pH 7.4) after treating with 400 μM KO_2. The spectrum was collected using ESI-MS (Advion ExpressIon Compact Mass Spectrometer) in negative mode.

Fluorescence experiments to quantify H_2S release from SOPD-Pep and SOPD-NAC

20 μL WSP-2 solution (500 μM stock in DMSO), 20 μL DMSO, and 20 μL pH 7.4 PBS were combined in a 1.5 mL centrifuge tube. 20 μL KO_2 (40 mM stock in 1/1 DMSO:H_2O v/v) and 20 μL Cys (40 mM in pH 7.4 PBS) were added in quick succession. Then, various volumes of Na_2S (20, 40, or 100 μL of 1.0 mM stock or 20 μL 10 mM stock in 10% DMSO in pH 7.4 PBS) were added, and the total volume was adjusted to 200 μL with 10% DMSO in pH 7.4 PBS. Final assay concentrations were 50 μM WSP-2, 4 mM KO_2, 4 mM Cys, and 100 μM, 200 μM, 500 μM, or 1 mM Na_2S. In the case of **SOPD-NAC** or **SOPD-Pep**, 100 μL solution (2 mM stock in 10% DMSO in pH 7.4 PBS) was added instead of Na_2S.

Each solution was vortexed and aged in the dark for 30 minutes, and each sample was then placed on the fluorimeter. Experiments were repeated 3 times each (n=3). Emission spectra were obtained using a QuantaMaster Model QM-200-4E emission spectrophotometer from Photon Technology, Inc. (PTI) equipped with a 350 nm LED and a Becker & Hickl GmbH PMH-100 PMT detector.

The excitation light source was a 75W Xe arc lamp (Newport). The detector was a thermoelectrically cooled Hamamatsu 1527 photomultiplier tube (PMT). The excitation wavelength was 385 nm and emission spectra from 420 nm to 550 nm was collected, using the peak emission at 456 nm for plotting in Figure S12.

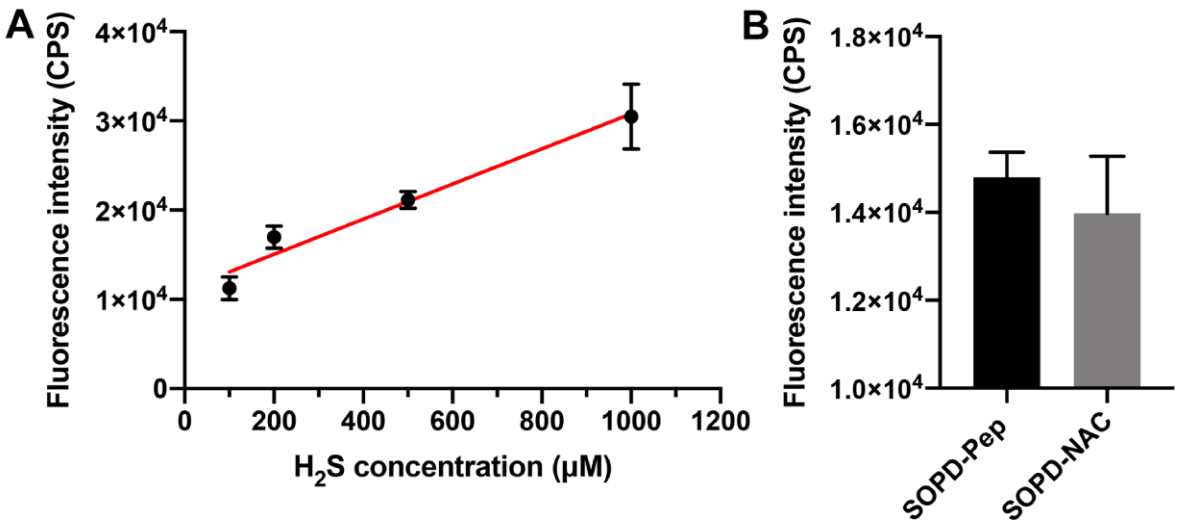

Figure S12. (A) The calibration curve of H_2S release from different concentrations of Na_2S measured by WSP-2 (Y=19.683X+11118). (B) Accordingly, the concentrations of H_2S released from 1 mM **SOPD-Pep** and **SOPD-NAC** were calculated to be 190 ± 30 μM and 150 ± 50 μM, respectively. Note that these values are lower bounds for the amount of persulfide or H_2S released in this timeframe and do not account for all possible side reactions.

Characterization of self-assembled peptides

Conventional transmission electron microscopy (TEM)

1 mM stock solutions of **SOPD-Pep** or **SOPD-Pep-Cont** in 10 mM phosphate buffer (PB) solution (pH 7.4) were prepared by direct dissolution of the lyophilized powders. Samples were allowed to age overnight. An aliquot of each solution was removed immediately prior to TEM sample preparation and diluted with PB to 100 μM. Next, 10 μL of this solution was deposited on a carbon-

coated copper grid (Electron Microscopy Services, Hatfield, PA, USA) and allowed to stand for 5 min. Excess solution was wicked away by a small piece of filter paper, and then DI water was deposited, allowed to stand for 40 sec, and then wicked away to wash away excess salts. Finally, 10 μL of a 2 wt % aqueous uranyl acetate (UA) solution was deposited on the grid for 5 min. A thin layer was generated after carefully wicking away excess UA. The sample grid was then allowed to dry at rt prior to imaging. Bright-field TEM imaging was performed on a Philips EM420 TEM operated at an acceleration voltage of 100 kV. TEM images were recorded by a slow scan CCD camera.

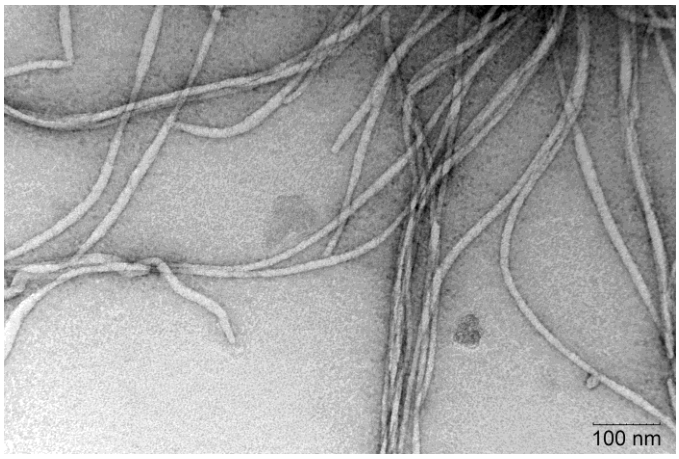

Figure S13. Conventional TEM characterization of nanoribbons formed by **SOPD-Pep-Cont**. The concentration of **SOPD-Pep-Cont** was 100 μM in PB (pH=7.4). TEM grid was stained by UA prior to imaging.

Circular dichroism (CD) spectroscopy

CD spectra of **SOPD-Pep** and **SOPD-Pep-Cont** from 190 nm to 320 nm were recorded on a Jasco J-815 spectropolarimeter (JASCO, Easton, MD, USA) using a 1 mm path length quartz UV-Vis absorption cell (Thermo Fisher Scientific, Pittsburgh, PA, USA). 100 μM samples diluted from a 1 mM stock solution in 10 mM phosphate buffer (pH=7.4) immediately before measurements were used in these experiments. A background spectrum of the solvent was acquired and subtracted from each sample spectrum. All measurements were conducted in triplicate.

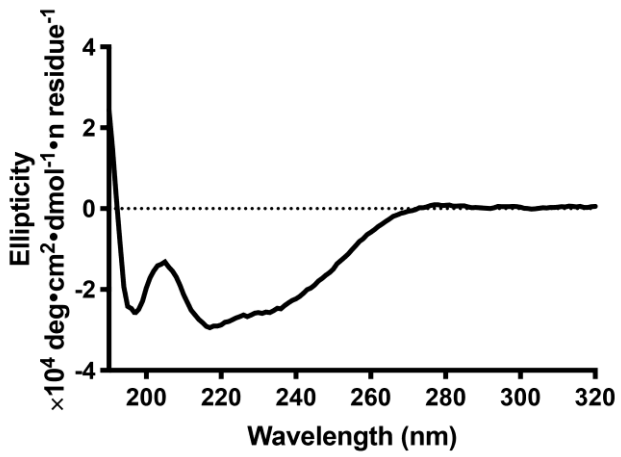

Figure S14. CD spectrum of **SOPD-Pep-Cont** in phosphate buffer (pH 7.4) at a concentration of 100 μM.

Cell viability assays

H9C2 cells were plated in a 96-well plate at a density of 5000 cells per well in 200 μL complete DMEM per well. After culturing for 24 h, cells were washed with 1X PBS three times before 195 μL serum-containing DMEM media was added. Next, 5 μL of stock **SOPD-NAC** or **SOPD-Pep** solution in DMSO was added to each well to make the final **SOPD-NAC** or **SOPD-Pep**

concentrations ranging from 20 to 200 µM. After incubation for 24 h, cells were washed three times with PBS and then treated with serum-free DMEM media (100 µL) and 10 µL Cell counting kit 8 solution (CCK-8, Dojindo, Rockville, MD). After incubation for another 3 h to allow for development of the CCK8 dye, absorbance was recorded at 450 and 750 nm using a BioTek Synergy Mx plate reader (BioTek, Winooski, VT). Worked-up data (absorbance at 750 nm subtracted from absorbance at 450 nm) were graphed using GraphPad InStat, version 3 (GraphPad Software, Inc., San Diego, CA). Mean values are reported together with the standard error of mean (SEM) representing the combination of 3 different experimental runs with five replicates per experiment. Cell viability assays on RAW 264.7 macrophage cells were also carried out in a similar way but the cell density was 7000 cells per well.

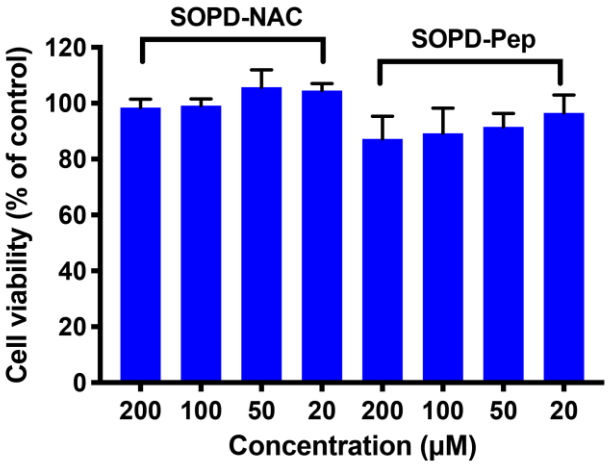

Figure S15. Cell viability of H9C2 cardiomyoctyes treated with different concentrations of **SOPD-NAC** or **SOPD-Pep** for 24 h.

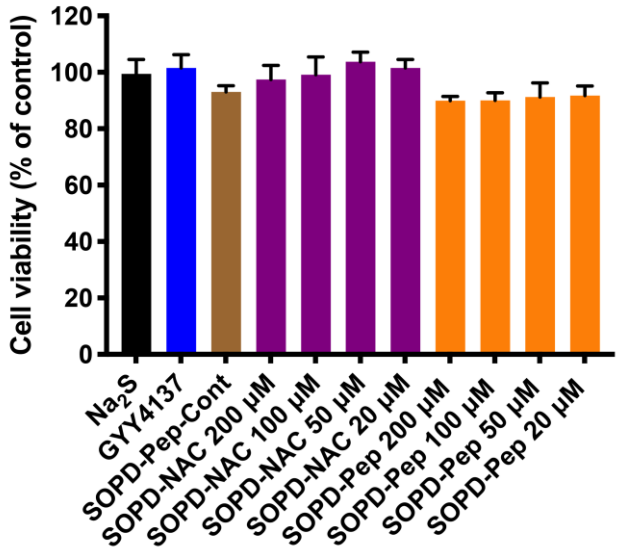

Figure S16. Cell viability of RAW 264.7 macrophage cells treated with Na_2S, GYY4137, **SOPD-Pep-Cont**, and different concentrations of **SOPD-NAC** or **SOPD-Pep** for 24 h. The concentrations of Na_2S, GYY4137, and **SOPD-Pep-Cont** were 100 µM.

Anti-inflammatory assays

RAW 264.7 macrophage cells were plated in a 96-well plate at a density of 7000 cells per well in 200 µL complete DMEM per well. After culturing for 24 h, cells were washed with 1X PBS three times before 190 µL of serum free DMEM media was added. Then cells were pre-incubated by adding an additional 5 µL of stock PMA (40 µg/mL-160 µg/mL) to each treatment well for 1 h before addition of 5 µL of 4 mM **SOPD-NAC** or **SOPD-Pep** solution in DMSO to each treatment well. After incubation for 4 h, cells were washed three times with PBS and then treated with serum-free DMEM media (100 µL) and 10 µL Cell counting kit 8 solution (CCK-8, Dojindo, Rockville, MD). After incubation for another 3 h to allow for development of the CCK8 dye, absorbance was recorded at 450 and 750 nm using a BioTek Synergy Mx plate reader (BioTek, Winooski, VT). Worked-up data (absorbance at 750 nm subtracted from absorbance at 450 nm) were graphed using GraphPad InStat, version 3 (GraphPad Software, Inc., San Diego, CA). For data analysis, multiple

comparisons were done using one-way ANOVA followed by Student-Newman-Keuls post-hoc tests for multiple pairwise examinations. Changes were identified as significant if *p* was less than 0.01. Mean values are reported together with the standard error of mean (SEM) representing the combination of 3 different experimental runs with five replicates per experiment.

In order to compare the anti-inflammation ability of different treat groups, similar cell assays were carried out. The only difference was that the PMA concentration added to the cells was 80 μg/mL. The treat groups were as follows (5 μL, 4 mM): **SOPD-NAC**, **SOPD-Pep**, **SOPD-Pep-Cont**, Na_2S, and GYY4137.

Fluorescence probe studies of H_2S release *in vitro*

Detection of H_2S release *in vitro* was analyzed using a turn-on fluorescent probe selective for H_2S (WSP-5, reported previously[1]). H9C2 cells were plated in a 24-well plate at a density of 0.1 million cells per well in 0.5 mL complete DMEM per well. After culturing for 24 h, cells were washed once with DMEM media before 490 μL serum-containing DMEM media was added. Then cells were treated with 10 μL of 10 mM **SOPD-NAC** or **SOPD-Pep** in DMSO or 10 μL of DMSO to bring the total volume to 500 μL. After incubating for 6 h, the media was removed, and cells were washed with 1X PBS three times. Next, the cells were incubated with 0.5 mL of serum-free DMEM media containing 2.5 mM WSP-5 (10 μL) and 5 mM CTAB (10 μL) for 30 min in the following groups: 250 mM BSO (10 μL) or serum-free DMEM media (10 μL). After washing with PBS three times, 0.5 mL of PBS was added to each well for imaging by fluorescence microscopy (Nikon Eclipse Ti-U) with FITC filter set. The magnification was 20X. Corrected total cell fluorescence (CTCF) intensity was estimated using the equation CTCF = integrated density − (area of selected cell) × (mean fluorescence of background). A rectangular drawing/selection tool in ImageJ was used to select a desired region with fluorescence, and its integrated density and area were

measured. Mean fluorescence intensity of the background was calculated by averaging the intensities of the selected areas that had no fluorescence.

Detection of reactive oxygen species (ROS) by the fluorescence probe *in vitro*

Detection of ROS generated *in vitro* was analyzed using a fluorescent probe selective for ROS (DHE). H9C2 cells were plated in a 24-well plate at a density of 0.6 million cells per well in 0.5 mL complete DMEM per well. After culturing for 24 h, cells were washed once with DMEM media before 487.5 μL serum-containing DMEM media was added. Then cells were treated with 12.5 μL of 8 mM **SOPD-NAC** or **SOPD-Pep** in DMSO or 12.5 μL of DMSO to bring the total volume to 500 μL. After incubating for 6 h, the media was removed, and cells were washed with 1X PBS three times. Next, the cells were incubated with 0.5 mL of serum-free DMEM media containing 1 mM DHE (5 μL) for 30 min in the following groups: 250 mM BSO (10 μL) or serum-free DMEM media (10 μL). After washing with PBS three times, 0.5 mL of PBS was added to each well for imaging by fluorescence microscopy (Nikon Eclipse Ti-U) with Cy3 filter set. The magnification was 20X. Corrected total cell fluorescence (CTCF) intensity was estimated using the equation CTCF = integrated density − (area of selected cell) × (mean fluorescence of background). A rectangular drawing/selection tool in ImageJ was used to select a desired region with fluorescence, and its integrated density and area were measured. Mean fluorescence intensity of the background was calculated by averaging the intensities of the selected areas that had no fluorescence.

References

1. B. Peng, W. Chen, C. R. Liu, E. W. Rosser, A. Pacheco, Y. Zhao, H. C. Aguilar, M. Xian, Fluorescent Probes Based on Nucleophilic Substitution-Cyclization for Hydrogen Sulfide Detection and Bioimaging. *Chem. Eur. J.* **2014**, *20*, 1010-1016.

2. C. R. Powell, K. M. Dillon, Y. Wang, R. J. Carrazzone, J. B. Matson, A Persulfide Donor Responsive to Reactive Oxygen Species: Insights into Reactivity and Therapeutic Potential. *Angew. Chem. Int. Ed.* **2018**, 57, 6324-6328.

3. B. Q. Xiong, C. H. Hu, H. T. Li, C. S. Zhou, P. L. Zhang, Y. Liu, K. W. Tang, CDI-promoted direct esterification of P(O)-OH compounds with phenols. *Tetrahedron Lett.* **2017**, *58*, 2482-2486.

4. X. Y. Gao, G. X. Feng, P. N. Manghnani, F. Hu, N. Jiang, J. Z. Liu, B. Liu, J. Z. Sun, B. Z. Tang, A two-channel fluorescent probe with AIE characteristics and its application for selective imaging of superoxide anions in living cells. *Chem. Commun.* **2017**, *53*, 1653-1656.

5. M. N. Hughes, H. G. Nicklin, The chemistry of pernitrites, Part 1: Kinetics of decomposition of pernitrous acid. *J. Chem. Soc. A* **1968**, 450-452.

Chapter 4: Polymeric persulfide prodrugs: Mitigating oxidative stress through controlled delivery of reactive sulfur species

Adapted with permission from: Dillon, K. M., et al. "Polymeric persulfide prodrugs: Mitigating oxidative stress through controlled delivery of reactive sulfur species." ACS Macro Letters **4**: 606-612.

4.1. Authors

Kearsley M. Dillon, Ryan J. Carrazzone, Yin Wang, Chadwick R. Powell, and John B. Matson

Department of Chemistry, Virginia Tech Center for Drug Discovery, and Macromolecules Innovation Institute, Virginia Tech, Blacksburg, VA 24061, United States

4.2. Abstract

Related biologically to the known gasotransmitter hydrogen sulfide (H_2S), persulfides (R–SSH) have recently been recognized as native signaling compounds and redox regulators in their own right. Reported here is the synthesis, characterization, and *in vitro* evaluation of a small molecule persulfide donor and its polymeric counterpart, both of which release *N*-acetyl cysteine persulfide (NAC-SSH) in response to esterases. The donors, termed EDP-NAC and poly(EDP-NAC), underwent controlled decomposition in response to porcine liver esterase, resulting in pseudo-first-order release half-lives of 1.6 h ± 0.3 h and 36.0 h ± 0.6 h, respectively. In cell experiments, slow-releasing poly(EDP-NAC) rescued H9C2 cardiomyocytes more effectively than EDP-NAC when cells were treated with 5-fluorouricil (5-FU), which induces sustained production of ROS. Neither

EDP-NAC nor poly(EDP-NAC) rescued MCF-7 breast cancer cells from 5-FU-induced oxidative stress, suggesting that polymeric persulfide donors could be used as adjuvants to reduce the deleterious cardiotoxic effects of many chemotherapeutics.

4.3. Introduction

Macromolecular prodrug systems offer a means to modulate the chemical, physical, and pharmacokinetic properties of a drug without extensively changing its chemical nature.[1] This drug delivery strategy can be particularly helpful for the delivery of drugs that are rapidly cleared, have narrow therapeutic indices, or generate adverse side effects. Both physical encapsulation or covalent attachment of a drug to a polymer can improve circulation time and extend release rates to maintain therapeutic efficacy without reaching supratherapeutic concentrations.[2-4] Due to their ability to modulate these important pharmacological properties of drugs, several polymer prodrug systems have exhibited therapeutic efficacy in a clinical setting. For example, in 1999, Duncan and Kopecek developed the first polymer-doxorubicin conjugates, which were studied in phase I and II clinical trials.[5] Despite this progress in delivery of conventional drugs, much less attention has been paid to polymers for delivery of reactive signaling molecules, which can have profound biological effects.[6-9] Due to their instability, reactive signaling molecules, such as reactive sulfur species (RSS), stand to benefit from polymer prodrug delivery even more than stable small molecule drugs, but such prodrugs are almost entirely unexplored.

Sulfur takes on oxidations states ranging from +2 to -6 in the body, with many types of RSS implicated in the (patho)physiological pathways that exist within oxidation states between the extremes.[10] Interest in the biological roles of RSS has increased dramatically following the 1996

discovery that hydrogen sulfide (H_2S) serves as an endogenous neuromodulator.[11] In the time since this initial report, many different types of H_2S-releasing compounds (termed H_2S donors) have been synthesized to aid in probing its signaling pathways and to realize its therapeutic potential. Thus far, H_2S donors with a variety of triggers have been developed, including water,[12-14] nucleophiles,[15-16] light,[17-18] and enzymes.[19-22] More recently, donors of related RSS, including carbonyl sulfide (COS),[23-24] sulfur dioxide (SO_2),[25-28] and persulfides (also called perthiols, R–SSH)[29-32] have also been developed. All of these donors increase our understanding of the roles that RSS play in a biological context, and some may hold therapeutic value in the form of prodrugs and drug conjugates.[6, 33]

In particular, persulfides are now of interest because recent advances in redox biology indicate that native persulfides carry out vital physiological functions as signaling products of H_2S.[34-37] Persulfides contain an internal sulfur atom with an oxidation state of 0 and are endogenously constructed *via* disulfide exchange reactions between H_2S and biologically relevant disulfides mediated by cystathionine gamma lyase (CSE) and cystathionine β-synthase (CBS). Due to the high abundance of their corresponding thiols, the most common persulfides in eukaryote systems are cysteine persulfide (Cys–SSH) and glutathione persulfide (G–SSH).[38] The physiological importance of persulfides is likely due to their enhanced nucleophilicity (*via* the alpha effect) relative to thiols.[39] This increase in nucleophilicity has multiple proposed effects on protein activity, where S-atom transfer from Cys–SSH or G–SSH generates persulfidated Cys residues on proteins.[40] For example, persulfidated proteins are generally more reactive than their native (i.e., unpersulfidated) analogs. Another outcome of protein persulfidation is protection of enzyme thiols from irreversible oxidation, where the terminal sulfur atom of a persulfide reacts with oxidants more readily than the internal sulfur atom.[41-42] Breaking the S–S bond in a reductive step then

regenerates the protein thiol, so the terminal sulfur atom acts as a sacrificial oxidant in the process. Thus, with multiple mechanisms to enhance or protect enzyme activity, persulfides appear to be important players in the reactive species interactome.[43]

Here we aimed to develop polymer persulfide donors, with the goal of extending their release half-life compared with small molecule persulfide donors and evaluate the biological effects resulting from sustained release. No polymeric persulfide donors have been reported, but currently available small molecule persulfide donors release persulfides in response to a variety of stimuli, including hydrogen peroxide (H_2O_2), esterase activity, pH changes, and addition of F^-.[29-32, 44] For example, Wang and coworkers reported an esterase-sensitive persulfide donor that utilized a 1,2-elimination reaction to release its persulfide payload (Scheme 1a), showing protective effects in myocardial ischemia/reperfusion injury.[31] The same group also recently reported the synthesis and characterization of a G–SSH donor using a trimethyl lock caging group (Scheme 1b).[45] Our lab recently developed a persulfide donor that responds to H_2O_2, utilizing a 1,6-elimination reaction to release *N*-acetyl cysteine persulfide (NAC–SSH), which rescued H9C2 cardiomyocytes from H_2O_2-induced oxidative stress as effectively or more effectively than a number of H_2S donors.[29] In spite of this recent progress in the development of persulfide donors, none thus far are capable of providing sustained persulfide release under specific release conditions. Persulfide prodrugs with longer half-lives could be more effective in mitigating chronic disease states (such as inflammation) than fast donors because fewer administrations would be required for the same level of therapeutic effects. Therefore, we hypothesized that a polymeric persulfide prodrug could provide longer lasting persulfide release and alleviate sustained oxidative stress more effectively than an equivalent small molecule by sterically shielding the cleavable bond from a triggering enzyme.

4.4. Results and Discussion

We envisioned that the ideal persulfide prodrug would be inert under physiological conditions but undergo controlled decomposition in response to a stimulus, resulting in the breakdown of any caging groups (or linkers) and release of the persulfide payload (Scheme 1c). To avoid premature release, the persulfide payload should be caged using a protecting group that is stable in biological media but responds to a stimulus to release the persulfide under desired conditions. Therefore, we envisioned that a benzyl linker capable of undergoing 1,6-elimination (sometimes called self-immolation)[46] would provide a means of protecting the persulfide, yet reveal it under conditions governed by the functionality installed at the *para* position. Several prodrug systems have utilized this linker to effectively release RSS, including COS and H_2S prodrugs and our previously reported H_2O_2-responsive persulfide prodrug.[22, 24, 29] Ester functionalities are responsive to biologically ubiquitous esterases and are easy to install on the benzyl linker, and release half-lives can be dramatically increased simply by installing bulkier esters.[47] Therefore, we set out to synthesize a modular, esterase-responsive persulfide prodrug with the potential for conjugation to a polymer backbone.

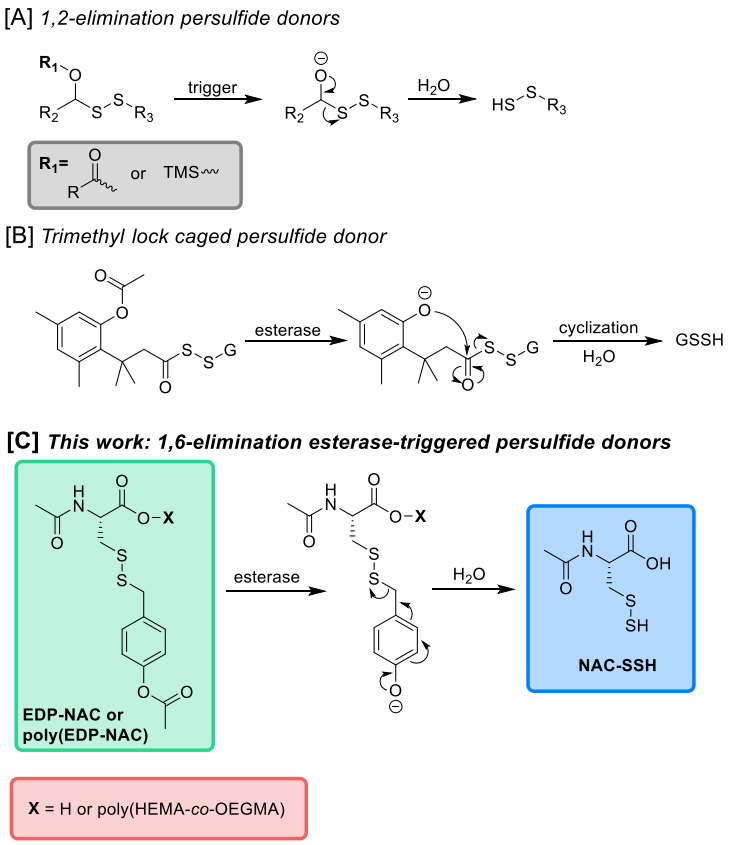

Scheme 1: Depiction of reported esterase-triggered persulfide donors and the small molecule and polymeric persulfide donors targeted here. [A] 1,2-Elimination persulfide donors; [B] Trimethyl lock caged persulfide donor with pendant glutathione (GSH) disulfide; [C] Small molecule and polymeric esterase-responsive 1,6-elimination persulfide donors (this work).

Given these design parameters, we first synthesized a small molecule persulfide donor, which we termed EDP-NAC (Ester Disulfide-Prodrug *N*-Acetyl Cysteine). EDP-NAC was synthesized in four simple steps with an overall yield of 44% (Scheme 2). First, *p*-cresol was acetylated with acetic anhydride in the presence of Na_2CO_3 as a proton scavenger. This product, *p*-tolyl acetate (**1**), was then brominated using *N*-bromosuccinimide (NBS) as a bromine source and azobisisobutyronitrile (AIBN) as a radical initiator. The resulting benzyl bromide (**2**) was then

converted into a thiol using thiourea as a nucleophile, followed by addition of *N*-butylamine to cleave the resulting thiouronium intermediate, generating *p*-(mercaptomethyl)phenyl acetate (**3**). Finally, reaction of thiol **3** with activated *N*-acetyl cysteine disulfide (NAC-pyDS) afforded EDP-NAC. EDP-NAC is water soluble up to low millimolar concentrations and dually tunable at both the ester and disulfide.

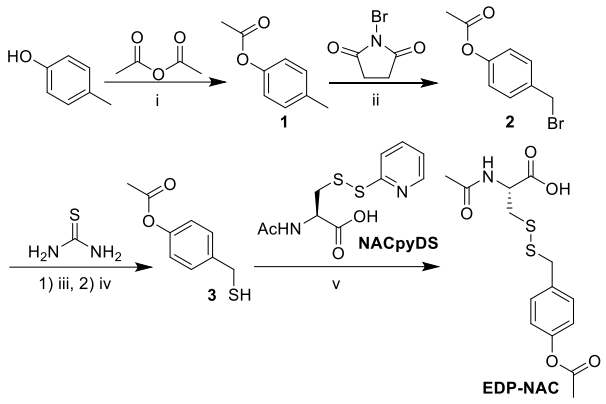

Scheme 2: Synthesis of EDP-NAC. Reaction conditions: i) Na_2CO_3, EtOAc, rt, 16 h; ii) AIBN, benzene, reflux, 16 h; iii) MeOH, rt, 16 h; iv) butylamine, $CHCl_3$, rt, 24 h; v) CH_2Cl_2, rt, 16 h

Persulfide-release from EDP-NAC was then evaluated utilizing fluorodinitrobenzene (FDNB), which has been shown to efficiently trap persulfides.[48] For all persulfide release experiments, we triggered release using porcine liver esterase (PLE), a representative esterase from this broad class of ubiquitous ester-hydrolyzing enzymes.[49] A one-dram vial was charged with a solution of EDP-NAC, FDNB, and water to give a clear, yellow solution. An aliquot was removed for a t=0 timepoint, then PLE was added to the reaction mixture, and additional aliquots were withdrawn at pre-determined time points for analysis by analytical HPLC (Figure 1, S18). At t=0, a single peak

was observed at an elution time of 3.8 min, corresponding to EDP-NAC. This peak decreased in intensity over time, and a new peak appeared at 4.9 min elution time over the course of an hour. This new peak showed the same elution time as authentic dinitrobenzene *N*-acetylcysteine disulfide (DNB-NAC), confirming that it was the product of the trapping reaction between FDNB and NAC-SSH (DNB-NAC, Figure S19). These results highlight the clean conversion from EDP-NAC to NAC persulfide.

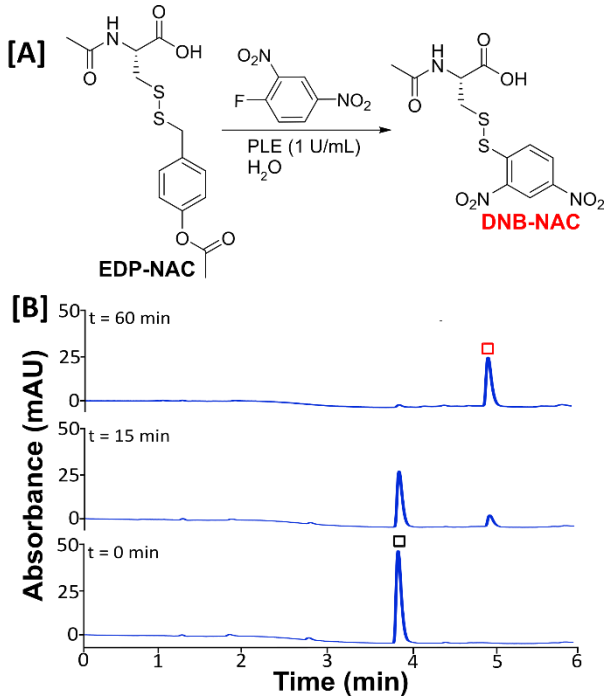

Figure 1: Persulfide trapping from EDP-NAC via reaction with FDNB. [A] Scheme depicting persulfide trapping using FDNB; [B] Analytical HPLC traces showing the loss of EDP-NAC and the production of persulfide adduct DNB-NAC over time. The peak eluting at 3.8 min (black square) corresponds to EDP-NAC while the peak at 4.9 min (red square) corresponds to the persulfide adduct DNB-NAC. Monitoring wavelength was 282 nm.

Convinced that the small molecule prodrug released NAC-SSH as intended, we set out to design a polymeric persulfide donor, termed poly(EDP-NAC) (Scheme 3). First, a block copolymer composed of 2-hydroxyethyl methacrylate and oligo(ethylene glycol) methacrylate, poly(HEMA-*co*-OEGMA), was synthesized via reversible addition-fragmentation chain-transfer (RAFT) polymerization. RAFT was chosen due to its ability to provide good control over the degree of polymerization and molar mass dispersity ($Đ_M$) of the resulting copolymers.[50] Next, poly(HEMA-*co*-OEGMA) (M_n = 10.4 kg/mol, $Đ_M$ = 1.28) was then coupled to EDP-NAC *via* EDC coupling at near 100% conversion to form poly(EDP-NAC) (M_n = 13.2 kg/mol, $Đ_M$ = 1.19). Comparative SEC traces of poly(HEMA-*co*-OEGMA) and poly(EDP-NAC) are included in Figure S22, showing a clear shift toward lower elution time after attachment of EDP-NAC. Additionally, poly(EDP-NAC) at 50% functionalization was synthesized using the same methods (Figure S14).

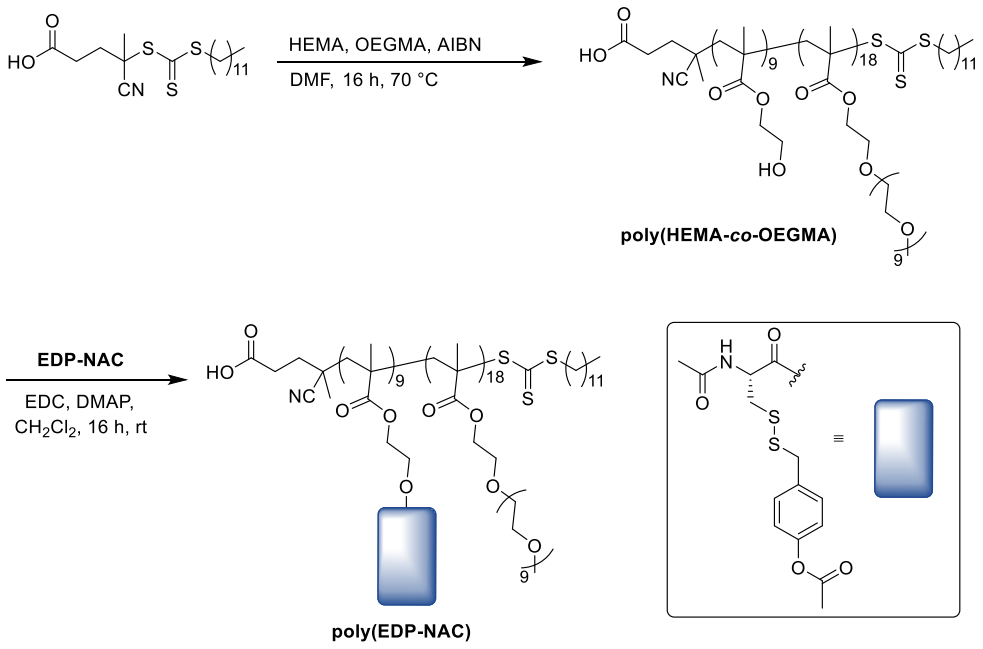

Scheme 3. Synthetic route to poly(HEMA-*co*-OEGMA) and poly(EDP-NAC) copolymers

With EDP-NAC and poly(EDP-NAC) in hand, we set out to compare their persulfide release kinetics. Because analytical HPLC is difficult with polymeric substrates, we used ^{1}H NMR spectroscopy to compare the half-lives between the small molecule and polymer prodrugs. First, EDP-NAC and poly(EDP-NAC) were each dissolved in DMSO-d_6 in an NMR tube, diluted with D_2O, and a t=0 timepoint was taken. Of note, poly(EDP-NAC) was much more water soluble than EDP-NAC, but a ratio of 1:4 DMSO-d_6:D_2O was used in both experiments for sake of consistency. Next, PLE was injected into each NMR tube, and spectra were collected at subsequent timepoints as shown in Figure 2.

By comparing ^{1}H NMR spectra over time for both EDP-NAC and poly(EDP-NAC), pseudo-first-order persulfide release half-lives were determined. Figure 2B shows stacked spectra for EDP-NAC treated with PLE. Before the addition of PLE (t=0 h), two aromatic signals corresponding to EDP-NAC were observed at 7.0 and 7.3 ppm (a and b, respectively). After addition of PLE (t=0.4 h), two new sets of signals appeared in the aromatic region (6.7 and 7.1 ppm, a' and b' respectively). These signals were attributed to the formation of *p*-hydroxybenzyl alcohol (pHBA), as confirmed by comparison to an authentic standard. No other aromatic signals were present in the ^{1}H NMR spectra, indicating clean conversion of EDP-NAC to pHBA. With these results, we measured a pseudo-first-order release half-life ($t_{1/2}$) of 1.6 h ± 0.3 h. Using a similar technique with dimethyl sulfone as an internal standard (Figure S20), the $t_{1/2}$ of 100% functionalized poly(EDP-NAC) was measured to be 36.0 h ± 0.6 h, while the $t_{1/2}$ of 50% functionalized poly(EDP-NAC) was measured to be 26 ± 3 h. A kinetics plot comparing EDP-NAC to 100% functionalized poly(EDP-NAC) under the same release conditions is shown in Figure 2C. Only 100% functionalized poly(EDP-NAC) was utilized in *in vitro* studies due to its longer half-life.

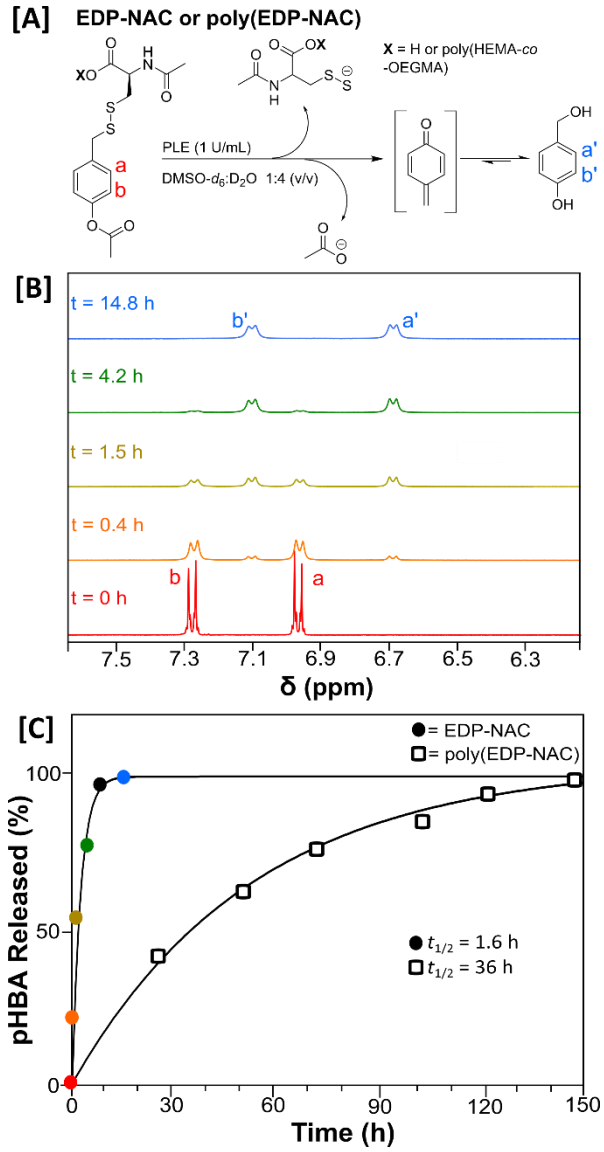

Figure 2: ^{1}H NMR analysis of pHBA release kinetics. [A] Proposed mechanism of pHBA release from EDP-NAC and poly(EDP-NAC); [B] ^{1}H NMR traces depicting disappearance of EDP-NAC and the appearance of pHBA; [C] Comparative kinetics plots of EDP-NAC and poly(EDP-NAC). Release half-lives were measured to be 1.6 h ± 0.3 h and 36.0 h ± 0.6 h for EDP-NAC and poly(EDP-NAC), respectively.

Persulfides, naturally-occurring biological reductants, possess the capacity to quench reactive oxygen species (ROS), and thus reduce inflammation. Thus, we set out to investigate the ability of EDP-NAC and poly(EDP-NAC) to quench ROS *in vitro*. First, however, we evaluated cell viability of EDP-NAC and poly(EDP-NAC). H9C2 cardiomyocytes were treated with EDP-NAC and incubated for 4 h before measuring viability. Both EDP-NAC and poly(EDP-NAC) exhibited no toxicity under these conditions, maintaining high cell viability up to concentrations of 400 μM prodrug (Figure S25A and B).

H_2O_2 is one of the most common naturally occurring ROS. We expected EDP-NAC, with its short persulfide release half-life, to be effective in combating toxicity induced by direct addition of H_2O_2 to cells. In contrast, 5-fluorouracil (5-FU) is a common cancer drug that produces ROS slowly over time; in fact, it is typically administered *via* bolus injection on a weekly schedule due to its sustained production of ROS over the course of multiple days.[51] Additionally, dosing of 5-FU in cancer patients is largely limited by off-target toxicity due to its narrow therapeutic window. For healthy cells exposed to 5-FU, we envisioned that poly(EDP-NAC) might be effective in mitigating ROS-induced toxicity due to its ability to produce persulfides in a sustained manner. Therefore, given the large discrepancies in half-life, we hypothesized that EDP-NAC would be better suited to quench ROS on a shorter timescale (direct H_2O_2 addition), while poly(EDP-NAC) would perform better in response to a sustained release of ROS (generated as a result of treatment with 5-FU) due to its extended persulfide release half-life.

To investigate the antioxidative properties of the prodrugs, H9C2 cardiomyocytes were exposed to H_2O_2 (100 μM) concomitantly with EDP-NAC or poly(EDP-NAC) for 1 h incubation time (Figure 3A). Cells receiving no persulfide donor (i.e., H_2O_2 only), were only 45% viable after H_2O_2 treatment. In contrast, EDP-NAC increased viability to 59% at 100 μM and 78% at 200 μM,

demonstrating the ability of EDP-NAC to rescue cells from the hazardous effects of H_2O_2. Poly(EDP-NAC) was not able to rescue cells as well under these conditions—treatment with 100 µM and 200 µM led to statistically smaller increases in viability over the H_2O_2-only control, reaching 51% and 57% viability, respectively. Therefore, consistent with our hypothesis, EDP-NAC was more effective in mitigating H_2O_2-induced oxidative stress than poly(EDP-NAC). Similar experiments were performed with KO_2 as a donor of superoxide, another type of endogenous reactive oxygen species, and the same trends were observed with generally lower cell viabilities. (Figure S24A).

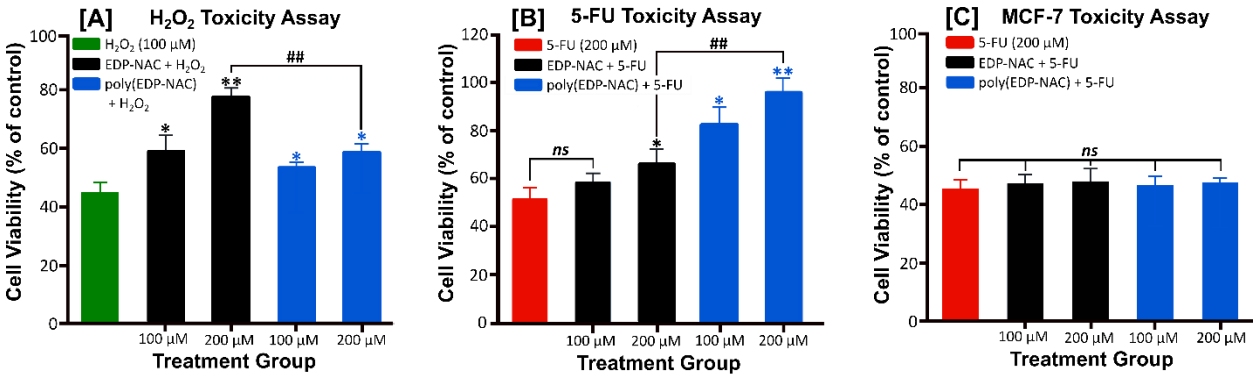

Figure 3: Cell viability of H9C2 (panels A and B) or MCF-7 cells (panel C) treated with EDP-NAC or poly(EDP-NAC). [A]: H9C2 H_2O_2 toxicity assay. H9C2 cells were treated with 100 µM H_2O_2 only (green bar) or co-treated with H_2O_2 and EDP-NAC (black bars) or H_2O_2 and poly(EDP-NAC) (blue bars) for 1 h exposure time. [B]: H9C2 5-FU toxicity assay. H9C2 cells were treated with 200 µM 5-FU only (red bar) or co-treated with 5-FU and EDP-NAC (black bars) or 5-FU and poly(EDP-NAC) (blue bars) for 4 h exposure time. [C]: MCF-7 5-FU toxicity assay. MCF-7 cells were treated with 5-FU only (red bar) or co-treated with 5-FU and EDP-NAC (black bars) or 5-FU and poly(EDP-NAC) (blue bars) for 4 h exposure time. Quantification of cell viability was

conducted using Cell Counting Kit-8 (CCK-8). *P<0.05 and **P<0.01 for comparisons against H_2O_2-only or 5-FU-only control treatment groups. ##P<0.01 for comparisons between EDP-NAC and poly(EDP-NAC) as indicated. Error bars indicate standard deviation of three separate experiments (n = 3, with 4 or 5 wells in each group in each experiment). Statistical analyses were conducted using a one-way analysis of variance (ANOVA) with a Student–Newman–Keuls post-hoc test.

Next, EDP-NAC and poly(EDP-NAC) were evaluated for their efficacy in rescuing H9C2 cells from 5-FU exposure. EDP-NAC and poly(EDP-NAC) were each co-administered with 5-FU (200 μM) for 4 h incubation time. Cells receiving no prodrug were only 51% viable after treatment with 5-FU. Co-treatment with poly(EDP-NAC) (200 μM) resulted in nearly 100% H9C2 viability under this timescale, whereas co-treatment with EDP-NAC (200 μM) only resulted in 65% viability. (Figure 3B) These findings are consistent with the extended half-life of poly(EDP-NAC) providing an appropriate amount of available persulfide to combat ROS produced slowly by 5-FU, whereas EDP-NAC is consumed at a rate that is most likely too fast to combat sustained ROS production.

Ideally, antioxidative effects would only be observed in non-cancer cells for EDP-NAC (or poly(EDP-NAC)) to be considered usable for co-administration in chemotherapy. Therefore, we investigated the ability of EDP-NAC and poly(EDP-NAC) to rescue MCF-7 breast cancer cells against 5-FU exposure. First, general toxicity assays were performed by treating MCF-7 cells with each prodrug for 4 h. No decrease in viability was observed up to 200 μM (Figure S25D). Next, EDP-NAC and poly(EDP-NAC) were each co-administered with 5-FU (200 μM) in MCF-7 cancer cells and incubated for 4 h. Neither EDP-NAC nor poly(EDP-NAC) rescued MCF-7 cells from 5-FU exposure, as viability was consistently around 50% in all treatment groups compared with an

untreated control group (Figure 3C). Additionally, we performed an identical MCF-7 toxicity assay for 24 h treatment time and observed similar outcomes, with viabilities near 40% for all treatment groups (Figure S24B). We hypothesize that the inability of EDP-NAC and poly(EDP-NAC) to rescue MCF-7 cells from 5-FU exposure results from a shift in redox balance of the cancer cells towards a more reducing environment, which contrasts with their naturally higher oxidative cell environment.[52]

Taken together, these cell experiments show that EDP-NAC was more effective in mitigating ROS-induced toxicity in healthy H9C2 cardiomyocytes by H_2O_2, an immediately available form of ROS. However, poly(EDP-NAC) was more effective in mitigating toxicity in H9C2 cells treated with 5-FU, a sustained ROS-inducer. Neither EDP-NAC nor poly(EDP-NAC) rescued MCF-7 breast cancer cells from 5-FU exposure, suggesting that persulfide donors like EDP-NAC and poly(EDP-NAC) could be useful in mitigating cardiotoxicity without hindering anticancer activity of oncology medications.

4.5. Conclusions

In summary, a polymeric persulfide prodrug, poly(EDP-NAC), was synthesized for the first time. Persulfide release, as characterized by ^{1}H NMR spectroscopy and analytical HPLC, was over an order of magnitude slower in poly(EDP-NAC) than a small molecule analog (EDP-NAC). In cell studies, EDP-NAC rescued H9C2 cardiomyocytes from H_2O_2 exposure more effectively than poly(EDP-NAC), while poly(EDP-NAC) rescued H9C2 cells exposed to 5-FU more effectively than EDP-NAC. Neither EDP-NAC nor poly(EDP-NAC) mitigated 5-FU-induced toxicity in MCF-7 breast cancer cells, suggesting that persulfide prodrugs may be appropriate for coadministration with chemotherapeutics to minimize off-target toxicity. This work highlights the importance of matching the release half-life of persulfide prodrugs with the appropriate disease condition, placing polymeric persulfide donors in a promising position to combat chronic disease states due to their extended release profiles and potentially extended circulation times in comparison to small molecule analogs. We envision that similar polymeric persulfide prodrug systems may be developed to afford a wide variety of materials for end-use applications including gels, coatings, and functional biomaterials that are properly tuned to combat specific disease indications.

4.6. Acknowledgements

This work was supported by the National Science Foundation (DMR-1454754) and the National Institutes of Health (R01GM123508). The authors thank Clay Arrington for performing TGA on polymer samples. The authors also thank Dr. Mehdi Ashraf-Khorassani for help with analytical HPLC and HRMS characterization of persulfide release and confirmation of molecular structure.

4.7. References

1. Meng, Q.; Hu, H.; Zhou, L.; Zhang, Y.; Yu, B.; Shen, Y.; Cong, H., Logical design and application of prodrug platforms. *Polym. Chem.* **2019,** *10* (3), 306-324.

2. Meng, Z.; Lv, Q.; Lu, J.; Yao, H.; Lv, X.; Jiang, F.; Lu, A.; Zhang, G., Prodrug Strategies for Paclitaxel. *Int. J. Mol. Sci.* **2016,** *17* (5), 796-801.

3. Dragojevic, S.; Ryu, J. S.; Raucher, D., Polymer-Based Prodrugs: Improving Tumor Targeting and the Solubility of Small Molecule Drugs in Cancer Therapy. *Molecules* **2015,** *20* (12), 21750-21769.

4. Senapati, S.; Mahanta, A. K.; Kumar, S.; Maiti, P., Controlled drug delivery vehicles for cancer treatment and their performance. *Signal. Transduct. Tar.* **2018,** *3* (1), 1-19.

5. Vasey, P. A.; Kaye, S. B.; Morrison, R.; Twelves, C.; Wilson, P.; Duncan, R.; Thomson, A. H.; Murray, L. S.; Hilditch, T. E.; Murray, T.; Burtles, S.; Fraier, D.; Frigerio, E.; Cassidy, J., Phase I Clinical and Pharmacokinetic Study of PK1 [N-(2-Hydroxypropyl)methacrylamide Copolymer Doxorubicin]: First Member of a New Class of Chemotherapeutic Agents-Drug-Polymer Conjugates. *Clin. Cancer Res.* **1999,** *5* (1), 83-94.

6. Powell, C. R.; Dillon, K. M.; Matson, J. B., A review of hydrogen sulfide (H_2S) donors: Chemistry and potential therapeutic applications. *Biochem. Pharmacol.* **2018,** *149*, 110-123.

7. Yang, G.; Sener, A.; Ji, Y.; Pei, Y.; Pluth, M. D., Gasotransmitters in Biology and Medicine: Molecular Mechanisms and Drug Targets. *Oxid. Med. Cell. Longev.* **2016,** *2016*, 1-2.

8. Urquhart, M. C.; Ercole, F.; Whittaker, M. R.; Boyd, B. J.; Davis, T. P.; Quinn, J. F., Recent advances in the delivery of hydrogen sulfide via a macromolecular approach. *Polym. Chem.* **2018,** *9* (35), 4431-4439.

9. Zhang, J.; Hao, X.; Sang, W.; Yan, Q., Hydrogen Polysulfide Biosignal-Responsive Polymersomes as a Nanoplatform for Distinguishing Intracellular Reactive Sulfur Species (RSS). *Small* **2017,** *13* (39), 1701601.

10. Álvarez, L.; Bianco, C. L.; Toscano, J. P.; Lin, J.; Akaike, T.; Fukuto, J. M., Chemical Biology of Hydropersulfides and Related Species: Possible Roles in Cellular Protection and Redox Signaling. *Antioxid. Redox. Signal.* **2017,** *27* (10), 622-633.

11. Abe, K.; Kimura, H., The possible role of hydrogen sulfide as an endogenous neuromodulator. *J. Neurosci.* **1996,** *16* (3), 1066-1071.

12. Li, L.; Whiteman, M.; Guan, Y. Y.; Neo, K. L.; Cheng, Y.; Lee, S. W.; Zhao, Y.; Baskar, R.; Tan, C.-H.; Moore, P. K., Characterization of a Novel, Water-Soluble Hydrogen Sulfide–Releasing Molecule (GYY4137). *Circulation* **2008,** *117* (18), 2351.

13. Nicolau, L. A. D.; Silva, R. O.; Damasceno, S. R. B.; Carvalho, N. S.; Costa, N. R. D.; Aragão, K. S.; Barbosa, A. L. R.; Soares, P. M. G.; Souza, M. H. L. P.; Medeiros, J. V. R., The hydrogen sulfide donor, Lawesson's reagent, prevents alendronate-induced gastric damage in rats. *Braz. J. Med. Biol. Res.* **2013,** *46*, 708-714.

14. Zhao, W.; Zhang, J.; Lu, Y.; Wang, R., The vasorelaxant effect of H_2S as a novel endogenous gaseous K(ATP) channel opener. *EMBO J.* **2001,** *20* (21), 6008-6016.

15. Zhao, Y.; Wang, H.; Xian, M., Cysteine-Activated Hydrogen Sulfide (H_2S) Donors. *J. Am. Chem. Soc.* **2011,** *133* (1), 15-17.

16. Foster, J. C.; Powell, C. R.; Radzinski, S. C.; Matson, J. B., *S*-Aroylthiooximes: A Facile Route to Hydrogen Sulfide Releasing Compounds with Structure-Dependent Release Kinetics. *Org. Lett.* **2014,** *16* (6), 1558-1561.

17. Fukushima, N.; Ieda, N.; Sasakura, K.; Nagano, T.; Hanaoka, K.; Suzuki, T.; Miyata, N.; Nakagawa, H., Synthesis of a photocontrollable hydrogen sulfide donor using ketoprofenate photocages. *Chem. Commun.* **2014,** *50* (5), 587-589.

18. Devarie-Baez, N. O.; Bagdon, P. E.; Peng, B.; Zhao, Y.; Park, C.-M.; Xian, M., Light-Induced Hydrogen Sulfide Release from "Caged" gem-Dithiols. *Org. Lett.* **2013,** *15* (11), 2786-2789.

19. Zheng, Y.; Yu, B.; Ji, K.; Pan, Z.; Chittavong, V.; Wang, B., Esterase-Sensitive Prodrugs with Tunable Release Rates and Direct Generation of Hydrogen Sulfide. *Angew. Chem. Int. Ed.* **2016,** *55* (14), 4514-4518.

20. Chauhan, P.; Bora, P.; Ravikumar, G.; Jos, S.; Chakrapani, H., Esterase Activated Carbonyl Sulfide/Hydrogen Sulfide (H_2S) Donors. *Org. Lett.* **2017,** *19* (1), 62-65.

21. Li, Z.; Organ, C. L.; Zheng, Y.; Wang, B.; Lefer, D. J., Novel Esterase-Activated Hydrogen Sulfide Donors Attenuate Myocardial Ischemia/Reperfusion Injury. *Circulation* **2016,** *134*, 17903.

22. Shukla, P.; Khodade, V. S.; SharathChandra, M.; Chauhan, P.; Mishra, S.; Siddaramappa, S.; Bulagonda, E. P.; Singh, A.; Chakrapani, H., "On Demand" Redox Buffering by H_2S Contributes to Antibiotic Resistance Revealed by a Bacteria-Specific H_2S Donor. *Chem. Sci.* **2017,** *8*, 4967-4972.

23. Powell, C. R.; Foster, J. C.; Okyere, B.; Theus, M. H.; Matson, J. B., Therapeutic Delivery of H_2S via COS: Small Molecule and Polymeric Donors with Benign Byproducts. *J. Am. Chem. Soc.* **2016,** *138* (41), 13477-13480.

24. Steiger, A. K.; Pardue, S.; Kevil, C. G.; Pluth, M. D., Self-Immolative Thiocarbamates Provide Access to Triggered H_2S Donors and Analyte Replacement Fluorescent Probes. *J. Am. Chem. Soc.* **2016,** *138* (23), 7256-7259.

25. Wang, W.; Ji, X.; Du, Z.; Wang, B., Sulfur dioxide prodrugs: triggered release of SO_2 via a click reaction. *Chem. Commun.* **2017,** *53* (8), 1370-1373.

26. Day, J. J.; Yang, Z.; Chen, W.; Pacheco, A.; Xian, M., Benzothiazole Sulfinate: a Water-Soluble and Slow-Releasing Sulfur Dioxide Donor. *ACS Chem. Biol.* **2016,** *11* (6), 1647-1651.

27. Malwal, S. R.; Sriram, D.; Yogeeswari, P.; Konkimalla, V. B.; Chakrapani, H., Design, Synthesis, and Evaluation of Thiol-Activated Sources of Sulfur Dioxide (SO_2) as Antimycobacterial Agents. *J. Med. Chem.* **2012,** *55* (1), 553-557.

28. Venkatesh, Y.; Kiran, K. S.; Shah, S. S.; Chaudhuri, A.; Dey, S.; Singh, N. D. P., One- and two-photon responsive sulfur dioxide (SO_2) donors: a combinatorial drug delivery for improved antibiotic therapy. *Org. Biomol. Chem.* **2019,** *17* (10), 2640-2645.

29. Powell, C. R.; Dillon, K. M.; Wang, Y.; Carrazzone, R. J.; Matson, J. B., A Persulfide Donor Responsive to Reactive Oxygen Species: Insights into Reactivity and Therapeutic Potential. *Angew. Chem. Int. Ed.* **2018,** *57* (21), 6324-6328.

30. Kang, J.; Xu, S.; Radford Miles, N.; Zhang, W.; Kelly Shane, S.; Day Jacob, J.; Xian, M., O→S Relay Deprotection: A General Approach to Controllable Donors of Reactive Sulfur Species. *Angew. Chem. Int. Ed.* **2018,** *57* (20), 5893-5897.

31. Zheng, Y.; Yu, B.; Li, Z.; Yuan, Z.; Chelsea, L.; Rishi, K.; Wang, S.; Lefer David, J.; Wang, B., An Esterase-Sensitive Prodrug Approach for Controllable Delivery of Persulfide Species. *Angew. Chem.* **2017,** *129* (39), 11911-11915.

32. Artaud, I.; Galardon, E., A Persulfide Analogue of the Nitrosothiol SNAP: Formation, Characterization and Reactivity. *Chembiochem* **2014,** *15* (16), 2361-2364.

33. Kaur, K.; Carrazzone, R. J.; Matson, J. B., The Benefits of Macromolecular/Supramolecular Approaches in Hydrogen Sulfide Delivery: A Review of Polymeric and Self-Assembled Hydrogen Sulfide Donors. *Antioxid. Redox. Signal.* **2020,** *32* (2), 79-95.

34. Kasamatsu, S.; Nishimura, A.; Morita, M.; Matsunaga, T.; Abdul Hamid, H.; Akaike, T., Redox Signaling Regulated by Cysteine Persulfide and Protein Polysulfidation. *Molecules* **2016,** *21* (12), 1721.

35. Yadav, P. K.; Martinov, M.; Vitvitsky, V.; Seravalli, J.; Wedmann, R.; Filipovic, M. R.; Banerjee, R., Biosynthesis and Reactivity of Cysteine Persulfides in Signaling. *J. Am. Chem. Soc.* **2016,** *138* (1), 289-299.

36. Cuevasanta, E.; Möller, M. N.; Alvarez, B., Biological chemistry of hydrogen sulfide and persulfides. *Arch. Biochem. Biophys.* **2017,** *617* (Supplement C), 9-25.

37. Filipovic, M. R.; Zivanovic, J.; Alvarez, B.; Banerjee, R., Chemical Biology of H_2S Signaling through Persulfidation. *Chem. Rev.* **2018,** *118* (3), 1253-1337.

38. Poole, L. B., The basics of thiols and cysteines in redox biology and chemistry. *Free Radic. Biol. Med.* **2015,** *80*, 148-157.

39. Ida, T.; Sawa, T.; Ihara, H.; Tsuchiya, Y.; Watanabe, Y.; Kumagai, Y.; Suematsu, M.; Motohashi, H.; Fujii, S.; Matsunaga, T.; Yamamoto, M.; Ono, K.; Devarie-Baez, N. O.; Xian, M.; Fukuto, J. M.; Akaike, T., Reactive cysteine persulfides and *S*-polythiolation regulate oxidative stress and redox signaling. *Proc. Natl. Acad. Sci.* **2014,** *111* (21), 7606.

40. Filipovic, M. R., Persulfidation (S-sulfhydration) and H_2S. *Handb. Exp. Pharmacol.* **2015,** *230*, 29-59.

41. Cheung, S. H.; Lau, J. Y. W., Hydrogen sulfide mediates athero-protection against oxidative stress via S-sulfhydration. *PLoS One* **2018,** *13* (3), e0194176.

42. Iciek, M.; Kowalczyk-Pachel, D.; Bilska-Wilkosz, A.; Kwiecień, I.; Górny, M.; Włodek, L., S-sulfhydration as a cellular redox regulation. *Biosci. Rep.* **2016,** *36* (2), e00304.

43. Cortese-Krott, M. M.; Koning, A.; Kuhnle, G. G. C.; Nagy, P.; Bianco, C. L.; Pasch, A.; Wink, D. A.; Fukuto, J. M.; Jackson, A. A.; van Goor, H.; Olson, K. R.; Feelisch, M., The Reactive Species Interactome: Evolutionary Emergence, Biological Significance, and Opportunities for Redox Metabolomics and Personalized Medicine. *Antioxid. Redox. Signal.* **2017,** *27* (10), 684-712.

44. Khodade, V. S.; Toscano, J. P., Development of S-Substituted Thioisothioureas as Efficient Hydropersulfide Precursors. *J. Am. Chem. Soc.* **2018,** *140* (50), 17333-17337.

45. Yuan, Z.; Zheng, Y.; Yu, B.; Wang, S.; Yang, X.; Wang, B., Esterase-Sensitive Glutathione Persulfide Donor. *Org. Lett.* **2018,** *20* (20), 6364-6367.

46. Dillon, K. M.; Powell, C. R.; Matson, J. B., Self-Immolative Prodrugs: Effective Tools for the Controlled Release of Sulfur Signaling Species. *Synlett* **2019,** *30* (05), 525-531.

47. Buchwald, P.; Bodor, N., Quantitative Structure−Metabolism Relationships: Steric and Nonsteric Effects in the Enzymatic Hydrolysis of Noncongener Carboxylic Esters. *J. Med. Chem.* **1999,** *42* (25), 5160-5168.

48. Sawahata, T.; Neal, R. A., Use of 1-fluoro-2,4-dinitrobenzene as a probe for the presence of hydrodisulfide groups in proteins. *Anal. Biochem.* **1982,** *126* (2), 360-364.

49. Wang, D.; Zou, L.; Jin, Q.; Hou, J.; Ge, G.; Yang, L., Human carboxylesterases: a comprehensive review. *Acta Pharm. Sin. B.* **2018,** *8* (5), 699-712.

50. Chiefari, J.; Chong, Y. K.; Ercole, F.; Krstina, J.; Jeffery, J.; Le, T. P. T.; Mayadunne, R. T. A.; Meijs, G. F.; Moad, C. L.; Moad, G.; Rizzardo, E.; Thang, S. H., Living Free-Radical Polymerization by Reversible Addition−Fragmentation Chain Transfer: The RAFT Process. *Macromolecules* **1998,** *31* (16), 5559-5562.

51. Saif, M. W.; Choma, A.; Salamone, S. J.; Chu, E., Pharmacokinetically Guided Dose Adjustment of 5-Fluorouracil: A Rational Approach to Improving Therapeutic Outcomes. *J. Natl. Cancer Inst.* **2009,** *101* (22), 1543-1552.

52. Hegedűs, C.; Kovács, K.; Polgár, Z.; Regdon, Z.; Szabó, É.; Robaszkiewicz, A.; Forman, H. J.; Martner, A.; Virág, L., Redox control of cancer cell destruction. *Redox Biol.* **2018,** *16*, 59-74.

4.8. Experimental

Materials and Methods

All reagents were obtained from commercial vendors and used as received unless otherwise stated. NMR spectra were measured on Agilent 400 MHz or Bruker 500 MHz spectrometers. ^{1}H and ^{13}C NMR chemical shifts are reported in ppm relative to internal solvent resonances. Solvents were used as received unless otherwise noted. PLE was purchased from Sigma Aldrich (15 U/mg). Yields refer to chromatographically and spectroscopically pure compounds unless otherwise stated. Thin-layer chromatography (TLC) was performed on glass-backed silica plates and visualized by UV unless otherwise stated. High-resolution mass spectra were taken on an Agilent Technologies 6230 TOF LC/MS mass spectrometer. LCMS experiments were performed on a Waters Acquity UPLC system equipped with a Kinetex EVO C18-functionalized silica column (C18 – 100 Å, 100 x 4.6 mm, H16-445733, 570-0069), diode array detector, and ESI mass spectrometer. Thermogravimetric analysis was performed with TGA-Q50, RT- 600 °C, 10 °C/min, N_2 fill gas, and 10 mg sample size.

Cell studies were conducted on an adherent H9C2 line of rat embryonic cardiomyocytes (ATCC, Manassas, VA, USA). Cultures were grown in Dulbecco's Modified Eagle Medium (DMEM, VWR, Radnor, PA), supplemented with 10 % fetal bovine serum (FBS, VWR, Radnor, PA). Cells were cultured at 37 °C in 5 % CO_2-air. The cultures were passaged after 70–80 % confluence was achieved. Cells were rinsed with PBS solution, and then released with trypsin and EDTA solution (VWR, Radnor, PA). The suspension of released cells was centrifuged at 1000 rpm for 5 min and then resuspended before plating for experiments. DNB-NAC was purified by preparative RP-HPLC using an Agilent Technologies 1260 Infinity HPLC system (Agilent Technologies, Santa Clara, CA) equipped with a fraction collector. Separations were performed using an Agilent PLRP-

S column (100 Å, 10 μm, 150 × 25 mm) monitoring at 220 nm. Fractions containing pure products were combined and lyophilized (FreeZone −105 °C, Labconco, Kansas City, MO), and then stored at −20 °C until needed.

Synthesis of 4-tolyl acetate **(1)**

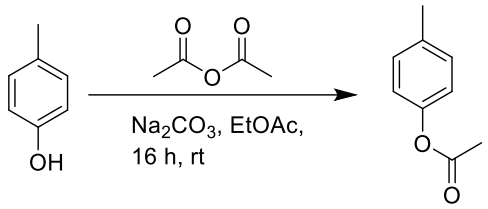

1

A round bottom flask was charged with *p*-cresol (5.0 g, 6 mmol), Na_2CO_3 (9.8 g, 92 mmol), acetic anhydride (14.2 g, 13.1 mL, 139 mmol), and EtOAc (100 mL). The reaction mixture was allowed to stir overnight (16 h). Salts were filtered off, and the resulting organic phase was washed with 10% NaOH (100 mL) to consume all remaining acetic anhydride, venting often to avoid pressure build-up. The organic layer was separated and dried over Na_2SO_4 and concentrated via rotary evaporation to yield a clear, colorless, viscous liquid. (6.7 g, 45 mmol, 96% yield). The product was used in the next step without further purification. ^{1}H NMR ($CDCl_3$): δ 7.20 (d, 2H), 7.00 (d, 2H), 2.37 (s, 3H), 2.30 (s, 3H) ^{13}C NMR ($CDCl_3$): δ 169.7, 148.5, 135.4, 129.6, 121.3, 21.0, 20.8.

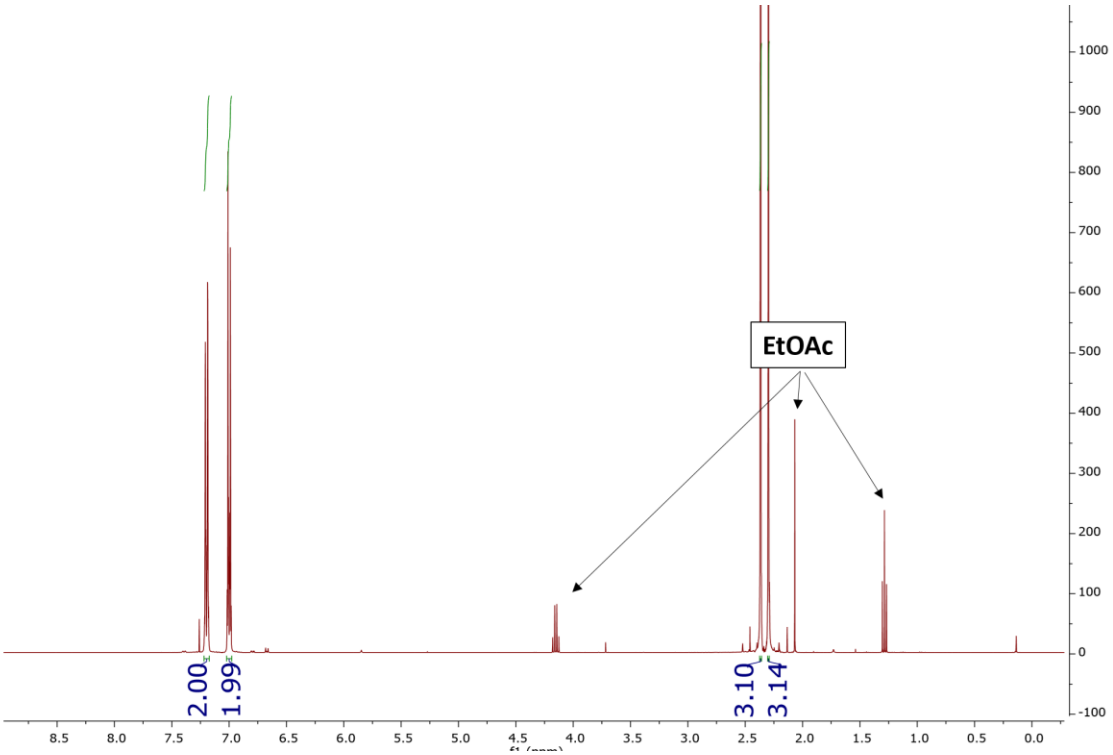

Figure S1. ^{1}H NMR spectrum of 4-tolyl acetate (1) ($CDCl_3$).

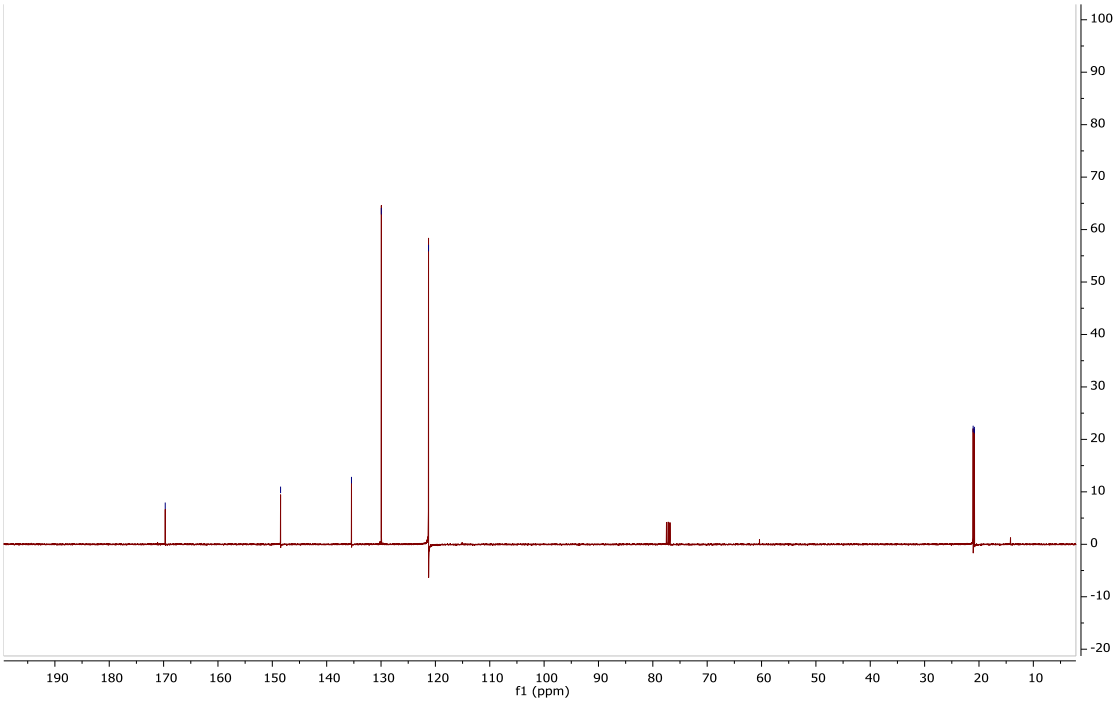

Figure S2. ^{13}C NMR spectrum of 4-tolyl acetate (1) ($CDCl_3$).

Synthesis of 4-(bromomethyl)phenyl acetate **(2)**

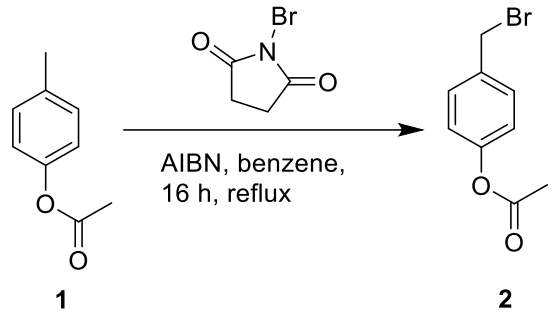

A flame-dried, 2-neck round bottom flask equipped with a septum and condenser was charged with compound **1** (6.0 g, 40 mmol), dry, degassed (bought in a container with a Sure Seal, bubbled with N_2 for 1 h) benzene (100 mL), and *N*-bromosuccinimide (8.5 g, 48 mmol) under N_2 flow. The mixture was stirred until all solids dissolved, yielding a clear, light yellow solution. Azobisisobutyronitrile (AIBN) (0.33 g, 2.0 mmol) was added in one portion under N_2 flow, and the reaction mixture was heated to reflux. The reaction was monitored by TLC (CH_2Cl_2) until starting material was consumed (~20 h). The reaction mixture was cooled to rt and washed successively with saturated $NaHCO_3$ (2 x 50 mL) and brine (50 mL). The organic layer was separated, dried over Na_2SO_4, and then concentrated via rotary evaporation to yield a brown, waxy solid. This crude product was then further purified via column chromatography, eluting with CH_2Cl_2. (Rf = 0.4, visualized with UV) The final product was isolated as a white solid (7.8 g, 40 mmol, 85% yield). ^{1}H NMR ($CDCl_3$): δ 7.30 (d, 2H) 7.15 (d, 2H), 3.5 (s, 2H), 2.26 (s, 3H). ^{13}C NMR ($CDCl_3$): δ 169.2, 149.7, 138.4, 129.6, 121.0, 29.8, 20.0.

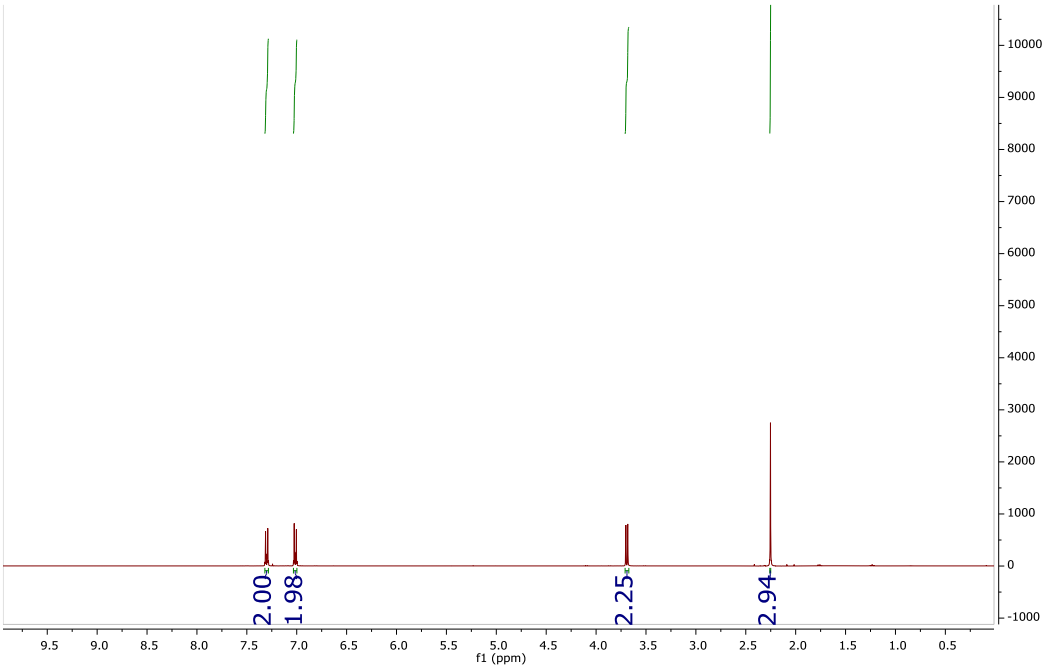

Figure S3. ^{1}H NMR spectrum of 4-(bromomethyl)phenyl acetate (2) ($CDCl_3$).

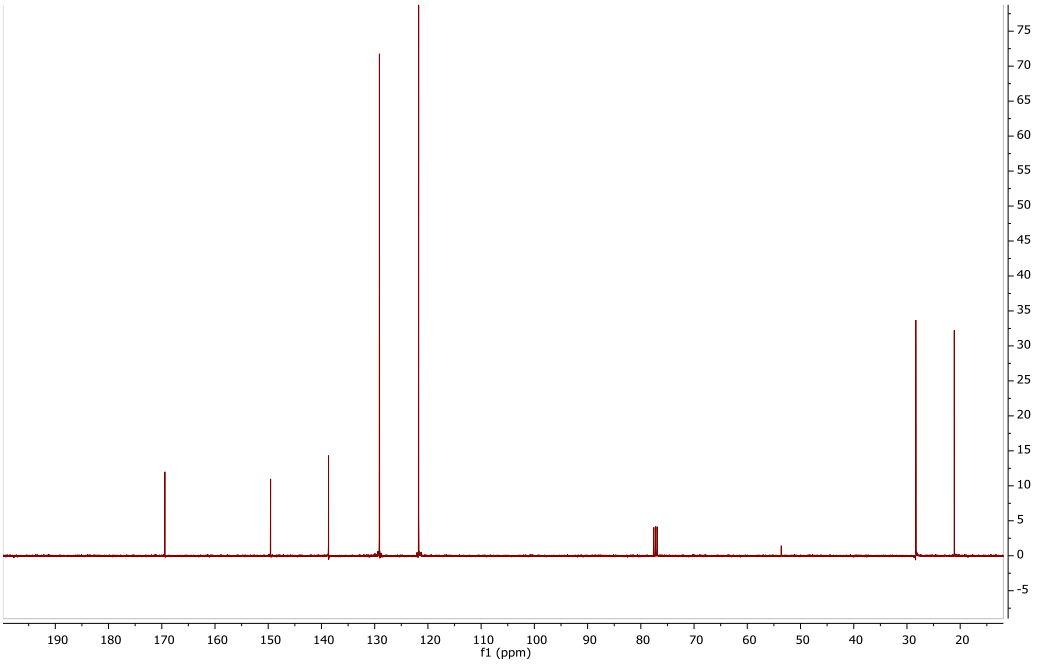

Figure S4. ^{13}C NMR spectrum of 4-(bromomethyl)phenyl acetate (2) ($CDCl_3$).

Synthesis of 4-(mercaptomethyl)phenyl acetate **(3)**

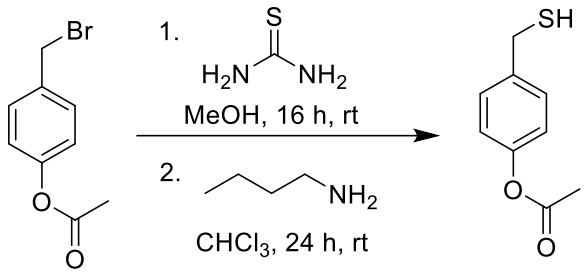

2 **3**

A two-neck round bottom flask equipped with a vacuum adaptor and a septum was charged with compound **2** (5.00 g, 21.8 mmol), MeOH (50 mL), and a stirbar. The resulting suspension was bubbled with N_2 for 15 min. Thiourea (2.49 g, 32.7 mmol) was then added in one portion under N_2, and the reaction mixture was stirred at rt. The solids dissolved slowly over the course of several hours to give a clear, light orange solution. Reaction progress was monitored by TLC (CH_2Cl_2) until starting material was consumed (16 h). The reaction mixture was then concentrated via rotary evaporation, and the thiouronium intermediate was subsequently suspended in $CHCl_3$ (50 mL). The suspension was degassed by bubbling with N_2 for 15 min. Butylamine (3.19 g, 4.3 mL, 43.7 mmol) was then injected via syringe. The resulting suspension slowly dissolved over the course of 24 h, yielding a bright yellow solution. This solution was washed with 1N HCl (50 mL) and brine (50 mL) in a separatory funnel. The organic layer was separated and dried over Na_2SO_4, and concentrated via rotary evaporation to yield a viscous, slightly yellow oil. The product was then further purified by silica gel chromatography, eluting with 25% EtOAc:hexanes, yielding a colorless, viscous oil (3.2 g, 75% yield) ^{1}H NMR ($CDCl_3$): δ 7.30 (d, 2H) 7.07 (d, 2H), 3.71 (d, 2H), 2.26 (s, 3H), 1.78 (s, 1H). ^{13}C NMR ($CDCl_3$): δ 169.1, 149.9, 139.4, 128.6, 121.0, 28.8, 21.2.

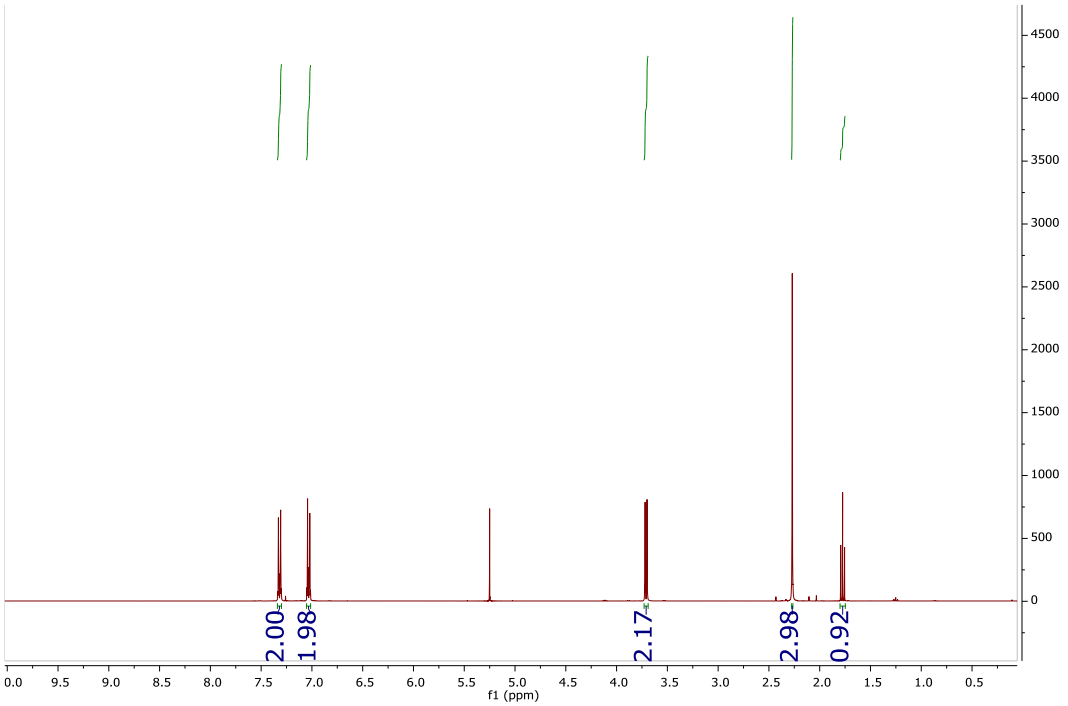

Figure S5. ^{1}H NMR spectrum of 4-(mercaptomethyl)phenyl acetate (3) ($CDCl_3$).

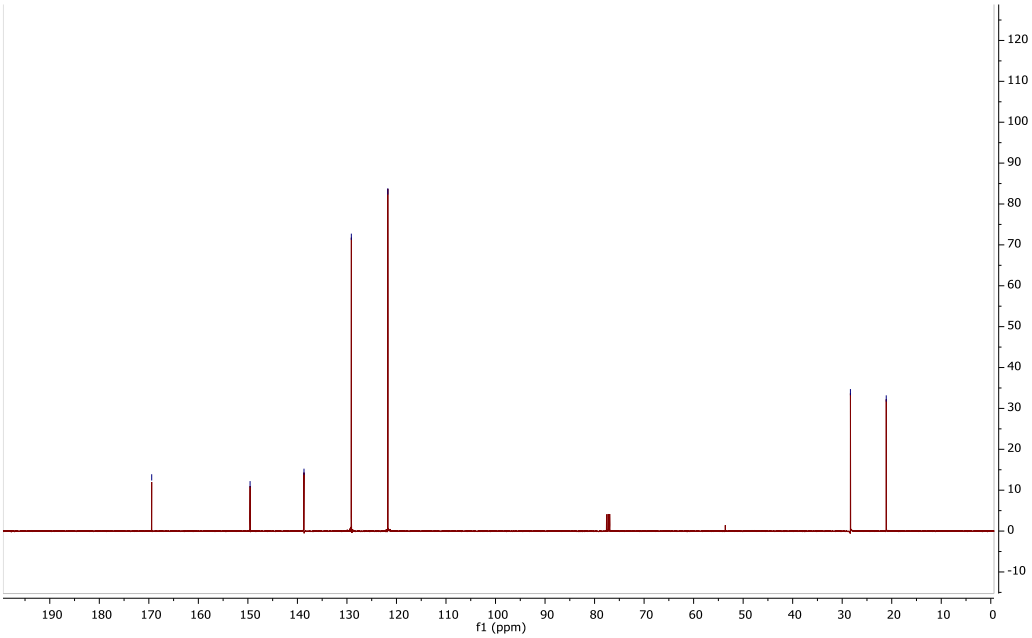

Figure S6. ^{13}C NMR spectrum of 4-(mercaptomethyl)phenyl acetate (3) ($CDCl_3$).

Synthesis of Activated N-Acetylcysteine Disulfide **(NAC-pyDS)**

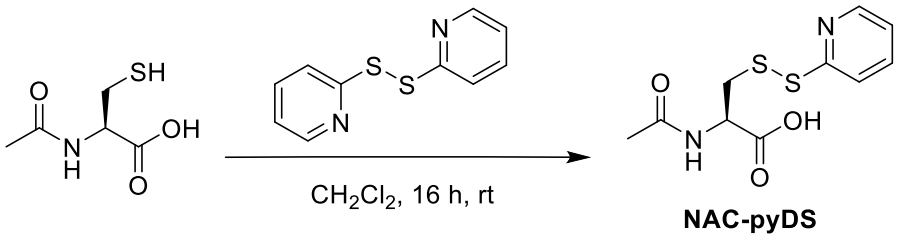

NAC-pyDS

A round bottom flask was charged with *N*-acetylcysteine (7.0 g, 42.9 mmol), CH_2Cl_2 (200 mL), and a stirbar to give a suspension. 2,2'-Dipyridyl disulfide (18.9 g, 85.8 mmol) was added in one portion resulting in a bright yellow suspension. The solids gradually dissolved over the course of several hours. The reaction mixture was stirred at rt (16 h), and reaction progress was monitored by TLC (EtOAc). The resulting yellow solution was concentrated via rotary evaporation, yielding a bright yellow solid. This crude product was then suspended in cold acetone, stirred for 30 minutes to dissolve any thiopyridone byproducts, and filtered, rinsing with copious amounts of cold acetone. This yielded a faintly yellow powder (8.4 g, 70% yield). ^{1}H NMR (DMSO-d_6): δ 12.97 (s, 1H), 8.46 (m, 1H), 8.42 (d, *J* = 7.9 Hz, 1H), 7.81 (m, 1H), 7.8 (m, 1H), 7.24 (m, 1H), 4.47 (m, 1H), 3.15 (m, 2H), 1.86 (s, 3H). ^{13}C NMR (DMSO-d_6): δ 171.88, 169.49, 158.77, 149.69, 137.86, 121.33, 119.34, 51.39, 39.93, 22.44.

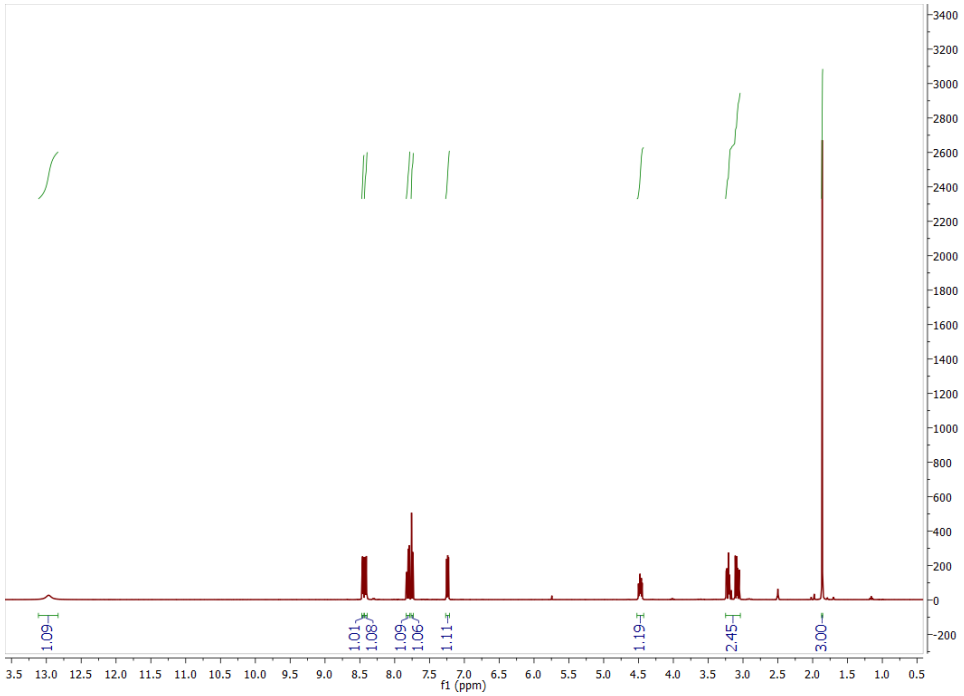

Figure S7. ^{1}H NMR spectrum of **NAC-pyDS** (DMSO-d_6).

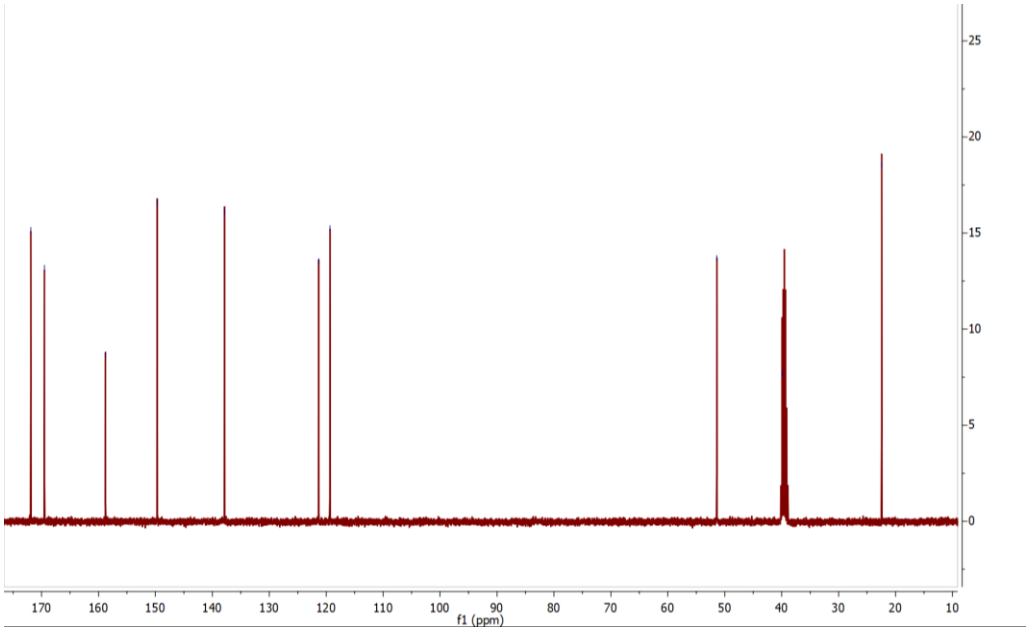

Figure S8. ^{13}C NMR spectrum of **NAC-pyDS** (DMSO-d_6).

Synthesis of 4-Benzylacetate *N*-Acetylcysteine Disulfide **(EDP-NAC)**

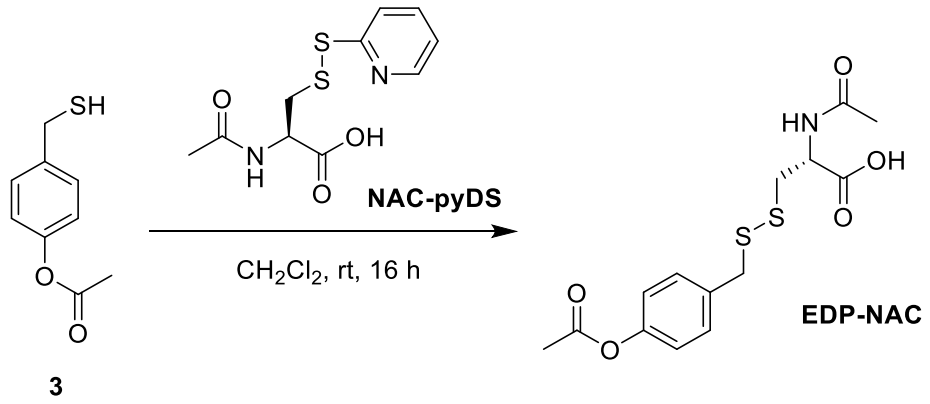

A single-neck roundbottom flask was charged with compound **3** (0.282 g, 1.55 mmol), CH_2Cl_2 (5 mL), **NAC-pyDS** (0.426 g, 1.56 mmol), and a stir bar, resulting in a light yellow suspension. The reaction mixture gradually became a clear, bright yellow solution over the course of 16 h. The reaction mixture was filtered to remove some small particulate matter, and then placed in the freezer overnight. The white, crystalline solid that was formed from this cooling was isolated by filtration and rinsed with cold CH_2Cl_2, resulting in light, white crystals. (0.328 g, 62 % yield). ^{1}H NMR (DMSO-d_6) δ 8.28 (d, 1H), 7.36 (d, 2H) 7.07 (d, 2H), 4.47 (m, 1H), 3.98 (d, 2H) 3.01 (m, 1H), 2.81 (m, 1H), 2.26 (s, 3H) 1.86 (s, 3H). ^{13}C NMR (DMSO-d_6): δ 172.5, 169.8, 169.6, 150.1, 135.4, 130.3, 122.2, 51.8, 49.0, 41.5, 22.9, 21.3. HRMS (ESI-TOF) calcd. for $C_{14}H_{16}NO_5S_2$ $[M-H]^-$ 342.0469, found 342.0472.

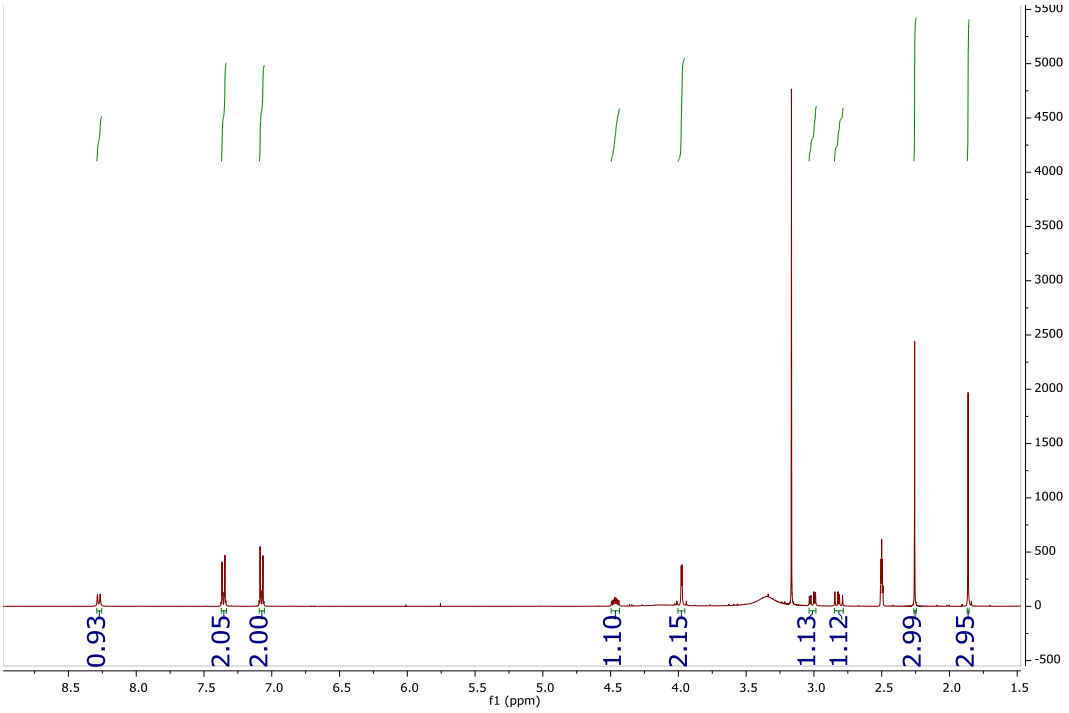

Figure S9. ^{1}H NMR spectrum of **EDP-NAC** (DMSO-d_6).

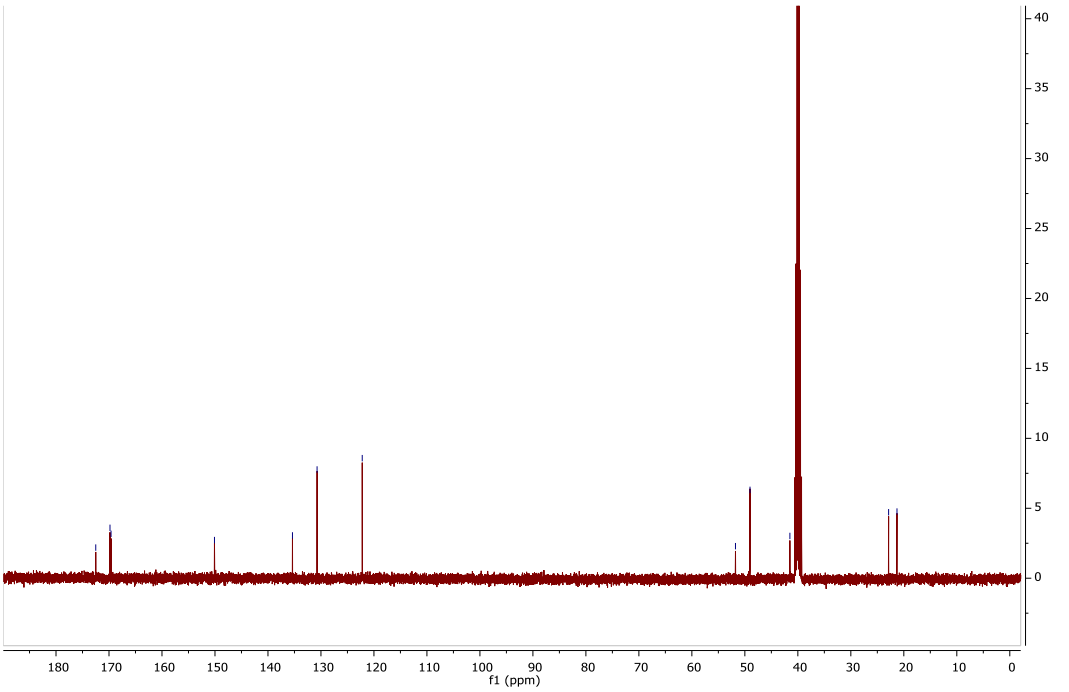

Figure S10. ^{13}C NMR spectrum of **EDP-NAC** (DMSO-d_6).

Synthesis of pHEMA-OEGMA:

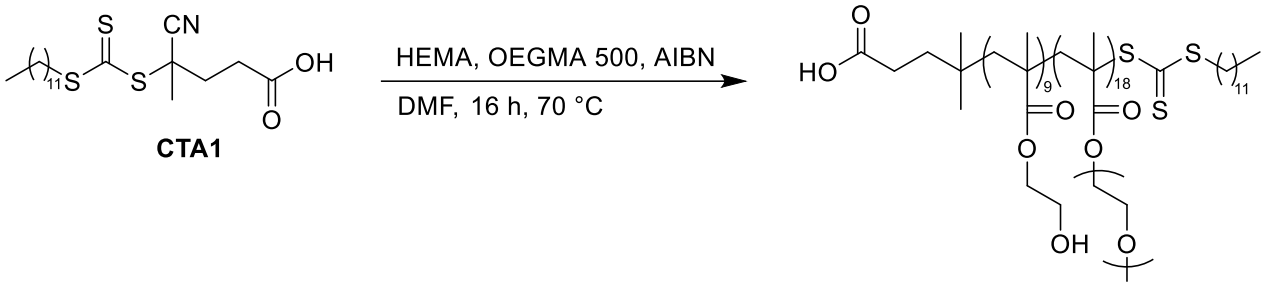

HEMA and OEGMA-500 were passed through basic alumina to remove inhibitor. A Schlenk flask was charged with HEMA (1.64 mL, 13.5 mmol), OEGMA-500 (3.60 mL, 27.0 mmol), AIBN (22.1 mg, 0.135 μmol), and RAFT chain transfer agent **CTA1** (544 mg, 1.35 mmol). DMF (4 mL) was then added, and the flask was subjected to four freeze-pump-thaw cycles. The flask was then back filled with nitrogen, sealed, and placed into an oil bath set to 70 °C. The reaction mixture was allowed to stir overnight. The polymer product was isolated by precipitating the reaction mixture twice into cold diethyl ether and dried overnight, resulting in a waxy yellow solid.

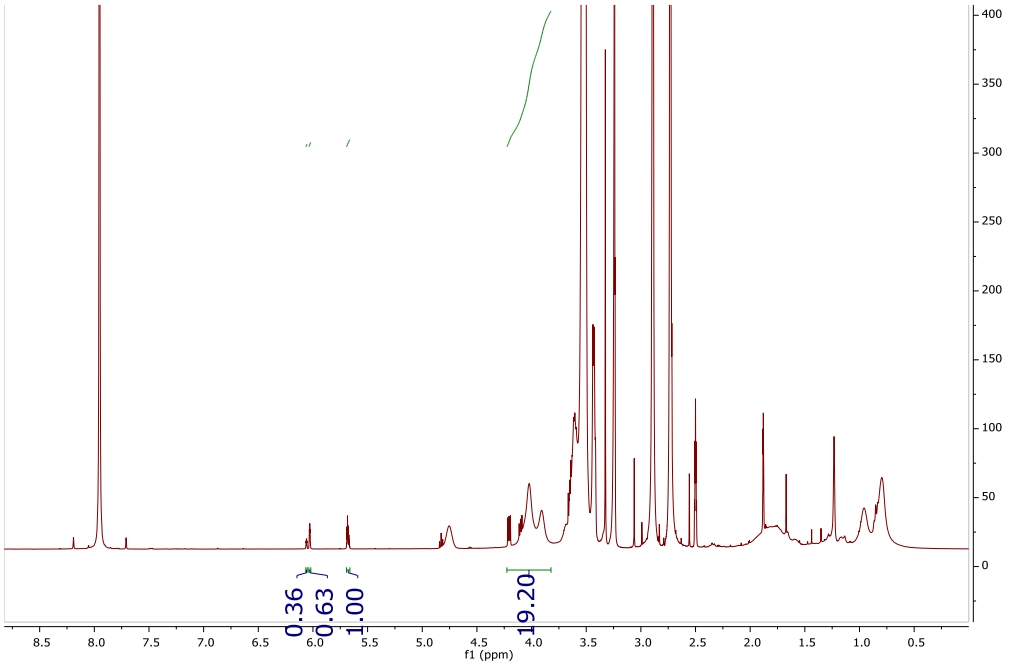

Figure S11. ^{1}H NMR spectrum of pHEMA-*co*-OEGMA at 95% conversion (DMSO-d_6).

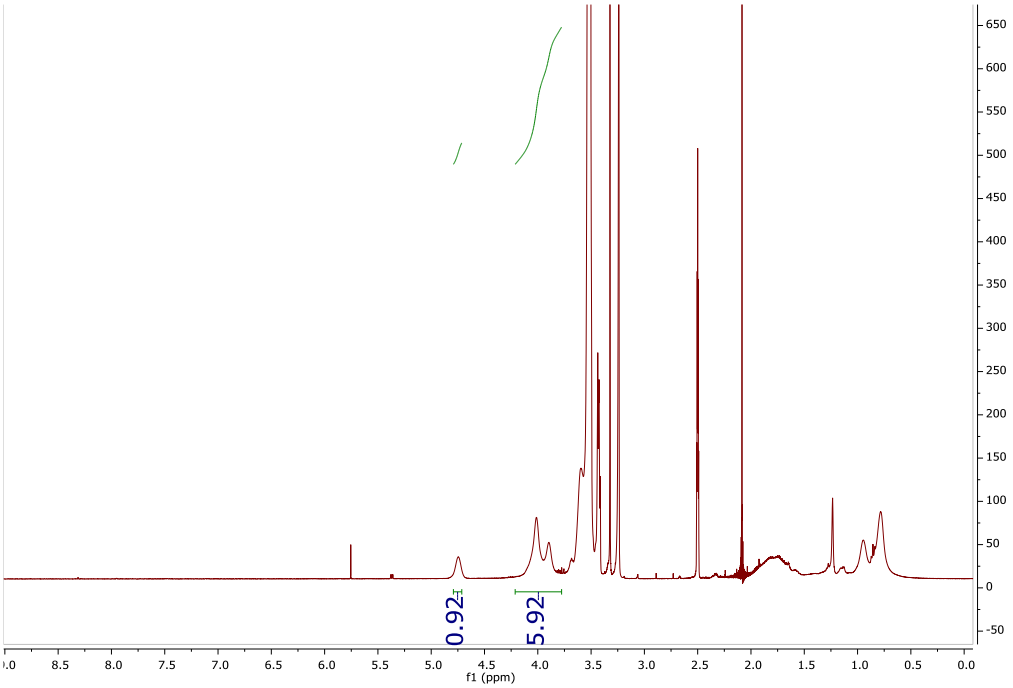

Figure S12. ^{1}H NMR spectrum of pHEMA-*co*-OEGMA after precipitation. Monomer incorporation was 1:2 HEMA:OEGMA (DMSO-d_6).

Synthesis of poly(EDP-NAC)

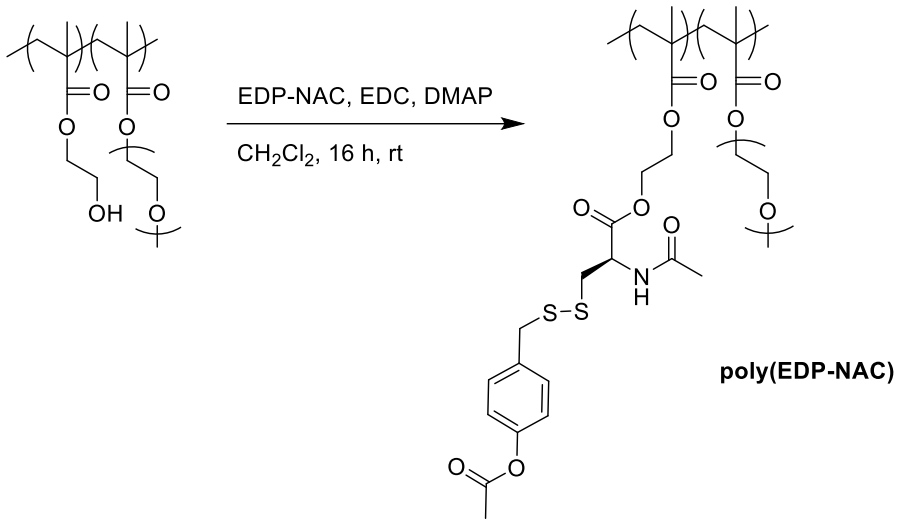

A two-neck roundbottom flask was charged with a stir bar and pHEMA-*co*-OEGMA (524 mg, 47.6 µmol), EDC (229 mg, 1.19 mmol), and DMAP (11.6 mg, 95.3 µmol). Anhydrous CH_2Cl_2 (4 mL) was then added, and the reaction mixture was stirred until homogenous. EDP-NAC (295 mg, 858 µmol) was then added under positive nitrogen pressure, and the reaction mixture was stirred for 16 h. The resulting pale yellow solution was then diluted with CH_2Cl_2 (25 mL), washed with 1N HCl (2 x 20 mL), saturated bicarbonate solution (2 x 20 mL), and brine (20 mL). The organic layer was separated and dried over Na_2SO_4. The organic solvent was concentrated *in vacuo* and polymer product was isolated by precipitating the reaction mixture twice into cold diethyl ether, yielding a waxy yellow solid. Based on ^1H NMR spectroscopy, esterification proceeded to near 100% conversion.

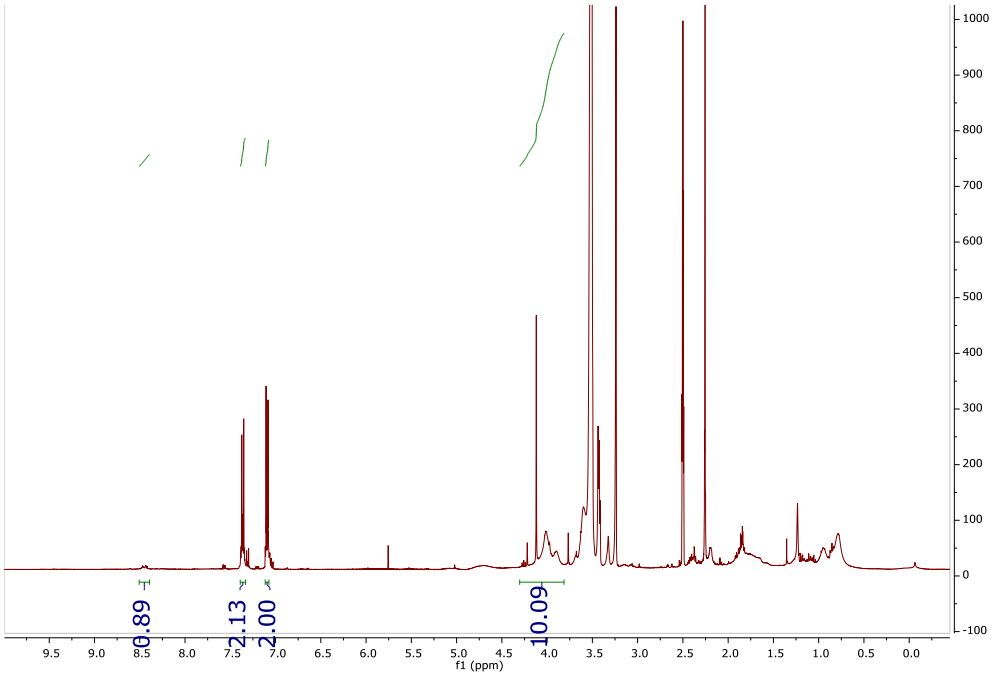

Figure S13. ^{1}H NMR spectrum of 100% functionalized poly(EDP-NAC) (DMSO-d_6).

Synthesis of 50% functionalized poly(EDP-NAC)

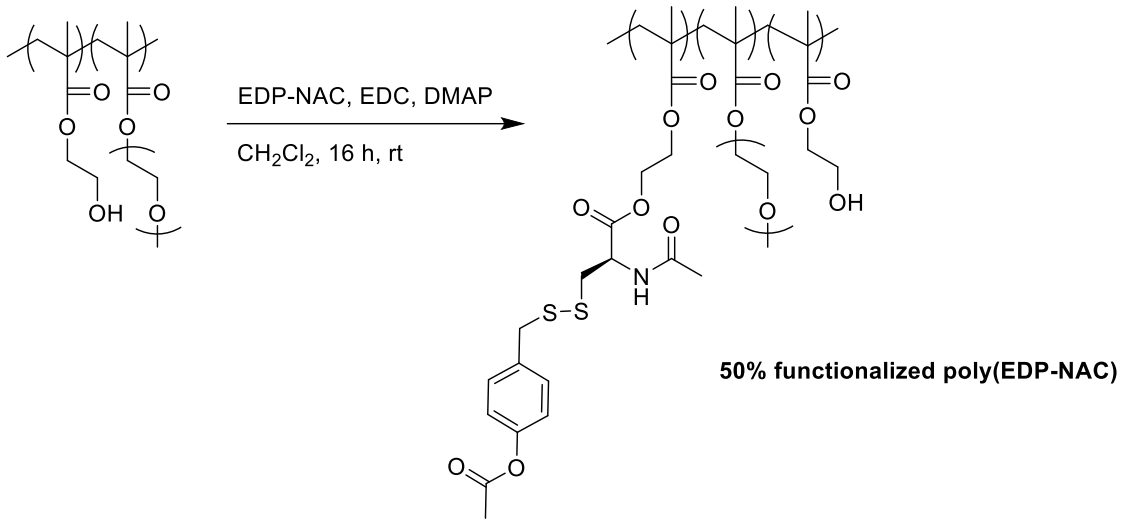

A two-neck roundbottom flask was charged with a stir bar and pHEMA-*co*-OEGMA (272 mg, 24.8 µmol), EDC (119 mg, 0.62 mmol), and DMAP (6.03 mg, 49.5 µmol). Anhydrous CH_2Cl_2 (2 mL) was then added, and the reaction mixture was stirred until homogenous. EDP-NAC (55.2 mg,

160 µmol) was then added under positive nitrogen pressure, and the reaction mixture was stirred for 16 h. The resulting pale yellow solution was then diluted with CH_2Cl_2 5 mL), washed with 1N HCl (2 x 5 mL), saturated bicarbonate solution (2 x 5 mL), and brine (5 mL). The organic layer was separated and dried over Na_2SO_4. The organic solvent was concentrated *in vacuo* and polymer product was isolated by precipitating the reaction mixture twice into cold diethyl ether, yielding a waxy yellow solid. Based on ^{1}H NMR spectroscopy, esterification proceeded to near 50% conversion.

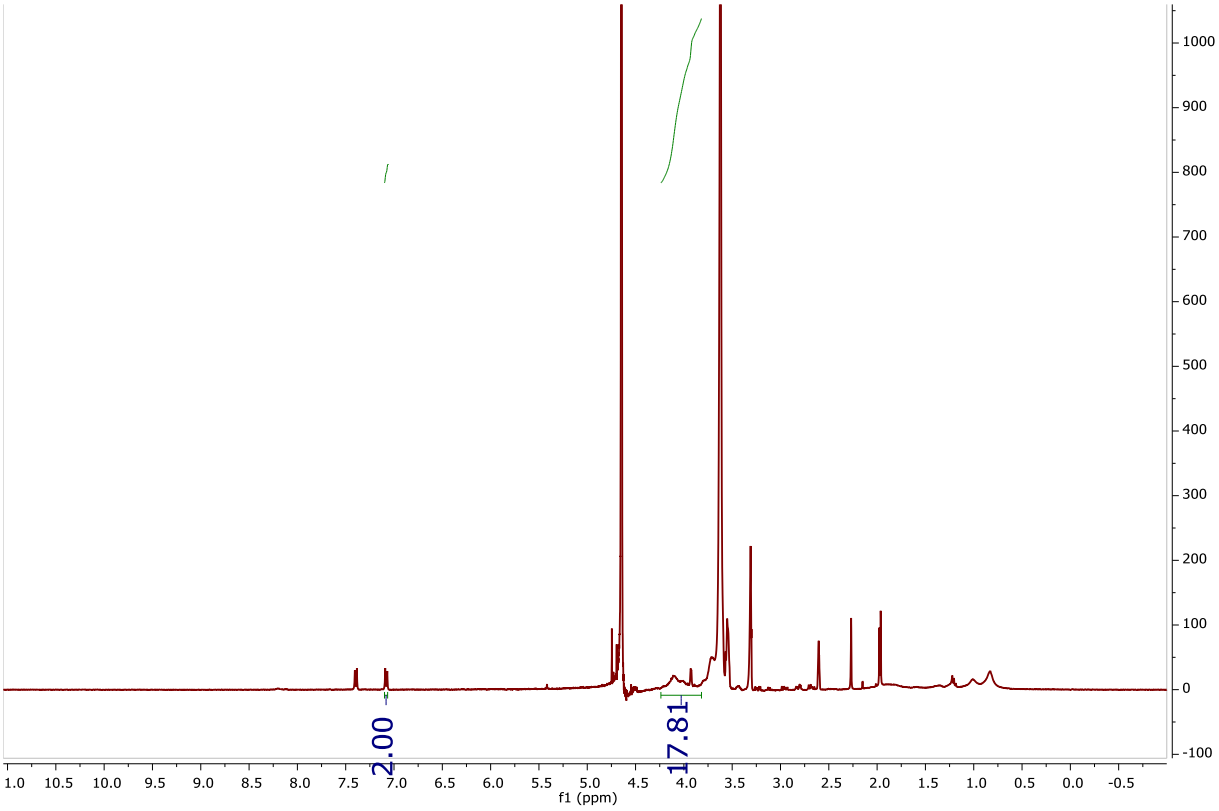

Figure S14. ^{1}H NMR spectrum of 50% functionalized poly(EDP-NAC) (D_2O).

Synthesis of 2,4-dinitrobenzene disulfide (DNBD)

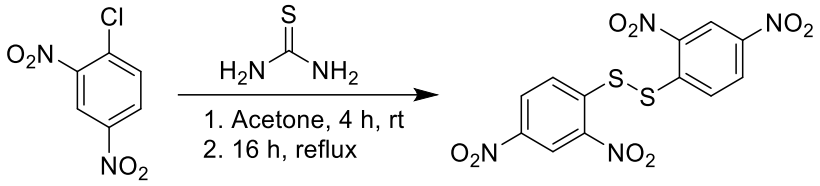

2,4-Chlorodinitrobenzene (5.00 g, 24.7 mmol) and thiourea (1.88 g, 24.7 mmol) were added to a round bottom flask charged with a stir bar. Acetone (50 mL) was added, and the reaction mixture was allowed to stir for 4 h. The resulting pale yellow solution was refluxed for 16 h, yielding a bright yellow precipitate. The acetone was removed via rotary evaporation, and the yellow solid was taken up in absolute ethanol. This slurry was stirred vigorously for 15 min, and the solids were isolated by filtration. The resulting yellow solid (4.20 g, 85 % yield) was used in the next step of synthesis without further purification. ^{1}H NMR (DMSO-d_6): δ 8.91 (s, 1H), 8.43 (d, 1H) 7.78 (d, 1H). ^{13}C NMR (DMSO-d_6): δ 149.2, 147.4, 137.9, 135.7, 128.5, 121.5.

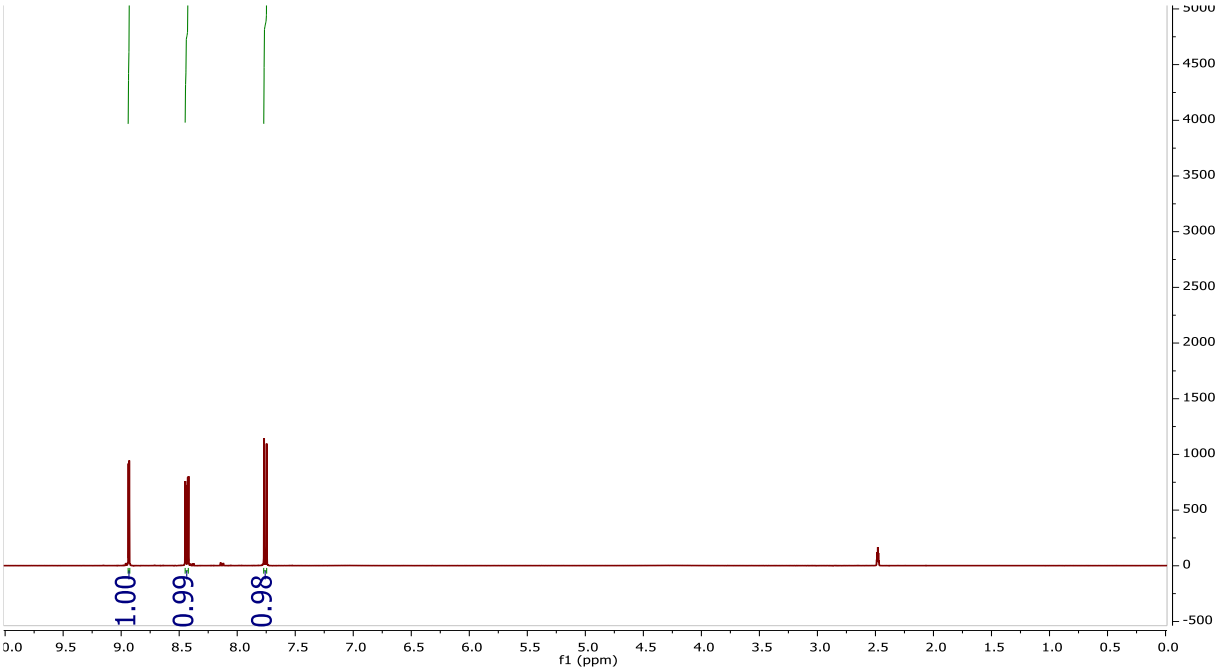

Figure S15. ^{1}H NMR spectrum of DNBD (DMSO-d_6).

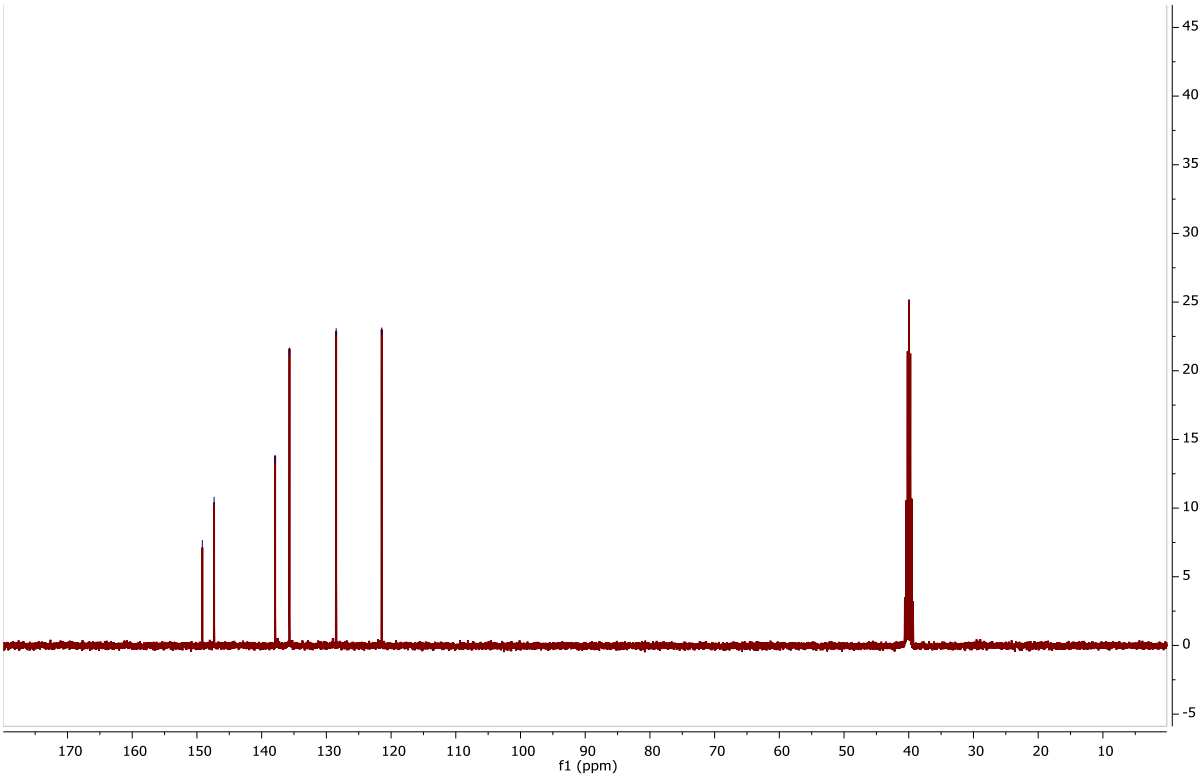

Figure S16. ^{13}C NMR spectrum of DNBD (DMSO-d_6).

Synthesis of persulfide adduct DNB-NAC

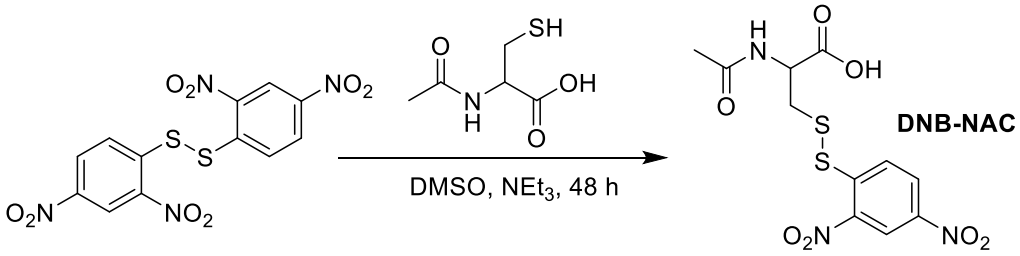

2,4-Dinitrobenzene disulfide (500 mg, 1.26 mmol) and NEt_3 (0.37 mL, 2.64 mmol) were dispensed into a two-neck round bottom flask charged with a stir bar. DMSO (8 mL) was then added, and the reaction mixture was bubbled with nitrogen gas for 20 min. The reaction mixture was placed under nitrogen flow and stirred until homogeneous, resulting in a yellow solution. NAC (205 mg, 1.26 mmol) was then added under nitrogen flow, and the reaction vessel was sealed and stirred for two days, yielding a bright red solution. The solution was then concentrated and precipitated into

CH_2Cl_2 (50 mL), and the solids were recovered by filtration. The resulting bright orange solid was then redissolved in a minimal amount of methanol (2 mL) and re-precipitated twice more in CH_2Cl_2 and recovered by filtration. The resulting pale orange solid was dissolved in 50 mL 1:1 CH_3CN:H_2O and purified using preparative reverse phase HPLC. 50 mg was purified in one 10 mL injection, resulting in 14 mg yield (26%) of a pale yellow powder. ^{1}H NMR (DMSO-d_6) δ 8.60 (s, 1H), 8.39 (d, 1H) 8.14 (d, 1H), 8.72 (d, 1H), 4.36 (m, 1H) 3.54 (d, 1H), 1.65 (s, 3H).

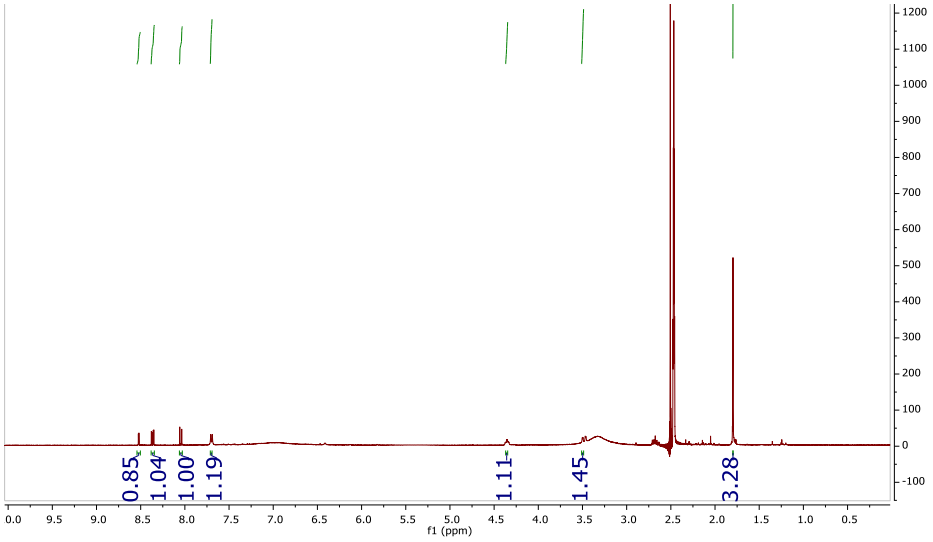

Figure S17. ^{1}H NMR spectrum of DNB-NAC (DMSO-d_6).

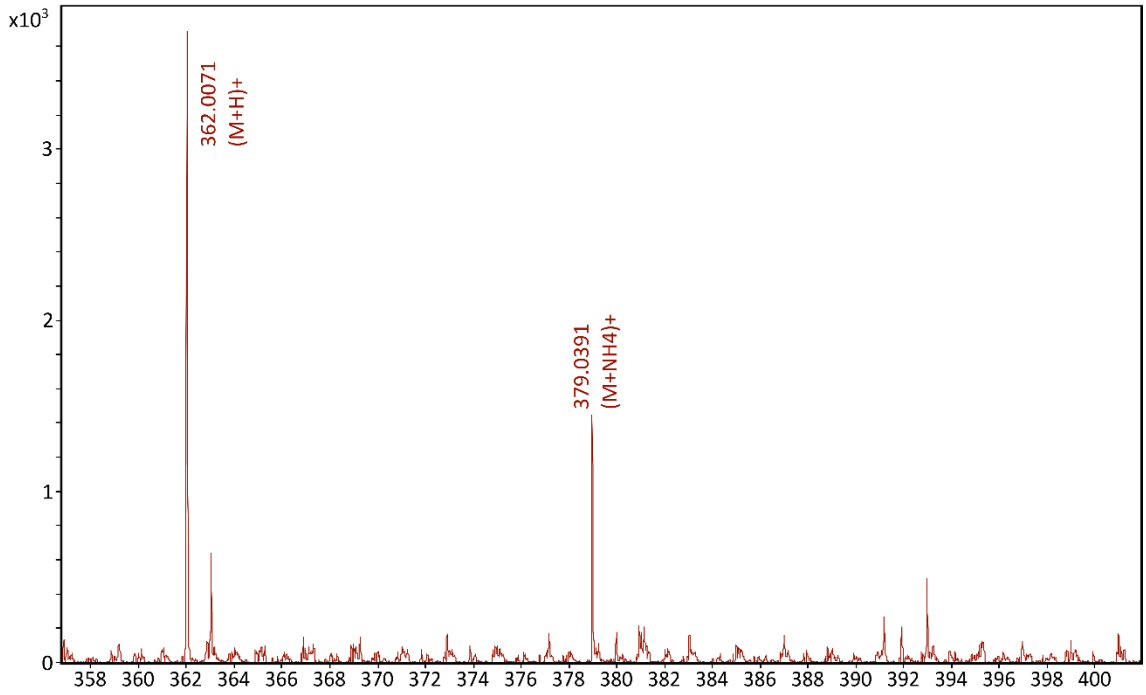

Figure S18. HRMS of DNB-NAC (ESI-TOF) calcd. for $C_{11}H_{12}N_3O_7S_2$ $[M+H]^+$ 362.0096, found 362.0071.

Persulfide Trapping:

Analysis of persulfide release by analytical HPLC: A one-dram vial was charged with a solution of EDP-NAC (100 µL; 20 mM in HPLC grade CH_3CN), FDNB (100 uL, 50 mM in HPLC grade CH_3CN) and diluted with water (0.8 mL) to give a clear, yellow solution. An aliquot (50 µL) was removed and diluted into water (0.95 mL) in a vial equipped with a screw cap lid with a rubber septum, which served as the t=0 time point. The aliquot was then analyzed by HPLC. Analytical HPLC method is as follows: 20 µL injection volume with an elution gradient starting at 5% CH_3CN in water (with 10 mM CH_2O_2 in both mobile phases), reaching 95% ACN over the course of 7 min, holding at this ratio of solvent for 1 min, and then ramping down from 95% to 5% CH_3CN over the course of 2 min. This chromatographic cycle was followed by a 5-min column equilibration at 5 % CH_3CN. After acquisition of the t=0 time point, PLE (10 µL, 1 mg/mL) was added to the reaction mixture. The vial was shaken thoroughly, and after 1 min the first aliquot was removed and diluted into water and injected into the HPLC in the same fashion as the zero min time point. Aliquots were then taken at 15 min intervals (up to 1 h) until the peak attributed to EDP-NAC disappeared. The UV detector readout was set to 282 nm. As shown in Figure S18 below, the peak eluting at 3.8 min (EDP-NAC) decays over time in response to PLE. The peak at 4.9 min increases over time and matches the elution time of DNB-NAC under the same HPLC conditions.

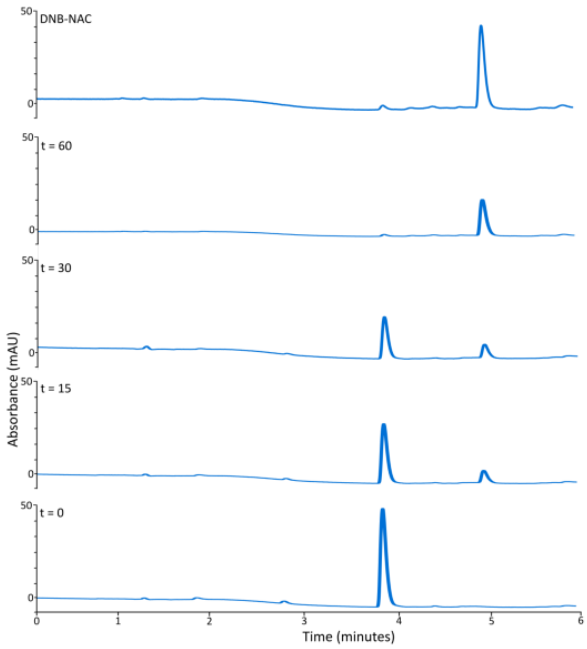

Figure S19. Chromatogram showcasing persulfide trapping from EDP-NAC in response to PLE. The top trace depicts the pre-synthesized standard DNB-NAC.

[1]H NMR Persulfide Release Kinetics:

EDP-NAC Kinetics

EDP-NAC (1.0 mg) was dissolved in 200 µL DMSO-d_6. D_2O (733 µL) was added, and a [1]H NMR spectrum was recorded for the t=0 time point. PLE (67 µL, 1 mg/mL stock dissolved in D_2O) was then added, and subsequent NMR scans were performed at intervals described in Scheme 3.

Poly(EDP-NAC) Kinetics

Poly(EDP-NAC) (3.7 mg) was dissolved in 108 µL DMSO-d_6. Dimethyl sulfone (92 µL, 1 mg/mL stock in DMSO-d_6) was then added to the solution of poly(EDP-NAC). D_2O (733 µL) was added, and a [1]H spectrum was recorded for the t=0 time point. PLE (67 µL, 1 mg/mL stock in D_2O) was then added and subsequent NMR scans were performed at intervals described in Scheme 3.

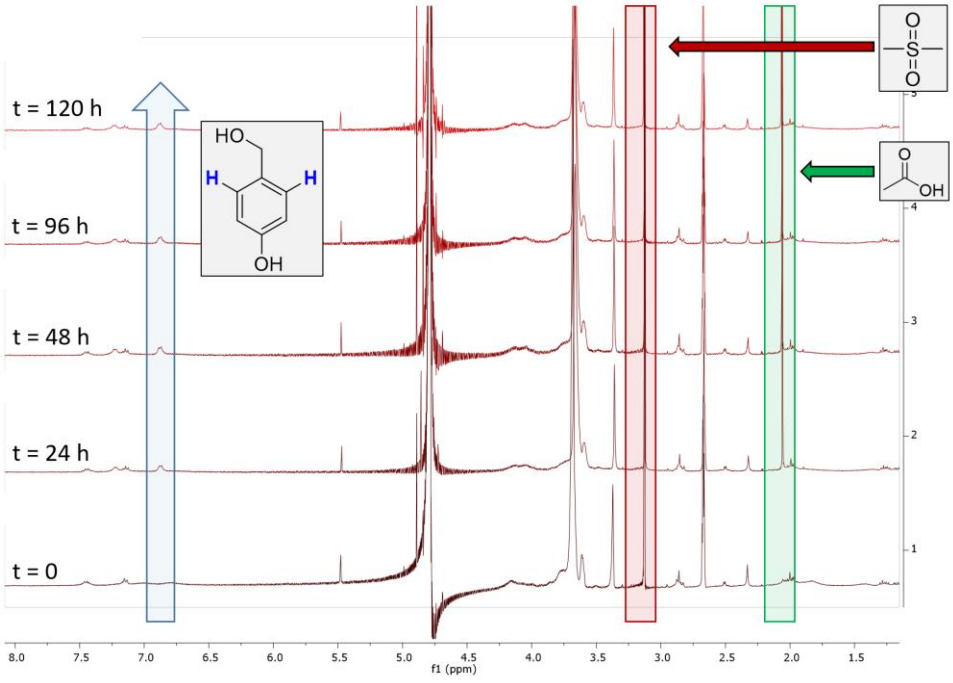

Figure S20. [1]H NMR Kinetics of 100% functionalized poly(EDP-NAC) in response to PLE. The resonance for 4-hydroxybenzyl alcohol emerges over time at 6.7 ppm (blue), as does the resonance

for acetic acid at 2.1 ppm (green). The resonance for the internal standard used in the study (dimethyl sulfone) is shown at 3.1 ppm (red).

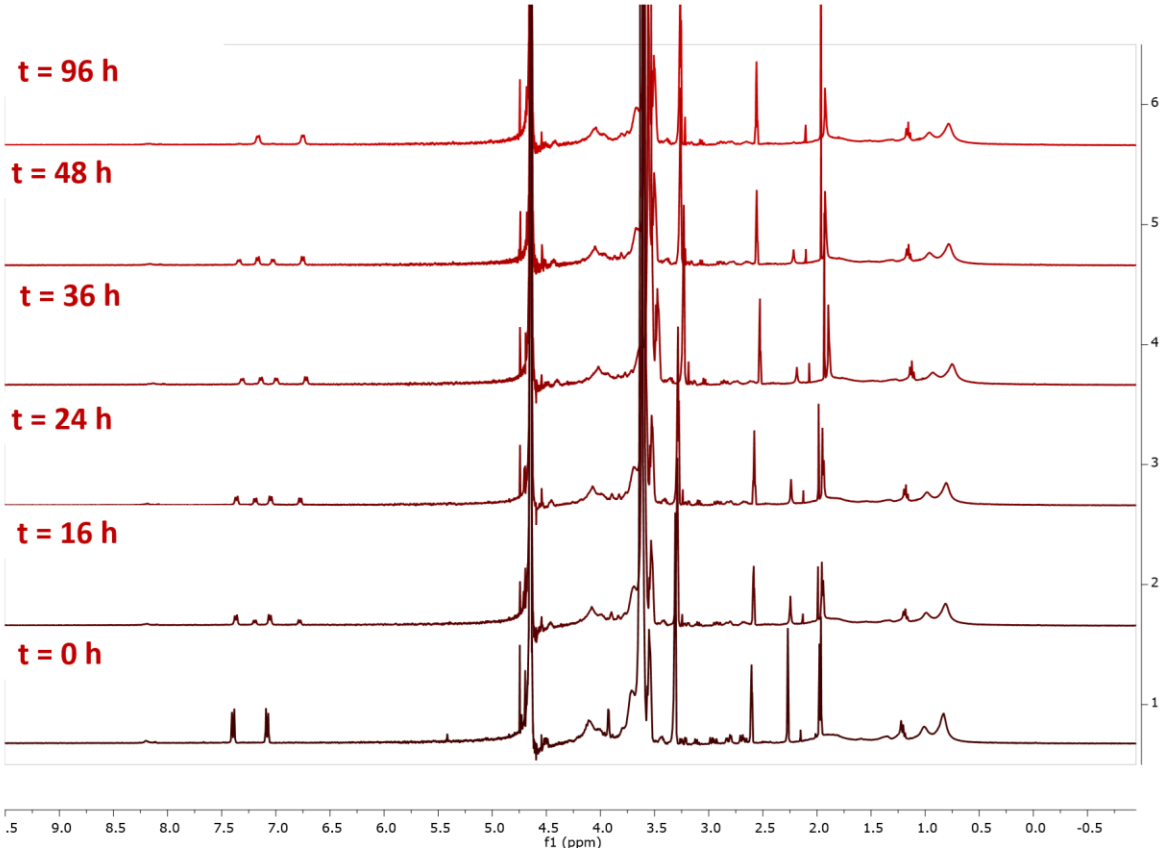

Figure S21. ^{1}H NMR kinetics traces with 50% functionalized poly(EDP-NAC). No internal standard was used in these experiments due to higher resolution on aromatic peaks relative to poly(EDP-NAC). The half-life of release was calculated to be 26 ± 3 h.

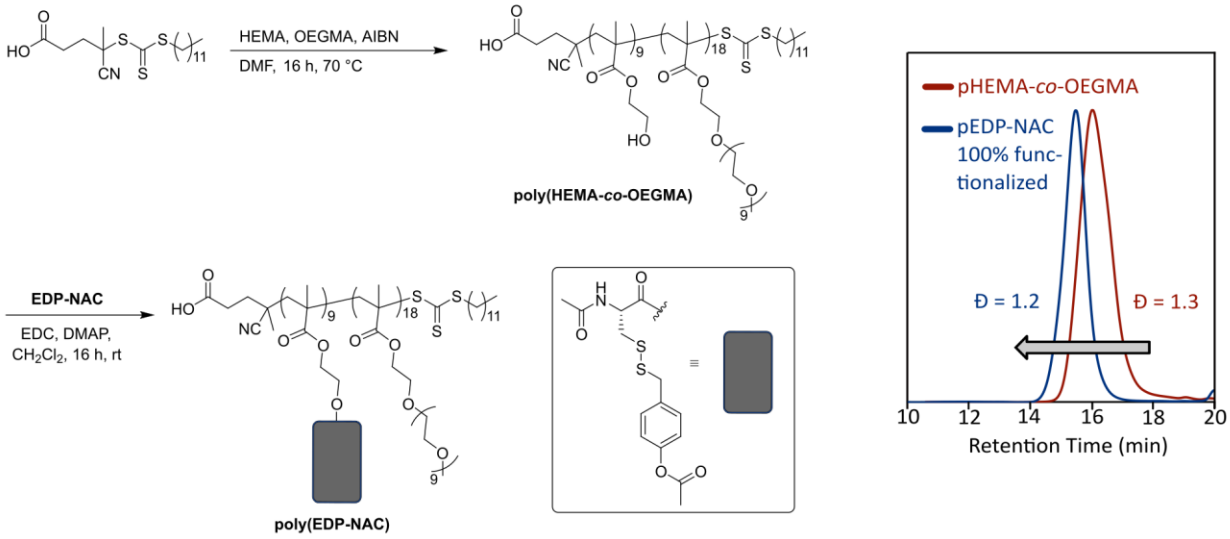

Polymer	M_n (SEC, Da)	$M_{n,theo}$ (^{1}H NMR, Da)	M_n, Endgroup analysis (^{1}H NMR, Da)	*Đ*
pHEMA-*co*-OEGMA	19 200	10 400	10 100	1.28
poly(EDP-NAC) 100% functionalized	25 100	13 200	13 000	1.19
poly(EDP-NAC) 50% functionalized	22 300	11 800	11 500	1.22

Figure S22. Synthetic scheme, SEC traces, and table describing the synthesis and SEC characterization of poly(EDP-NAC).

Thermogravimetric analysis (TGA) of poly(EDP-NAC)

Two aliquots of poly(EDP-NAC) (50 mg each) were dissolved in HPLC grade THF (10 mL). One batch (labeled GPC-THF) was then concentrated to dryness via rotary evaporation at room temperature to remove THF, leaving any tightly bound residual bound water behind. The second batch (labeled HV) was then dried using high vacuum to remove all solvents. TGA was then performed with a TGA-Q50, ramping from rt to 600 °C at 10 °C/min with N_2 fill gas and a 10 mg sample size. According to these results (Figure S21), poly(EDP-NAC) consists of 9 wt.% water. This bound water likely contributes in part to the observed discrepancies in M_n calculated by SEC and ^{1}H NMR due to inaccurate measurements of injected mass and therefore d*n*/d*c*.

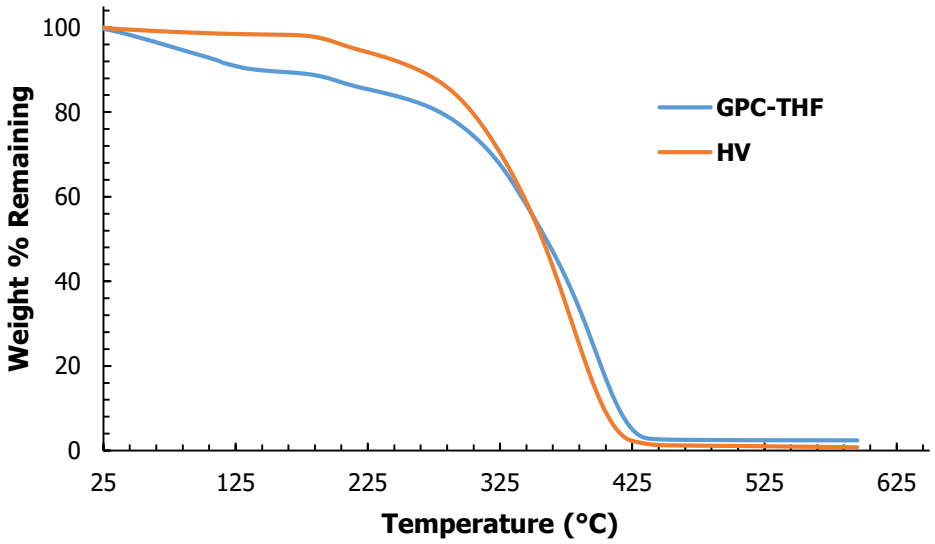

Figure S23. TGA of poly(EDP-NAC) dissolved in THF (**GPC-THF**) and then rotovapped to remove THF but not bound water, and poly(EDP-NAC) dried using high vacuum before TGA analysis (**HV**).

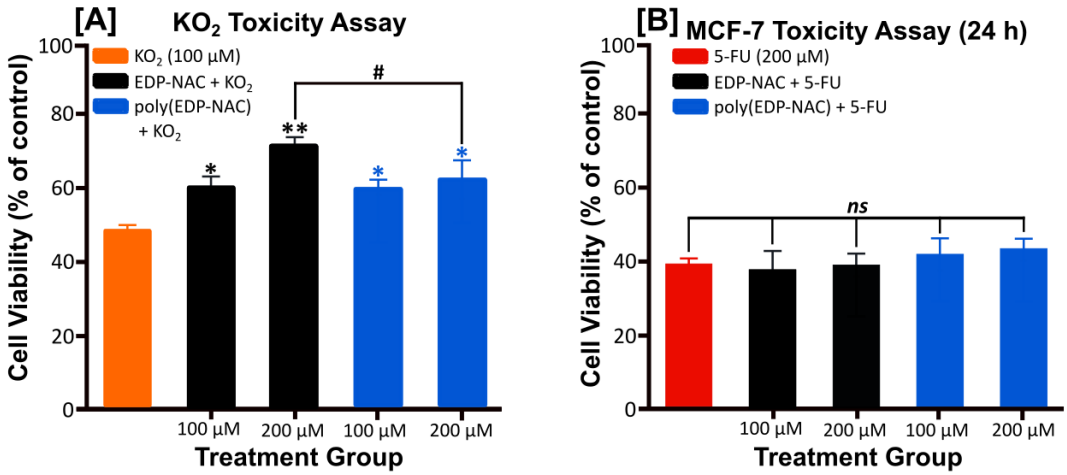

Figure S24. Additional toxicity experiments. [A]: H9C2 KO_2 toxicity assay. H9C2 cells were treated with 100 µM KO_2 only (orange bar) or co-treated with KO_2 and EDP-NAC (black bars) or KO_2 and poly(EDP-NAC) (blue bars) for 1 h exposure time. [B]: 24 h MCF-7 5-FU toxicity assay. MCF-7 cells were treated with 5-FU only (red bar) or co-treated with 5-FU and EDP-NAC (black bars) or 5-FU and poly(EDP-NAC) (blue bars) for 24 h exposure time.

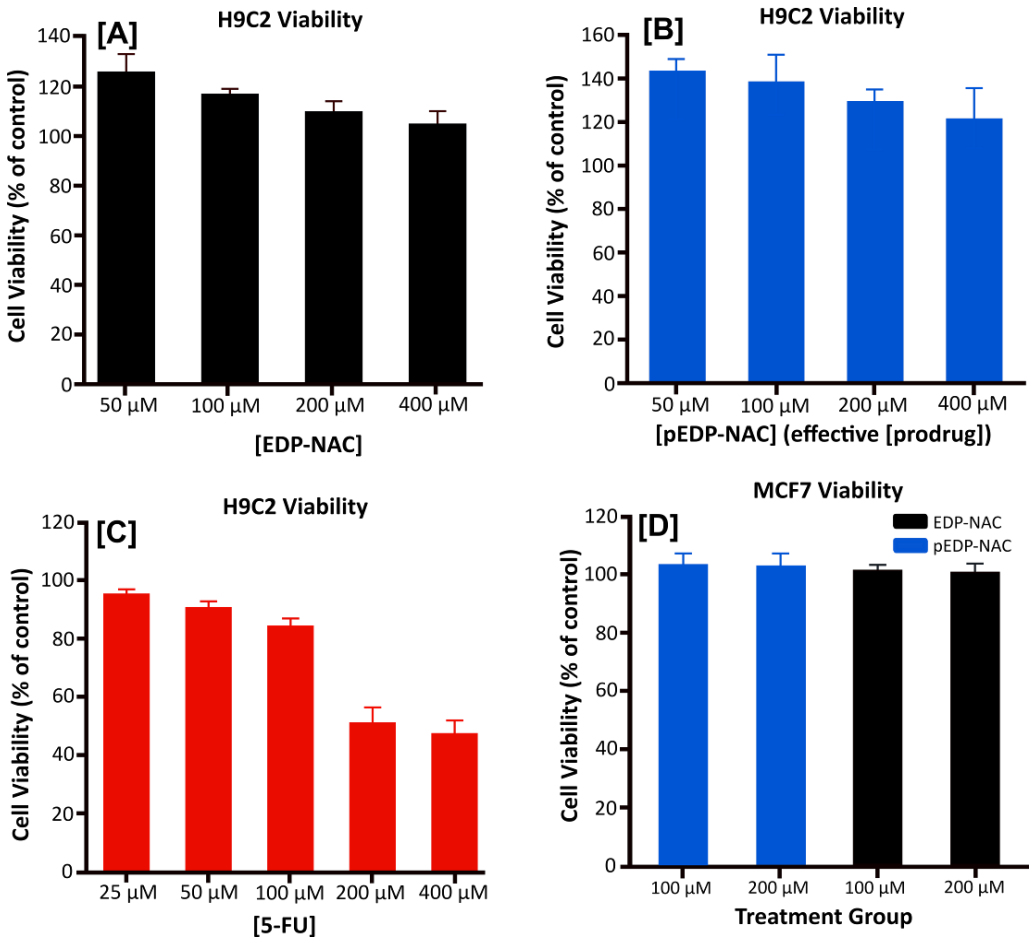

Figure S25. Control viability experiments. [A]: Basic H9C2 cell viability assay with EDP-NAC at various concentrations compared to PBS control; [B]: H9C2 cell viability assay with poly(EDP-NAC) at various effective prodrug concentrations compared to PBS control; [C]: H9C2 cell viability assay with 5-FU compared to PBS control; [D]: MCF-7 cell viability with either EDP-NAC or poly(EDP-NAC) compared to PBS control. No significant change in cell viability was observed upon addition of EDP-NAC or poly(EDP-NAC) in MCF-7 cells under these conditions.

Dynamic Light Scattering Time Study with poly(EDP-NAC)

poly(EDP-NAC) (10 mg/mL in 1:4 DMSO:DI H_2O final concentration) was exposed to PLE (1 U/mL final concentration) for 7 d. 0.2 mL of the reaction mixture was diluted into 1.8 mL 1:4 DMSO: DI H_2O (making a 1mg/mL solution) and filtered before putting the sample on the DLS instrument. A freshly prepared sample with no added PLE (1 mg/mL poly(EDP-NAC) in 1:4 DMSO:DI H_2O) was used as the t = 0 measurement.

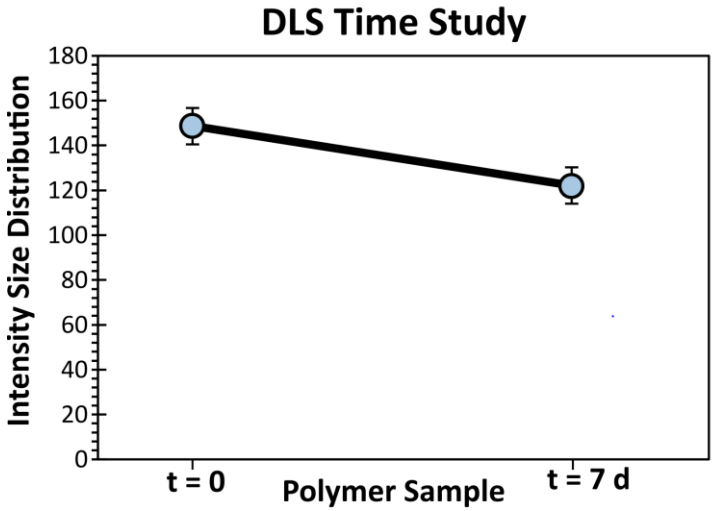

Figure S26. DLS time study with poly(EDP-NAC). Aggregate size decreased slightly upon exposure to PLE for 7 d, but aggregates remained after complete cleavage by PLE, suggesting cleavage by PLE has little effect on persulfide release from self-assembled polymeric prodrugs in solution.

Chapter 5: Targeted Delivery of Persulfides to the Gut: Effects on the Microbiome

Adapted with permission from: Dillon, K. M., et al. "Targeted Delivery of Persulfides to the Gut: Effects on the Microbiome." Angewandte Chemie **60**: 6061-6067.

5.1. Authors

Kearsley M. Dillon,[§] Holly A. Morrison,[†] Chadwick R. Powell,[§] Ryan J. Carrazzone,[§] Veronica M. Ringel-Scaia,[†] Ethan W. Winckler,[§] R. McAlister Council-Troche,[†] Irving C. Allen,[†] John B. Matson[§]

† Department of Biomedical Sciences and Pathobiology, Virginia-Maryland College of Veterinary Medicine, Virginia Tech, Blacksburg, Virginia 24061, United States

§ Department of Chemistry, Virginia Tech Center for Drug Discovery, and Macromolecules Innovation Institute, Virginia Tech, Blacksburg, Virginia 24061, United States

5.2. Abstract

Persulfides (R-SSH) have been hypothesized as potent redox modulators and signaling compounds. Reported here is the synthesis, characterization, and *in vivo* evaluation of a persulfide donor that releases *N*-acetyl cysteine persulfide (NAC-SSH) in response to the prokaryote-specific enzyme nitroreductase. The donor, termed NDP-NAC, decomposed in response to *E. coli* nitroreductase, resulting in release of NAC-SSH. NDP-NAC elicited gastroprotective effects in mice that were not observed in animals treated with control compounds incapable of persulfide

release or in animals treated with Na_2S. NDP-NAC induced these effects by the upregulation of beneficial small and medium chain fatty acids and through increasing growth of *Turicibacter sanguinis*, a beneficial gut bacterium. It also decreased the populations of *Synergistales* bacteria, opportunistic pathogens implicated in gastrointestinal infections. This work represents the first example of targeted delivery of persulfides and reveals the possibility of maintaining gut health or treating microbiome-related diseases with reactive sulfur species such as persulfides.

5.3. Introduction

Hydrogen sulfide (H_2S) has been under investigation as a biological signaling gas (gasotransmitter) since its physiological signaling capacity was discovered in 1996.[1] To aid in understanding its (patho)physiological roles, many different types of donors have been synthesized with a variety of triggers, including water,[2-5] nucleophiles,[6-7] light,[8-9] and enzymes.[10-12] Some may hold therapeutic value in the form of prodrugs and drug conjugates.[13] More recently, additional work has been conducted in the synthesis of compounds that release a variety of related reactive sulfur species (RSS) including carbonyl sulfide (COS),[14-16] sulfur dioxide (SO_2),[17-19] and persulfides (R-SSH),[20-24] with the goal of understanding the specific roles of each of these RSS in the greater reactive species interactome.[25] Of these RSS, persulfides have received considerable interest lately because of their role as likely H_2S signaling products, coupled with advances in redox biology showing that native persulfides carry out specific, anti-oxidative physiological functions.[26-28] Several persulfide-releasing compounds (termed persulfide donors) release their payload under a variety of conditions, including changes in pH,[23] and addition of fluoride,[29] hydrogen peroxide,[21] or esterases.[20, 22] These donors provide insight into persulfide interactions

from a systemic perspective, but it is difficult to determine the role(s) persulfides may serve in specific areas of the body due to a lack of persulfide donors with targeting capabilities.

One particular area where persulfides may play important physiological and/or pathophysiological roles is in the gut.[30-31] The gut microbiome is a promising drug target because many links have been discovered connecting microbiome health and composition to a variety of human diseases. The effects of exogenously delivered H_2S in the microbiome are controversial; some studies have shown beneficial effects of H_2S in the regeneration of colon epithelial tissues by decreasing local inflammation,[32] while others have found harmful effects, such as inhibiting colonocyte respiration and increasing inflammation.[33] The discrepancies in the observed outcomes of exogenously delivered H_2S may be a result of inconsistent delivery methods and concentrations, combined with the use of H_2S donors capable of reaching the bloodstream and exerting off-target effects. As for other RSS, little is known; for example, there exist no studies evaluating the effect of persulfides in the microbiome due to a lack of persulfide donors specifically activated in the gut.

We sought to address this lack of targeted persulfide donors and gap in knowledge in how persulfide delivery affects the gut microbiome by synthesizing a persulfide donor that responds to the prokaryote enzyme nitroreductase (NR). NRs are located specifically in bacteria, sequestered mostly in the mouth, skin, and intestines in mammals. Pharmacologically, NRs have been utilized to trigger the release of a variety of compounds ranging from prodrug systems[34-35] to chemical probes used in imaging.[36-37] For example, Dubikovskaya developed an NR-responsive caged luciferin probe for use in gene-directed enzyme prodrug therapy. The probe fluoresced exclusively in the presence of NR, yielding a novel method to view NR transformed cancer cells.[36] Chakrapani et al. reported the synthesis and characterization of an NR-responsive nitric oxide (NO)-releasing prodrug.[34] The donor was stable in PBS buffer, but released NO selectively in response to NR.

Chakrapani also synthesized an NR-responsive H_2S prodrug by combining *p*-nitrobenzyl thiol with a ketone to form a thioketal.[38] The donor released H_2S in the presence of bacteria and mediated cytoplasmic redox potential upon exposure to H_2O_2; however, it also significantly increased antibiotic resistance. Inspired by these studies and intrigued by the possibility of generating persulfides specifically in the gut, we set out to synthesize and evaluate an NR-triggered persulfide donor.

5.4. Results and Discussion

Using a similar design strategy to a previously reported H_2O_2-reponsive persulfide donor,[21] we synthesized a new persulfide donor termed NDP-NAC for Nitroreductase Disulfide Prodrug- *N*-acetylcysteine (Scheme 1). NRs utilize a 2-electron reduction mechanism employing nicotinamide adenine dinucleotide (NADH) as a cofactor. The *para* positioned nitro ($R\text{-}NO_2$) group is first reduced to a nitroso (R-NO) intermediate, then reduced to a hydroxylamine (R-NHOH), and finally to an amine ($R\text{-}NH_2$) group.[39] In the case of NDP-NAC, we envisioned that this free amine (or hydroxylamine) could undergo a 1,6-elimination mechanism, resulting in the concomitant release of *N*-acetylcysteine persulfide (NAC-SSH) and *p*-aminobenzyl alcohol (pABA).

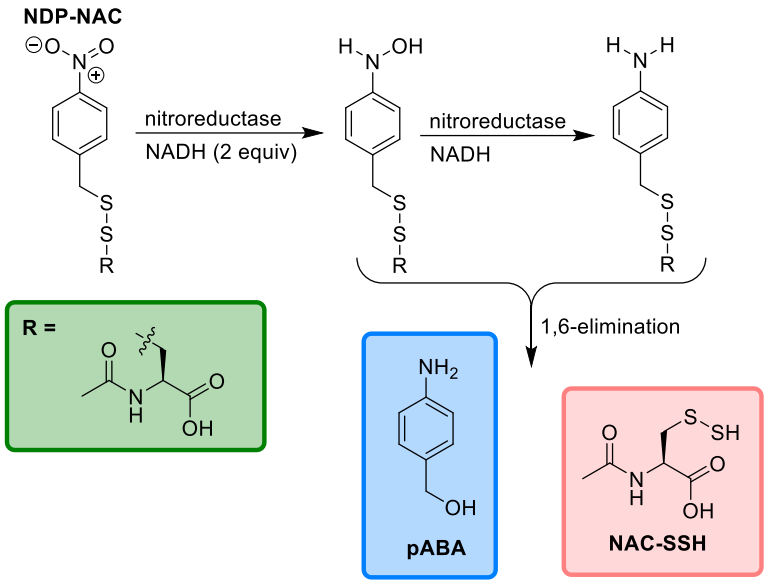

Scheme 1. Proposed mechanism of persulfide release from NDP-NAC. 1,6-elimination may proceed via the hydroxylamine or amine intermediates.

NDP-NAC was synthesized in 4 steps (Scheme 2). First, *p*-nitrotoluene was brominated using *N*-bromosuccinimide (NBS), yielding *p*-nitrobenzyl bromide (**1**). Next, thiourea was added, and subsequent aminolysis using hexylamine yielded *p*-nitrobenzyl thiol (**2**). The resulting thiol was added to the activated disulfide of NAC (NACpyDS) in a disulfide exchange reaction to afford the prodrug in a 35% overall yield with only one column purification step required throughout the synthesis.

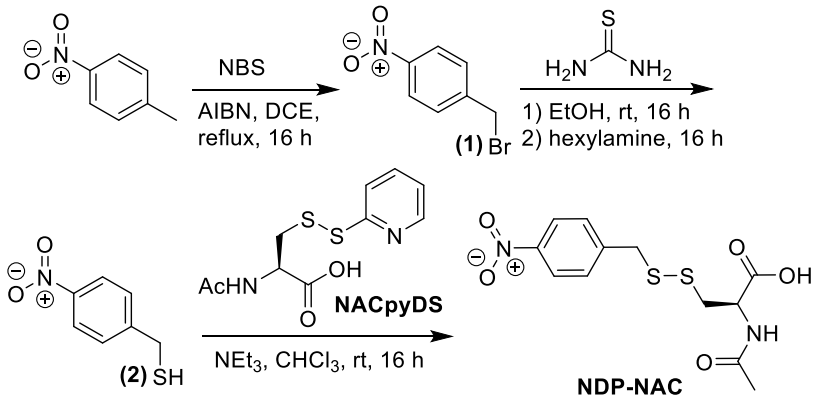

Scheme 2. Synthesis of NDP-NAC.

Due to their inherent instability, persulfides are difficult to detect directly by high resolution mass spectrometry (HRMS), so electrophilic trapping reagents such as *N*-ethylmaleimide (NEM), iodoacetamide (IAM),[40] or dinitrofluorobenzene (DNFB)[20] are commonly used. The reaction of a persulfide with these trapping agents forms a disulfide that typically can withstand MS ionization conditions, whereas the persulfide itself mostly disproportionates into H_2S and a thiol or forms trisulfides when directly analyzed.[24] We attempted to trap the persulfide using NEM, IAM, and DNFB, and we found that DNFB worked best in this system.

In the experimental setup, NDP-NAC, DNFB, and NADH were dissolved in pH 8.0 PBS and added to a vial with a screwcap lid, and an aliquot was removed for a zero timepoint (t = 0). Exact procedures for dilution and analysis are described in the supporting information. NR was then added to the reaction mixture, and aliquots were removed every 30 min. After a brief workup step to remove excess NADH, each aliquot was analyzed by analytical HPLC (Figures 1, S15). The peak corresponding to NDP-NAC (elution time 4.0 min) decreased in intensity over time as a new peak (6.1 min) evolved, which we determined corresponded to the trapped persulfide adduct (DNB-NAC, Figure S10) based on comparison to an authentic sample. After 2 h, NDP-NAC had

been consumed, and DNB-NAC remained. The conversion of NDP-NAC into DNB-NAC indicated that NDP-NAC efficiently released its persulfide payload in the presence of NR.

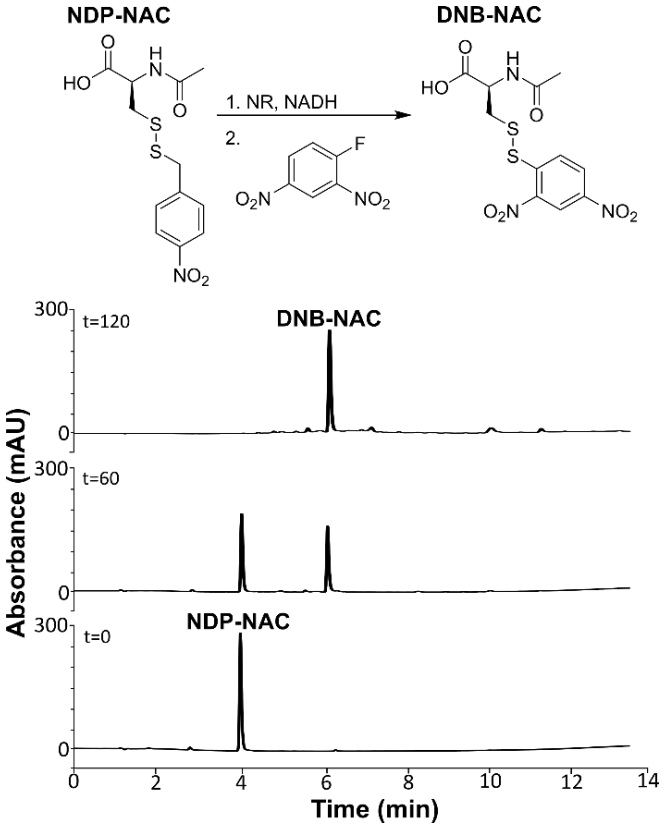

Figure 1. Analytical HPLC chromatogram series depicting persulfide release from NDP-NAC over time using DNFB as a trapping reagent. The peak eluting at 4.0 min corresponds to NDP-NAC while the peak at 6.1 min corresponds to the persulfide adduct DNB-NAC. Reactions were performed at 22 °C in pH 8.0 phosphate buffer (the pH level stabilized at 7.8) at 100 µM NDP-NAC. Monitoring wavelength was 282 nm.

Next, we set out to determine the persulfide release half-life from NDP-NAC using ^{1}H NMR spectroscopy (Figure 2). NDP-NAC and NADH were dissolved in a mixture of DMSO-d_6 and deuterated phosphate buffer (dPB) at pD = 8 (1:4 v/v). This pD value was chosen to mimic the mildly basic conditions of the intestines, where most gut bacteria are located. A zero timepoint

was taken, NR was then added to the NMR tube, and subsequent scans were taken over the course of several hours. As shown in the zero timepoint spectrum, a clear doublet (a) corresponding to NDP-NAC was observed at 7.42 ppm. After the addition of NR, a new doublet (a'), which we attribute to pABA, was observed at 7.15 ppm. Other signals in the aromatic region were due to NADH and NAD^+, the oxidation product of NADH, including the three new signals above 8.6 ppm. By 10.7 h, complete disappearance of NDP-NAC was observed. A decomposition half-life ($t_{1/2}$) of 1.5 h ± 0.3 h (n=3) was calculated from these experiments (Figure S16). We and others have observed similar discrepancies between the half-lives observed in ^{1}H NMR and HPLC experiments previously,[41] and we attributed them to slower 1,6-elimination rates in organic solvents relative to aqueous solvent mixtures.[42] Although replication of the complex gut microbiome environment is not possible in these NMR and HPLC experiments, taken together they show that NDP-NAC generates NAC-SSH in response to nitroreductase over the course of hours under the mildly basic conditions present in the intestines.

Furthermore, we next evaluated the reactivity of NDP-NAC with Cys to assess the potential for biological reductants to hamper the prodrug's ability to release persulfides. NDP-NAC and Cys (2 eq) were dissolved in 1:4 DMSO-d_6:pD 8.0 dPB or 1:4 DMSO-d_6:pD 2.5 dPB. In both cases, no substantial changes to the ^{1}H NMR spectrum of NDP-NAC were observed after 24 h at rt (Figures S17 and S18), suggesting that NDP-NAC is stable in the presence of thiols under these conditions.

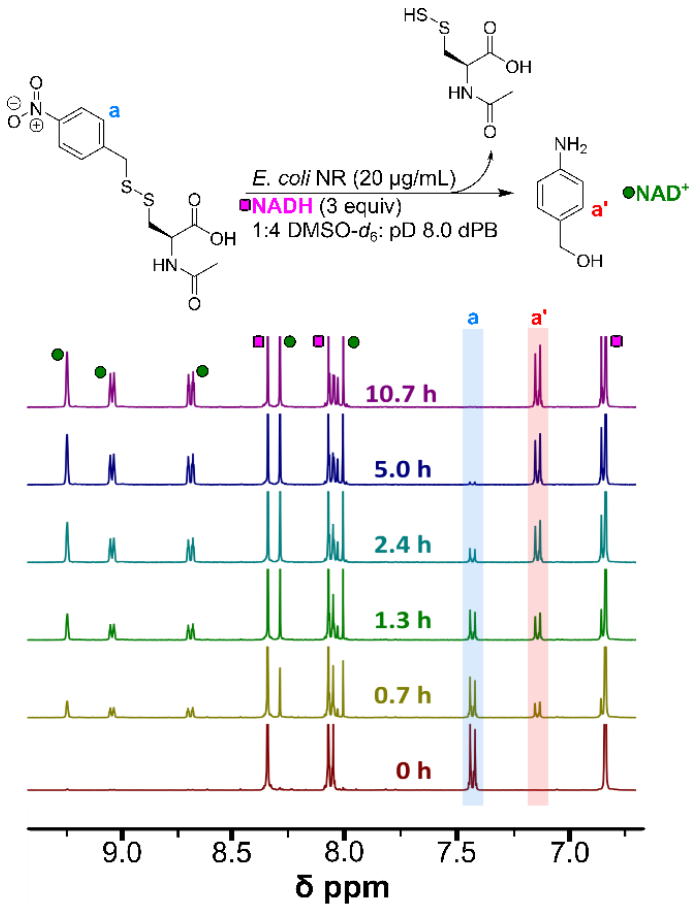

Figure 2. ^{1}H NMR analysis of NDP-NAC decomposition kinetics. The half-life was calculated to be 1.5 h ± 0.3 h (n = 3). Reactions were performed at 22 °C in pD 8.0 phosphate buffer (the pD level stabilized at 8.1) at 3.6 mM NDP-NAC.

We then aimed to determine the effects of exogenous delivery of persulfides in the microbiome. However, we first needed to establish whether NDP-NAC was toxic to human cells. NDP-NAC cell viability was conducted on H9C2 cardiomyocytes as a representative normal mammalian cell line (Figure 3A). NDP-NAC was nontoxic up to 400 μM, inducing proliferation to a small degree at lower levels compared with untreated controls. Of note, cell viability greater than 100% in these experiments is likely due to artifacts of the CCK-8 assay.[43]

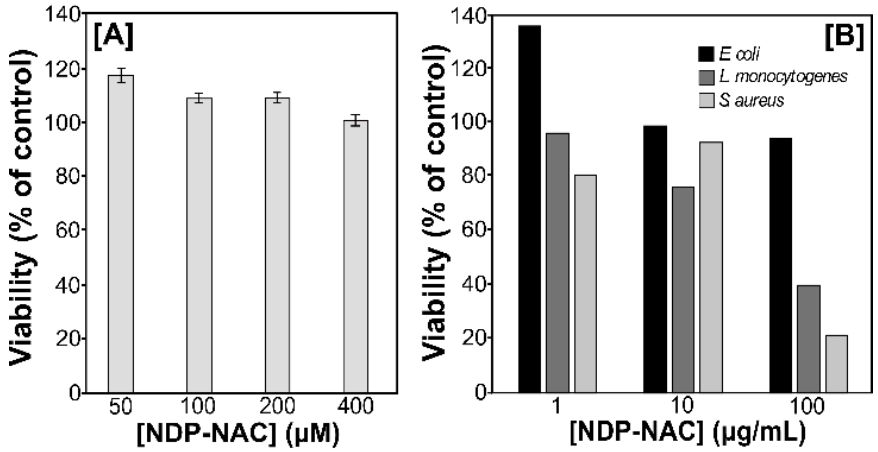

Figure 3. Summary of eukaryote and bacteria viability after treatment with NDP-NAC. A) H9C2 viability after treatment with NDP-NAC at various concentrations. Viability was quantified using cell counting kit 8 (CCK-8), comparing treatment groups to an untreated control. Results are expressed as the mean ± SEM (n = 3, 3–5 wells per experiment). B) Bacteria viability in response to NDP-NAC at various concentrations after 24 h culture in agar plates. Viability is reported with respect to control plates with no NDP-NAC.

Next, the toxicity of NDP-NAC to prokaryotes that are commonly located in the gut was evaluated (Figure 3B). An aqueous solution of NDP-NAC at either 1, 10, or 100 µg/mL was added to molten agar and stirred until homogeneous. Agar plates were prepared, and then *E. coli*, *L. monocytogenes*, and *S. aureus* were then used to inoculate the plates. After 24 h in culture, NDP-NAC exhibited no toxicity towards *E. coli*, a common inhabitant of the human gut. However, NDP-NAC did elicit a dose-dependent decrease in viability in *L. monocytogenes* and *S. aureus*, two opportunistic pathogens.

With these results in hand, we set out to investigate effects on general bacteria populations elicited by NDP-NAC and various controls in the mouse microbiome. Two compounds that are similar in

structure to NDP-NAC were synthesized as control compounds for use in these studies (Figure 4A). Benz-NAC, which is analogous to NDP-NAC but lacks the nitro group, was prepared as a control compound that could not release a persulfide but was otherwise structurally similar. NDP-TE, which possesses a thioether linkage instead of a disulfide linkage, was synthesized as a second control compound that could undergo decomposition in response to nitroreductases but would release a thiol (NAC) instead of a persulfide. Despite potentially low bioavailability due to the oral gavage method used for delivery, Na_2S was utilized as a model H_2S donor control in these experiments due to its widespread use as a simple, instantaneous H_2S donor that lacks byproducts. After mice (n = 5 with five treatment groups: NDP-NAC, Benz-NAC, NDP-TE, Na_2S, and PBS vehicle only) were given single daily gavages of NDP-NAC (100 µL, 100 µg/mL), control compounds (100 µL, 100 µg/mL) or PBS vehicle (100 µL) over 5 d, feces were harvested and plated on agar. Morphology assessments were conducted, and individual, morphologically unique colonies were picked and cultured to logarithmic growth phase in this biased screening approach. Each specimen was identified to at least the genera level using matrix-assisted laser desorption/ionization-time of flight (MALDI-TOF) mass spectrometry.

The types of bacteria discovered in this approach were quite different in animals treated with NDP-NAC versus all others (Figure 4B). As expected, animals that received PBS only were rich in *Bacillus* species with no unique or non-*Bacillus* species. *Bacillus* species are quite prevalent in a healthy gut microbiome. Mice treated with Benz-NAC also elicited no microbiome change, whereas NDP-TE and Na_2S elicited minor changes (two and one unique or non-*Bacillus* species, respectively). However, in animals treated with NDP-NAC, we recovered 8 unique or non-*Bacillus* species, including *Enterococcus faecalis*, *Bacillus cereus*, and *Staphylococcus lentus*, which are all common probiotic bacteria found in commercial supplements. While we recognize this prodrug

may react in unintended ways in the complex gut environment, these findings suggested that NDP-NAC was capable of regulating the microbiome, warranting a deeper search into possible effects on metabolism within the gut.

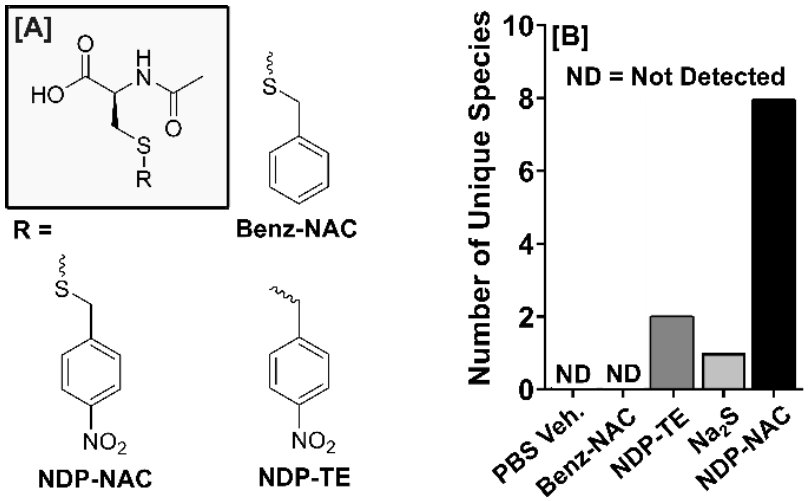

Figure 4. Summary of structural analogs of NDP-NAC used in MALDI-TOF. A) Chemical structures NDP-NAC and controls Benz-NAC (lacking nitro group) and NPD-TE (a thioether in place of a disulfide) used in MALDI-TOF analysis. B) Broad identification of the bacteria present in the mouse gastrointestinal microbiome upon treatment with NDP-NAC or various controls using biased sampling and MALDI-TOF.

To expand upon the findings associated with the microbiome population changes, we also sought to determine the effects of the altered microbiome on functional and metabolic processes of biological and physiological relevance by evaluating short and medium chain fatty acids (SCFAs and MCFAs) in the fecal specimens using gas chromatography.[44] SCFA/MCFA analysis revealed mostly minor differences in metabolites evaluated using NDP-NAC, Benz-NAC, NDP-TE, and vehicle-treated groups. However, we did observe a nine-fold increase in heptanoic acid production

between NDP-NAC and PBS-treated groups (Figure S19). In the gastrointestinal tract, heptanoic acid plays key roles in lipid transport, peroxidation, and metabolism; decreased levels have been found in patients with Crohn's disease, ulcerative colitis, and pouchitis.[45] Together, these data suggest that NDP-NAC may exhibit gastroprotective and anti-inflammatory effects.[46-48] Mouse blood plasma samples were also analyzed using ultra high performance liquid chromatography with tandem mass spectrometry (UPLC-MS/MS). No trace of NDP-NAC or pABA was detected in any of the six mouse plasma samples (LOD = 0.1 ng/mL, see Supporting Information). These results suggest that the NDP-NAC does not pass through the intestinal epithelial cell barrier and its effects appear to be contained within the gastrointestinal tract, likely indicating that the prodrug is metabolized directly by the bacteria or at least in close proximity. Likewise, no adverse effects were observed in animals treated with NDP-NAC. In summary, NDP-NAC induced changes in the mouse microbiome, affecting the types of bacterial species present and the production of metabolites, that were not observed in either of the control molecules or Na_2S.

Building upon these findings, we next repeated our animal studies (same administration method, dose, and numbers of animals, but only using NDP-NAC and PBS-vehicle treatment groups) and utilized a more robust, non-biased screening approach to better define microbiome population differences between the NDP-NAC-treated and untreated animals. Feces were harvested from mice at the end of the 5-day study, with collection directly from the colon at necropsy; tissue scraping was conducted to also recover adherent populations. Fecal specimens were flash frozen upon sterile collection, followed by nucleic acid extraction for shotgun metagenomics analysis.

Consistent with the biased screening assessments noted above, treatment with NDP-NAC resulted in changes in microbiome populations, with significant differences noted between the PBS vehicle- and NDP-NAC-treated animals. Sample clustering with taxonomic abundance revealed that the

majority of the PBS vehicle-treated animals clustered together (Figure 5A). However, treatment with NDP-NAC generated two distinct groups that were significantly different in composition at the phylum level compared to the PBS vehicle (Figure 5B). Further assessments by LEfSe (linear discriminant analysis effect size) analysis revealed that the differences between the PBS vehicle- and NDP-NAC-treated animals were due to decreased members of the genus *Pseudoflavonifractor* and at the species level decreased *clostridium*, *eubacterium*, *clostridiales*, *lachnoclostridium*, *pseudoflavonifractor*, and *acutalibacter* species in the microbiome isolated from the vehicle-treated animals. Conversely, the microbiome from the NDP-NAC-treated animals had a significant increase in members of the *Turicibacter* genus, specifically *Turicibacter sanguinis* species. Intriguingly, *T. sanguinis* has recently been identified as a highly relevant gut bacterium that naturally expresses a neurotransmitter sodium symporter-related protein homologous to mammalian SERT, which is a host 5-HT (serotonin) transporter.[49] *T. sanguinis* blooms in the GI tract can alter a broad range of host genes impacting multiple biochemical pathways, including increases in those important for lipid and steroid metabolism and decreasing systemic triglyceride levels and inguinal adipocyte size.[49] In addition to *T. sanguinis* being increased in the NDP-NAC-treated animals, additional metastats analysis was conducted, which relies on a non-parametric *t*-test for detecting differentially abundant features in metagenomic studies. Results revealed a significant decrease in the relative abundance of *Synergistales* bacterium in NDP-NAC-treated animals (Figure 5C). *Synergistales* bacteria are a recently identified family of anaerobic, gram-negative, opportunistic pathogens that are implicated in the formation and progression of cysts, abscesses, periodontal disease, and gastrointestinal infections.[50-52]

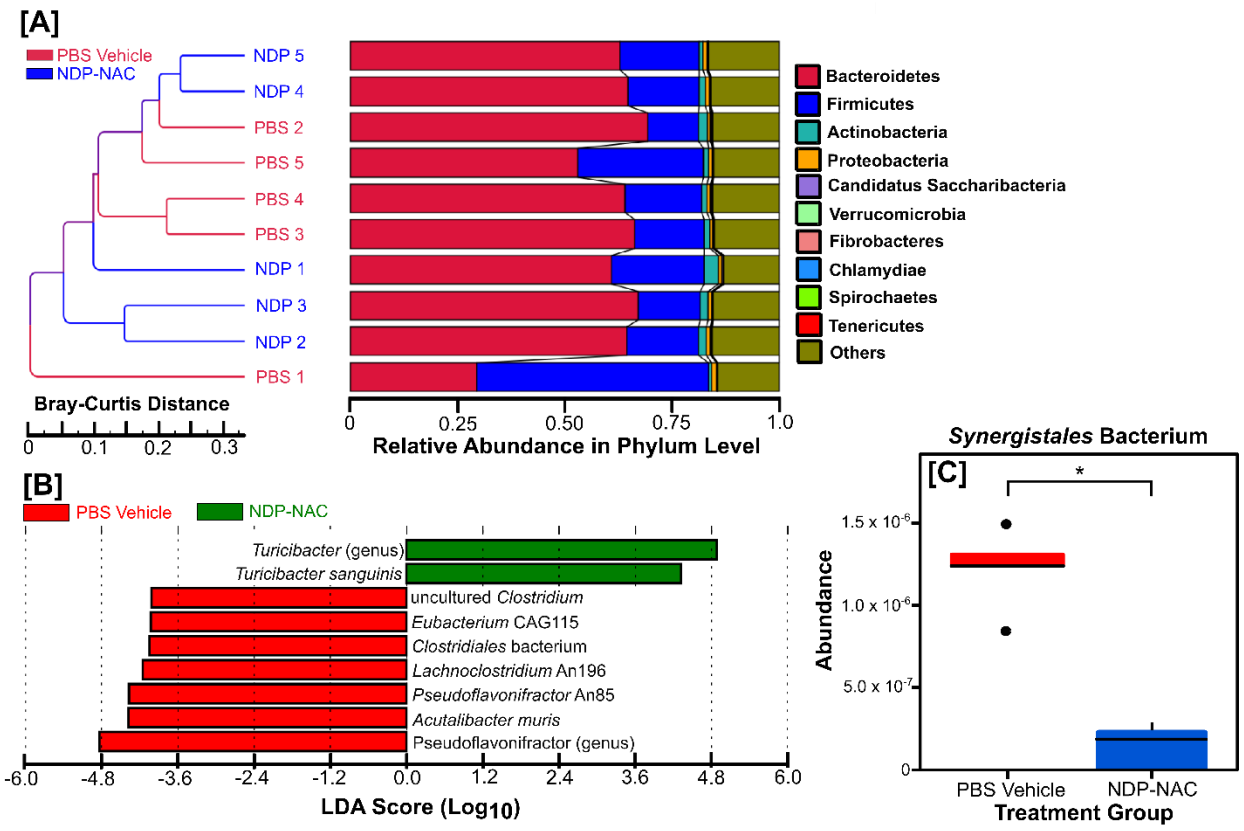

Figure 5. Sample clustering with taxonomic abundance. A) Sample clustering analysis based on Bray-Curtis distance highlighting the similarity of samples from each animal. The distance was calculated according to relative taxonomic abundance, and the data shown were generated by combining the clustering results and relative abundances of different samples at the phylum level. B) LEfSe analysis identifying genomic features (taxa) characterizing the significant differences between the microbiome populations among treatment groups. The histogram of the LDA scores shows the species whose LDA scores are larger than the set threshold (4 set by default). C) Metastats analysis demonstrating a significant decrease in the relative abundance of *Synergistales* bacterium in mice treated with NDP-NAC. *$p<0.05$

Finally, to gain additional insight into the microbial metabolic processes impacted by NDP-NAC, we also utilized shotgun metagenomics and to assemble protein sequence data to predict microbial

protein function. This analysis identified changes in only three functions following NDP-NAC treatment: genetic information processing/translation, lipid metabolism, and endocrine and metabolic diseases (Figure 6). The increased translation and lipid metabolism differences are highly consistent with the findings associated with the increased *Turicibacter sanguinis* levels (Figure 5B) as this bacterium significantly impacts lipid metabolism, triglyceride levels, and host genetic functions.[49] These findings are also consistent with the observed changes in heptanoic acid (Figure S19), which is critical for lipid transport and metabolism. We also found that in contrast to previous reports on H_2S delivery to the gut,[38] genetic markers for antibiotic resistance did not increase in the NDP-NAC treatment group (Figures S23, S24, and S25).

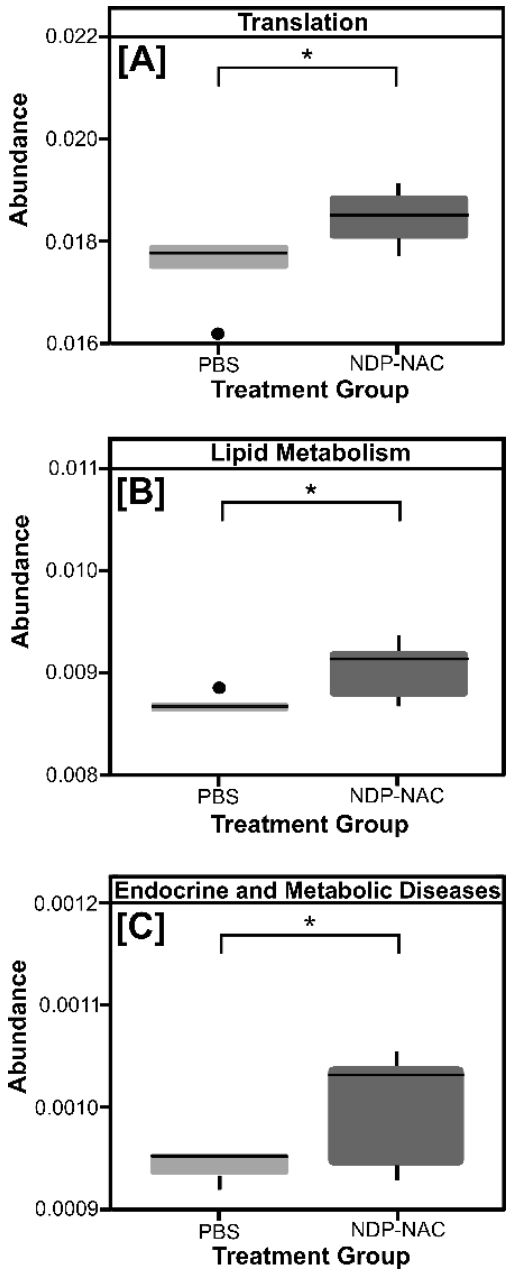

Figure 6. Metastats analysis of functional differences. Three functions, whose abundances were significantly different between the PBS vehicle- and NDP-NAC-treatment groups, were identified from shotgun metagenomic analyses: (A) genetic information processing/translation, (B) lipid metabolism, (C) endocrine and metabolic diseases. *$p<0.05$

5.5. Conclusions

In summary, NDP-NAC, a nitroreductase-responsive persulfide prodrug, which to our knowledge represents the first persulfide donor with targeting capabilities, released persulfides in the presence of microbial nitroreductase with a half-life on the order of hours. NDP-NAC significantly impacted the composition and function of the host microbiome in mice treated with the prodrug compared with mice treated with non-persulfide releasing control compounds and Na_2S, an H_2S donor. Changes elicited by NDP-NAC created favorable niches for the expansion of a limited repertoire of bacteria species, including *Turicibacter sanguinis*, that appear to have robust host effects impacting metabolism and overall gastrointestinal health. Conversely, NDP-NAC also demonstrated clear suppressive effects on a diverse range of opportunistic and pathogenic bacteria in the gut. This includes limiting *Synergistales* bacteria, which are associated with a variety of human health issues. Thus, NDP-NAC enhances several health-promoting bacteria while limiting the growth of various pathogenic bacteria. This work adds to the body of knowledge in the rapidly growing field of gut microbiome health, showing that controlled delivery of RSS to the gut may be useful for modulating the gastrointestinal microbiome during disease states, shifting the balance from dysbiosis to homeostasis.

5.6. Acknowledgements

This work was supported by the National Institutes of Health (R01GM123508), the National Science Foundation (DMR-1454754), the Virginia Tech Center for Drug Discovery, and the Dreyfus foundation. The authors thank Dr. Mehdi Ashraf-Khorassani for assistance with LCMS, Dr. Kristin Eden for her animal model expertise, and Elizabeth Smiley for fatty acid analysis. The authors also acknowledge Novogene Co., Ltd. for their genome sequencing and bioinformatics work.

5.7. References

1. Abe, K.; Kimura, H., The possible role of hydrogen sulfide as an endogenous neuromodulator. *J. Neurosci.* **1996,** *16* (3), 1066-1071.

2. Li, L.; Whiteman, M.; Guan, Y. Y.; Neo, K. L.; Cheng, Y.; Lee, S. W.; Zhao, Y.; Baskar, R.; Tan, C.-H.; Moore, P. K., Characterization of a Novel, Water-Soluble Hydrogen Sulfide–Releasing Molecule (GYY4137). *Circulation* **2008,** *117* (18), 2351.

3. Nicolau, L. A. D.; Silva, R. O.; Damasceno, S. R. B.; Carvalho, N. S.; Costa, N. R. D.; Aragão, K. S.; Barbosa, A. L. R.; Soares, P. M. G.; Souza, M. H. L. P.; Medeiros, J. V. R., The hydrogen sulfide donor, Lawesson's reagent, prevents alendronate-induced gastric damage in rats. *Braz. J. Med. Biol. Res.* **2013,** *46*, 708-714.

4. Zhao, W.; Zhang, J.; Lu, Y.; Wang, R., The vasorelaxant effect of H_2S as a novel endogenous gaseous K(ATP) channel opener. *EMBO J.* **2001,** *20* (21), 6008-6016.

5. Kang, J.; Li, Z.; Organ, C. L.; Park, C.-M.; Yang, C.-t.; Pacheco, A.; Wang, D.; Lefer, D. J.; Xian, M., pH-Controlled Hydrogen Sulfide Release for Myocardial Ischemia-Reperfusion Injury. *J. Am. Chem. Soc.* **2016,** *138* (20), 6336-6339.

6. Zhao, Y.; Wang, H.; Xian, M., Cysteine-Activated Hydrogen Sulfide (H_2S) Donors. *J. Am. Chem. Soc.* **2011,** *133* (1), 15-17.

7. Foster, J. C.; Powell, C. R.; Radzinski, S. C.; Matson, J. B., *S*-Aroylthiooximes: A Facile Route to Hydrogen Sulfide Releasing Compounds with Structure-Dependent Release Kinetics. *Org. Lett.* **2014,** *16* (6), 1558-1561.

8. Fukushima, N.; Ieda, N.; Sasakura, K.; Nagano, T.; Hanaoka, K.; Suzuki, T.; Miyata, N.; Nakagawa, H., Synthesis of a photocontrollable hydrogen sulfide donor using ketoprofenate photocages. *Chem. Commun.* **2014,** *50* (5), 587-589.

9. Devarie-Baez, N. O.; Bagdon, P. E.; Peng, B.; Zhao, Y.; Park, C.-M.; Xian, M., Light-Induced Hydrogen Sulfide Release from "Caged" gem-Dithiols. *Org. Lett.* **2013,** *15* (11), 2786-2789.

10. Zheng, Y.; Yu, B.; Ji, K.; Pan, Z.; Chittavong, V.; Wang, B., Esterase-Sensitive Prodrugs with Tunable Release Rates and Direct Generation of Hydrogen Sulfide. *Angew. Chem. Int. Ed.* **2016,** *55* (14), 4514-4518.

11. Chauhan, P.; Bora, P.; Ravikumar, G.; Jos, S.; Chakrapani, H., Esterase Activated Carbonyl Sulfide/Hydrogen Sulfide (H_2S) Donors. *Org. Lett.* **2017,** *19* (1), 62-65.

12. Li, Z.; Organ, C. L.; Zheng, Y.; Wang, B.; Lefer, D. J., Novel Esterase-Activated Hydrogen Sulfide Donors Attenuate Myocardial Ischemia/Reperfusion Injury. *Circulation* **2016,** *134*, 17903.

13. Powell, C. R.; Dillon, K. M.; Matson, J. B., A review of hydrogen sulfide (H_2S) donors: Chemistry and potential therapeutic applications. *Biochem. Pharmacol.* **2018,** *149*, 110-123.

14. Powell, C. R.; Foster, J. C.; Okyere, B.; Theus, M. H.; Matson, J. B., Therapeutic Delivery of H_2S via COS: Small Molecule and Polymeric Donors with Benign Byproducts. *J. Am. Chem. Soc.* **2016,** *138* (41), 13477-13480.

15. Steiger, A. K.; Pardue, S.; Kevil, C. G.; Pluth, M. D., Self-Immolative Thiocarbamates Provide Access to Triggered H_2S Donors and Analyte Replacement Fluorescent Probes. *J. Am. Chem. Soc.* **2016,** *138* (23), 7256-7259.

16. Powell, C. R.; Foster, J. C.; Swilley, S. N.; Kaur, K.; Scannelli, S. J.; Troya, D.; Matson, J. B., Self-amplified depolymerization of oligo(thiourethanes) for the release of COS/H_2S. *Polym. Chem.* **2019,** *10* (23), 2991-2995.

17. Wang, W.; Ji, X.; Du, Z.; Wang, B., Sulfur dioxide prodrugs: triggered release of SO_2 via a click reaction. *Chem. Commun.* **2017,** *53* (8), 1370-1373.

18. Day, J. J.; Yang, Z.; Chen, W.; Pacheco, A.; Xian, M., Benzothiazole Sulfinate: a Water-Soluble and Slow-Releasing Sulfur Dioxide Donor. *ACS Chem. Biol.* **2016,** *11* (6), 1647-1651.

19. Malwal, S. R.; Sriram, D.; Yogeeswari, P.; Konkimalla, V. B.; Chakrapani, H., Design, Synthesis, and Evaluation of Thiol-Activated Sources of Sulfur Dioxide (SO_2) as Antimycobacterial Agents. *J. Med. Chem.* **2012,** *55* (1), 553-557.

20. Zheng, Y.; Yu, B.; Li, Z.; Yuan, Z.; Chelsea, L.; Rishi, K.; Wang, S.; Lefer David, J.; Wang, B., An Esterase-Sensitive Prodrug Approach for Controllable Delivery of Persulfide Species. *Angew. Chem.* **2017,** *129* (39), 11911-11915.

21. Powell, C. R.; Dillon, K. M.; Wang, Y.; Carrazzone, R. J.; Matson, J. B., A Persulfide Donor Responsive to Reactive Oxygen Species: Insights into Reactivity and Therapeutic Potential. *Angew. Chem. Int. Ed.* **2018,** *57* (21), 6324-6328.

22. Yuan, Z.; Zheng, Y.; Yu, B.; Wang, S.; Yang, X.; Wang, B., Esterase-Sensitive Glutathione Persulfide Donor. *Organic Letters* **2018,** *20* (20), 6364-6367.

23. Artaud, I.; Galardon, E., A Persulfide Analogue of the Nitrosothiol SNAP: Formation, Characterization and Reactivity. *Chembiochem* **2014,** *15* (16), 2361-2364.

24. Khodade, V. S.; Toscano, J. P., Development of S-Substituted Thioisothioureas as Efficient Hydropersulfide Precursors. *J. Am. Chem. Soc.* **2018,** *140* (50), 17333-17337.

25. Cortese-Krott, M. M.; Koning, A.; Kuhnle, G. G. C.; Nagy, P.; Bianco, C. L.; Pasch, A.; Wink, D. A.; Fukuto, J. M.; Jackson, A. A.; van Goor, H.; Olson, K. R.; Feelisch, M., The Reactive Species Interactome: Evolutionary Emergence, Biological Significance, and Opportunities for Redox Metabolomics and Personalized Medicine. *Antioxid. Redox. Signal.* **2017,** *27* (10), 684-712.

26. Kasamatsu, S.; Nishimura, A.; Morita, M.; Matsunaga, T.; Abdul Hamid, H.; Akaike, T., Redox Signaling Regulated by Cysteine Persulfide and Protein Polysulfidation. *Molecules* **2016,** *21* (12), 1721.

27. Yadav, P. K.; Martinov, M.; Vitvitsky, V.; Seravalli, J.; Wedmann, R.; Filipovic, M. R.; Banerjee, R., Biosynthesis and Reactivity of Cysteine Persulfides in Signaling. *J. Am. Chem. Soc.* **2016,** *138* (1), 289-299.

28. Cuevasanta, E.; Möller, M. N.; Alvarez, B., Biological chemistry of hydrogen sulfide and persulfides. *Arch. Biochem. Biophys.* **2017,** *617* (Supplement C), 9-25.

29. Kang, J.; Xu, S.; Radford Miles, N.; Zhang, W.; Kelly Shane, S.; Day Jacob, J.; Xian, M., O→S Relay Deprotection: A General Approach to Controllable Donors of Reactive Sulfur Species. *Angew. Chem. Int. Ed.* **2018,** *57* (20), 5893-5897.

30. Barton, L. L.; Ritz, N. L.; Fauque, G. D.; Lin, H. C., Sulfur Cycling and the Intestinal Microbiome. *Dig. Dis. Sci.* **2017,** *62* (9), 2241-2257.

31. Carbonero, F.; Benefiel, A. C.; Alizadeh-Ghamsari, A. H.; Gaskins, H. R., Microbial pathways in colonic sulfur metabolism and links with health and disease. *Front. Physiol.* **2012,** *3*, 448-448.

32. Wallace, J. L.; Motta, J.-P.; Buret, A. G., Hydrogen sulfide: an agent of stability at the microbiome-mucosa interface. *Am. J. Physiol. Gastrointest. Liver Physiol.* **2018,** *314* (2), G143-G149.

33. Beaumont, M.; Andriamihaja, M.; Lan, A.; Khodorova, N.; Audebert, M.; Blouin, J.-M.; Grauso, M.; Lancha, L.; Benetti, P.-H.; Benamouzig, R.; Tomé, D.; Bouillaud, F.; Davila, A.-M.; Blachier, F., Detrimental effects for colonocytes of an increased exposure to luminal hydrogen sulfide: The adaptive response. *Free Radical Biol. Med.* **2016,** *93*, 155-164.

34. Sharma, K.; Sengupta, K.; Chakrapani, H., Nitroreductase-activated nitric oxide (NO) prodrugs. *Bioorg. Med. Chem. Lett.* **2013,** *23* (21), 5964-5967.

35. Searle, P. F.; Chen, M.-J.; Hu, L.; Race, P. R.; Lovering, A. L.; Grove, J. I.; Guise, C.; Jaberipour, M.; James, N. D.; Mautner, V.; Young, L. S.; Kerr, D. J.; Mountain, A.; White, S. A.; Hyde, E. I., Nitroreductase: A prodrug-activating enzyme for cancer gene therapy. *Clin. Exp. Pharmacol. Physiol.* **2004,** *31* (11), 811-816.

36. Vorobyeva, A. G.; Stanton, M.; Godinat, A.; Lund, K. B.; Karateev, G. G.; Francis, K. P.; Allen, E.; Gelovani, J. G.; McCormack, E.; Tangney, M.; Dubikovskaya, E. A., Development of a Bioluminescent Nitroreductase Probe for Preclinical Imaging. *PLoS One* **2015,** *10* (6), e0131037.

37. Zhu, D.; Xue, L.; Li, G.; Jiang, H., A highly sensitive near-infrared ratiometric fluorescent probe for detecting nitroreductase and cellular imaging. *Sens. Actuators B Chem.* **2016,** *222*, 419-424.

38. Shukla, P.; Khodade, V. S.; SharathChandra, M.; Chauhan, P.; Mishra, S.; Siddaramappa, S.; Bulagonda, E. P.; Singh, A.; Chakrapani, H., "On Demand" Redox Buffering by H_2S Contributes to Antibiotic Resistance Revealed by a Bacteria-Specific H_2S Donor. *Chem. Sci.* **2017,** *8*, 4967-4972.

39. Miller, A.-F.; Park, T. J.; Ferguson, L. K.; Pitsawong, W.; Bommarius, S. A., Informing Efforts to Develop Nitroreductase for Amine Production. *Molecules* **2018,** *23* (2), 211.

40. Chatterji, T.; Keerthi, K.; Gates, K. S., Generation of reactive oxygen species by a persulfide (BnSSH). *Bioorg. Med. Chem. Lett.* **2005,** *15* (17), 3921-3924.

41. Dillon, K. M.; Powell, C. R.; Matson, J. B., Self-Immolative Prodrugs: Effective Tools for the Controlled Release of Sulfur Signaling Species. *Synlett* **2019,** *30* (5), 525-531.

42. Schmid, K. M.; Jensen, L.; Phillips, S. T., A Self-Immolative Spacer That Enables Tunable Controlled Release of Phenols under Neutral Conditions. *J. Org. Chem.* **2012,** *77* (9), 4363-4374.

43. Lin, J.; Akiyama, M.; Bica, I.; Long, F. T.; Henderson, C. F.; Goddu, R. N.; Suarez, V.; Baker, B.; Ida, T.; Shinkai, Y.; Nagy, P.; Akaike, T.; Fukuto, J. M.; Kumagai, Y., The Uptake and Release of Polysulfur Cysteine Species by Cells: Physiological and Toxicological Implications. *Chem. Res. Toxicol.* **2019,** *32* (3), 447-455.

44. Ringel-Scaia, V. M.; Qin, Y.; Thomas, C. A.; Huie, K. E.; McDaniel, D. K.; Eden, K.; Wade, P. A.; Allen, I. C., Maternal Influence and Murine Housing Confound Impact of NLRP1 Inflammasome on Microbiome Composition. *J. Innate Immun.* **2019,** *11* (5), 416-431.

45. De Preter, V.; Machiels, K.; Joossens, M.; Arijs, I.; Matthys, C.; Vermeire, S.; Rutgeerts, P.; Verbeke, K., Faecal metabolite profiling identifies medium-chain fatty acids as discriminating compounds in IBD. *Gut* **2015,** *64* (3), 447.

46. Maslowski, K. M.; Vieira, A. T.; Ng, A.; Kranich, J.; Sierro, F.; Yu, D.; Schilter, H. C.; Rolph, M. S.; Mackay, F.; Artis, D.; Xavier, R. J.; Teixeira, M. M.; Mackay, C. R., Regulation of inflammatory responses by gut microbiota and chemoattractant receptor GPR43. *Nature* **2009,** *461* (7268), 1282-1286.

47. Wlodarska, M.; Kostic, A. D.; Xavier, R. J., An integrative view of microbiome-host interactions in inflammatory bowel diseases. *Cell Host Microbe* **2015,** *17* (5), 577-591.

48. Kim, Y. I., Short-Chain Fatty Acids in Ulcerative Colitis. *Nutr. Rev.* **1998,** *56* (1), 17-24.

49. Fung, T. C.; Vuong, H. E.; Luna, C. D. G.; Pronovost, G. N.; Aleksandrova, A. A.; Riley, N. G.; Vavilina, A.; McGinn, J.; Rendon, T.; Forrest, L. R.; Hsiao, E. Y., Intestinal serotonin and fluoxetine exposure modulate bacterial colonization in the gut. *Nature* **2019,** *4* (12), 2064-2073.

50. Jumas-Bilak, E.; Carlier, J.-P.; Jean-Pierre, H.; Citron, D.; Bernard, K.; Damay, A.; Gay, B.; Teyssier, C.; Campos, J.; Marchandin, H., Jonquetella anthropi gen. nov., sp. nov., the first member of the candidate phylum 'Synergistetes' isolated from man. *Int. J. Syst. Evol. Microbiol.* **2007,** *57* (12), 2743-2748.

51. Horz, H.-P.; Citron, D. M.; Warren, Y. A.; Goldstein, E. J. C.; Conrads, G., Synergistes group organisms of human origin. *J. Clin. Microbiol.* **2006,** *44* (8), 2914-2920.

52. Vartoukian, S. R.; Palmer, R. M.; Wade, W. G., The division "Synergistes". *Anaerobe* **2007,** *13* (3), 99-106.

5.8. Experimental

Materials and Methods

All reagents were obtained from commercial vendors and used as received unless otherwise stated. *E. coli* NR was purchased from Sigma-Aldrich. NMR spectra were measured on Agilent 400 MHz or Bruker 500 MHz spectrometers. ^{1}H and ^{13}C NMR chemical shifts are reported in ppm relative to internal solvent resonances. Solvents were used as received unless otherwise noted. Yields refer to chromatographically and spectroscopically pure compounds unless otherwise stated. Thin-layer chromatography (TLC) was performed on glass-backed silica plates and visualized by UV unless otherwise stated. High-resolution mass spectra were taken on an Agilent Technologies 6230 TOF LC/MS mass spectrometer. LCMS experiments were performed on a Waters Acquity UPLC system equipped with a Kinetex EVO C18-functionalized silica column (C18 – 100 Å, 100 x 4.6 mm, H16-445733, 570-0069), diode array detector, and ESI mass spectrometer.

Cell studies were conducted on an adherent H9C2 line of rat embryonic cardiomyocytes (ATCC, Manassas, VA, USA). Cultures were grown in Dulbecco's Modified Eagle Medium (DMEM, VWR, Radnor, PA), supplemented with 10 % fetal bovine serum (FBS, VWR, Radnor, PA). Cells were cultured at 37 °C in 5 % CO_2-air. The cultures were passaged after 70–80 % confluence was achieved. Cells were rinsed with PBS solution, and then released with trypsin and EDTA solution (VWR, Radnor, PA). The suspension of released cells was centrifuged at 1000 rpm for 5 min.

All experiments were conducted in accordance with the NIH Guide for the Care and Use of Laboratory Animals and were conducted under the approval of the Virginia Tech Institutional Animal Care and Use Committee (IACUC; #19-134) and the Virginia-Maryland College of Veterinary Medicine.

Synthesis of 4-(nitrobenzyl) bromide (**1**)

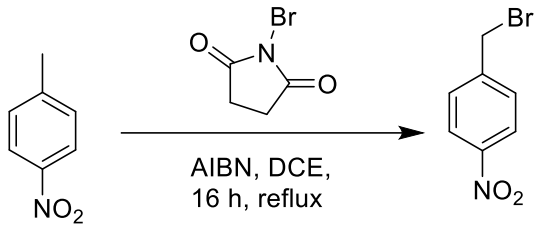

(1)

A flame-dried, 2-neck round bottom flask equipped with a septum and condenser was charged with 4-nitrotoluene (6.45 g, 47.0 mmol), dry 1,2-dichloroethane (150 mL), and *N*-bromosuccinimide (9.21 g, 51.7 mmol) under N_2 flow. The mixture was stirred until homogeneous, yielding a clear, light yellow solution. Azobisisobutyronitrile (AIBN) (0.386 g, 2.35 mmol) was added in one portion under N_2 flow, and the reaction mixture was degassed with N_2 for 30 minutes. The reaction was then heated to reflux under N_2 flow. Reaction progress was monitored by TLC (CH_2Cl_2) until starting material was consumed (~16 h). The reaction mixture was cooled to rt and washed successively with saturated $NaHCO_3$ (2 x 50 mL) and brine (50 mL). The organic layer was separated, dried over Na_2SO_4, and then concentrated via rotary evaporation to yield a brown, waxy solid. This crude product was then further purified via column chromatography, eluting with 1:1 CH_2Cl_2:hexanes. (Rf = 0.4, visualized with UV) The final product was isolated as white solid (8.90 g, 4.10 mmol, 82% yield). The product may also be recrystallized from boiling ethanol to reach higher purity. ^{1}H NMR ($CDCl_3$): δ 8.16 (d, 2H) 7.49 (d, 2H), 4.43 (s, 2H). ^{13}C NMR ($CDCl_3$): δ 169.2, 149.7, 138.4, 129.6, 34.9. These chemical shifts match literature precedence.[1]

Synthesis of 4-(nitrobenzyl) thiol (**2**)

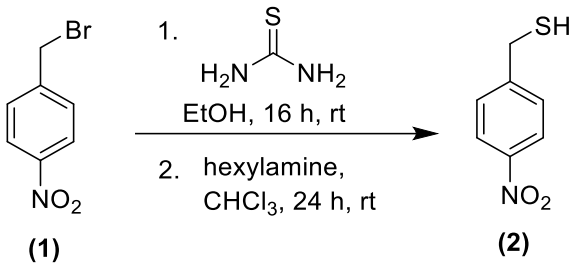

A two-neck round bottom flask equipped with a hose-barb adaptor and a septum was charged with compound **1** (4.00 g, 18.5 mmol), EtOH (50 mL), and a stirbar. The resulting suspension was bubbled with N_2 for 15 min. Thiourea (2.11 g, 27.8 mmol) was then added in one portion under N_2, and the reaction mixture was stirred at rt. The solids dissolved slowly over the course of several hours to give a clear, light orange solution. Reaction progress was monitored by TLC (CH_2Cl_2) until starting material was consumed (16 h). The reaction mixture was then concentrated via rotary evaporation, and the thiouronium intermediate was subsequently suspended in CH_2Cl_2 (100 mL) in the same two-neck round bottom flask. The suspension was degassed with N_2 for 30 min. Hexylamine (2.06 g, 2.7 mL, 20.4 mmol) was then injected. The resulting suspension slowly dissolved over the course of 4 h, yielding a bright yellow solution. After stirring for 24 h, this solution was washed with 1N HCl (50 mL) and brine (50 mL). The organic layer was separated and dried over Na_2SO_4, and concentrated via rotary evaporation to yield a viscous, yellow oil with a rancid smell. The product was then further purified by silica gel chromatography, eluting with 25% EtOAc:hexanes, yielding a white solid (2.6 g, 75% yield) ^{1}H NMR ($CDCl_3$): δ 8.15 (d, 2H) 7.50 (d, 2H), 3.82 (d, 2H), 1.84 (t, 1H). ^{13}C NMR ($CDCl_3$): δ 148.6, 129.1, 124.1, 28.5. These chemical shifts match literature precedence.[2]

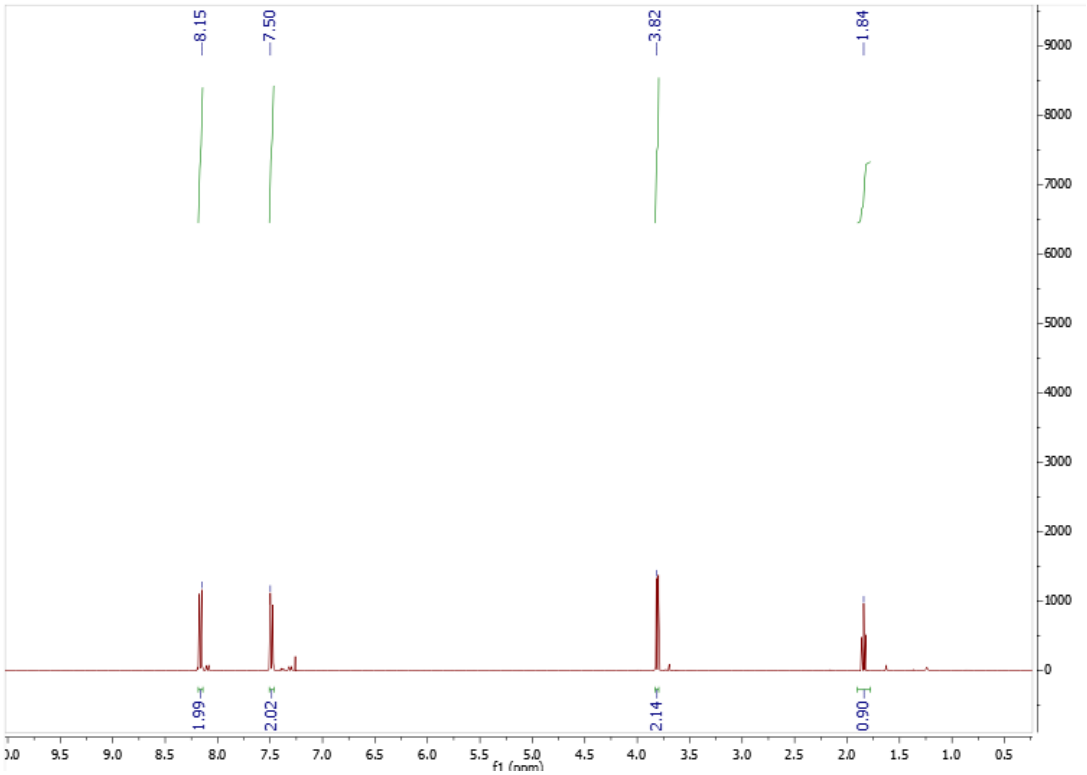

Figure S1. ^{1}H NMR spectrum of 4-(nitrobenzyl) thiol (2).

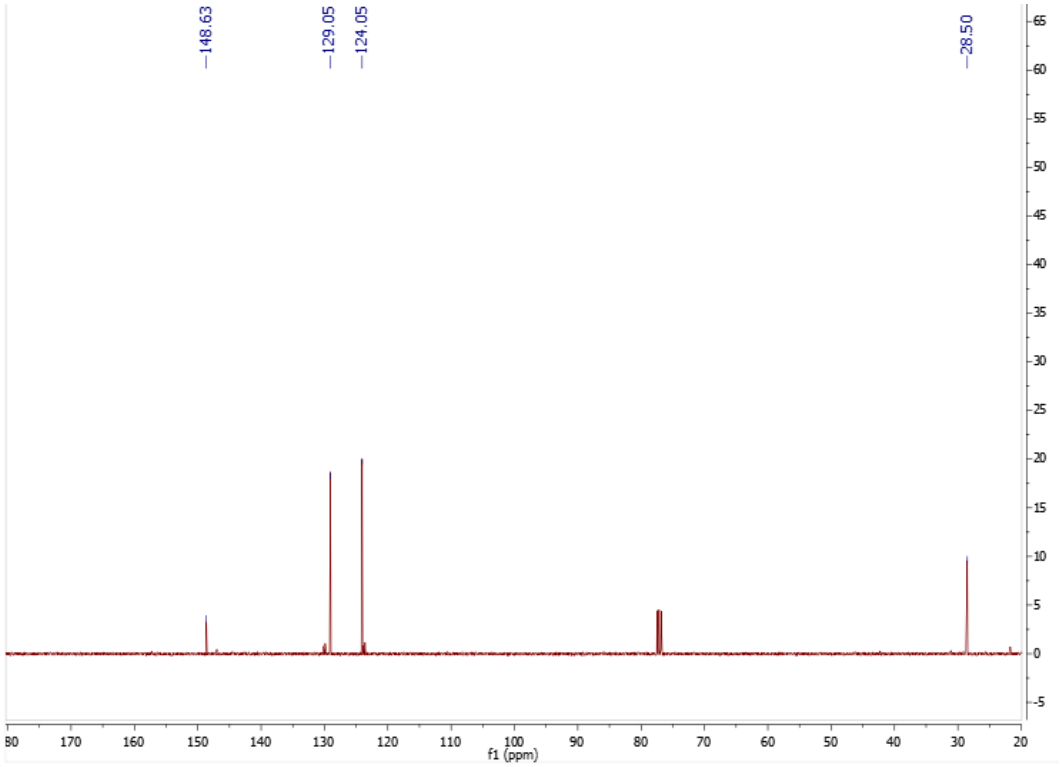

Figure S2. ^{13}C NMR spectrum of 4-(nitrobenzyl) thiol (2).

Synthesis of **NAC-pyDS**

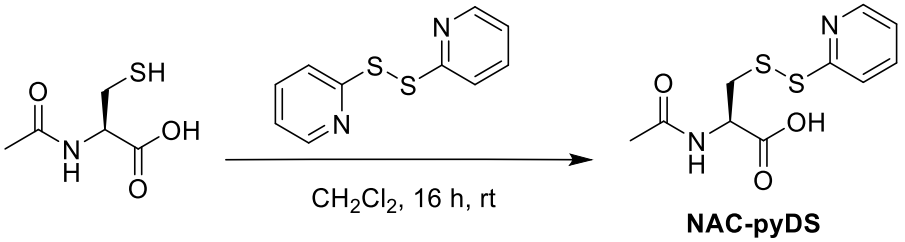

A round bottom flask was charged with *N*-acetylcysteine (7.0 g, 42.9 mmol), CH_2Cl_2 (200 mL), and a stirbar to give a suspension. 2,2'-Dipyridyl disulfide (18.9 g, 85.8 mmol) was added in one portion resulting in bright yellow suspension. The reaction mixture gradually dissolved over the course of several hours. The reaction mixture was stirred at rt (16 h), and reaction progress was monitored by TLC (EtOAc). The resulting yellow solution was concentrated via rotary evaporation, yielding a bright yellow solid. This crude product was then suspended in cold acetone, stirred for 30 min to dissolve any thiopyridone byproducts, and filtered, rinsing with copious amounts of cold acetone. This yielded a faintly yellow powder (8.4 g, 70% yield). ^{1}H NMR (DMSO-d_6): δ 12.97 (s, 1H), 8.46 (m, 1H), 8.42 (d, *J* = 7.89 Hz, 1H), 7.81 (m, 1H), 7.75 (m, 1H), 7.24 (m, 1H), 4.47 (m, 1H), 3.15 (m, 2H), 1.86 (s, 3H). ^{13}C NMR (DMSO-d_6): δ 171.88, 169.49, 158.77, 149.69, 137.86, 121.33, 119.34, 51.39, 39.93, 22.44. Spectroscopic data agree with literature precedence.[3]

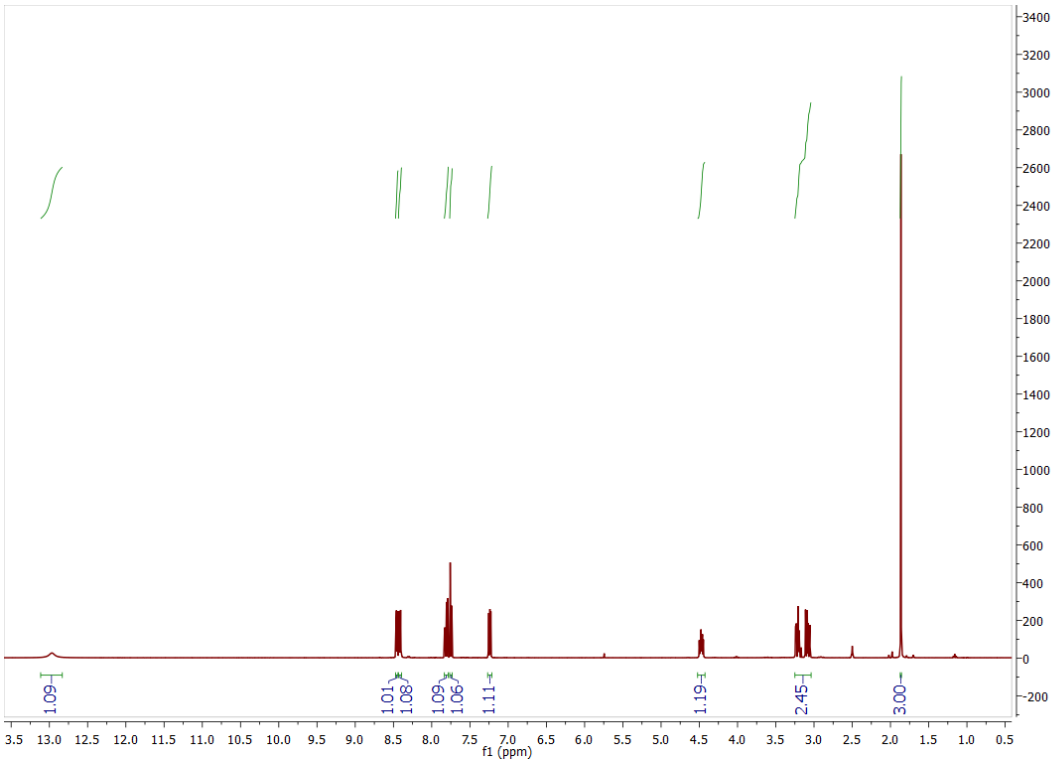

Figure S3. ^{1}H NMR spectrum of **NAC-pyDS**.

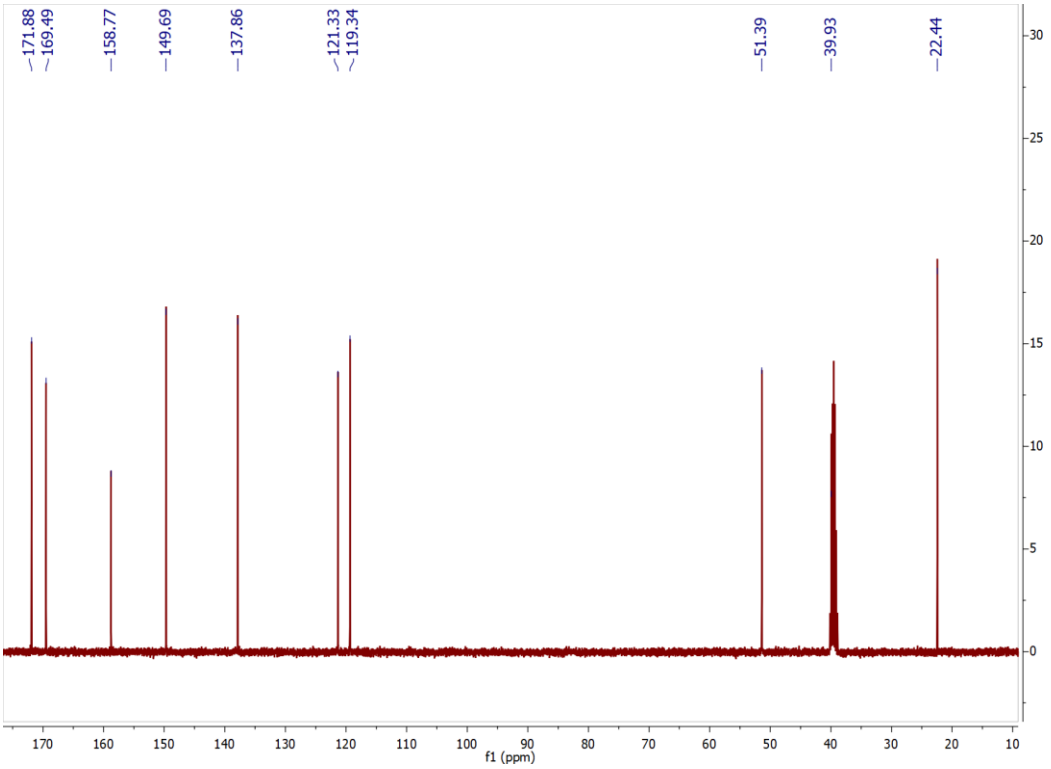

Figure S4. ^{13}C NMR spectrum of **NAC-pyDS**.

Synthesis of **NDP-NAC**

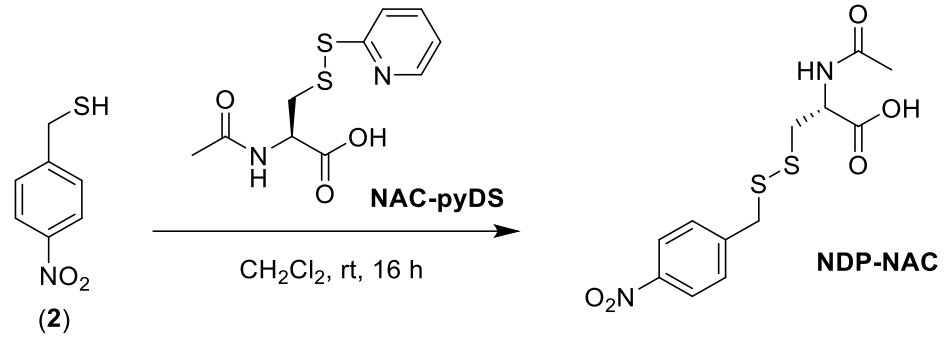

A roundbottom flask was charged with compound **2** (2.12 g, 12.5 mmol), CH_2Cl_2 (50 mL), **NAC-pyDS** (3.41 g, 12.5 mmol), and a stir bar, resulting in a light yellow suspension. The reaction mixture gradually became homogeneous, yielding a bright yellow solution over the course of 16 h. The reaction mixture was then filtered to remove some small particulates and placed in the freezer overnight. The solid that was formed was recovered by filtration and rinsed with cold CH_2Cl_2, resulting in airy, white crystals. (2.30 g, 56 % yield). ^{1}H NMR (DMSO-d_6) δ 8.29 (d, 1H), 8.20 (d, 2H) 7.61 (d, 2H), 4.44 (m, 1H), 4.11 (m, 2H), 2.92 (m, 1H) 2.75 (m, 1H), 1.85 (s, 3H). ^{13}C NMR (DMSO-d_6): δ 172.4, 169.9, 147.1, 146.4, 130.9, 124.0, 51.5, 40.9, 39.7, 22.8. HRMS (ESI-TOF) calcd. for $C_{12}H_{14}N_2O_5S_2$ $[M-H]^-$ 329.0266, found 329.0270.

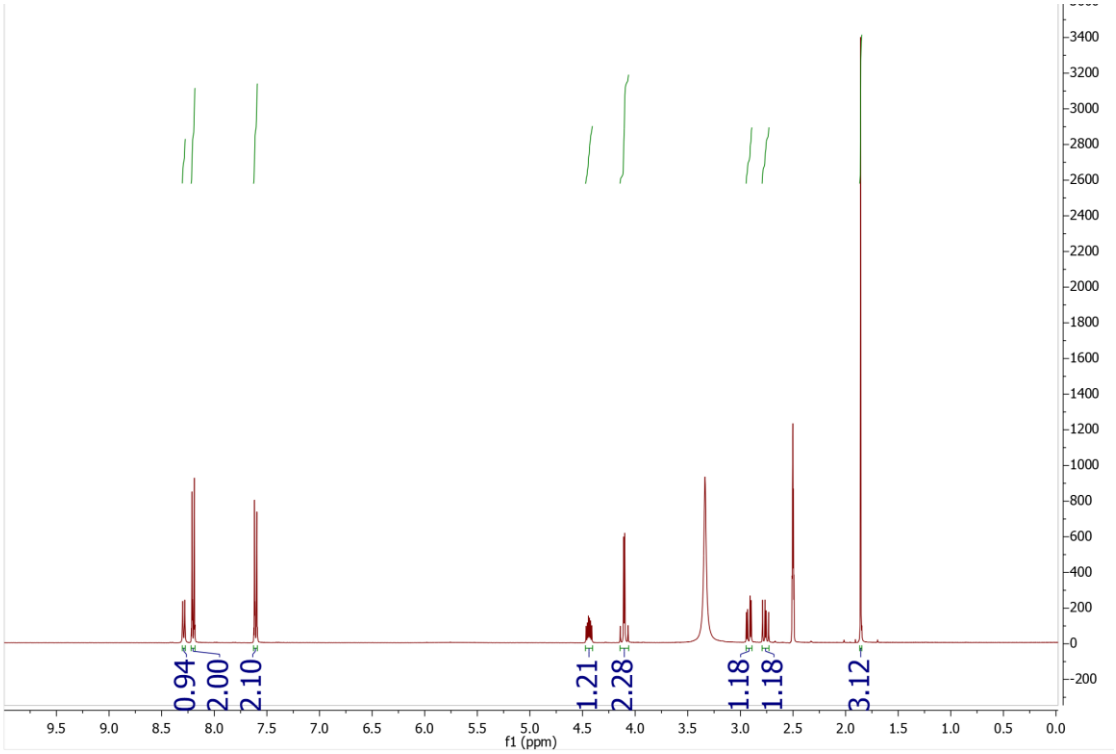

Figure S5. ^{1}H NMR spectrum of **NDP-NAC**.

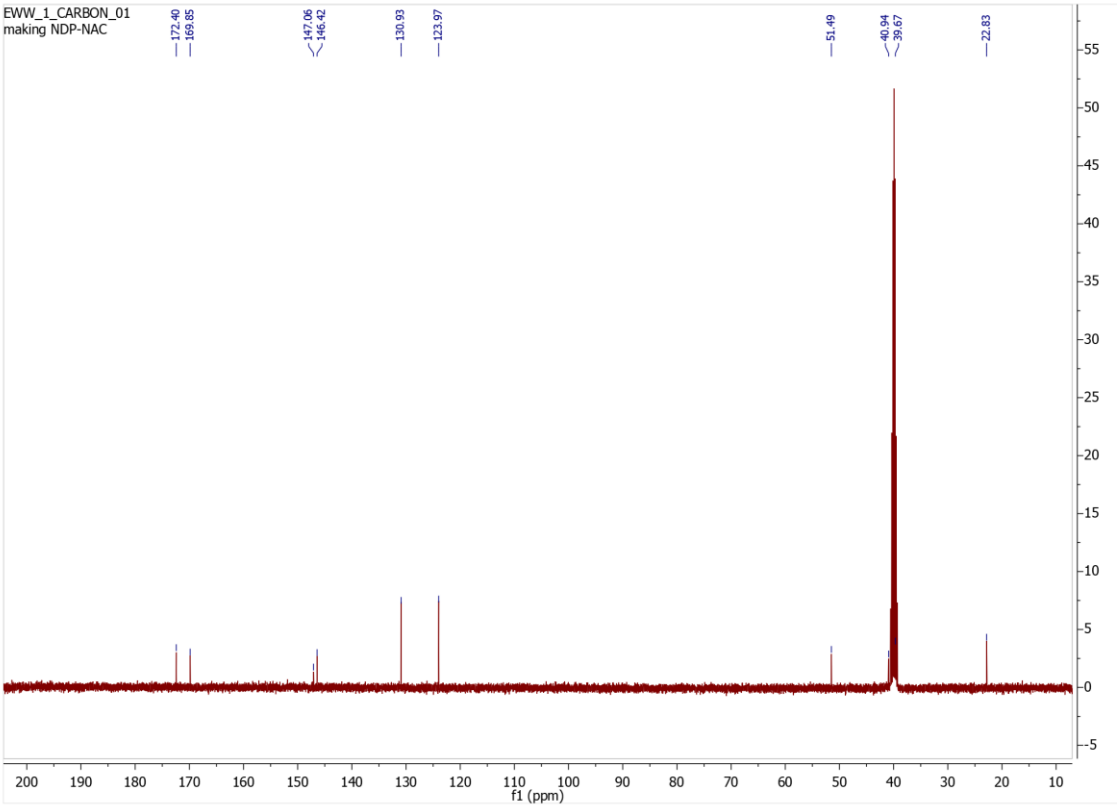

Figure S6. ^{13}C NMR spectrum of **NDP-NAC**.

Synthesis of 2,4-dinitrobenzene disulfide (DNBD)

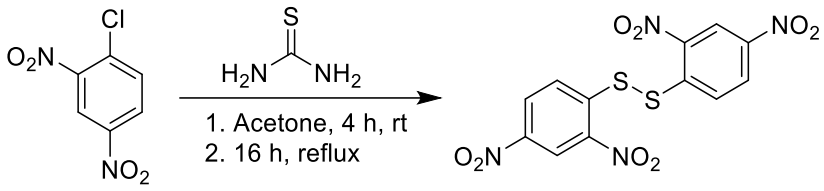

2,4-Chlorodinitrobenzene (5.00 g, 24.7 mmol) and thiourea (1.88 g, 24.7 mmol) were added to a round bottom flask charged with a stir bar. Acetone (50 mL) was added, and the reaction mixture was allowed to stir for 4 h. The resulting pale yellow solution was refluxed overnight for 16 hours, yielding a bright yellow precipitate. Acetone was removed via rotary evaporation, and the yellow solid was taken up in EtOH (absolute). This slurry was stirred vigorously for 15 minutes while heating to reflux, and then the crude product was recovered by hot filtration. The resulting yellow solid (4.20 g, 85 % yield) was used in the next step of synthesis without further purification. ^{1}H NMR (DMSO-d_6) δ 9.12 (s, 1H), 8.39 (d, J = 2.2 Hz, 1H) 7.60 (d, J = 2.2 Hz, 1H). ^{13}C NMR (DMSO-d_6) δ 148.7, 146.9, 137.5, 135.3, 128.1, 121.0.

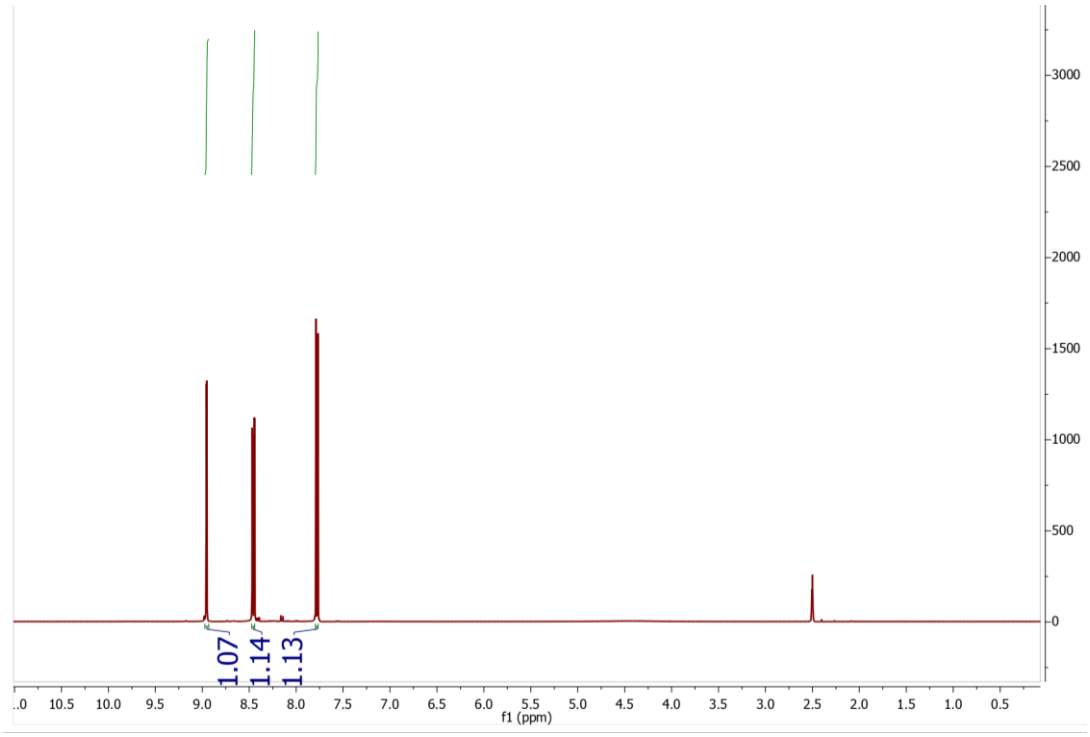

Figure S7. ^{1}H NMR spectrum of DNBD.

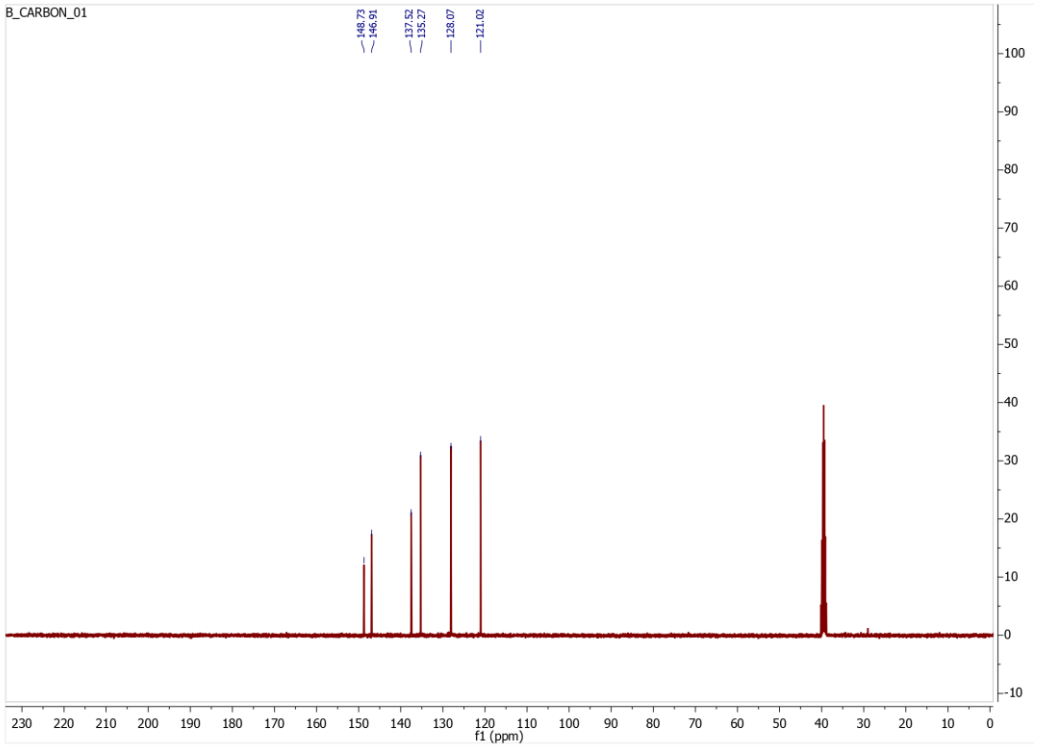

Figure S8. ^{13}C NMR spectrum of DNBD.

Synthesis of persulfide adduct DNB-NAC

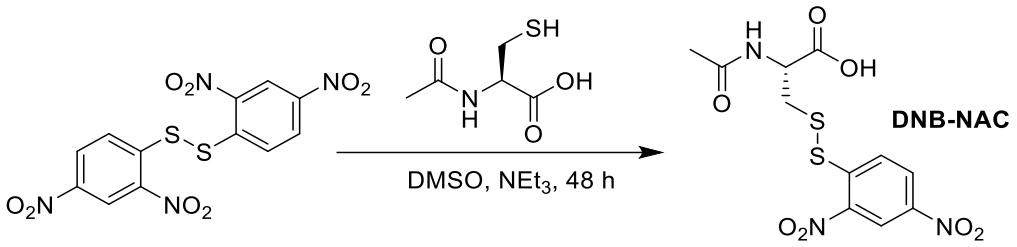

2,4-Dinitrobenzene disulfide (500 mg, 1.26 mmol) and NET_3 (0.37 mL, 2.64 mmol) were added to a two-neck round bottom flask charged with a stir bar. DMSO (8 mL) was then added, and the reaction mixture was degassed for 20 min. The reaction mixture was placed under nitrogen flow and stirred until homogeneous, resulting in a yellow solution. NAC (205 mg, 1.26 mmol) was then added under nitrogen flow, and the reaction vessel was sealed and stirred for two d, yielding a bright red solution. The solution was then concentrated, precipitated into CH_2Cl_2 (50 mL), and filtered. The resulting bright orange solid was then redissolved in a minimal amount of methanol (2 mL) and re-precipitated twice more from CH_2Cl_2. The resulting pale orange solid was dissolved in 50 mL 1:1 CH_3CN:H_2O and purified using reverse-phase preparation HPLC. HPLC was performed using an Agilent Technologies 1260 Infinity HPLC system (Agilent Technologies, Santa Clara, CA) equipped with a fraction collector. Separations were performed using an Agilent PLRP-S column (100 Å, 10 μm, 150 × 25 mm) monitoring at 220 nm. The compound was eluted using a solvent gradient of 2% CH_3CN in H_2O to 100% CH_3CN over 30 min, with 0.1% NH_4OH added to each mobile phase to aid in solubility. A 50 mg injection of crude product yielded 4 mg yield (8%) of a pale yellow powder. ^1H NMR (DMSO-d_6) δ 8.60 (s, 1H), 8.39 (d, 1H) 8.14 (d, 1H), 8.72 (d, 1H), 4.36 (m, 1H) 3.54 (d, 1H), 1.65 (s, 3H). HRMS (ESI-TOF) calcd. for $C_{11}H_{12}N_3O_7S_2$ $[M+H]^+$ 362.0096, found 362.0071

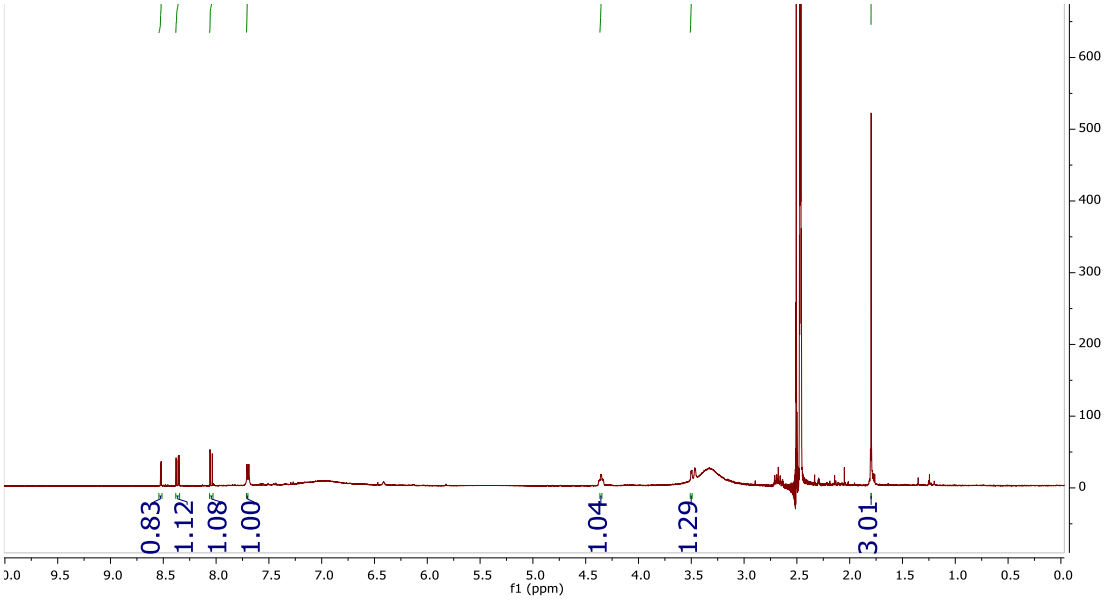

Figure S9. ^{1}H NMR spectrum of **DNB-NAC**.

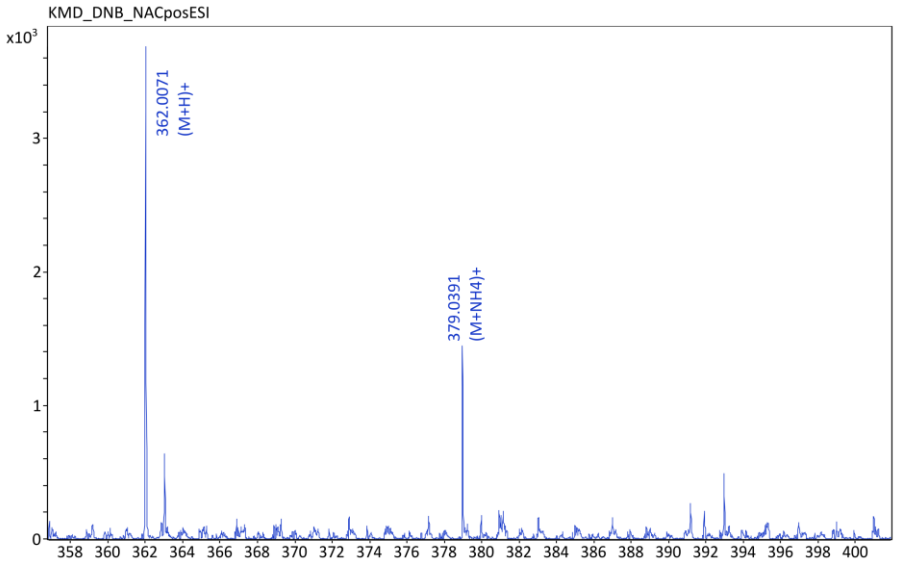

Figure S10. HRMS (ESI-TOF) calcd. For **DNB-NAC**. $C_{11}H_{12}N_3O_7S_2$ $[M+H]^+$ 362.0096, found 362.0071

Synthesis of NDP-NAC-thioether (**NDP-TE**)

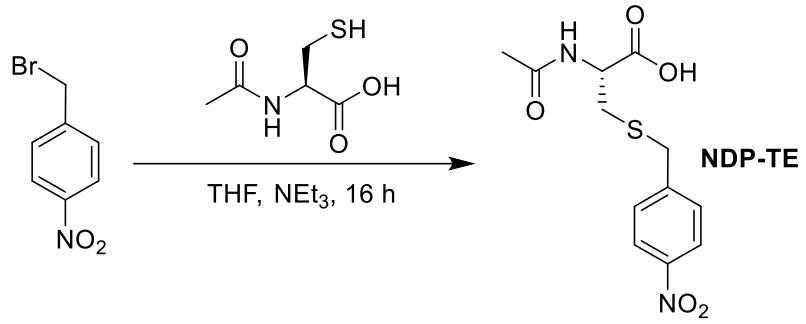

To a two-neck round bottom flask charged with a stirbar was added 4-(nitrobenzyl) bromide (1.00 g, 4.63 mmol) and NET_3 (0.97 mL, 6.94 mmol). THF (10 mL) was then added, and the reaction mixture was degassed for 20 min. The reaction mixture was placed under nitrogen flow and stirred until homogeneous, resulting in a yellow solution. **NAC** (906 mg, 5.55 mmol) was then added under nitrogen flow, and the reaction vessel was sealed and stirred for 16 h, yielding a suspension of white triethylamine salts. Reaction progress was monitored by TLC in CH_2Cl_2. The salts were filtered off, and the solvent was removed via rotary evaporation. The resulting off-white solid was then taken up in 1:1 CH_2Cl_2: EtOAc and purified via column chromatography using gradient elution from 1:1 CH_2Cl_2: EtOAc to 100% EtOAc. The product, a colorless, crystalline solid, was isolated in a 73% yield (1.00 g). ^{1}H NMR (DMSO-d_6) δ12.84 (s, 1H), 8.27 (d, *J* = 4.6 Hz, 1H), 8.19 (d, *J* = 2.1 Hz, 2H) 7.55 (d, *J* = 2.1 Hz, 2H), 4.38 (m, 1H), 3.88 (s, 2H), 2.78 (m, 1H), 2.66 (m, 1H), 1.87 (s, 3H). ^{13}C NMR (DMSO-d_6) δ172.11, 169.37, 146.8, 146.43, 130.12, 123.59, 51.65, 34.62, 32.44, 22.37. HRMS (ESI-TOF) calcd. for $C_{12}H_{15}N_2O_5S_1$ $[M+H]^+$ 299.0701, found 299.0704.

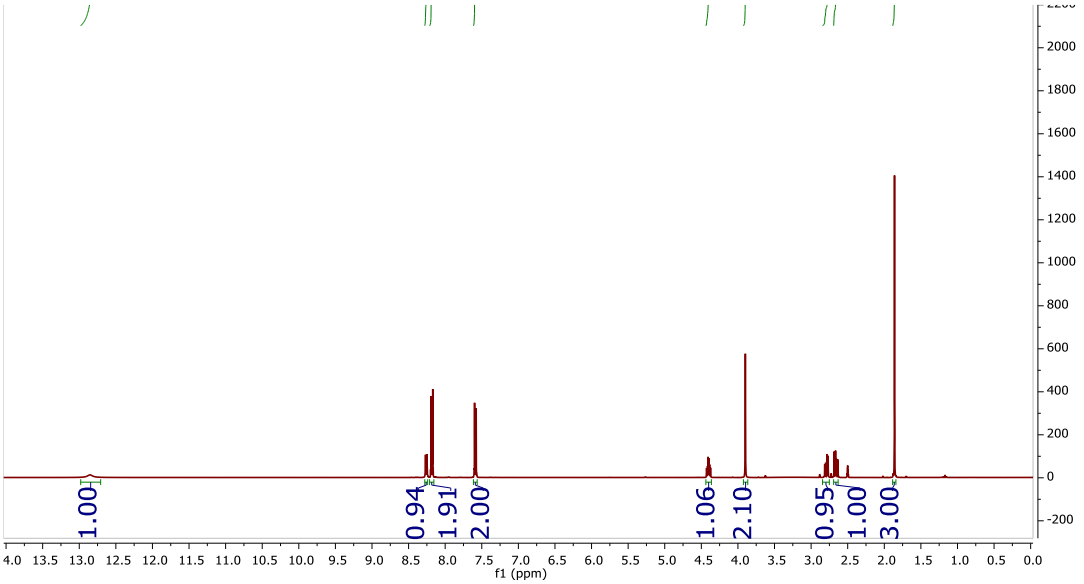

Figure S11. ^{1}H NMR spectrum of **NDP-TE**

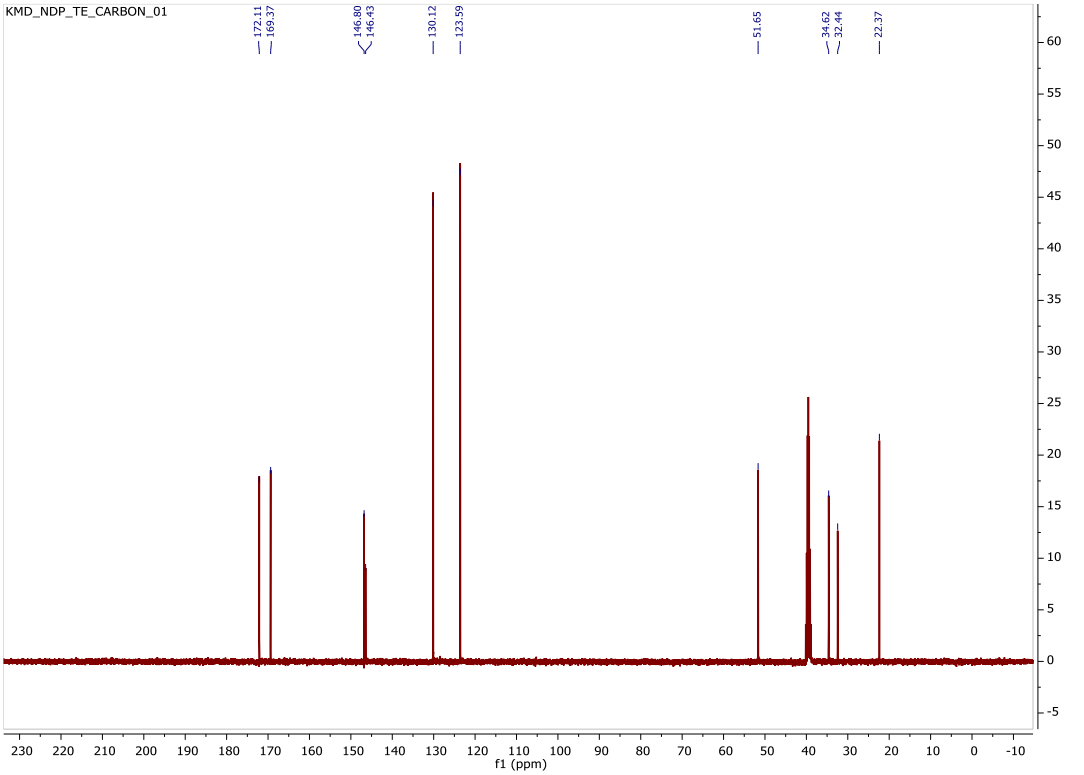

Figure S12. ^{13}C NMR spectrum of **NDP-TE**

Synthesis of benzyl-NAC disulfide (**Benz-NAC**)

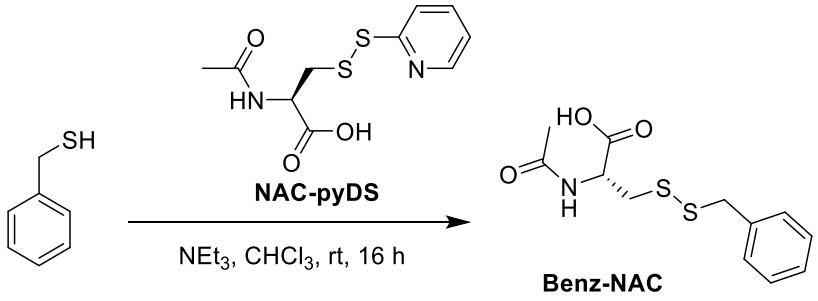

A single neck round bottom flask was charged with **NAC-pyDS** (0.7 g, 2.4 mmol) and $CHCl_3$ (5 mL) to form a suspension. Benzyl mercaptan (0.26 mL, 2.0 mmol) and NET_3 (0.42 mL, 3.0 mmol) were added sequentially via syringe. The reaction mixture was stirred for 4 h at rt, monitoring reaction progress by TLC (25 % EtOAc in hexanes, UV visualization). Once complete conversion was observed, the reaction mixture was diluted with $CHCl_3$ (10 mL), washed successively with 1 N HCl (2 x 10 mL) and brine (10 mL), dried over Na_2SO_4, and concentrated by rotary evaporation. The resulting yellow powder was purified by silica gel chromatography eluting with a gradient of 0% to 15 % MeOH in CH_2Cl_2, yielding an off-white solid (0.356 g, 62 % yield). ^{1}H NMR (DMSO-d_6): δ 12.94 (s, 1H), 8.30 (d, *J* = 4.7, 1H), 7.37-7.23 (m, 5H), 4.46 (m, 1H), 3.97 (m, 2H), 2.99-2.71 (m, 2H), 1.86 (s, 3H). ^{13}C NMR (DMSO-d_6): δ 172.10, 169.39, 137.37, 129.30, 128.44, 127.31, 51.25, 41.92, 39.45, 22.45. HRMS (ESI-TOF) calcd. for $C_{12}H_{16}NO_3S_2$ $[M+H]^+$ 286.0571, found 286.0567. Calcd. for $C_{12}H_{15}NNaO_3S_2$ $[M+Na]^+$ 309.0414, found 309.0419.

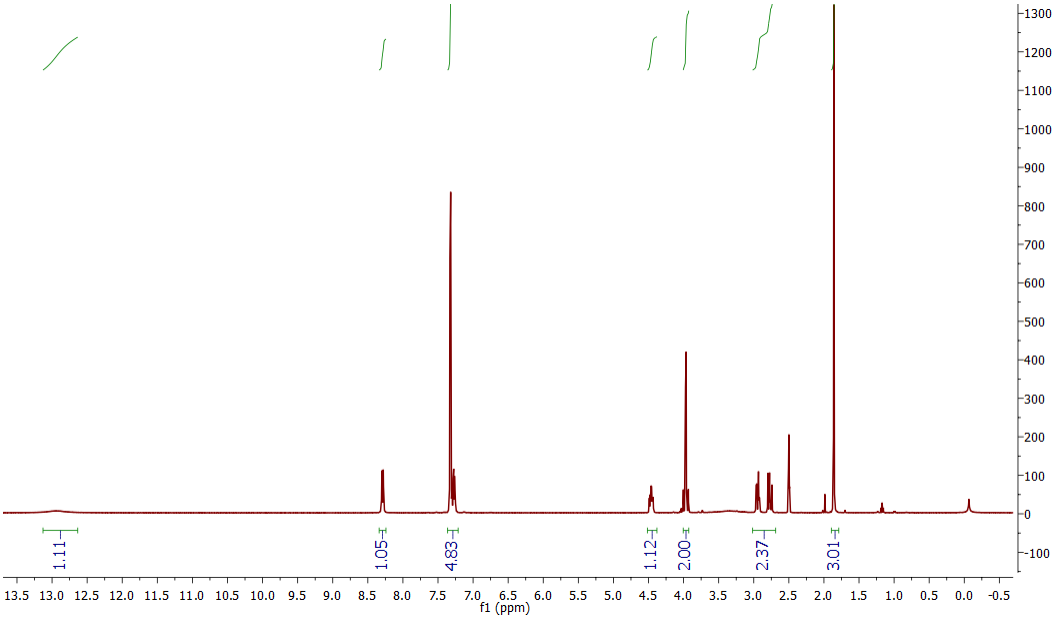

Figure S13. ^{1}H NMR spectrum of **Benz-NAC**

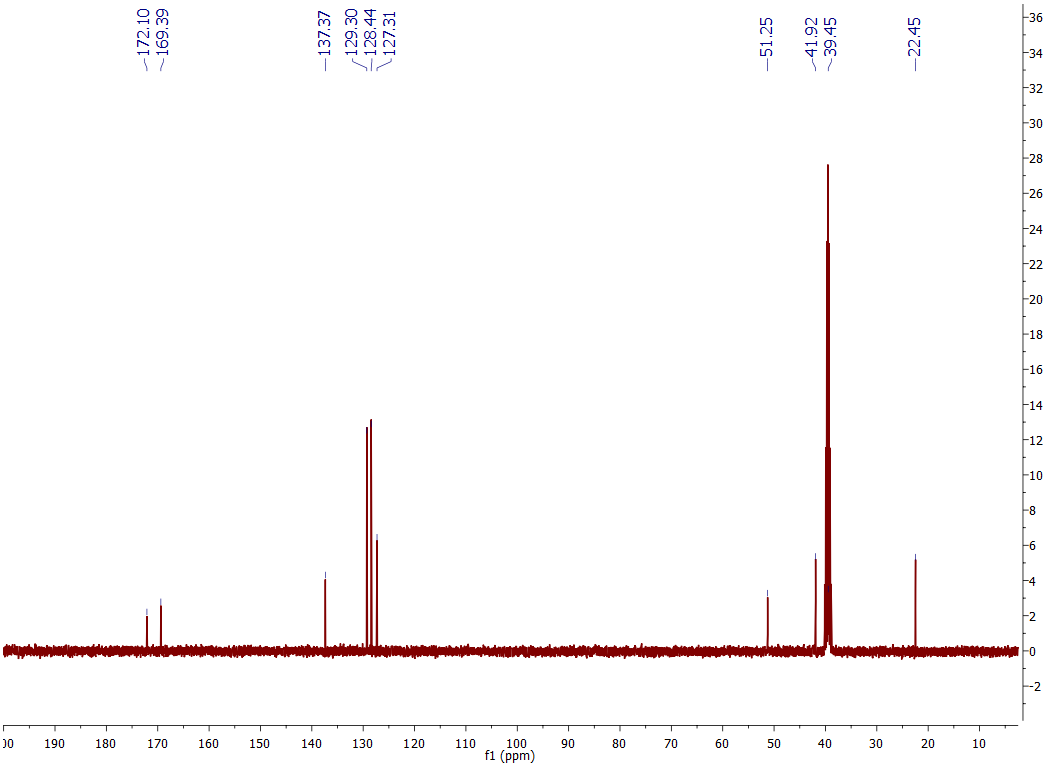

Figure S14. ^{13}C NMR spectrum of **Benz-NAC**

Persulfide Trapping:

Analysis of persulfide release by LCMS was carried out as follows: A one-dram vial was charged with a solution of NDP-NAC (100 µL; 1 mM in HPLC grade CH_3CN), NADH (100 µL, 5 mM in LCMS H_2O), 2,4 -dinitrofluorobenzene (DNFB, 100 µL, 5 mM in HPLC CH_3CN) and diluted with 1X pH 8.0 PBS (made with LCMS H_2O, 0.7 mL) to give a clear, colorless solution. An aliquot (50 µL) was removed and diluted into CH_3CN (0.95 mL) in a vial equipped with a screw cap lid with a rubber septum. After removal of an aliquot to serve as the t=0 timepoint, nitroreductase (10 µL, 1 mg/mL stock) was added to the reaction mixture. The vial was shaken thoroughly, and after 1 min the first aliquot was removed and diluted with CH_3CN (1 mL). This process was repeated every 30 min for 2 h. The aliquots were then cooled in a dry ice/acetone bath until cloudy (~1 min) and centrifuged for 5 min at 2000 rpm. The supernatant was decanted into vials and the (small) pellet that formed (most likely charged impurities, NADH/NAD^+) was discarded. The samples were then analyzed by LCMS as follows: 20 µL injection volume eluting 5 to 95% CH_3CN in water with 10 mM trifluoroacetic acid (TFA) in each mobile phase over the course of 10 min, holding at 95% CH_3CN for 2 min, and then ramping down from 95 to 5% CH_3CN in water over 2 min. This chromatographic cycle was followed by a 5-min column equilibration in 5 % CH_3CN in water. Experiments were run at room temperature (22 °C). The UV detector readout was set to 282 nm. As shown in Figure S11, the peak eluting at 4.0 minutes (NDP-NAC) declines in intensity after addition of nitroreductase. The peak at 6.1 minutes matches the elution time of DNB-NAC under the same LCMS conditions. For these experiments, the pH level during the reaction was 7.8. We did not observe DNFB reduction by *E. coli* nitroreductase under these conditions.

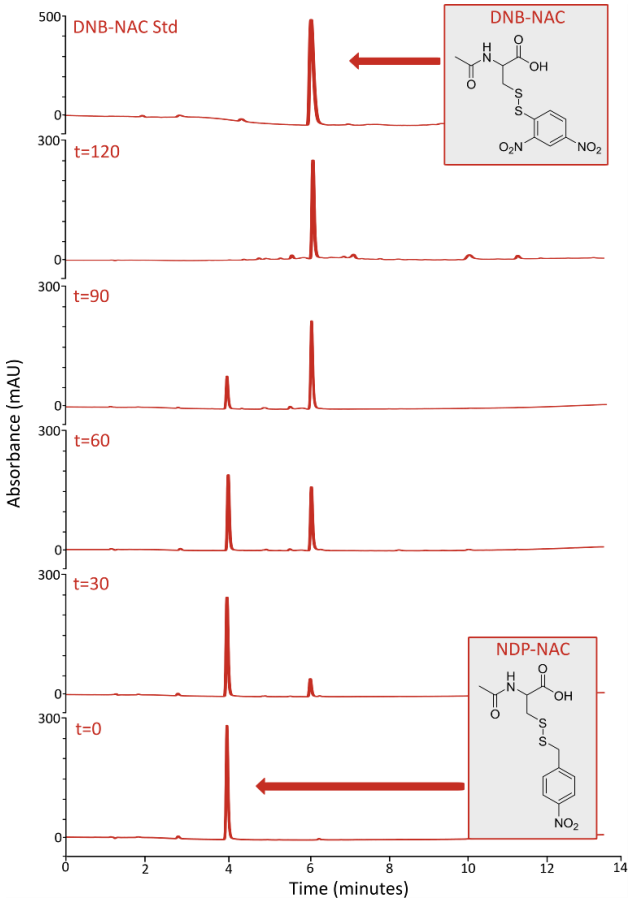

Figure S15. Chromatogram series depicting persulfide trapping from NDP-NAC in response to nitroreductase. The peak eluting at 4.0 minutes corresponds to NDP-NAC, whereas the peak that increases in intensity over time (6.1 minutes) corresponds to the persulfide adduct DNB-NAC standard.

<u>^{1}H NMR *p*-ABA Release Kinetics:</u>

NDP-NAC (1.0 mg) and NADH (5 equiv) were dissolved in 200 µL DMSO-d_6. pD 8.0 dPB (733 µL) was added, and a first ^{1}H NMR time point was collected. Nitroreductase (20 µg dissolved in 67 µL pD 8.0 dPB) was then added, the NMR tube was capped, and subsequent ^{1}H NMR scans

were performed at intervals described in Figure 2. Experiments were conducted at room temperature (22 °C) and the pD level during the reaction was pD = 8.1.

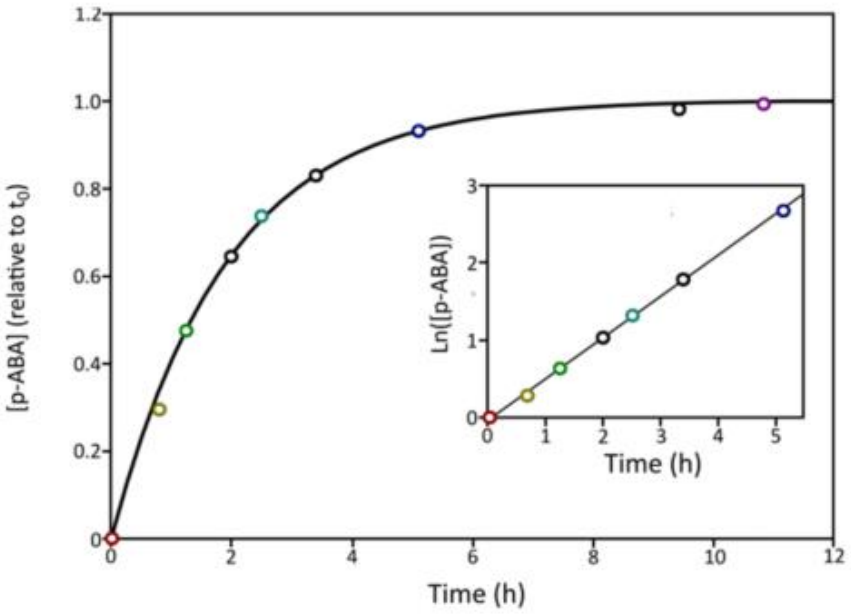

Figure S16. Pseudo-first order plot of ^{1}H NMR release kinetics depicting pABA release from NDP-NAC.

<u>Thiol-disulfide exchange control experiments:</u>

NDP-NAC (2 mg/mL) and Cys (2 eq) were dissolved in 1:4 DMSO-d_6:pD 8.0 dPB or 1:4 DMSO-d_6:pD 2.5 dPB. Under both mildly basic and strongly acidic conditions, no substantial changes to the ^{1}H NMR spectra were observed after 24 h at rt. However, Cys oxidation to cystine was observed.

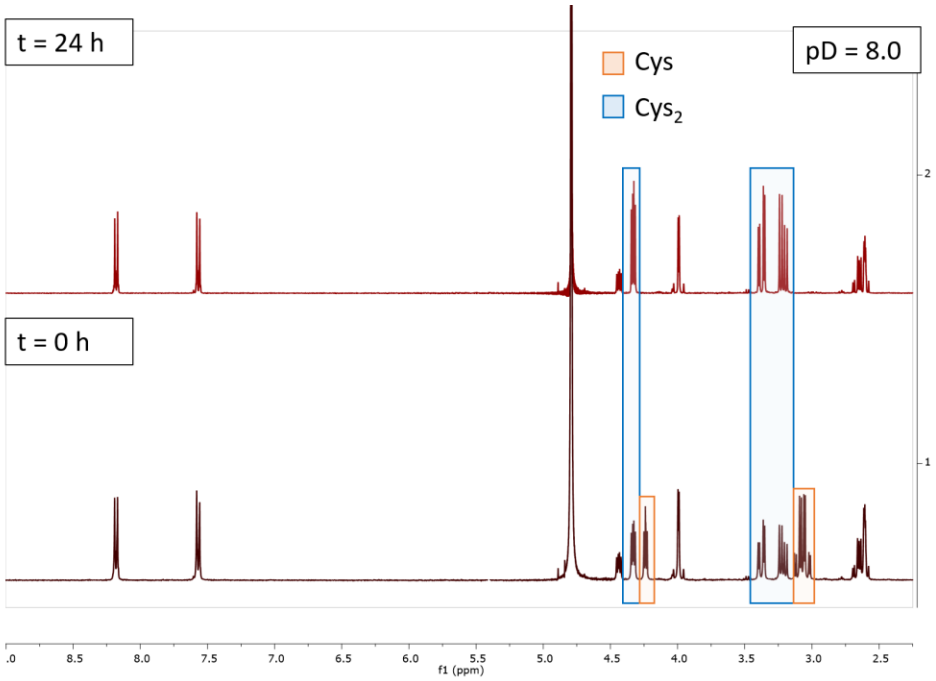

Figure S17. Thiol-disulfide exchange control experiment utilizing NDP-NAC and Cys at pD 8.0. No change in signals attributed to NDP-NAC (not boxed) were observed, although oxidation of Cys to cystine (Cys_2) was noted (boxed peaks).

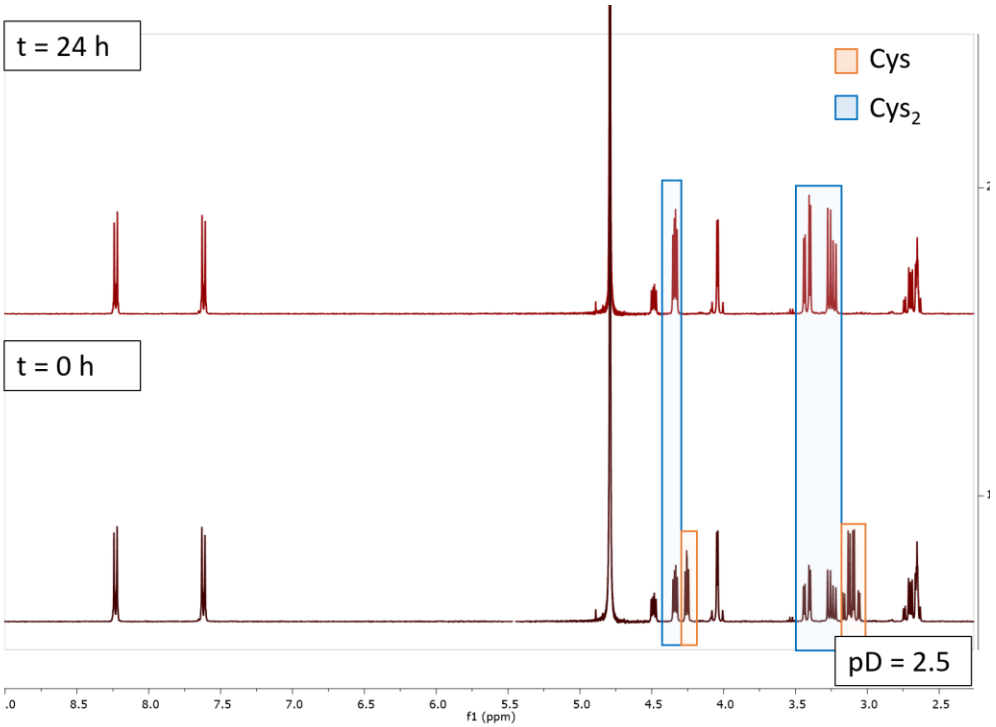

Figure S18. Thiol-disulfide exchange control experiment utilizing NDP-NAC and Cys at pD 2.5. No change in signals attributed to NDP-NAC (not boxed) were observed, although oxidation of Cys to cystine (Cys_2) was noted (boxed peaks).

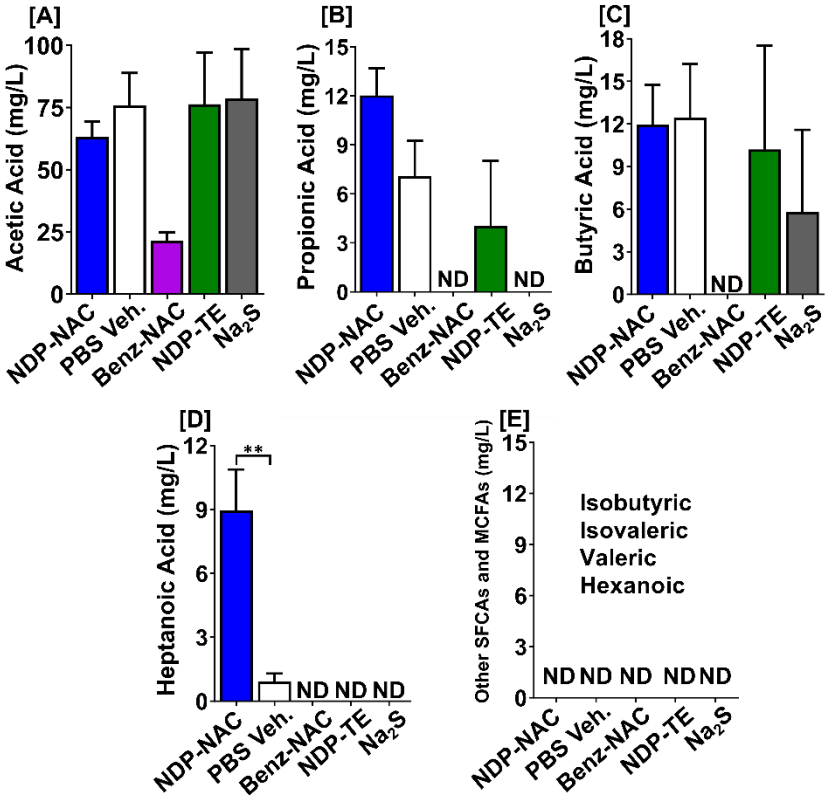

Figure S19. Short and medium chain fatty acid profiles (SCFA and MCFA) of mouse excrement after daily treatment with NDP-NAC or indicated control. ** designates $p < 0.01$ for comparisons between treatment groups indicated with brackets. Isobutyric, isovaleric, valeric, and hexanoic acid concentrations were below the level of detection, which is typical for these types of experiments. ND = not detected (below limit of detection, LOD). Acetic acid LOD = 2 mg/mL, LOD = 1 mg/mL for all other SCFA/MCFAs. Statistical analysis was performed using ANOVA with Tukey's *post-hoc* test.

H9C2 Cell Viability Assays:

For eukaryote experiments, H9C2 cells were plated at a density of 5000 cells per well in a volume of 180 μL serum-containing media per well in a 96-well plate and cultured for 24 h before

treatment. Cell viability data was analyzed using a BioTek Synergy Mx plate reader (BioTek, Winooski, VT). Cell viability assays were performed by using Cell counting kit 8 (CCK-8, Dojindo, Rockville, Md.). H9C2 cardiomyocytes in a 96-well plate (n = 5 for each group) were treated with various concentrations of NDP-NAC and allowed to age 4 h in serum-containing media. After incubation with NDP-NAC or controls for an additional 4 h, the cells were then washed with 1X PBS buffer three times. After washing, fresh DMEM (100 μL) without FBS and 10 v/v % CCK-8 solution was added, and the cells were incubated for 3 h. Absorbance was recorded then at 450 and 750 nm.

Bacterial Cell Viability Assays:

Escherichia coli, Listeria monocytogenes, and Staphylococcus aureus were acquired and validated from the American Type Culture Collection and cultured following standard procedures defined by the vendor. Sub-cultures were streaked on nutrient agar containing either 0, 1, 10, or 100 μg/ml of NDP-NAC. Percent viability was determined by colony forming unit assessments.

Ultra High Performance Liquid Chromatography with Tandem Mass Spectrometry (UPLC-MS/MS) analysis of NDP-NAC in mouse plasma

Mouse plasma samples were run at the VA-MD College of Veterinary Medicine Analytical Research Laboratory by McAlister Council-Troche. Plasma concentrations of NDP-NAC and *p*-aminobenzyl alcohol (pABA) were determined by UPLC-MS/MS after protein precipitation with 5% (v/v) formic acid (FA) in CH_3CN.

NDP-NAC, pABA, and NAC-pyDS were used as reference standards, with NAC-pyDS being used as the internal standard (IS). Stock solutions of both compounds were initially made up in CH_3CN and then separately diluted in CH_3CN to their final standard concentrations.

Plasma samples were prepared by combining 100 µL of plasma, 20 µL of NAC-pyDS (200 ng/mL in CH_3CN), and 300 µL of CH_3CN with 5% FA in 0.6 mL microcentrifuge tubes. The protein-precipitated samples were briefly shaken and then vortexed for 30 sec before being centrifuged (Eppendorf Microcentrifuge Model 5415R) at 16,100 g for 10 min. The resulting supernatant solutions were then transferred to fresh 4 mL glass vials and dried under nitrogen at 40 °C. The dried samples were then reconstituted in 200 µL of 10/90/1 CH_3CN/H_2O/FA, and then vortexed for 5 min to completely dissolve the sample residue. The reconstituted samples were then transferred to fresh 0.6 mL microcentrifuge tubes and centrifuged for another 10 min at 16,100 g. The supernatants were then transferred to 2 mL amber vials with low volume inserts before being placed in the refrigerated autosampler of the UPLC-MS/MS for analysis.

Sample extracts were subjected to chromatographic separation performed on a Waters H-Class UPLC system with a Phenyl column (Waters Acquity UPLC BEH Phenyl, 100 mm length x 2.1 mm ID x 1.7 µm) and matching guard column (Waters Acquity UPLC BEH Phenyl VanGuard Pre-Column, 5 mm length x 2.1 mm ID x 1.7 µm) maintained at 40 °C. 5 µL sample was injected onto the column using a refrigerated autosampler maintained at 8 °C. Mobile phase A consisted of 1% (v/v) FA in H_2O, and mobile phase B consisted of 1% (v/v) FA in CH_3CN. The mobile phase was delivered to the UPLC column at a flow rate of 0.4 mL/min. The gradient elution is shown below in Table S1.

Time (min)	%A (1%FA in H_2O)	%B (1%FA in CH_3CN)
0.00	98	2
0.25	98	2
3.25	2	98
3.75	2	98
3.76	98	2
5.75	98	2

Table S1. UPLC gradient method used for the chromatographic separation of NDP-NAC, pAB, and NAC-pyDS.

In order to keep the MS clean, the divert valve was used to transfer the column effluent to the MS from 0.5 to 3.75 min. From 0 to 0.5 and 3.75 to 6.0 minutes, all the column effluent was transferred to waste. The retention times of pABA, NDP-pyDS, and NDP-NAC were approximately 0.75, 3.17, and 3.18 minutes, respectively. The UPLC column effluent was pumped directly without any split into a triple-quadrupole mass spectrometer (Waters Xevo TQD) equipped with a Z Spray ionization source which was operated in positive-ion electrospray mode (ESI+) using multiple reaction monitoring (MRM). The parent and product ion transitions for the compounds of interest are shown in Table S2.

Analyte	Parent Ion (amu)	Product Ion (amu)	Cone Energy (V)	Collision Energy (eV)	Quant/Qual Transition
pABA	124.0 $[M+H]^+$	94.0	36	14	Quantifier
	124.0 $[M+H]^+$	89.0	36	20	Qualifier 1
	124.0 $[M+H]^+$	77.0	36	22	Qualifier 2

NDP-NAC	331.1 $[M+H]^+$	162.0	22	12	Quantifier
	331.1 $[M+H]^+$	116.0	22	30	Qualifier 1
	331.1 $[M+H]^+$	199.9	22	22	Qualifier 2
NAC-pyDS (IS)	286.0 $[M+H]^+$	162.1	20	10	Quantifier
	286.0 $[M+H]^+$	91.0	20	38	Qualifier 1
	286.0 $[M+H]^+$	116.0	20	32	Qualifier 2

Table S2. MRM transitions and specific mass spectrometry tuning parameters for the quantification of pAB and NDP-NAC.

Commercial software (MassLynx) was used to analyze the data. Tuning was performed on each analyte by direct infusion of standard solution (0.1 ng/µL) at a rate of 10 µL/min. Mass spectrometer parameters used for the detection of pABA, NDP-NAC, and NAC-pyDS are shown in Table S3.

Parameter	**Value**
Capillary (kV)	3.40
Cone (V)	20
RF (V)	2.50
Extractor (V)	3.00
Source Temperature (°C)	150
Desolvation Temperature (°C)	600
Cone Gas Flow (L/Hr)	10
Desolvation Gas Flow (L/Hr)	1000

Table S3. Mass spectrometer tuning parameters for the detection of pABA, NDP-NAC, and NAC-pyDS.

A six-point calibration curve made up in blank mouse plasma was prepared in the same manner as the samples but was spiked with a range of approximately 2 to 95 ng/mL plasma for both pABA and NDP-NAC.

A linear calibration curve was constructed for both compounds of interest using the MassLynx software to determine analyte concentration in samples based on the sample/IS ratio. The coefficient of determination (R^2) for all curves was >0.99, and all standard values were within ±10% of the expected range. *The system had a limit of detection (LOD) of approximately 0.06 ng NDP-NAC/mL plasma and approximately 0.1 ng* p*ABA/mL plasma, as determined by the signal-to-noise ratio, and the limit of quantification (LOQ), determined by the lowest concentration on a linear regression line of the calibration curve, was 2 ng/mL plasma for both analytes*. The calibration curves used in the NDP-NAC and pABA analyses are shown in Figures S14 and S15, respectively. **Neither NDP-NAC nor *p*ABA were detected in any of the six mouse plasma samples that were tested.**

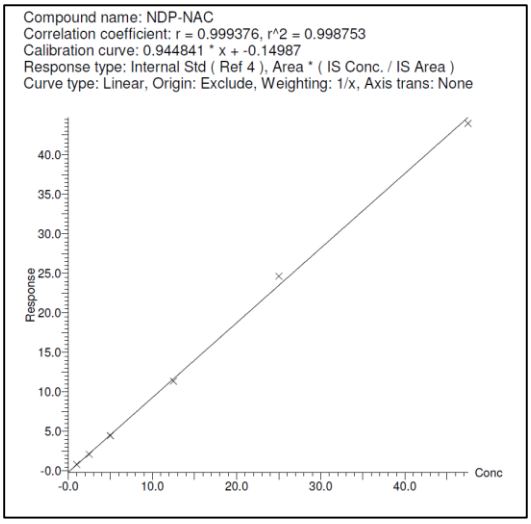

Figure S20. Linear calibration curve used in the analysis of NDP-NAC in mouse plasma. It should be noted that the concentration range on the x-axis is in ng NDP-NAC / mL solution. This is easily converted to plasma concentrations by multiplying by the reconstitution volume (0.2 mL) and dividing by the plasma volume (0.1 mL).

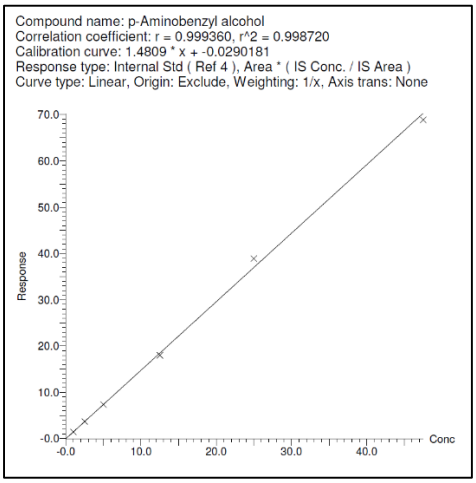

Figure S21. Linear calibration curve used in the analysis of pABA in mouse plasma. It should be noted that the concentration range on the x-axis is in ng pABA/mL solution. This is easily converted to plasma concentrations by multiplying by the reconstitution volume (0.2 mL) and dividing by the plasma volume (0.1 mL).

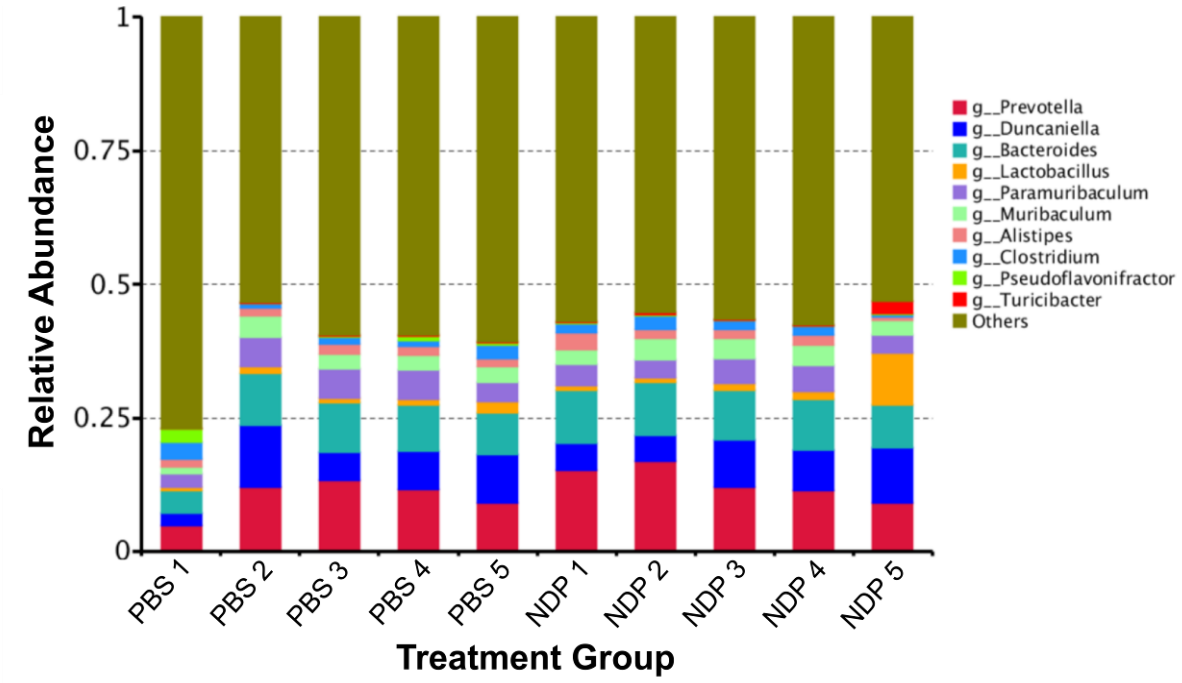

Figure S22. Stacked bar graph depicting overall bacterial populations after treatment with NDP-NAC/vehicle controls and collection and processing of feces. No significant difference in general populations was observed.

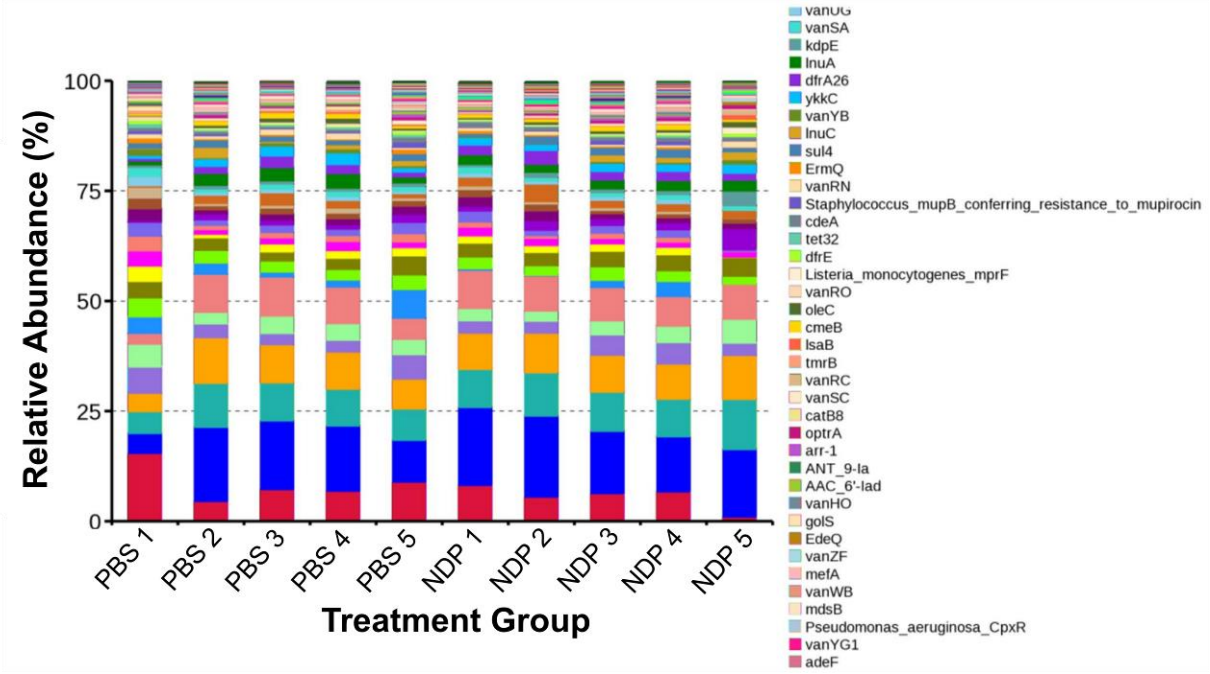

Figure S23. Stacked bar graph showcasing differences in genes associated with antibiotic resistance (ARG) after treatment with NDP-NAC/vehicle controls and collection and processing of feces. No significant difference in ARG observed.

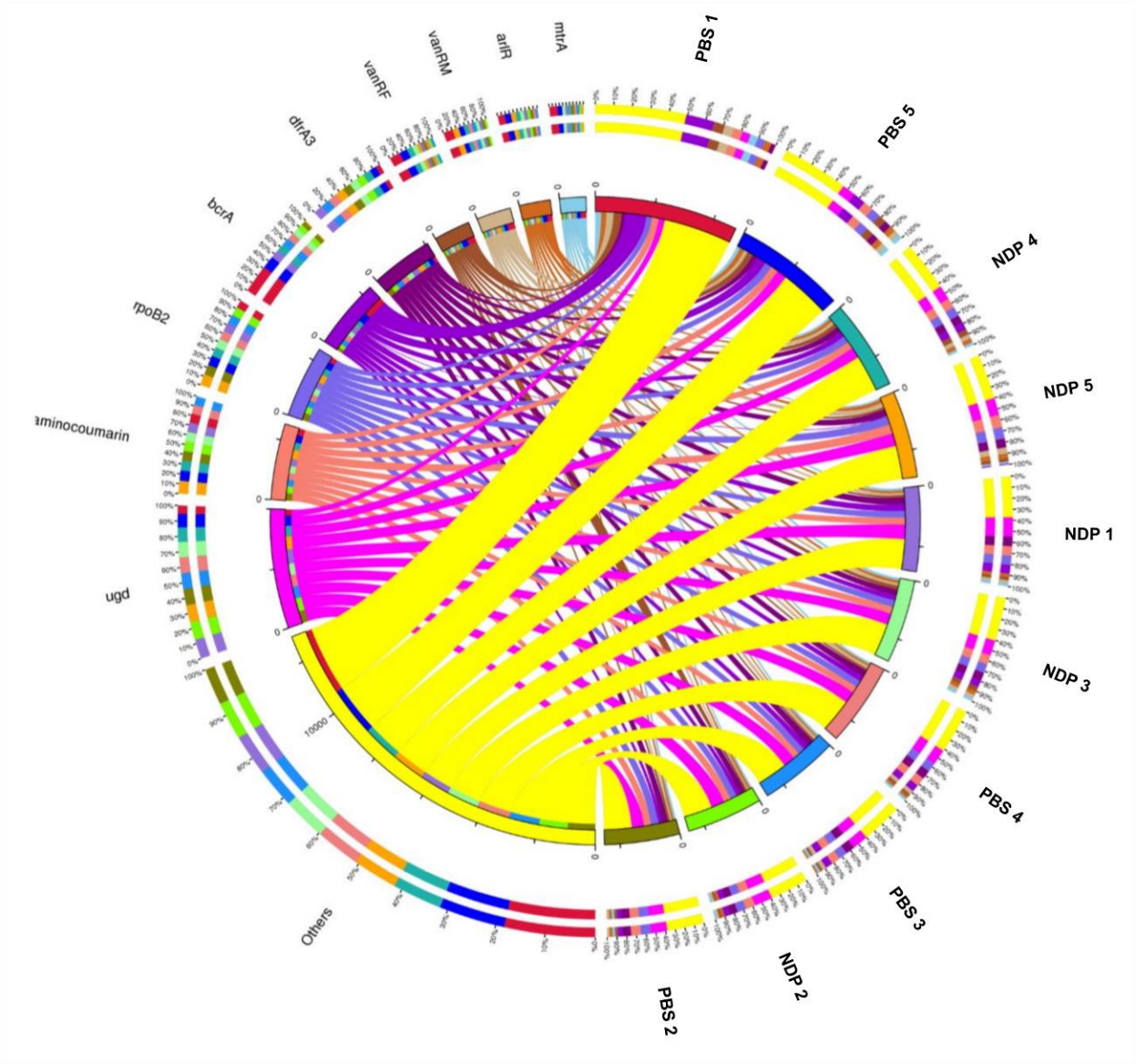

Figure S24. Circle plot showcasing differences in genes associated with antibiotic resistance after treatment with NDP-NAC/vehicle controls and collection and processing of feces. No significant differences in number of ARG observed.

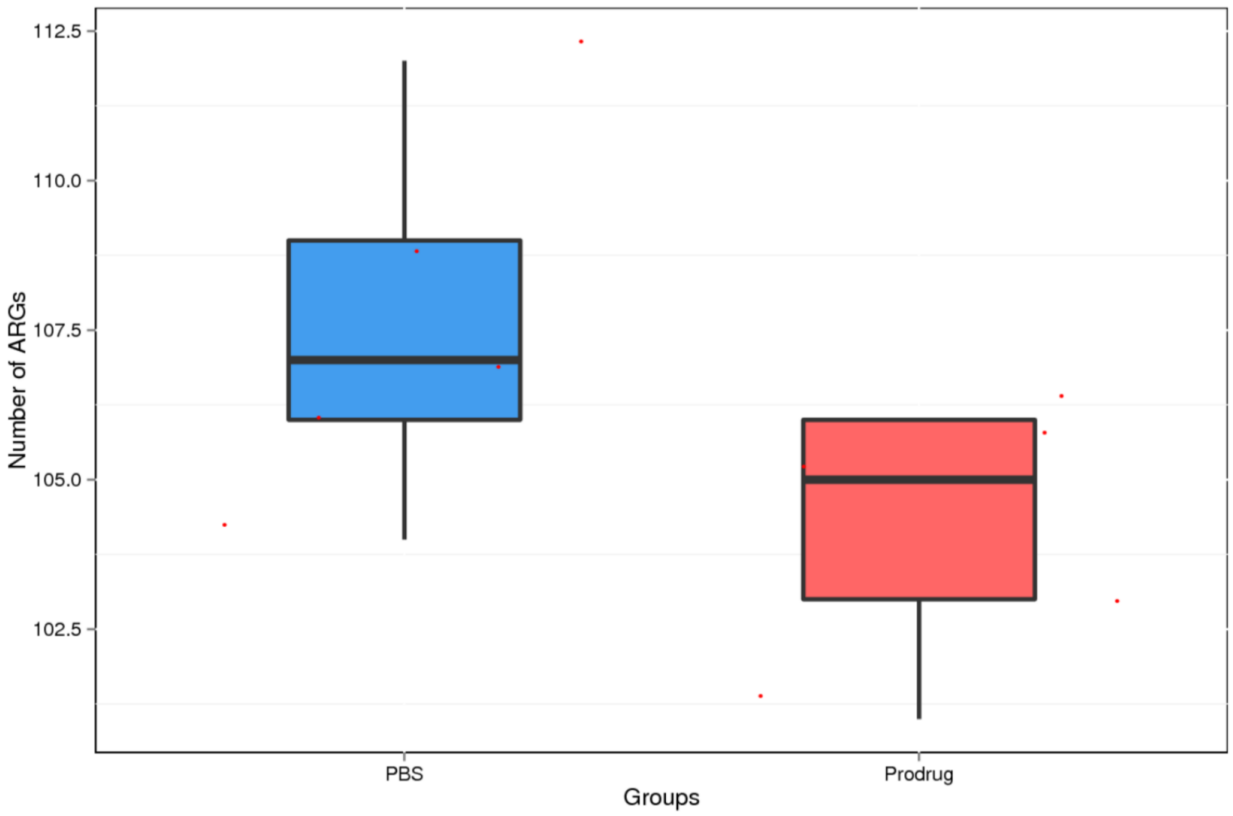

Figure S25. Box plot highlighting average number of ARG in the NDP-NAC treatment group compared to PBS vehicle. ARG in the NDP-NAC treatment group trended downward on average as compared to the PBS vehicle.

References:

1. D. Cantillo, O. de Frutos, J. A. Rincon, C. Mateos, C. O. Kappe, A Scalable Procedure for Light-Induced Benzylic Brominations in Continuous Flow. J. *Org. Chem.* **2014**, *79* (7), 223-229.

2. P. Molina, M. Alajarin, M. J. Vilaplana, A. R. Katritzky, One pot conversion of alkyl halides into thiols under mild conditions. *Tetrahedron Lett.* **1985**, *26* (3), 469-472.

3. R. S. Navath, B. Wang, S. Kannan, R. Romero, R. M. Kannan, Stimuli-responsive star poly(ethylene glycol) drug conjugates for improved intracellular delivery of the drug in neuroinflammation. *J. Controlled Release* ***2010***, *142* (21), 447-456.

Chapter 6: Conclusions and Future Outlook

Chapter 2: This chapter introduces the first self-immolative persulfide prodrug, termed BDP-NAC. This donor responded to H_2O_2 preferentially over other oxidants and reductants to generate its product. *In vitro* cell viability experiments revealed BDP-NAC was non-toxic up to 200 μM in the absence of exogenous H_2O_2. However, BDP-NAC was more effective at rescuing the H9C2 cells in the presence of H_2O_2 than several control compounds, including a compound that lacked the Bpin trigger functionality required for persulfide release (BDP-Control), and a Bpin derivative containing an OH functionality instead of a disulfide (Bpin-OH) delivered **simultaneously** with common biologically-relevant thiols and **H_2S donors**.

Taken together, these findings suggested that persulfides may be more potent bioreductants than H_2S and thus warranted further investigation, stimulating the conception, synthesis, and evaluation of all other persulfide donors in this dissertation. At this point in the field, there were very few discrete persulfide donors, so any biological findings, especially those that compared persulfide and H_2S release under the same conditions, provided foundational insights into persulfide reactivity and potential biological uses. For years, many researchers hypothesized that the total sulfane sulfur pool contributed broadly to the biological activity that was observed upon exogenous delivery of H_2S or persulfides,[1] partly because similar antioxidant activity was observed in different tissues using different H_2S donors and early persulfide donors. However, none of these early experiments adequately compared persulfide donors with structurally analogous control compounds delivered simultaneously with H_2S donors. This work provided seminal findings that suggested that persulfides may have rich, unique biological activity apart from H_2S.

Of note, all persulfide donor systems in this dissertation only release NAC-SSH. Because of the synthetic route used to make BDP-NAC (and all other donors), any thiol may theoretically be appended (instead of NAC) and then released as an analogous persulfide. This opens the door to many possibilities for researchers to append other naturally or non-naturally occurring thiols to similar donors, yielding persulfides with different reactivity. Comparisons between different persulfides released from similar prodrug systems are limited at this point, but one can imagine how beneficial a comprehensive comparison between various released persulfides under different biological conditions may allow researchers to understand which physicochemical properties of persulfides are most important to achieve maximal cellular protection from various forms of ROS/inflammation.

Chapter 3: Chapter 3 focused on the superoxide-responsive persulfide prodrug SOPD-NAC and SOPD-Pep. This prodrug system utilized the same benzyl-based self-immolative scaffold as BDP-NAC, but with an attached superoxide ($O_2^{\bullet -}$)-responsive diphenylphosphinate functionality. Broadly, this manuscript compared a small molecule persulfide donor, SOPD-NAC, to peptide-based nanoassemblies (SOPD-Pep). The structure of the peptide-based donor, termed SOPD-Pep, was synthesized to be structurally analogous to SOPD-NAC, substituting NAC for the peptide sequence Bz-Cys-Phe-Phe-Glu. The trigger specificity of the diphenylphosphinate group in both the small molecule persulfide donor and peptide was verified using the WSP-2 fluorescent probe, observing no differences in these fluorescence assays between the SOPD-NAC or SOPD-Pep. Taken together, these findings confirmed that both the small molecule and peptide could release persulfides in response to $O_2^{\bullet -}$ with similar efficacy.

Fluorescence microscopy was then employed to investigate whether H_2S could be released inside cells in the presence of exogenously delivered $O_2^{\bullet -}$. In these experiments, L-buthionine-(*S,R*)-sulfoximine (BSO) was used as an oxidant, and WSP-5 was used as an H_2S-sensitive probe to monitor H_2S accumulation in the cells. Pretreatment of cells with SOPD-Pep, followed by subsequent addition of WSP-5 and BSO, dramatically increased fluorescence intensity. Importantly, the small molecule persulfide donor SODP-NAC showed limited increase in fluorescence, which was attributed to increased cellular retention of peptide assemblies compared with this small molecule due to its nanoscale size. These findings regarding different cellular uptake of small molecule and peptide-based persulfide prodrugs introduced another variable that researchers must consider when designing biologically appropriate persulfide donors in the future. In other words, it highlights how persulfide donors can appear similar after evaluation by ^{1}H NMR spectroscopy, HPLC, and fluorescence experiments, but the donors' ultimate use (in cells or animals) could be limited by poor cellular uptake.

Many opportunities for the expansion and improvement of peptide-based persulfide donors are available to researchers. Namely, numerous changes could be made to peptide-based donors by changing the appended amino acid sequence, affording potentially robust biological targeting and/or desirable material properties (e.g., localized release from self-assembling peptide hydrogels). Because of the rapid iteration possible via the amendment of pendant amino acids, one can imagine a variety of peptide-based persulfide donors with a plethora of biological uses.

Chapter 4: Chapter 4 focused on the esterase-responsive persulfide prodrugs EDP-NAC and poly(EDP-NAC). This donor system compared antioxidant behavior of an esterase-responsive small molecule and polymeric persulfide donor. Most small molecule persulfide donors at this time in the field were limited in half-life range (generally minutes to hours). To ameliorate this

lack of donors that exhibited long release times, donors with extended persulfide release kinetics were designed via the attachment of a self-immolative benzyl disulfide prodrug to a polymeric scaffold. ^{1}H NMR spectroscopy was then utilized to measure the decomposition kinetics of the persulfide donors in response to PLE, observing decomposition half-lives of 1.6 and 36 h for EDP-NAC and poly(EDP-NAC), respectively.

Atypical for other persulfide donor systems, this large range of persulfide release rates allowed for comparison of the effects of fast and slow-releasing persulfide donors in a variety of cell assays. In an H_2O_2-induced cytotoxicity assay, EDP-NAC rescued cells from H_2O_2, where poly(EDP-NAC) showed limited ability to rescue cells using this immediate form of ROS. However, when H9C2 cardiomyocytes were treated with 5-fluorouricil (5-FU), a sustained inducer of ROS production, poly(EDP-NAC) showed a much greater ability to rescue cells than EDP-NAC, indicating that persulfide release half-lives must be on the same timescale of intracellular ROS production to achieve maximal cellular protection from oxidative stress. Furthermore, this work suggests that polymeric persulfide donors may be uniquely poised to solve some biological problems that small molecule donors cannot, simply due to the massive increase in half-life that one can achieve by appending water soluble (or potentially self-assembling amphiphilic) polymers to persulfide donors.

Poly(EDP-NAC) is one of very few literature examples of polymeric persulfide donors. Because this area of the field remains underexplored, there are many opportunities for the expansion and improvement of this existing system. Degree of polymerization, monomer choice, and polymer topology are only a few examples of variables researchers could leverage to synthesize many polymeric persulfide donors. Should it prove feasible, elucidation of these polymers' mechanical and thermal properties would inform researchers of the practical utility of these polymers in "real

world" applications ranging from cell culture scaffolds to coatings and other functional materials. Targeting groups, fluorophores, and other drugs could be included through covalent or non-covalent interactions in the polymers or polymer assemblies to achieve robust biological targeting capabilities and widely tunable release rates. Additionally, this system may provide opportunities for further comparisons between persulfide and H_2S-releasing polymers with similar half-lives.

Chapter 5: Chapter 5 focused on the nitroreductase-responsive persulfide prodrug NDP-NAC. Because biological links between host and microbe health and reactive sulfur species have been established, a persulfide donor that responded to bacterial stimuli might prove useful in the discovery of the biological roles persulfides potentially enact at the host-bacterial interface. The donor, termed NDP-NAC, released NAC-SSH and *p*-aminobenzyl alcohol as a byproduct in response to bacterial nitroreductase (NR), as confirmed by ^{1}H NMR spectroscopy and HPLC.

NDP-NAC uniquely enabled a study of exogenous persulfide delivery on general bacterial populations in the mouse microbiome. After gavage and feces harvesting, the number of unique non-*Bacillus* species present were counted using MALDI-TOF analysis, yielding 8 unique species present in the NDP-NAC treatment group, and negligible changes in a control group treated with a similar compound that lacked the ability to release persulfides, and a group treated with Na_2S (an H_2S donor). Using the samples from the same mice, short and medium chain fatty acid (SCFA and MCFA) analysis revealed NDP-NAC-treated animals produced higher concentrations of heptanoic acid, an MCFA that performs gastroprotective roles in Crohn's disease and ulcerative colitis. Furthermore, significant alterations in genes responsible for translation, lipid metabolism, and endocrine and metabolic diseases were revealed utilizing shotgun metagenomics analysis. Persulfide release from NDP-NAC elicited substantial changes in the mouse microbiome, reducing the population of niche pathogens and increasing populations of generally beneficial bacteria,

suggesting that delivery of persulfides to the gut may be useful for modulating the microbiome to treat various diseases.

This work served as the first example in the literature of a tissue-specific persulfide donor. Importantly, these findings suggested that persulfides may enact unique biological effects in the microbiome apart from H_2S, and that they may exert specific biological functions other than serving as quenchers of ROS and/or basic redox modulators. There are several ongoing collaborations between the Virginia-Maryland College of Veterinary Medicine and Indiana University, and other proposed collaborative opportunities for the purpose of elucidating specific bacterial species/protein targets. Findings from these collaborative activities could possibly provide insight into a biological mechanism of action by which NDP-NAC modulates the microbiome, further guiding researchers to design improved versions of donors.

Importantly, persulfide donors that utilize enzyme triggers that are localized in specific tissues are desirable to treat acute disease conditions, like localized inflammation (oxidative stress), in order to minimize off-target effects. Nitroreductase is just the first example of several possible compartmentalized enzymes that may prove useful in the development of tissue-specific, enzyme-responsive persulfide donors. One can foresee researchers leveraging the reactivity of other compartmentalized enzymes in the coming years, yielding specialized chemical tools to help elucidate biological roles of persulfides in specific tissues under specific conditions.

References

1. Ishigami, M.; Hiraki, K.; Umemura, K.; Ogasawara, Y.; Ishii, K.; Kimura, H., A Source of Hydrogen Sulfide and a Mechanism of Its Release in the Brain. *Antioxid. Redox. Signal.* **2008,** *11* (2), 205-214.

Appendix A: Fluorescence detection of H_2S through formation of pyrene excimers

Adapted with permission from: Ernesto Cuevasanta, Ana Denicola, Matías N. Möller, Manuela Pose, Kearsley M. Dillon, Beatriz Alvarez, and John B. Matson. "Fluorescence detection of H_2S through formation of pyrene excimers" *In preparation*

A.1. Authors

Kearsley M. Dillon and John B. Matson

Department of Chemistry, Virginia Tech Center for Drug Discovery, and Macromolecules Innovation Institute, Virginia Tech, Blacksburg, VA 24061, United States

A.2. Introduction

H_2S has been recognized as a key player in many important biological processes.[1] Despite this realization of its biological importance, H_2S remains challenging to quantify in the biological setting, as the presence of many different chemical species in complex media complicate results.[2] In particular, cross-reactivity with various cellular reductants (i.e., Cys, GSH) appears to be one of the main issues with currently used quantifiers of H_2S concentrations. Our collaborators originally envisioned a system that utilized pyrene-linked maleimides would be appropriate to solve this problem, as one equiv of H_2S could react twice with the maleimide functionalities, yielding bridged pyrene dimers that would form excimers in solution.[3] Thiols and persulfides could also add to the maleimide, but only once, resulting in two differently fluorescent species that are easily distinguishable. In other words, a system that leveraged the large Stokes shift difference

between excimers and monomers would allow for adequate measuring of H_2S concentrations even in the presence of thiols.

A.3. Results and Discussion

A pyrene-based H_2S sensor (MEBP) was synthesized for the purposes of quantification of H_2S in the presence of biological reductants (Scheme 1). The synthesis of MEBP was accomplished in four steps, starting with a Diels-Alder reaction using furan and maleic anhydride. The resulting oxanorbornene anhydride (**1**) was then treated with ethanolamine in MeOH, rotovapped, and then refluxed in toluene using a Dean Stark trap to distill off furan in a retro Diels-Alder reaction, yielding hydroxyethyl maleimide (**2**). Notably, the furan group in this synthesis was utilized as a protecting group to shield the reactive maleimide from ethanolamine, thus Diels-Alder and retro Diels-Alder had to be performed to minimize unwanted reactivity.[4] The alcohol was then coupled to pyrene butyric acid using an EDC coupling reaction, affording **MEBP** in fair total yields.

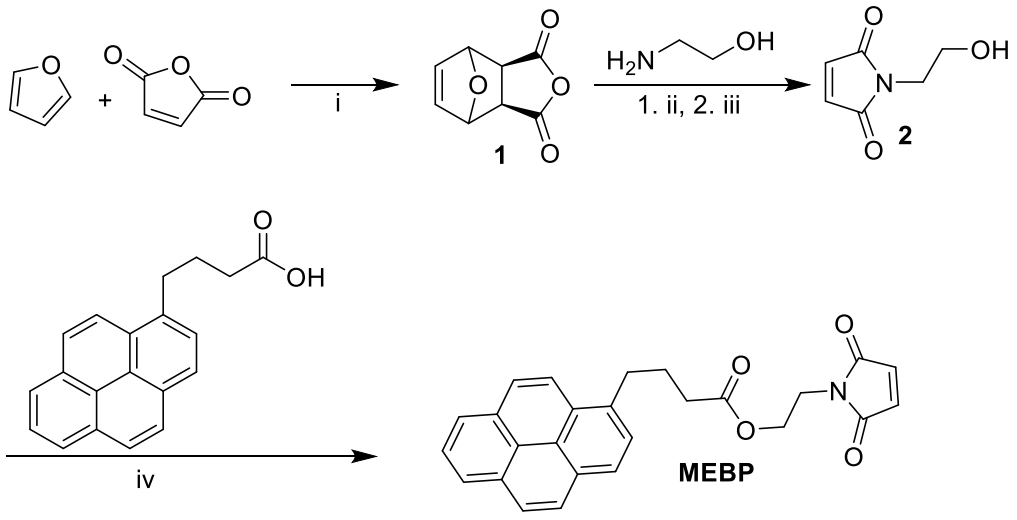

Scheme 1: Synthesis of MEBP. Reaction conditions: i) Et_2O, rt, 12 h; ii) MeOH, 0 °C, 1 h; iii) toluene, reflux, 16 h, Dean-Stark apparatus; iv) EDC, DMAP, THF, rt, 16 h

The mechanism of action that the probe utilizes to quantify H_2S release first entails the reaction of one equivalent of H_2S to the maleimide functionality of MEBP, generating a thiol through a Michael reaction. Another MEBP unit then reacts with this thiol, yielding a coupled MEBP bridged with a thioether linkage (Scheme 2).

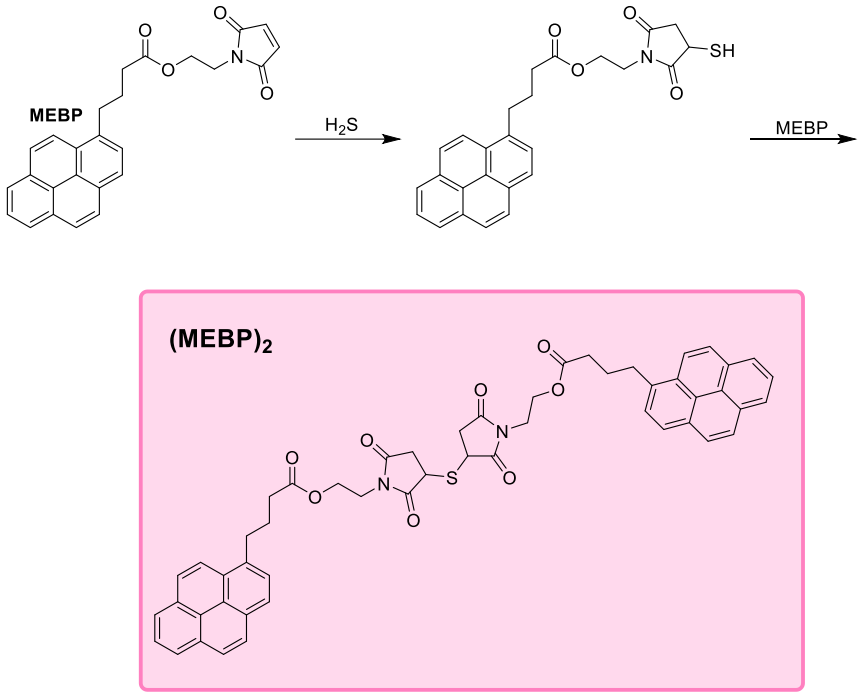

Scheme 2: Mechanism of H_2S reaction with MEBP

This bridged pyrene dimer then exhibits aggregation-induced emission (AIE), fluorescing at a higher wavelength than unimeric pyrenes, which are easily distinguishable. We also proposed this difference in emission wavelength would allow researchers to quantify H_2S concentrations in the presence of biological thiols because only one equivalent of MEBP could react with thiols and this emission wavelength would be easily distinguishable from the pyrene dimer. To provide evidence of stacked pyrene excimer formation, MEBP was treated with Na_2S (0.1 equiv) in a CH_3CN:H_2O (50:1) mixture. An immediate color change occurred upon addition of Na_2S, changing the solution from a pale yellow color to bright pink. HRMS was then utilized to confirm the formation of the

bridged pyrene dimer (Figure S6). Work is ongoing in this project, and we expect a manuscript to form from this work in the near future.

A.4. References

1. Wang, R., Physiological Implications of Hydrogen Sulfide: A Whiff Exploration That Blossomed. *Physiol. Rev.* **2012,** *92* (2), 791-896.

2. Ibrahim, H.; Serag, A.; Farag, M. A., Emerging analytical tools for the detection of the third gasotransmitter H2S, a comprehensive review. *J. Adv. Res.* **2021,** *27* (6), 137-153.

3. Mei, J.; Leung, N. L. C.; Kwok, R. T. K.; Lam, J. W. Y.; Tang, B. Z., Aggregation-Induced Emission: Together We Shine, United We Soar! *Chem. Rev.* **2015,** *115* (21), 11718-11940.

4. Discekici, E. H.; St. Amant, A. H.; Nguyen, S. N.; Lee, I.-H.; Hawker, C. J.; Read de Alaniz, J., Endo and Exo Diels–Alder Adducts: Temperature-Tunable Building Blocks for Selective Chemical Functionalization. *J. Am. Chem. Soc.* **2018,** *140* (15), 5009-5013.

A.5. Experimental

Synthesis of *exo* oxanorbornene anhydride (**1**).

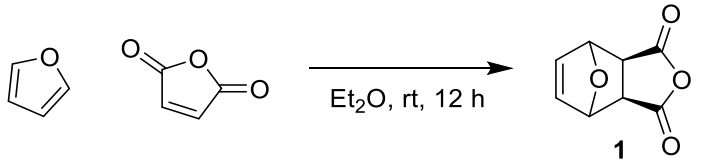

To a 250 mL, flame-dried, two-neck round bottom flask equipped with a septum and an N_2 inlet was added maleic anhydride (10.8 g, 110 mmol) and Et_2O (70 mL) under N_2 flow. Furan (22 mL, 311 mmol) was then added directly to the flask from a graduated cylinder. The flask was sealed with a septum, and the reaction mixture was allowed to stir for 12 h at room temperature under N_2 flow. A white precipitate formed that was collected by filtration and washed with 50 mL cold Et_2O. This white powder (16.1 g, 88% yield) was used in the next step without further purification. NMR spectra were consistent with previous reports.[1] ^{1}H-NMR (δ, $CDCl_3$): 6.58 (2H, t, J = 1.0 Hz), 5.46 (2H, t, J = 1.0 Hz), 3.17 (2H, s)

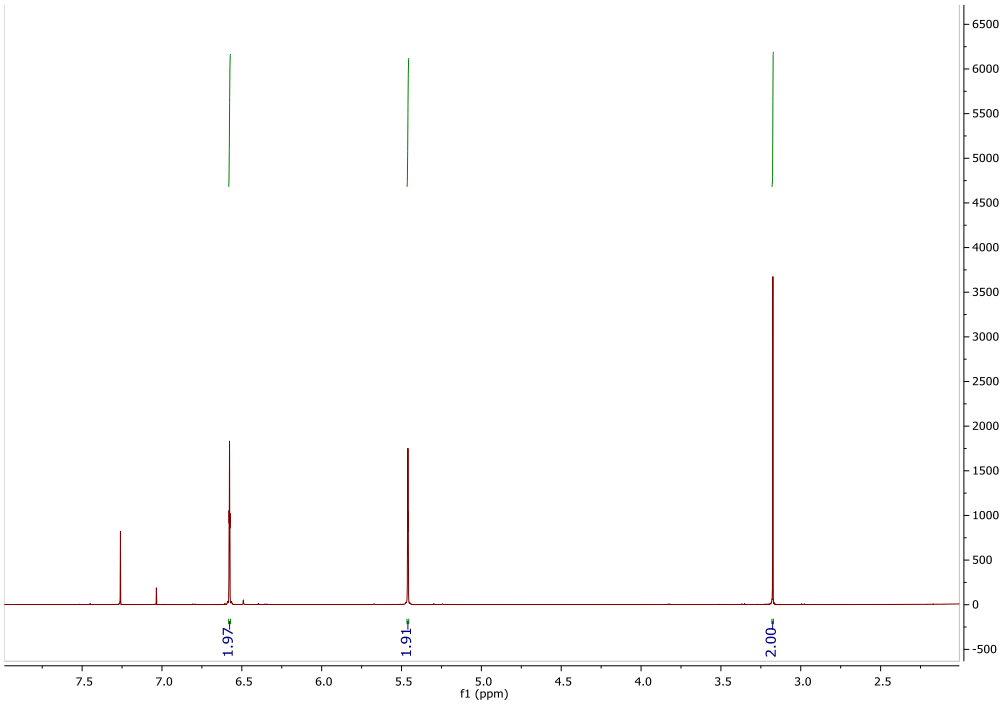

Figure S1: ^{1}H NMR spectrum of *exo* oxanorbornene anhydride

Synthesis of *N*-(2-hydroxyethyl)maleimide (**2**).

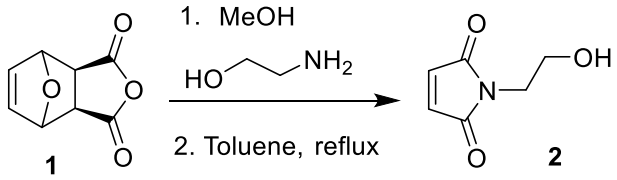

To a flame-dried round bottom flask, anhydride (**1)** (8.7 g, 52 mmol) degassed methanol (80 mL) was transferred via cannula from a Strauss flask and the solution was cooled to 0 °C on an ice bath. A solution of ethanolamine (3.5 mL, 58 mmol) in degassed methanol (15 mL) was dripped in slowly with an addition funnel over 30 min. The reaction mixture was allowed to warm up to room temperature and stirred for 1 h. A reflux condenser was then added to the flask, and the reaction mixture was heated at reflux for 16 h. The reaction mixture was then concentrated via rotary evaporator to yield an off-white solid, which was taken up in CH_2Cl_2 (100 mL) and washed with water in a separatory funnel (3 x 25 mL). The organic layer was removed, dried over Na_2SO_4, and

concentrated in vacuo to yield a white powder, which was immediately carried to the next reaction step without further purification. Next, degassed toluene (80 mL) and a reflux condenser were added to the 250 mL round bottom flask containing the first product, and the reaction mixture was heated at reflux for 16 h under positive nitrogen flow. A distillation apparatus was assembled, and distillation was carried out at 90 °C for 8 h at atmospheric pressure to remove excess furan and prevent Diels-Alder recombination. Once furan had ceased distilling, the remaining toluene was removed via rotary evaporation to yield the desired product as off-white crystals (6.3 g, 79% yield). NMR spectra were consistent with previous reports.[2] ^{1}H-NMR (δ, $CDCl_3$): 6.73 (2H, s), 3.77 (2H, m), 3.71 (2H, m)

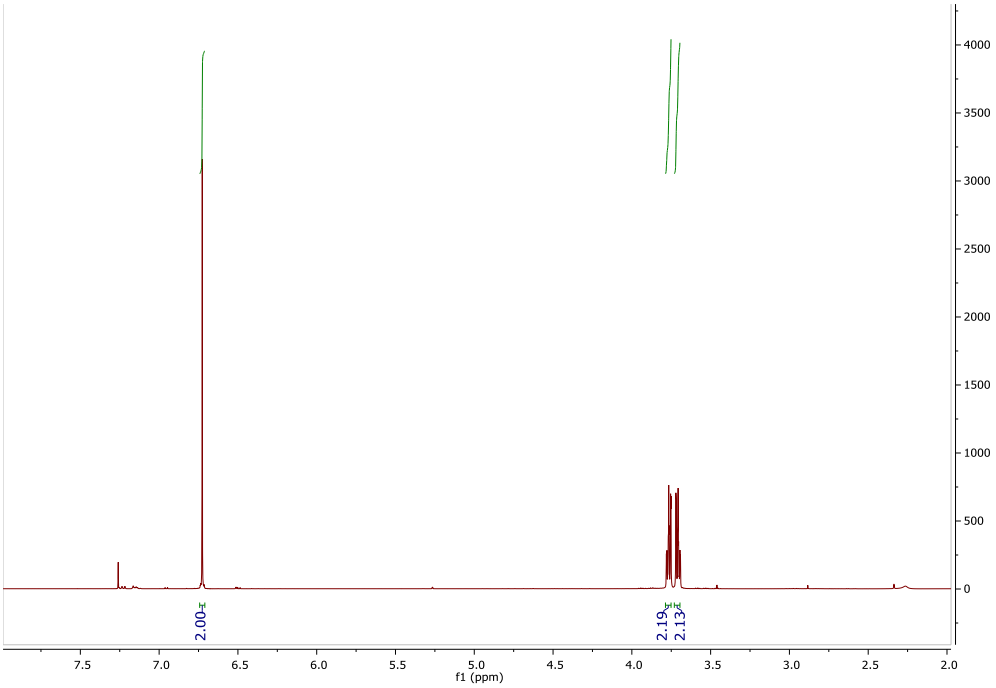

Figure S2. ^{1}H NMR spectrum of *N*-(2-hydroxyethyl)maleimide

Synthesis of MEBP (**3**).

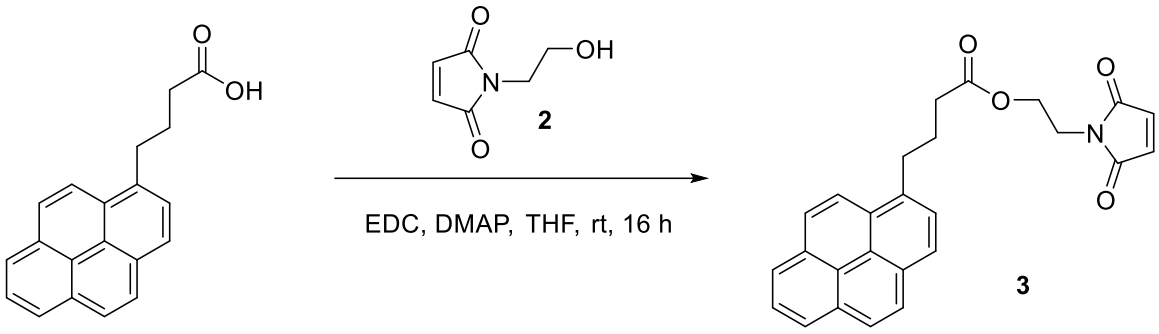

To a flame-dried, two-neck, round bottom flask, equipped with a stopper and a septum, 4-(1-pyrenyl)butyric acid (150 mg, 0.52 mmol) and anhydrous THF (10 mL, via cannula from a Strauss flask) were added under N_2 flow. To this suspension, ethyl-3-(3-dimethylaminopropyl)carbodiimide (EDC, 400 mg, 2.5 mmol) and 4-dimethylaminopyridine (DMAP, 3.0 mg, 26 µmol) were added. The reaction mixture was allowed to stir for 30 min at rt until homogeneous. To this amber solution, *N*-(2-hydroxyethyl)maleimide **(2)** (77 mg, 0.56 mmol) was added under N_2 flow, and the reaction mixture was allowed to stir for 16 h at rt, monitoring reaction progress by TLC (DCM, UV visualization). The reaction mixture was then concentrated via rotary evaporation to yield an orange waxy solid, which was taken up in CH_2Cl_2 (20 mL) and then washed with 1 N HCl (10 mL), deionized water (2 x 10 mL), and brine (10 mL). The organic layer was then removed and dried over Na_2SO_4. The product was dry-loaded onto silica and purified by column chromatography, eluting with 25% EtOAc in hexanes (Spot 2, R_f = 0.3, visualized with UV) to yield the product as a yellow waxy solid (140 mg, 65%). ^{1}H-NMR (δ, $CDCl_3$): 8.30 (1H, d, *J* = 9.5 Hz), 8.18-8.10 (4H, m), 8.02-7.97 (3H, m), 7.87 (1H, d, *J* = 7.7 Hz), 6.63 (2H, s), 4.5 (2H, t, *J* = 5.3 Hz) 3.8 (2H, t, *J* =5.3 Hz), 3.37 (2H, t, *J* = 7.6 Hz), 2.44 (2H, t, *J* = 7.5 Hz), 2.17 (2H, quint, *J* = 7.6 Hz**)** ^{13}C-NMR (δ, $CDCl_3$): 173.3, 170.4, 135.7, 134.2, 131.4,

130.9, 130.0, 128.8, 127.6, 127.44, 127.36, 126.8, 125.9, 125.1, 125.0, 124.97, 124.88, 124.83, 124.4, 61.5, 36.9, 33.7, 32.7, 26.6.

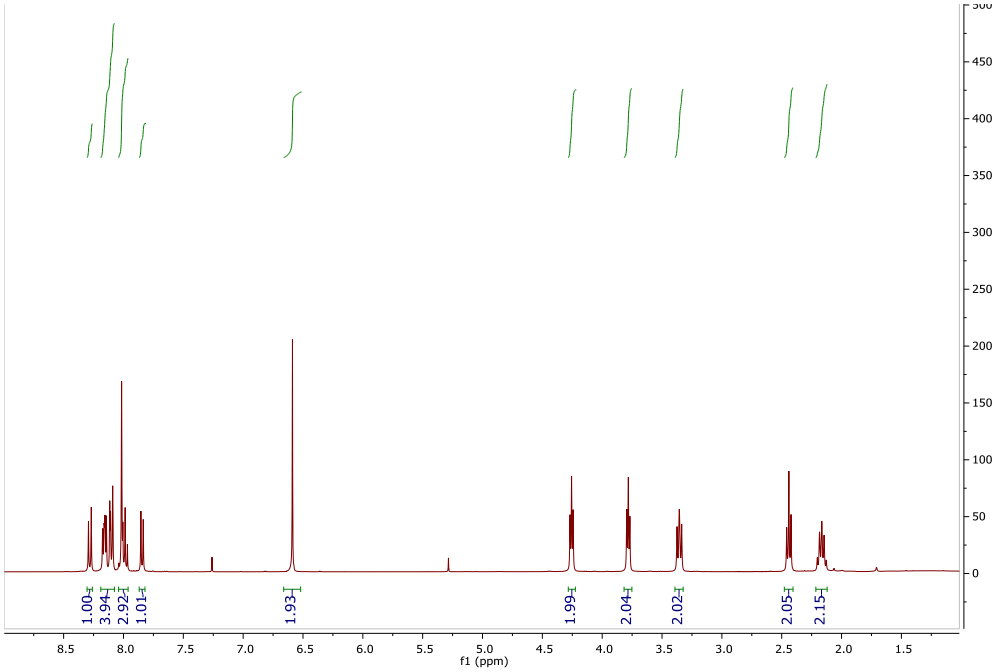

Figure S3. ^{1}H NMR spectrum of MEBP

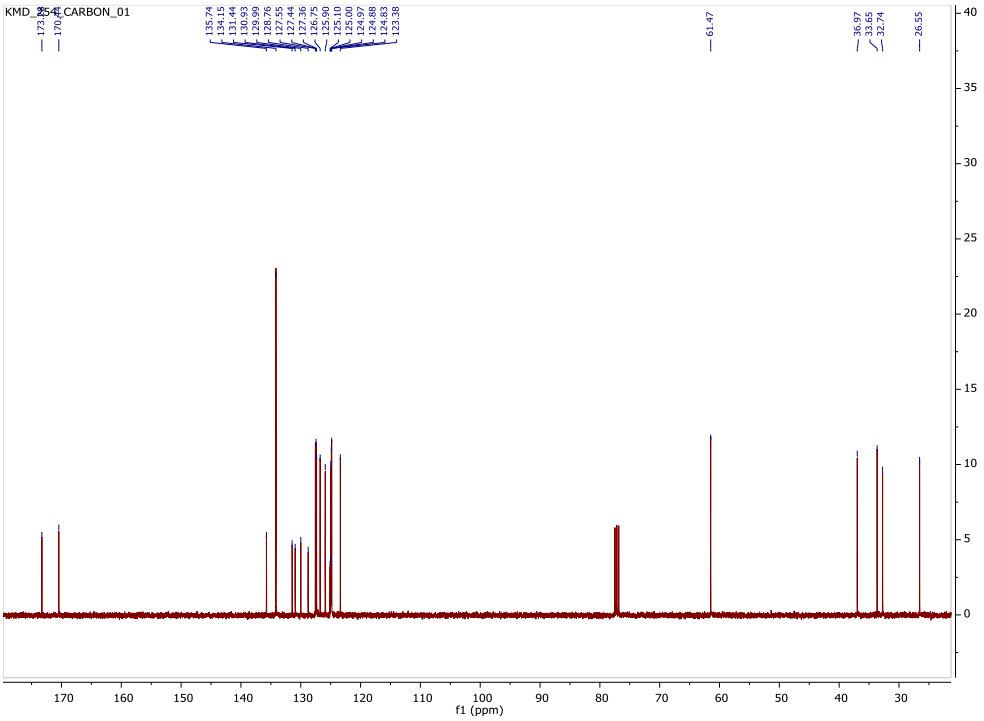

Figure S4. ^{13}C NMR spectrum of MEBP

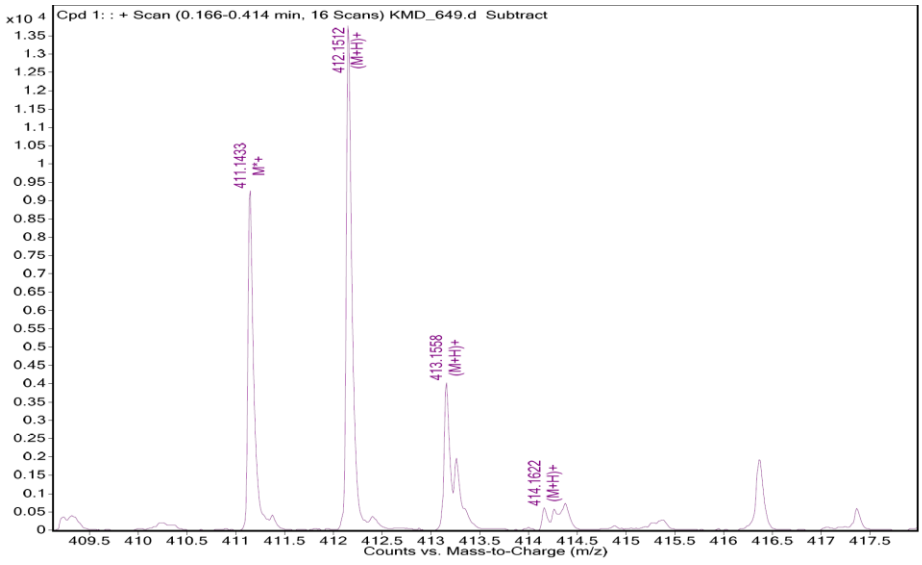

Figure S5. HRMS (ESI-TOF): Calculated for $C_{25}H_{19}NO_4$ $[M+H]^+$ 412.1548, found 412.1512.

Analysis of MEBP reaction with Na_2S

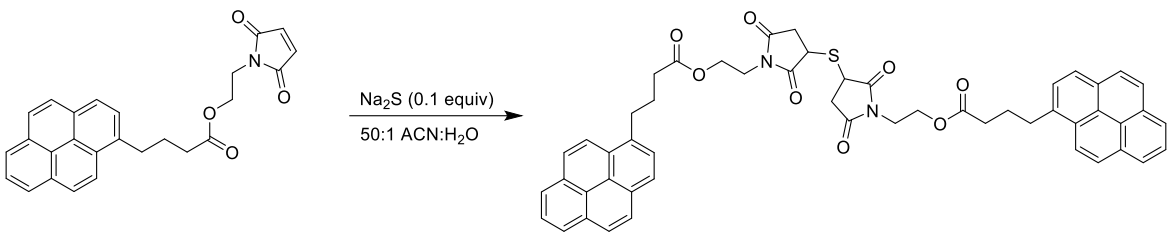

MEBP (1.0 mg, 2.4 µmol) was dissolved in LC-MS grade ACN (1.0 mL) creating a clear, colorless solution. Na_2S (1.0 mg), stored in a glove box under a nitrogen atmosphere, was dissolved in LC-MS grade H_2O (1.0 mL). 20 µL Na_2S stock solution (0.26 µmol) was then injected into the solution of MEPB. The resulting pink solution was analyzed by HRMS.

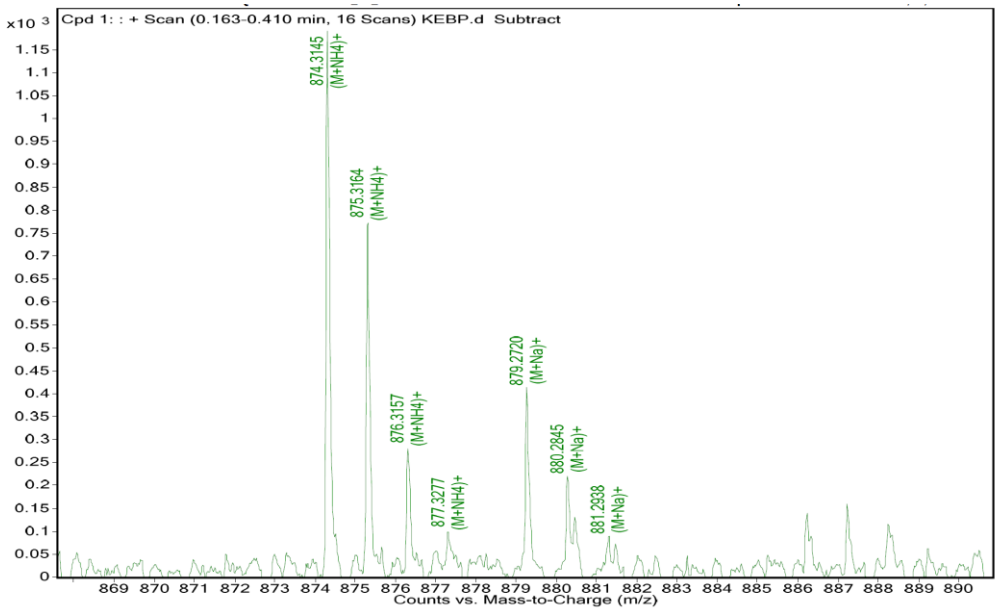

Figure S6. MS (ESI-TOF) spectrum of $(MEPB)_2$-S. A peak was observed at m/z = 874.3145, consistent with the $[M+NH_4]^+$ adduct of the expected product (calculated m/z = 874.3162). The other peak observed at m/z = 879.2720 was consistent with the sodium adduct $[M+Na]^+$ (calculated 879.2716).

Experimental references:

1. McCluskey, A.; Ackland, S. P.; Bowyer, M. C.; Baldwin, M. L.; Garner, J.; Walkom, C. C.; Sakoff, J. A., Cantharidin Analogues: Synthesis and Evaluation of Growth Inhibition in a Panel of Selected Tumor Cell Lines. *Bioorg* **2003**, *31* (2), 68-79.

2. Linares, I. A. P.; de Oliveira, K. T.; Perussi, J. R., Chlorin Derivatives Sterically-Prevented from Self-Aggregation with High Antitumor Activity for Photodynamic Therapy. *Dyes Pigm.* **2017**, *145* (17), 518-527.

Appendix B: Synthesis of peptide thioacids for H_2S delivery

B.1. Authors:

Kearsley M. Dillon and John B. Matson

Department of Chemistry, Virginia Tech Center for Drug Discovery, and Macromolecules Innovation Institute, Virginia Tech, Blacksburg, VA 24061, United States

B.2 Introduction:

Peptide-based H_2S donors have been reported in the literature for a variety of biological applications.[1-2] A major limitation of these donors is that they require the covalent attachment of a presynthesized H_2S donor, and thus result in byproducts that may cause undesired biological effects. In this work, a peptide was designed that was expected to release H_2S without the attachment of a separate synthetic H_2S donor, avoiding any issues with byproducts. The peptide sequence Ac-VPLSLG-C(O)SH was chosen to leverage reactivity with matrix metalloprotein-9 (MMP-9),[3] an enzyme involved in wound repair, as it was believed there might be a synergistic effect if H_2S release could be localized where wound repair was occurring (decreasing inflammation, aiding wound repair). MMP-9 cleaves between the serine and leucine residues in this sequence, resulting in the release of a dipeptide NH_2-LG-C(O)SH. It was proposed that this dipeptide would then cyclize, forming a diketopiperizine with the release of H_2S.

B.3. Results and Discussion:

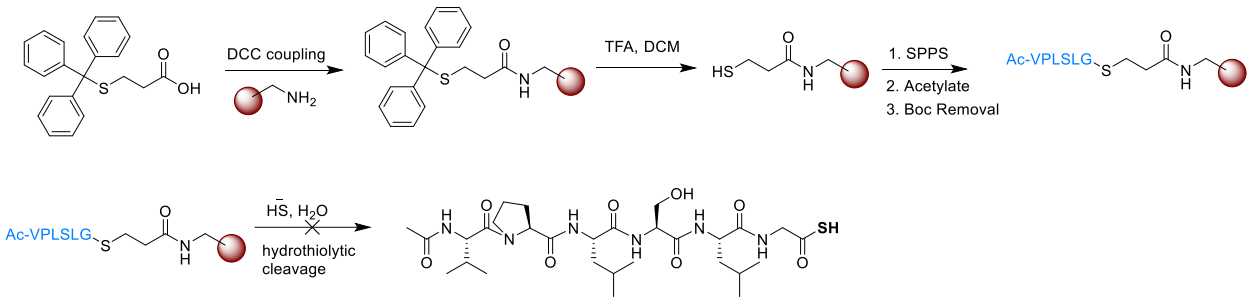

Scheme 1. Proposed synthesis of Ac-VPLSLG-C(O)SH. Hydrothiolytic cleavage was unsuccessful in this synthesis.

First, a peptide was synthesized according to Scheme 1 (above). This approach involved first the synthesis of a modified resin using trityl protected mercaptopropionic acid, followed by standard solid phase peptide synthesis. Although the reaction product of this reaction following hydrothiolytic cleavage should yield the desired peptide thioacid, this compound was never observed. Instead, Ac-VPLSLG-C(O)OH was observed in good yields under a variety of conditions (Figure 1, predicted mass 626 amu). Thus, additional reactions were performed to try to convert the resulting carboxylic acid into a thioacid functionality.

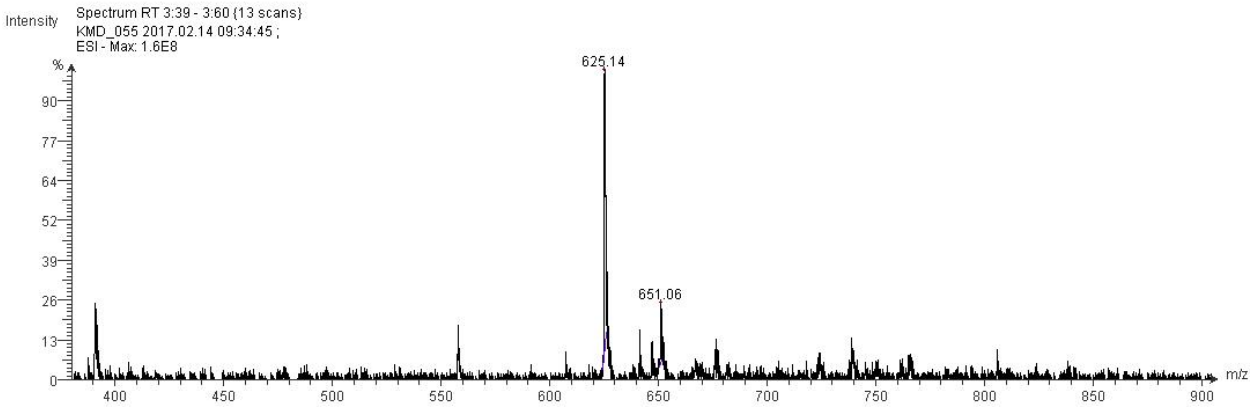

Figure 1. MS confirmation of Ac-VPLSLG-C(O)OH

Although several conditions were utilized to attempt to convert the carboxylic acid into the thioacid, one main approach was extensively studied. Using Lawesson's reagent (LR), several research groups had shown the conversion of small peptides and many organic ketones into their sulfur-based derivative (thioacids and thioketones, respectively).[4] We utilized microwave irradiation to speed up the conversion of carboxylic acid to thioacid, an approach also commonly employed in the literature (Figure 2).

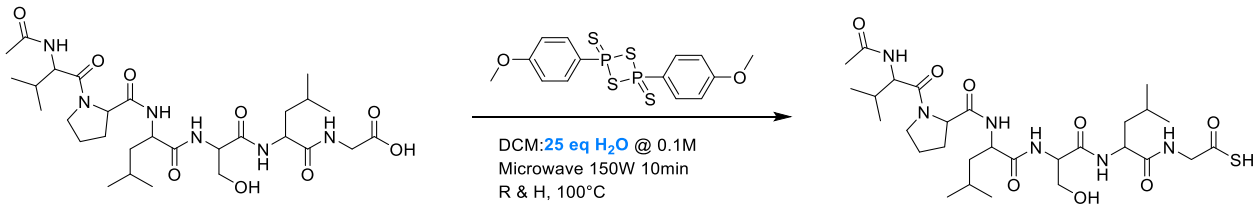

Figure 2. Synthesis of Ac-VPLSLG-C(O)SH via Lawesson's reagent. Base additive highlighted in blue, with H_2O shown in this case.

After many attempts of thioacid synthesis with Lawesson's reagent varying a variety of experiment parameters, it was apparent that a particular mass that was present in the MS spectrum that was indicative of the reaction not proceeding to completion (Figure 3).

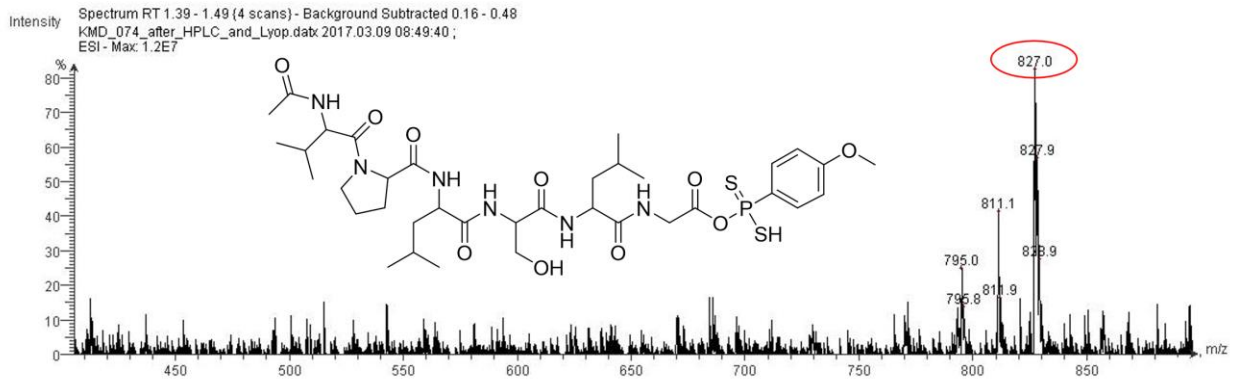

Figure 3. Mass spectrum of Lawesson's reagent peptide adduct. Circled mass corresponds to Ac-VPLSLG-LR adduct (predicted mass 828 amu).

According to the reaction mechanism (Figure 4), Lawesson's reagent first cleaves in response to heat and/or irradiation, yielding a thiophosphonium salt that is then reactive towards carboxylic acids and ketones. Based on MS analysis, the reaction of Ac-VPLSLG-C(O)OH and Lawesson's reagent was getting stuck at the point at which a base was needed to perform proton transfer, allowing for rearrangement to occur with subsequent release of Ac-VPLSLG-C(O)SH.

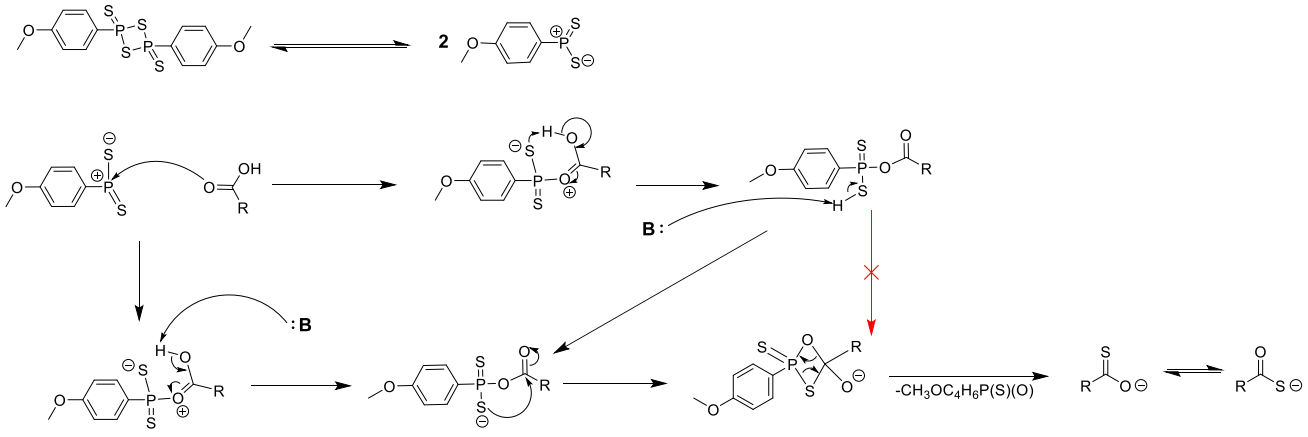

Figure 4. Lawesson's reagent reaction mechanism.

Because the thiophosphonium salt is a good electrophile, the chosen base (proton transfer agent) must not be nucleophilic. A variety of base additives were used in many different reactions and concentrations during the microwave reaction of LR and Ac-VPLSLG-C(O)SH to try to achieve higher conversion to thioacid. In model reactions with *N*-acetyl glycine, moderate conversion to thioacid was observed using all chosen base additives (Figure 5), but no productive reaction was observed when trying these additives under the same conditions using Ac-VPLSLG-C(O)OH.

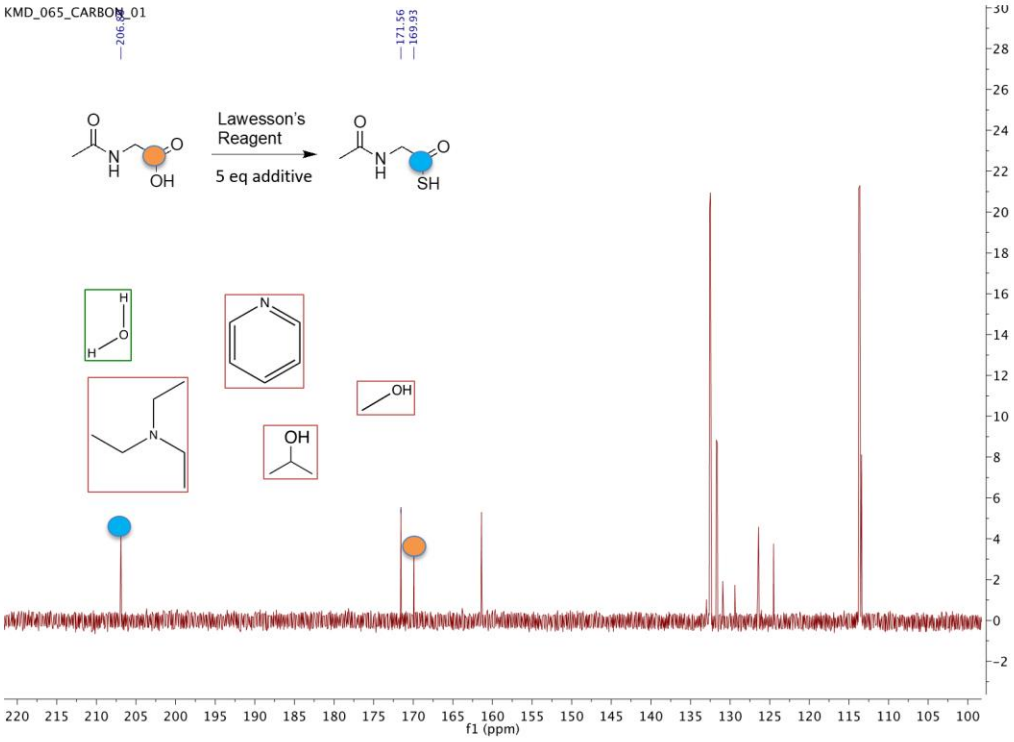

Figure 5. Exemplary ^{13}C NMR spectrum of *N*-acetyl glycine thoacid and listed base additives. The reaction with water as an additive is shown in the above spectrum.

Unfortunately, this series of work yielded minimal results, and research efforts were shifted to the persulfide-releasing prodrugs that were discussed in earlier chapters in this dissertation. The synthesis of peptide thioacids for H_2S delivery may still be possible, but creative chemistries will

have to be utilized to do so, and it is predicted that the usage of a disulfide intermediate may be critical in this newly designed synthesis.

B.4. References

1. Qian, Y.; Kaur, K.; Foster, J. C.; Matson, J. B., Supramolecular Tuning of H_2S Release from Aromatic Peptide Amphiphile Gels: Effect of Core Unit Substituents. *Biomacromolecules* **2019,** *20* (2), 1077-1086.

2. Qian, Y.; Matson, J. B., Gasotransmitter delivery via self-assembling peptides: Treating diseases with natural signaling gases. *Adv. Drug Deliv. Rev.* **2017,** *110-111* (Supplement C), 137-156.

3. Mohan, R.; Chintala, S. K.; Jung, J. C.; Villar, W. V. L.; McCabe, F.; Russo, L. A.; Lee, Y.; McCarthy, B. E.; Wollenberg, K. R.; Jester, J. V.; Wang, M.; Welgus, H. G.; Michael Shipley, J.; Senior, R. M.; Elizabeth Fini, M., Matrix metalloproteinase gelatinase B (MMP-9) coordinates and effects epithelial regeneration. *J. Biol. Chem.* **2002,** *277* (3), 2065-2072.

4. Ozturk, T.; Ertas, E.; Mert, O., Use of Lawesson's Reagent in Organic Syntheses. *Chem. Rev.* **2007,** *107* (11), 5210-5278.